Cardiff
Catalysis Institute

Sefydliad Catalysis
Caerdydd

Water purification by Catalytic Wet Air Oxidation (CWAO)

Korrin Saunders

Supervisors: Prof. Stan Golunski[a], Prof. Stuart Taylor[a], Dr. Pawel Plucinski[b]

[a]Cardiff University   [b]University of Bath

Thesis submitted in accordance with the requirement of Cardiff University

for the degree of Doctor of Philosophy

September 2019

Acknowledgements

Abstract

The generation of hazardous wastewaters from industrial and domestic processes, poses a serious environmental threat if left untreated and allowed to enter water sources. Current techniques for removing toxic organic pollutants from wastewaters include biological, thermal and chemical treatment, but they are often coupled with an inability to degrade high concentrations of pollutants, long biological degradation lifetimes or the release of harmful emission gases. As we steer towards more sustainable and environmentally friendly techniques, advanced oxidation processes have become increasingly popular. Wet Air Oxidation (WAO) and subsequently, Catalytic Wet Air Oxidation (CWAO), is proving to be one of the most economical and environmentally friendly processes for the removal of toxic organic compounds found in industrial wastewater streams. Using oxygen as a clean source of oxidant, CWAO oxidises the pollutants, over a catalyst, to CO_2 and H_2O. The addition of a catalyst offers increased reaction rates and less severe operating conditions, which in turn leads to lower capital costs. Phenol was selected as a model pollutant, for CWAO.

Building on previous research, alternate catalyst compositions are investigated with particular attention paid to the wettability of catalyst support. Noble metals supported on silicon carbides were investigated for the CWAO of phenol and bisphenol-A (BPA) in a trickle bed reactor (TBR). Complete phenol conversion was observed for Pt/SiC at 7 $bar_{(g)}$ and 160 °C, with 99.9 % selectivity towards CO_2. The partial substitution of platinum with ruthenium was investigated, as well as the effect of surface area of the silicon carbide support.

An explanation is proposed for the increased reaction rates seen when using comparatively hydrophobic catalyst supports; the presence of gas bubbles within the catalyst pores on a hydrophobic support allows for a secondary mass transfer route of oxygen directly from the gas phase to the catalyst surface, prohibited by the more typical hydrophilic catalysts.

The catalysts screened were characterised using a number of techniques including, powder x-ray diffraction (XRD), N_2 adsorption BET specific surface area, thermogravimetric analysis (TGA), temperature programmed reduction (TPR), scanning election microscopy (SEM), energy dispersive x-rays (EDX), x-ray photoelectron spectroscopy (XPS) and helium pycnometry porosity measurements.

Table of Contents

Chapter 3: Experimental

Chapter 4: Addition of ruthenium to platinum catalysts for CWAO of phenol

Chapter 5: Effect of surface area on silicon carbide catalysts for CWAO of phenol

Chapter 6: The CWAO of bisphenol-A

x

Chapter 1

Introduction to wastewater treatment

1.1 Environmental concerns of wastewater

The generation of wastewater, from both industrial and domestic processes, leads to hazardous organic pollutants which, if left untreated, can cause severe problems for our ecosystems. Therefore, with the growing concern for the environment, and ever-stricter government water quality regulations, it is necessary to develop greener and more efficient processes to treat such pollutants.

A large majority of industrial processes use water as either a solvent or reaction transport medium[1]; the resulting contaminated wastewater can have far reaching effects if discharged into streams and rivers. The chemical content of these effluents may vary from inorganic pollutants from an electroplating process to toxic organic compounds from pesticide manufacturing[2]. Organic pollutants in particular can cause severe problems for aquatic life[3], affecting the metabolism, survival, growth and reproductive capabilities of certain species[4].

Efficient and economic technologies for the removal of toxic organic contaminants in wastewater streams are imperative to produce reusable process water and environmentally friendly effluents[5].

1.2 Sources of wastewater

Wastewater can come from a variety of different sources; a substantial proportion of industrial processes generate wastewater containing a broad range of chemicals. The biochemical content of this wastewater is dependent upon the

industry in which it was generated. Pulp and paper mills, copper-ore/deep mines[6], paint shops, oil refineries, plastics and resin manufaturing[7] are just a few industries that give way to wastewater containing difficult to break down, non-biodegradable, toxic organic compounds[8]. Each of these industries, and countless others produce wastewater that requires treatment if it is to be safely discharged into the environment.

The majority of agriculture and industrial processes have wastewater management procedures in place, however not all are designed to degrade toxic organic pollutants, and in some cases these pollutants can pass through untreated into rivers and streams[9].

1.3 Common pollutants and legislation

To control and prevent excess discharge of harmful contaminants entering the environment, the European Union set regulations regarding the limits of pollutants allowed to safely enter UK watercourses. The level of pollution can be measured using biochemical oxygen demand (BOD) and chemical oxygen demand (COD), which measure the concentration of oxygen required to fully oxidise the biochemical and chemical content of water to CO_2 and H_2O[10].

Table 1.1 Average pollutant concentrations found in untreated wastewater, US EPA 2015[11]

Pollutant	Unit	Average total concentration
Total Kjeldahl Nitrogen (TKN)	mg L^{-1}	34.9
Ammonia as N	mg L^{-1}	13.1
Nitrate as N	mg L^{-1}	91.4
BOD	mg L^{-1}	8.2
COD	mg L^{-1}	345
Total Suspended Solids (TSS)	mg L^{-1}	14,500
Total Phosphorous (TP)	mg L^{-1}	4.02
Chloride	mg L^{-1}	7,1820
Sulphate	mg L^{-1}	13,300
Total Dissolved Solids (TDS)	mg L^{-1}	33,300
Selenium	µg L^{-1}	3,130
Calcium	mg L^{-1}	3,290,000

Table 1.1 shows an example of pollutant concentrations found in wastewater associated with Flue Gas Desulfurization (FGD) processes by the United States Environmental Protection Agency (EPA) in 2015[11]. As well as the COD and BOD, ammonia, nitrate and phosphorous concentrations are all regulated. Ammonia is one of the more common pollutants discharged into water streams; food processing industries, fertilizer production and textile manufacturing are all industries which generate highly concentrated ammonia wastewaters[12].

Removal of phosphorous from wastewaters is also paramount, as it can contribute to eutrophication, causing excess growth of photosynthesising organisms[13]. Excess algae on the surface of lakes and rivers, restricts the sunlight reaching plant life at lower depths, which consequently restricts photosynthesis, depleting the oxygen concentration in the body of water. As a result of the reduced oxygen, fish and other marine animals can suffocate.

The nature of pollutants and their concentrations are as varied as the industries in which they are generated; the concentrations of specific effluents will

also vary over time from the same industrial plant[2]. Regulations concerning water quality are becoming ever stricter; in the UK, regulations are set based on the particular industry, nature of pollutants and waterbody the effluent is being discharged into.

As an example, the trade effluent discharge limits set by the Singapore government under the Environmental Protection and Management Regulations are presented in Table 1.2[14].

Table 1.2 Regulations for the discharge of trade effluents set by the Singapore government[14]

No.	List of Substances	Limit (mg L^{-1})
1	Biological oxygen demand (BOD) 5 days at 20 ^{o}C	20
2	Chemical oxygen demand (COD)	60
3	Total suspended solids	30
4	Total dissolved solids	1,000
5	Chloride (chloride ion)	250
6	Sulphate (SO$_4$)	200
7	Sulphide (sulphur)	0.2
8	Cyanide (CN)	0.1
9	Detergents (linear alkylate sulphonate as methylene blue active species)	5
10	Grease and oil (hydrocarbon)	1
11	Grease and oil (non-hydrocarbon)	1
12	Arsenic	0.01
13	Barium	1
14	Tin	5
15	Iron (Fe)	1
16	Beryllium	0.5
17	Boron	0.5
18	Manganese	0.5
19	Phenolic compounds (phenol)	Nil

Organic pollutants are of particular concern due to their persistence and ability to bioaccumulate, some can remain in the environment in excess of 100 years[15]. One such compound is phenol and its derivatives; it is also the only compound listed in Table 1.2 which has a limit of zero for discharge in controlled watercourses.

1.3.2 Phenol as a model pollutant

Phenol and phenolic compounds are among the most common organic pollutants typically found in wasterwaters[16]. An estimated 6 million tonnes of phenol are produced each year[17]. Phenol compounds are important chemical precursors for many industrial processes, they are widely used as raw materials for the production of petrochemicals, pesticides, plastics and pharmaceuticals[18,19]. As a result, these compounds are commonly encountered in the industrial effluents and surface water associated with such processes. Furthermore, phenol is a frequent intermediate product in the reaction pathway of higher molecular weight aromatic compounds also encountered in wastewaters[20]. The molecular structure of phenol can be seen in Figure 1.1.
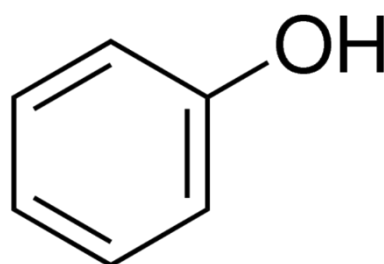
Figure 1.1 Molecular structure of phenol

Unfortunately, phenol is both toxic and corrosive, and, if allowed to enter water streams, it can cause severe problems for aquatic life[3]. Phenol affects the metabolism, survival, growth and reproductive capabilities of aquatic life, as well as causing skin irritation and damage to kidney, liver and lung function in humans[21]; ingestion of doses larger than 1 g can be fatal to adults[22]. Concentrations of <1 mg L^{-1} can cause significant taste and odour problems and

the European Economic Community (EEC) directive mandate phenol concentration should not exceed 0.5 pg L^{-1} in drinking water[23,24].

The high toxicity and frequency of which phenol is used make it a model organic pollutant for wastewater treatment methods[25]. This project will focus on the removal of phenol, which has been investigated numerous times in the literature[26-30], setting a good catalyst benchmark.

1.3.2.1 Oxidation pathway and possible reaction intermediates

The complete oxidation of phenol to CO_2 and H_2O can proceed *via* several different pathways, and under non-optimal conditions partial oxidation can result in numerous intermediates. The potential pathways and reaction intermediates for phenol oxidation proposed by Devlin *et al.*[31] is presented in Figure 1.2.
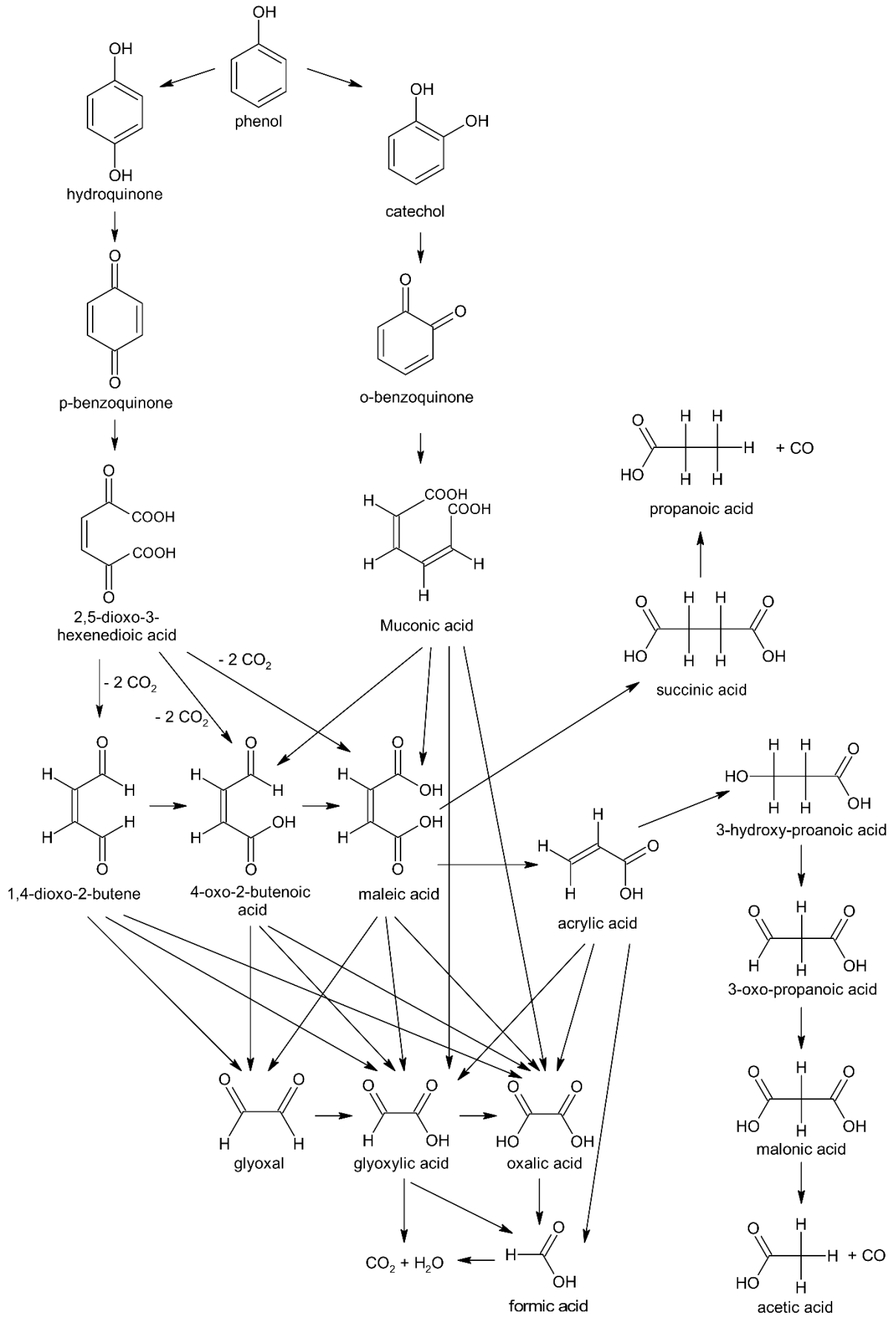
Figure 1.2 Possible reaction pathways for the oxidation of phenol[31]

The initial step of oxidation can occur in either the *ortho* or *para* position, resulting in catechol or hydroquinone, followed by *o*-benzoquinone and *ρ*-benzoquinone respectively. Further oxidation can then proceed *via* numerous pathways, with a possible 15 different organic intermediates before complete oxidation to CO_2 and H_2O. Devlin *et al.*[31] proposed this reaction schematic after isolating the majority of the compounds in the reaction media, however a few compounds were considered too short lived to isolate, but were consistent with the sequential devolvement of the reaction scheme.

Duprez *et al.*[32] and Santos *et al.*[33] also proposed similar reaction schematics (shown in Figures 1.3 and 1.4 respectively) reinforcing the validity of the pathway.
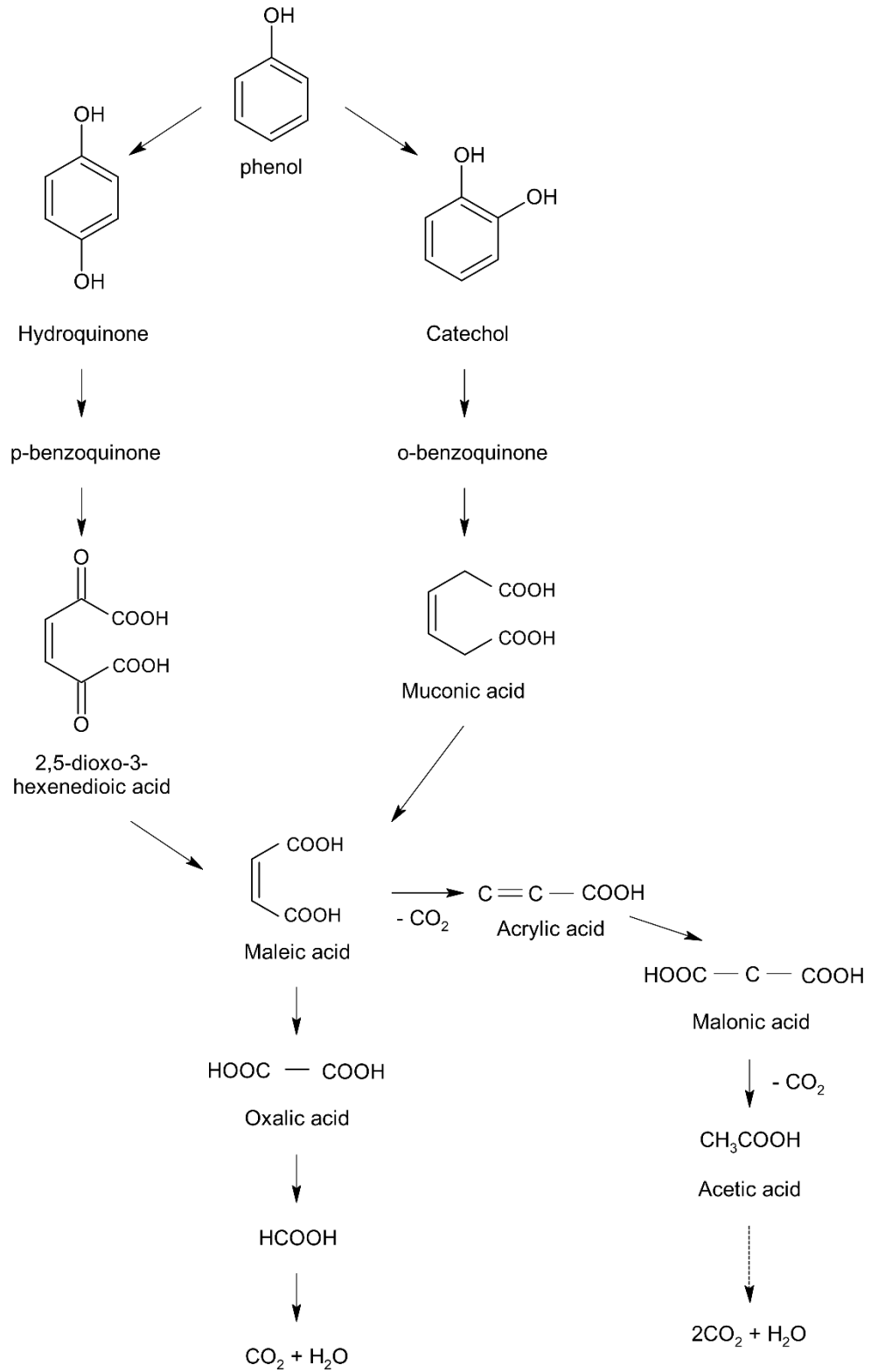
Figure 1.3 Phenol oxidation pathway proposed by Dupres et al.[32]
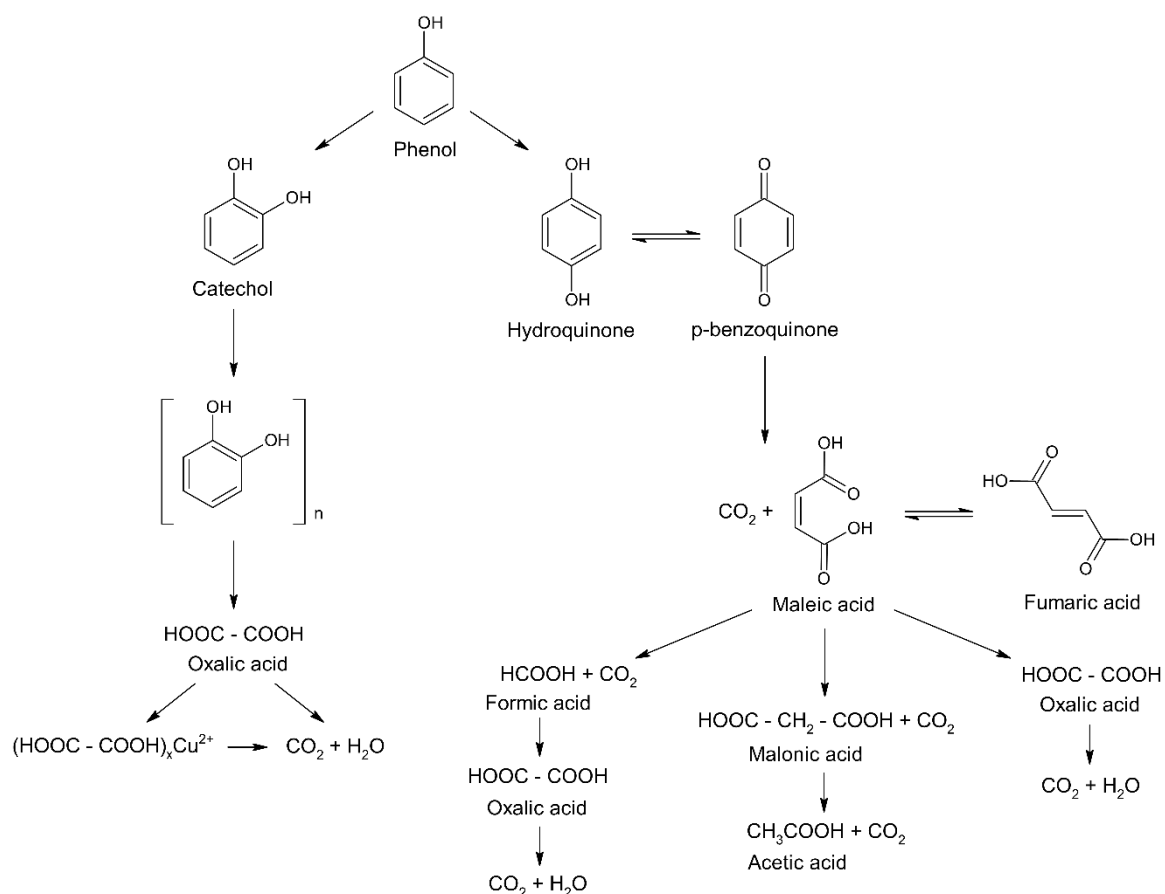
Figure 1.4 Phenol oxidation pathway proposed by Santos et al.[33]

Acetic acid is a common end product in oxidation reactions of various organic compounds, and the oxidation of this carboxylic acid is thought to be a rate limiting factor for the complete oxidation of phenol[32]. Oxalic and maleic acid were also observed as stable side products.

The potential for polymerization reactions during phenol oxidation, leading to the formation of complex molecules was reported by Levec *et al.*[34]. The proposed polymer reaction pathway is displayed in Figure 1.5.
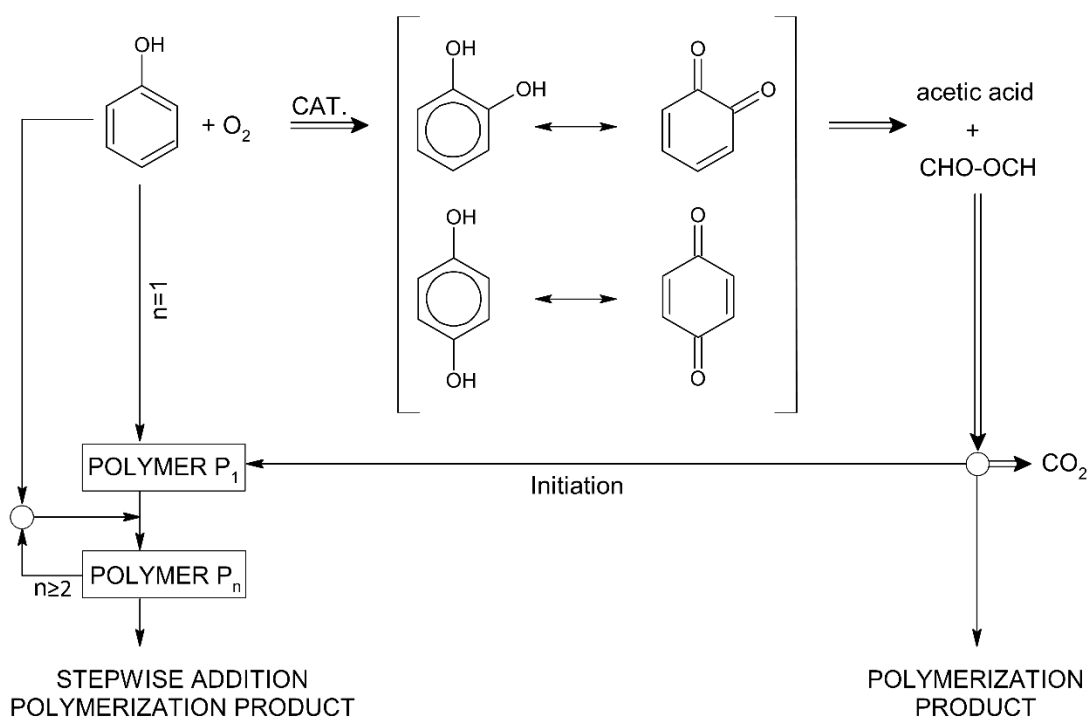
Figure 1.5 Reaction schematic for phenol oxidation with potential polymerisation[34]

Polymerization can occur *via* the reaction between phenol and partial oxidation product glyoxal, or by polymerisation of glyoxal with itself. Alejandre *et al.*[35] also observed polymerisation in this manner during the oxidation of phenol.

Cyclic intermediates hydroquinone and *p*-benzoquinone are considerably more toxic than phenol, and if they remain as stable intermediate products there is a risk of increased toxicity of the wastewater during treatment[36]. Coupled with the possibility of numerous other reaction intermediates, the reaction success cannot be described in terms of purely phenol conversion. The complete oxidation and selectivity towards CO_2 and H_2O must also be considered.

1.4 Wastewater treatment methods

A diverse range of treatment methods are available to treat industrial wastewaters. The chosen treatment method for a particular effluent steam is governed by a number of factors, such as the chemical content (organic or inorganic), the concentration of pollutants and the volume of water to be treated[2].

Frequently more than one treatment process, run in sequence or parallel, is required for total degradation of pollutants[37].

For phenolic wastewaters, the treatment methods can be separated into various categories, including biological, thermal and oxidation processes.

1.4.1 Adsorption processes

Historically, adsorption has been used for the treatment of aqueous organic and inorganic pollutants. High surface area materials such as activated carbon, clay and zeolites adsorb certain contaminants onto their surface, thus removing them from the wastewater[38,39].

Adsorption processes gained popularity as they could be used continuously and require minimal plant modification. Once saturated, the adsorbent must undergo a costly regeneration process or be disposed of by incineration or placed in landfill[40]. Neither disposal method is desirable, as the pollutants either still exist in the environment, or contribute to hazardous emissions; diminishing both the minimal cost and low environmental impact of the process.

1.4.2 Biological treatment

The most common depolluting method is biological treatment[41], typically applied to residual wastewaters; microorganisms are used to degrade pollutants. The process, however, often suffers from long residence times and is not suited to treatment of toxic contaminants due to biomass poisoning[25].

Typically, biological methods use raw materials which are environmentally abundant, such as algae and sea weed, or wastes from other industrial processes, such as activated sludge[16]. The use of such materials is responsible for the low costs often associated with biosorption, as well as making it one of the eco-friendlier processes for wastewater treatment.

The use of activated sludge for the anaerobic digestion of organic pollutants in wastewater can be considered an optimisation of wastewater treatment plants, as it reduces the amount of sludge being disposed of, as well as producing biogas during the degradation of organic matter, which can be recycled as an energy source for other industrial processes[42].

Despite such optimisations existing for conventional biological wastewater treatments, they are applied to wastewaters with low effluent concentrations and suffer from long residence times[43]. Biodegradation of toxic compounds such as phenol can be very slow and require move advanced treatment methods for complete removal.

1.4.3 Thermal treatment

Thermal treatment includes methods such as incineration, which, unlike biological degradation, is more suited to wastewaters with a high concentration of pollutants. Temperatures between 1000 – 1700 °C are required to combust aqueous contaminants[44], however, the process is extremely energy extensive, requiring high operating temperatures and pressures to not only combust the pollutants, but to also vaporize the water.

Thermal treatment is typically chosen for wastewaters with concentrations of low value hydrocarbons greater than 100 g L^{-1}, and can offer complete destruction of pollutants[17,45]. However, incineration also comes with a high carbon footprint and releases considerable emissions of other hazardous compounds, such as dioxins, NO_x and furans[46], which merely shifts the environmental problem rather than presenting a solution.

Due to the substantial energy requirements associated with incineration, the process is also accompanied by significant operating costs. To help cover these high costs, thermal treatment is often utilised in industrial plants that require an additional energy supply. The heat or steam is recovered and redirected elsewhere within the plant, helping reduce net costs[47].

Incineration is not suited to wastewaters with low concentrations of toxic organic compounds (TOCs), if concentrations are too low additional fuel needs to be added leading to further operational expense[48]. Thermal treatment methods suffer from high economic and environmental consequences, and therefore other wastewater treatment methods must to be considered.

1.4.4 Advanced oxidation processes (AOP)

Adsorption, biological and thermal treatment processes all have their advantages, however neither are suited to wastewaters which contain toxic organic pollutants in intermediate concentrations. Such wastewaters are too toxic for biological treatment, yet too dilute to incinerate[49]. Coupled with the desire for more environmentally friendly methods, interest has moved toward advanced oxidation processes (AOPs).

AOPs rely on the production of radicals, such as hydroxyl radicals ($\cdot OH$), to oxidise contaminants to CO_2 and H_2O[50]. The oxidant responsible for generation of radicals commonly include hydrogen peroxide, oxygen and ozone. AOPs have shown success in the oxidation of large majority of organic compounds typically present in industrial wastewaters[51].

The first and most common AOP is the Fenton method, in which pollutants are degraded by a mixture of a soluble iron salt and hydrogen peroxide (H_2O_2), known as the Fenton's reagent[52]. H_2O_2 decomposes catalytically in the presence of Fe(II) salt, producing hydroxyl radicals ($\cdot OH$) with a high oxidation capacity[53].

$$Fe^{3+} + H_2O_2 \rightarrow Fe^{2+} + HO_2 \cdot + H^+ \qquad \textit{Equation 1.1}$$
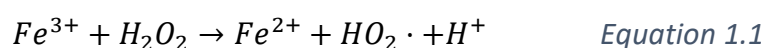
The Fenton method can be improved by the addition of ultraviolet (UV) light (UV-Fenton); which can accelerate the reduction of Fe^{3+}. The Fenton method is attractive as it shows very high activity towards the oxidation of organic compounds in wastewaters, and the components are widely available[53,54]. However, large quantities of concentrated H_2O_2 are expensive and potentially

explosive[55]. Another drawback is the significant cost increase when coupled with the addition of UV light[56].

Peroxidation is another common AOP, in which ozone (O_3) and H_2O_2 are used for the production of highly reactive $HO\cdot$ and $O_2^-\cdot$ species.

$$O_3 + HO_2^- \rightarrow O_2 + HO \cdot + O_2^- \cdot \qquad \textit{Equation 1.2}$$
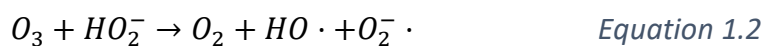
Ozone can be used by itself for the production of radicals, however the addition of hydrogen peroxide can enhance the decomposition rate of O_3, producing larger quantities of $\cdot OH$ radicals[52]; making peroxidation more efficient than ozonation alone. Unfortunately, as with the Fenton method, there is a considerable cost for large quantities of the chosen oxidant, in this case ozone.

To help combat the high cost of AOPs, focus has moved towards wet air oxidation (WAO), which uses oxygen as a clean source of oxidant for the production of hydroxyl radicals and subsequent oxidation of organic pollutants in wastewaters.

1.5 Wet air oxidation (WAO)

Wet air oxidation (WAO) can oxidise complex organic pollutants into carbon dioxide, water and simpler biodegradable forms. The use of oxygen as a clean source of oxidant, makes it one of the more environmentally friendly AOP technologies. The oxidizing power of the system relies on the solubility of oxygen in water at elevated temperatures and pressures, and the increased reaction rates and production of free radicals that accompany these high temperatures[57]. WAO can cope with water streams that are too dilute for incineration, but too concentrated for biological treatment, without the release of any hazardous emissions such as NO_x, SO_2 and HCl[58].

High temperatures and pressures are required to promote the solubility of atmospheric oxygen in the wastewater. The oxygen subsequently interacts with

the water, resulting in the formation of hydroxide ions[17], which in turn promote the oxidation of organic pollutants.

$$O_2 + 2H_2O + 4e^- \rightarrow 4OH^- \hspace{2cm} \textit{Equation 1.3}$$
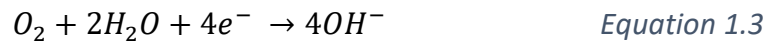
WAO can be applied to the majority of organic compounds typically encountered in wastewaters. It can be preferential over other treatment methods due to the lower operational costs, however, the operational costs can increase depending on the reaction conditions, wastewater composition and extent of oxidation required[33,57].

Due to the positive affect high temperatures have on initial reaction rates and oxygen solubility[59], WAO is carried out at elevated temperatures, typically reaching >200 °C[60]. If the reaction were to remain at atmospheric pressure, under such temperatures, the aqueous phase would be converted to steam. For the oxidation of phenol, it has been suggested that the reactions occur predominately in the liquid phase[61], thus high pressures are necessary to maintain the wastewater in this state. Figure 1.6 demonstrates the temperature and pressure range at which water will remain in the liquid phase.
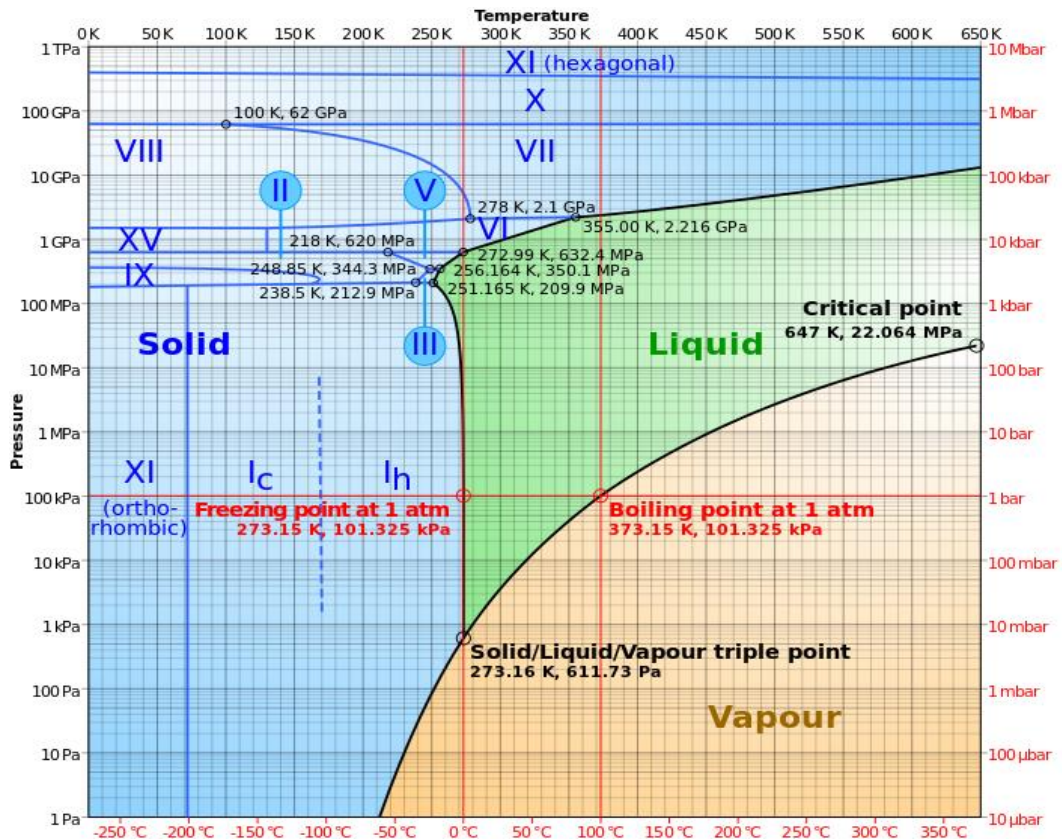
Figure 1.6 Diagram of water phases at varying temperatures and pressures[62]

A major drawback of WAO is the low solubility of oxygen in the reaction media[8] and the necessary high pressures have the added bonus of increasing the concentration of dissolved oxygen, therefore aiding the oxidation rate. Pressures upwards of 200 bar are not uncommon in WAO processes[63].

When considering reactor design, the use of oxygen as an oxidant has significant safety implications. Oxygen behaves differently to air or compressed air, and under high pressures, such as those in a cylinder, oxygen can react violently with common materials such as grease or oil; other materials may also catch fire spontaneously. A faulty valve or hose, resulting in a small increase in oxygen concentration, coupled with a poor ventilation can significantly increase the risk of a fire. The subsequent fire will also be more vigorous in the oxygen enriched atmosphere and the destructive capabilities increased due to the higher temperature of the flame[64].

Consequently, compressed air is commonly used as a safer source of oxygen. Air is readily available and as such also comes at much lower costs, compared with pure oxygen[65].

1.6 Catalytic wet air oxidation (CWAO)

The efficiency of WAO can be largely improved by the addition of a catalyst; catalytic wet air oxidation (CWAO) introduces a catalyst into the reaction, lowering the oxidation energy barrier, allowing the reaction to be carried out at significantly lower temperatures and pressures. Typically, WAO operates at high temperatures (180 – 315 °C) and pressures (20 – 200 bar)[58], however, with the use of a catalyst, operation costs can be halved[66].

Furthermore, a higher degree of oxidation can be achieved with CWAO, with most organic contaminants able to be fully oxidised to carbon dioxide and water, without any simple, biodegradable intermediates remaining[25]. Complete mineralization of pollutants removes the need for a secondary biological treatment step, which is common for WAO processes[67].

The use of CWAO, together with compressed air as a low cost, abundant oxidant and the use of a catalyst to significantly reduce operating conditions, represents an energy efficient, low-cost solution to wastewater treatment.

1.7 Conclusion

This chapter summarises the various methods available for the treatment of toxic organic wastewaters, including typical pollutants encountered in wastewater and the legislation which governs the limits of their safe release into the environment. Among them, phenol and its derivatives were shown to be an appropriate model pollutant due to its increased toxicity and frequency of use.

Of the treatment methods discussed, wet air oxidation (WAO) and subsequentially catalytic wet air oxidation (CWAO) were chosen as promising technologies. The environmentally friendly choice of oxidant and application over a wide range of pollutants allows for an efficient alternative to biological and thermal wastewater treatment methods.

1.8 References

(1)   Levec, J.; Pintar, A. Catalytic wet-air oxidation processes: A review. *Catal. Today* **2007,** *124* (3-4), 172.

(2)   Mahajani, V. V.; Joshi, J. B.; Mishra, V. S.; Mahajani, V. V.; Joshi, J. B. Wet Air Oxidation. *Industrial & engineering chemistry research.* **1995,** *34* (1), 2.

(3)   Weber, M.; Weber, M. In *Phenolic Resins: A Century of Progress*; Pilato, L., Ed.; Springer Berlin Heidelberg: Berlin, Heidelberg, **2010**.

(4)   Kolpin, D. W.; Furlong, E. T.; Meyer, M. T.; Thurman, E. M.; Zaugg, S. D.; Barber, L. B.; Buxton, H. T. Pharmaceuticals, hormones, and other organic wastewater contaminants in US streams, 1999-2000: A national reconnaissance. *Environmental Science & Technology* **2002,** *36* (6), 1202.

(5)   Stüber, F.; Font, J.; Fortuny, A.; Bengoa, C.; Eftaxias, A.; Fabregat, A. Carbon materials and catalytic wet air oxidation of organic pollutants in wastewater. *Topics in Catalysis* **2005,** *33* (1), 3.

(6)   Kasperczyk, D.; Urbaniec, K. Application of a compact trickle-bed bioreactor to the biodegradation of pollutants from the ventillation air in a copper-ore mine. *Journal of Cleaner Production* **2015,** *87*, 971.

(7)   Kasperczyk, D.; Urbaniec, K.; Barbusinski, K.; Rene, E. R.; Colmenares-Quintero, R. F. Application of a compact trickle-bed bioreactor for the removal of odor and volatile organic compounds emitted from a wastewater treatment plant. *Journal of Environmental Management* **2019,** *236*, 413.

(8)   Monteros, A. E. d. l.; Lafaye, G.; Cervantes, A.; Del Angel, G.; Barbier Jr, J.; Torres, G. Catalytic wet air oxidation of phenol over metal catalyst (Ru,Pt) supported on TiO_2–CeO_2 oxides. *Catalysis Today* **2015,** *258, Part 2*, 564.

(9)   Luo, Y. L.; Guo, W. S.; Ngo, H. H.; Nghiem, L. D.; Hai, F. I.; Zhang, J.; Liang, S.; Wang, X. C. C. A review on the occurrence of micropollutants in the aquatic environment and their fate and removal during wastewater treatment. *Science of the Total Environment* **2014,** *473*, 619.

(10)   Pisarevsky , A.; Polozova, P.; Russian Journal of Applied Chemistry, **2005**; Vol. 78.

(11)   Andalib, M.; Mathematical Modeling of Biological Selenium Removal from Flue Gas Desulfurization (FGD) Wastewater Treatment. *Proceedings of the Water Environment Federation,* **2016,** 228.

(12)   Karri, R. R.; Sahu, J. N.; Chimmiri, V. Critical review of abatement of ammonia from wastewater. *Journal of Molecular Liquids* **2018,** *261*, 21.

(13)   Duenas, J. F.; Alonso, J. R.; Rey, A. F.; Ferrer, A. S. Characterisation of phosphorous forms in wastewater treatment plants. *Journal of Hazardous Materials* **2003,** *97* (1-3), 193.

(14)   http://www.nea.gov.sg/anti- pollution-radiation-protection/water-pollution-control/allowable-limits, **2019**.

(15)   Lin, K.; The effect of organic pollution on the abundance and distribution of aquatic oligochaetes in an urban water basin, Taiwan. *Hydrobiologia* **2008,** *596*, 213.

(16)   Aksu, Z.; Gonen, F. Biosorption of phenol by immobilized activated sludge in a continuous packed bed: prediction of breakthrough curves. *Process Biochemistry* **2004,** *39* (5), 599.

(17)   Busca, G.; Berardinelli, S.; Resini, C.; Arrighi, L. Technologies for the removal of phenol from fluid streams: A short review of recent developments. *Journal of Hazardous Materials* **2008,** *160* (2-3), 265.

(18)   Kumaran, P.; Paruchuri, Y. L. Kinetics of phenol biotransformation. *Water Research* **1997,** *31* (1), 11.

(19)   Rocha, M. A. L.; Del Angel, G.; Torres-Torres, G.; Cervantes, A.; Vazquez, A.; Arrieta, A.; Beltramini, J. N. Effect of the Pt oxidation state and Ce^{3+}/Ce^{4+} ratio on the Pt/TiO_2-CeO_2 catalysts in the phenol degradation by catalytic wet air oxidation (CWAO). *Catalysis Today* **2015,** *250*, 145.

(20)   Santos, A.; Yustos, P.; Quintanilla, A.; Ruiz, G.; Garcia-Ochoa, F. Study of the copper leaching in the wet oxidation of phenol with CuO-based catalysts: Causes and effects. *Applied Catalysis B-Environmental* **2005,** *61* (3-4), 323.

(21)   Lunagomez Rocha, M. A.; Del Angel, G.; Torres-Torres, G.; Cervantes, A.; Vazquez, A.; Arrieta, A.; Beltramini, J. N. Effect of the Pt oxidation state and Ce^{3+}/Ce^{4+} ratio on the Pt/TiO_2-CeO_2 catalysts in the phenol degradation by catalytic wet air oxidation (CWAO). *Catalysis Today* **2015,** *250*, 10.

(22)   Michalowicz, J.; Duda, W. Phenols - Sources and toxicity. *Polish Journal of Environmental Studies* **2007,** *16* (3), 347.

(23)   Drinking Water Directive 80/778/EEC, Commission of the European Communities: Brussels, **1980**.

(24)   Yang, S. X.; Zhu, W. P.; Wang, J. B.; Chen, Z. X. Catalytic wet air oxidation of phenol over CeO_2-TiO_2 catalyst in the batch reactor and the packed-bed reactor. *Journal of Hazardous Materials* **2008,** *153* (3), 1248.

(25)   Kim, K. H.; Ihm, S. K. Heterogeneous catalytic wet air oxidation of refractory organic pollutants in industrial wastewaters: A review. *Journal of Hazardous Materials* **2011,** *186* (1), 16.

(26)   Massa, P.; Ivorra, F.; Haure, P.; Cabello, F. M.; Fenoglio, R. Catalytic wet air oxidation of phenol aqueous solutions by 1% $Ru/CeO_2-Al_2O_3$ catalysts prepared by different methods. *Catalysis Communications* **2007,** *8* (3), 424.

(27)   Eftaxias, A.; Font, J.; Fortuny, A.; Fabregat, A.; Stuber, F. Kinetics of phenol oxidation in a trickle bed reactor over active carbon catalyst. *Journal of Chemical Technology and Biotechnology* **2005,** *80* (6), 677.

(28)   Hamoudi, S.; Larachi, F.; Sayari, A. Wet oxidation of phenolic solutions over heterogeneous catalysts: Degradation profile and catalyst behavior. *Journal of Catalysis* **1998,** *177* (2), 247.

(29)   Chen, H.; Sayari, A.; Adnot, A.; Larachi, F. Composition-activity effects of Mn-Ce-O composites on phenol catalytic wet oxidation. *Applied Catalysis B-Environmental* **2001,** *32* (3), 195.

(30)   Alvarez, P. M.; McLurgh, D.; Plucinski, P. Copper oxide mounted on activated carbon as catalyst for wet air oxidation of aqueous phenol. 1. Kinetic and mechanistic approaches. *Industrial & Engineering Chemistry Research* **2002,** *41* (9), 2147.

(31)   Devlin, H. R.; Harris, I. J. Mechanism of the oxidation of aqueous phenol with dissolved oxygen. *Industrial & Engineering Chemistry Fundamentals* **1984,** *23* (4), 387.

(32)   Duprez, D.; Delanoe, F.; Barbier-Jr, J.; Isnard, P.; Blanchard, G. Catalytic oxidation of organic compounds in aqueous media. *Catalysis Today* **1996,** *29* (1-4), 317.

(33)   Santos, A.; Yustos, P.; Quintanilla, A.; Rodriguez, S.; Garcia-Ochoa, F. Route of the catalytic oxidation of phenol in aqueous phase. *Applied Catalysis B-Environmental* **2002,** *39* (2), 97.

(34)   Levec, J.; Pintar, A. Catalytic oxidation of aqueous solutions of organics – an effective method for removal of toxic pollutants from waste waters. *Catalysis Today* **1995,** *24* (1-2), 51.

(35)   Alejandre, A.; Medina, F.; Fortuny, A.; Salagre, P.; Sueiras, J. E. Characterisation of copper catalysts and activity for the oxidation of phenol aqueous solutions. *Applied Catalysis B-Environmental* **1998,** *16* (1), 53.

(36)   Santos, A.; Yustos, P.; Gomis, S.; Ruiz, G.; Garcia-Ochoa, F. Reaction network and kinetic modeling of wet oxidation of phenol catalyzed by activated carbon. *Chemical Engineering Science* **2006,** *61* (8), 2457.

(37)   Erjavec, B.; Kaplan, R.; Djinovic, P.; Pintar, A. Catalytic wet air oxidation of bisphenol A model solution in a trickle-bed reactor over titanate nanotube-based catalysts. *Applied Catalysis B-Environmental* **2013,** *132*, 342.

(38)   Lin, S. H.; Juang, R. S. Adsorption of phenol and its derivatives from water using synthetic resins and low-cost natural adsorbents: A review. *Journal of Environmental Management* **2009,** *90* (3), 1336.

(39)   Fortuny, A.; Font, J.; Fabregat, A. Wet air oxidation of phenol using active carbon as catalyst. *Applied Catalysis B-Environmental* **1998,** *19* (3-4), 165.

(40)   Smith, K. M.; Fowler, G. D.; Pullket, S.; Graham, N. J. D. Sewage sludge-based adsorbents: A review of their production, properties and use in water treatment applications. *Water Research* **2009,** *43* (10), 2569.

(41)   Janecki, D.; Szczotka, A.; Burghardt, A.; Bartelmus, G. Modelling wet-air oxidation of phenol in a trickle-bed reactor using active carbon as a

catalyst. *Journal of Chemical Technology & Biotechnology* **2016,** *91* (3), 596.

(42) Appels, L.; Baeyens, J.; Degreve, J.; Dewil, R. Principles and potential of the anaerobic digestion of waste-activated sludge. *Progress in Energy and Combustion Science* **2008,** *34* (6), 755.

(43) Clara, M.; Kreuzinger, N.; Strenn, B.; Gans, O.; Kroiss, H. The solids retention time - a suitable design parameter to evaluate the capacity of wastewater treatment plants to remove micropollutants. *Water Research* **2005,** *39* (1), 97.

(44) Eftaxias, A.; Font, J.; Fortuny, A.; Fabregat, A.; Stuber, F. Nonlinear kinetic parameter estimation using simulated annealing. *Computers & Chemical Engineering* **2002**, 26 (12)

(45) Debellefontaine, H.; Chakchouk, M.; Foussard, J. N.; Tissot, D.; Striolo, P. Treatment of organic aqueous wastes: Wet air oxidation and Wet Peroxide Oxidation. *Environ Pollut* **1996,** *92* (2), 155.

(46) Bhargava, S. K.; Tardio, J.; Prasad, J.; Foger, K.; Akolekar, D. B.; Grocott, S. C. Wet oxidation and catalytic wet oxidation. *Industrial & Engineering Chemistry Research* **2006,** *45* (4), 1221.

(47) Fytili, D.; Zabaniotou, A. Utilization of sewage sludge in EU application of old and new methods - A review. *Renewable & Sustainable Energy Reviews* **2008,** *12* (1), 116.

(48) Heimbuch, J. A.; Wilhelmi, A. R. Wet air oxidation – a treatment means for aqueous hazardous waste streams. *Journal of Hazardous Materials* **1985,** *12* (2), 187.

(49) Oller, I.; Malato, S.; Sanchez-Perez, J. A. Combination of Advanced Oxidation Processes and biological treatments for wastewater decontamination-A review. *Science of the Total Environment* **2011,** *409* (20), 4141.

(50) Andreozzi, R.; Caprio, V.; Insola, A.; Marotta, R. Advanced oxidation processes (AOP) for water purification and recovery. *Catalysis Today* **1999,** *53* (1), 51.

(51) Gogate, P. R.; Pandit, A. B. A review of imperative technologies for wastewater treatment I: oxidation technologies at ambient conditions. *Advances in Environmental Research* **2004,** *8* (3-4), 501.

(52) Oturan, M. A.; Aaron, J. J. Advanced Oxidation Processes in Water/Wastewater Treatment: Principles and Applications. A Review. *Critical Reviews in Environmental Science and Technology* **2014,** *44* (23), 2577.

(53) Zazo, J. A.; Casas, J. A.; Mohedano, A. F.; Rodriguez, J. J. Catalytic wet peroxide oxidation of phenol with a Fe/active carbon catalyst. *Applied Catalysis B-Environmental* **2006,** *65* (3-4), 261.

(54) Neyens, E.; Baeyens, J. A review of classic Fenton's peroxidation as an advanced oxidation technique. *Journal of Hazardous Materials* **2003,** *98* (1-3), 33.

(55) Zhang, M. H.; Dong, H.; Zhao, L.; Wang, D. X.; Meng, D. A review on Fenton process for organic wastewater treatment based on optimization perspective. *Science of the Total Environment* **2019,** *670*, 110.

(56)   Chan, Y. J.; Chong, M. F.; Law, C. L.; Hassell, D. G. A review on anaerobic-aerobic treatment of industrial and municipal wastewater. *Chemical Engineering Journal* **2009,** *155* (1-2), 1.

(57)   Kolaczkowski, S. T.; Plucinski, P.; Beltran, F. J.; Rivas, F. J.; McLurgh, D. B. Wet air oxidation: a review of process technologies and aspects in reactor design. *Chemical Engineering Journal* **1999,** *73* (2), 143.

(58)   Luck, F. Wet air oxidation: past, present and future. *Catalysis Today* **1999,** *53* (1), 81.

(59)   Tromans, D. Temperature and pressure dependent solubility of oxygen in water: a thermodynamic analysis. *Hydrometallurgy* **1998,** *48* (3), 327.

(60)   Pintar, A. Catalytic processes for the purification of drinking water and industrial effluents. *Catalysis Today* **2003,** *77* (4), 451.

(61)   Lavelle, K.; McMonagle, J. B. Mass transfer effects in the oxidation of aqueous organic compounds over a hydrophobic solid catalyst. *Chemical Engineering Science* **2001,** *56* (17), 5091.

(62)   Zhang, X.; Sun, P.; Yan, T. T.; Huang, Y. L.; Ma, Z. S.; Zou, B.; Zheng, W. T.; Zhou, J.; Gong, Y. Y.; Sun, C. Q. Water's phase diagram: From the notion of thermodynamics to hydrogen-bond cooperativity. *Progress in Solid State Chemistry* **2015,** *43* (3), 71.

(63)   Matatov-Meytal, Y. I.; Sheintuch, M. Catalytic abatement of water pollutants. *Industrial & Engineering Chemistry Research* **1998,** *37* (2), 309.

(64)   European Industrial Gas Association, Fire hazards of oxygen and oxygen enriched atmospheres. *EIGA*, 2018; Vol. Doc 04/18.

(65)   Lafaye, G.; Barbier, J.; Duprez, D. Impact of cerium-based support oxides in catalytic wet air oxidation: Conflicting role of redox and acid-base properties. *Catalysis Today* **2015,** *253*, 89.

(66)   Cybulski, A.; Trawczyński, J. Catalytic wet air oxidation of phenol over platinum and ruthenium catalysts. *Appl. Catal. B: Environmental* **2004** *47*, 1

(67)   Perkow, H.; Steiner, R.; Vollmuller, H.; Wet air oxidation: a review, *Ger. Chem. Eng*, **1981**; Vol. 4.

Chapter 2

Catalysts for CWAO

2.1 Introduction to catalysis

Catalysis is used extensively throughout industrial processes to help reduce the severity of reaction conditions, production of emissions and operational costs. It is estimated that a catalyst is involved at some stage in the commercial production of approximately 90 % of all chemical products[1]. Concerning WAO, the addition of a catalyst can also result in a higher degree of oxidation for organic pollutants[2].

A catalyst is able to reduce the activation energy (E_a) of a reaction by providing an alternative pathway with a lower energy barrier, without itself being consumed. If the energy necessary for a reaction to proceed is lowered, the percentage of species with sufficient energy to react is increased, and therefore the rate of reaction increases.
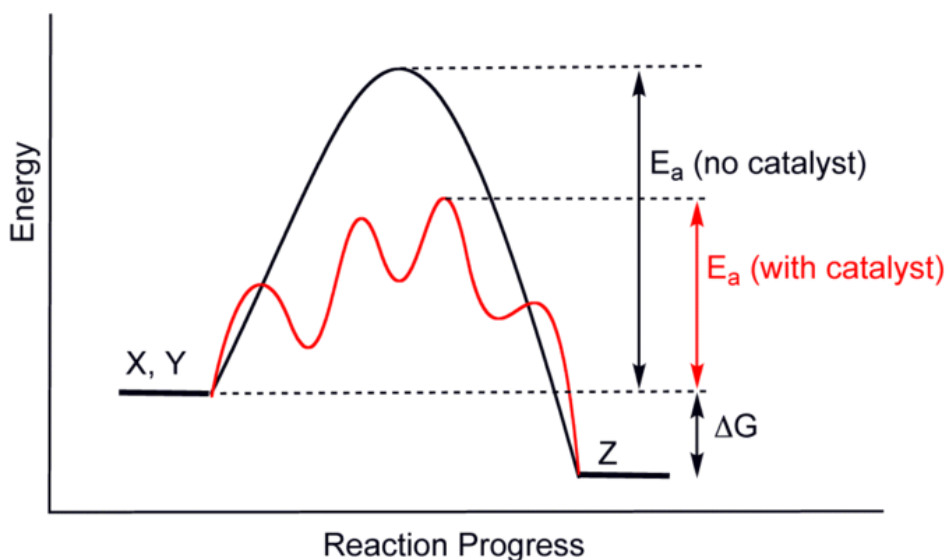
Figure 2.1 Illustration of the activation energy of a catalysed and uncatalyzed reaction[3]

It is possible to calculate the activation energy of a reaction by use of the Arrehnius equation:

$$k = Ae^{\frac{-E_a}{RT}}$$

Equation 2.1, Arrhenius equation, where k = the rate constant, A = pre-exponential factor, E_a = activation energy, R = universal gas constant, T = temperature

Typically, a catalyst activates one or more reactants, which then react, before being released back into the reaction media, during which the chemical structure of the catalyst is restored, allowing it to continue activating new reactants.

Generally speaking, the majority of catalytic processes can be divided into two groups, heterogeneous and homogeneous. Homogeneous catalysts are those which are present in the same phase as the reactants, whilst heterogeneous catalysts are present in a different phase.

2.1.1 Homogeneous catalysis

Homogeneous catalysts are those that exist in the same phase as the reactants, typically the liquid phase. One of the main advantages of homogenous processes is the increased catalytic activity due to the optimal contact between the catalyst and reactants, as both exist in the same solution. The catalytic active sites, which can be a rate limiting factor for catalysed reactions, can also be increased by simply increasing the concentration of catalyst.

Copper salts have shown high activities for homogeneous CWAO[4-7], however, the recovery of the catalyst after treatment is necessary to prevent further contamination of the water by the toxic copper ion. The Ciba-Geigy process, used commercially for pharmaceutical wastewaters, uses cupric salts which are recovered as cupric sulphide and then recycled back into the reactor[2,8]. The copper salts have shown high selectivity towards CO_2 but homogeneous metal complexes such as these often suffer from reduced thermal stability at temperatures above 250 °C[9].

The main disadvantage encountered with homogeneous catalysis is the catalyst recovery step. The separation of the products from the catalyst (and vice versa) can be complex, resulting in additional costs and often a portion of the catalyst can be lost[10].

2.1.2 Heterogenous catalysis

Heterogeneous catalysts are present in a separate phase to reactants, typically, but not always, the catalyst is a solid material used in conjunction with liquid or gas phase reactants. For CWAO, a solid catalyst is either mixed with the wastewater in the case of batch processes, or contained within a reactor bed, over which the wastewater flows in the case of continuous processes.

Solid catalysts exist in a wide variety of forms such as metal oxides or mixed metal oxides, supported metal catalysts and zeolites. The choice of appropriate catalyst is dependent upon many factors, including but not limited to, the reaction and reactants to be catalysed, selectivity towards desired product(s), stability of the catalyst under the reaction conditions and cost.

Concerning CWAO, the majority of the focus has been on heterogeneous catalysis, with the catalyst in the solid phase, the polluted wastewater in the liquid phase and the oxidant (O_2) present in the gas phase. Solid catalysts are preferred as they can be easily separated from the reaction medium in batch or continuous processes, making them better suited over homogeneous catalysts, which require an additional recovery step. Solid catalysts also exhibit higher thermal stability compared to homogeneous liquid catalysts, allowing for the oxidation reaction to be conducted at elevated temperatures, increasing the reaction rate.

2.2 Reactors for heterogenous CWAO

CWAO processes require a reactor capable of handling the tri-phase catalytic reaction. The reactor needs to accommodate efficient mixing of a solid catalyst, aqueous pollutants and gas phase oxidant, and, in the case of batch processes, the separation of the catalyst after water treatment.

2.2.1 Batch reactors

Much of the CWAO examples in the literature are conducted in batch processes, and often these batch processes can compete with the catalytic activities seen for similar continuous processes. Increased agitation, or stirring, can increase the mass transfer of oxygen to the catalyst surface which allows the catalyst to achieve higher activity. The method at which the reactor facilitates efficient mass transfer is dependent upon the choice of reactor.

2.2.1.1 Continuous stirred tank reactor (CTSR)

A continuous stirred tank reactor (CSTR) can accommodate both homogeneous and heterogeneous catalysts for CWAO. The catalyst and a fixed volume of the reagents are stirred for a sufficient time at a specified temperature and pressure, during which oxidation can occur. Once complete, the products and any remaining reactants are separated from the catalyst, for solid catalysts this is typically achieved using filters. Figure 2.2 illustrates a typical CSTR set-up.
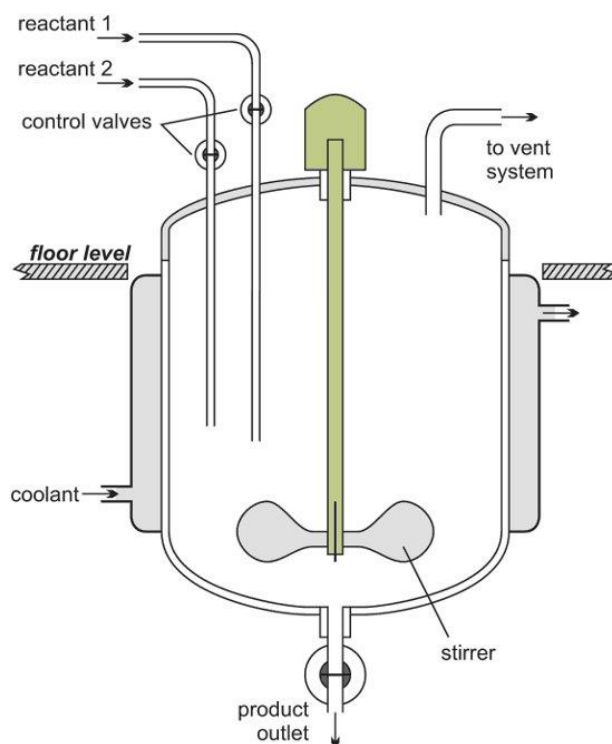
Figure 2.2 Illustration of a CSTR batch reactor[11]

Yang *et al.*[12] observed complete phenol conversion over a CeO_2-TiO_2 catalyst after 150 minutes in a batch CSTR, however catalyst activity decreased after multiple cycles, declining to 65 % phenol conversion after the third cycle. The high ratio of organic compounds to solid catalyst enhanced the formation of heavy polymers which irreversibly adsorbed to the catalyst surface resulting in deactivation. When the same catalyst was utilised in a continuous flow packed bed reactor, no deactivation was observed over the 100 hour testing period. Levec *et al.*[13] and Stuber *et al.*[14] also reported similar findings, with phenol more likely to form poly-aromatic species when treated in batch reactors, which can result in poisoning of the catalyst surface.

Pintar *et al.*[15] stated that the formation of polymers during the oxidation of phenol can arise from two different reactions taking place within the liquid phase - initial polymer formation from the reaction between glyoxal and phenol, followed by the step-wise addition of phenol, and secondly, the polymerisation of glyoxal with other glyoxal molecules. Alejandre *et al.*[16] also reached a similar conclusion, noting that the homogeneous polymerisation reaction markedly reduced the extent of total oxidation, resulting in catalyst deactivation by

irreversibly bound polymer species. The presence of glyoxal, a partial oxidation product of phenol, can be considered an initiator for these polymerisation reactions.

When switching from a batch process (the majority were carried out in batch Slurry reactors) to a continuous flow packed bed reactor (typically a trickle bed reactor) however, the polymerisation reactions were suppressed[12-18]. The characteristic high solid catalyst to liquid pollutant ratio of such reactors was considered responsible for the lack of polymerisation.

Pintar *et al.*[18] concluded that when using a reactor with high solid to liquid ratio, the propagation and termination reaction steps are limited to a very thin liquid film near the catalyst surface, thus reactions between the adsorbed species are favoured over those in the liquid phase, such as polymerisation.

The initial set-up costs for CSTR's are typically lower than for continuous flow reactors, however the longer residence times associated with batch processing and the reactor down time between batches can increase the operational costs. Coupled with the increase in probability of polymerisation of organic pollutants, resulting in catalyst deactivation by fouling, the CWAO of phenol is better suited to continuous processes.

2.2.2 Continuous reactors

The advantages of continuous processes are numerous, along with reduced labour requirements, reduced time and energy expenditure; a continuous CWAO process also allows higher quantities of effluent to be treated over the same time period[19].

Multi-phase reactors, capable of handling solid, liquid and gas phase components in continuous operation can typically be divided into three categories, bubble column reactors, fluidized bed reactors and fixed bed reactors.

2.2.2.1 Bubble column reactor

A bubble column reactor, as the name suggests, uses bubbles of gas flowed vertically upwards through a column containing a mixture of the catalyst and reactants. The gas bubbles are introduced by a sparger at the bottom of the reactor, causing constant agitation facilitating mass transfer. Bubble column reactors can be characterised by their efficient mass and heat transfer.

Figure 2.3 illustrates the standard set-up of a bubble column reactor. In continuous operation, the gas and liquid suspension flow concurrently upward through the column and the suspension that leaves the column is recycled to a feed tank[20].
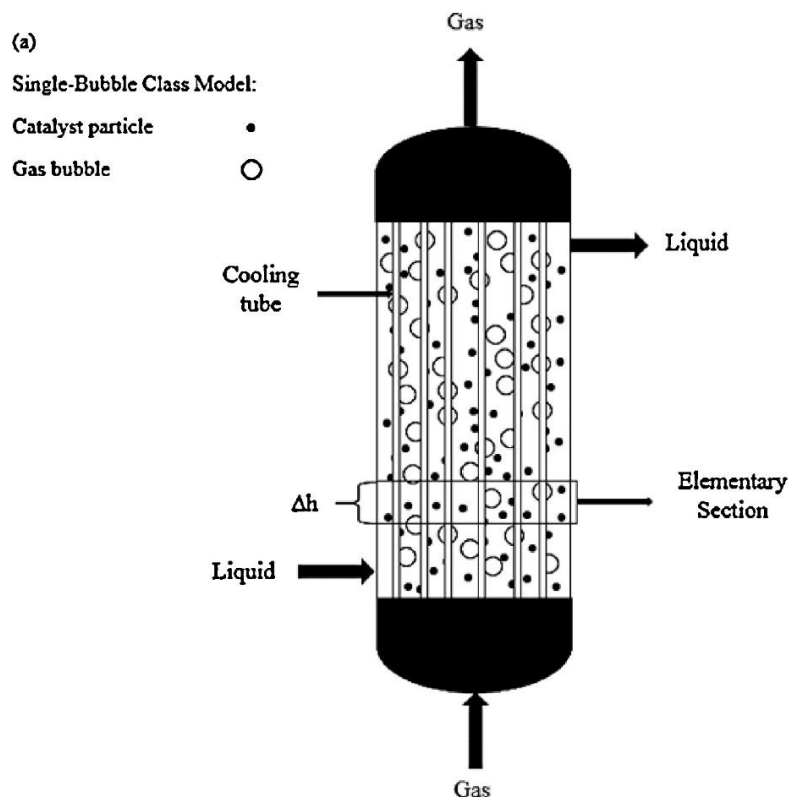
Figure 2.3 Illustration of a bubble column reactor[21]

Bubble column reactors require lower quantities of catalyst compared to fixed bed reactors, due to higher catalytic efficiency as a result of better mixing between the catalyst particles and reactants[21].

Much like batch reactors however, the high liquid to catalyst ratio and long residence time of phenol pollutants makes them more susceptible to polymerisation, therefore increasing the potential for catalyst poisoning.

2.2.2.2 Slurry reactor

In slurry reactors, similar to a bubble column reactor, the catalyst particles are mixed with the liquid pollutants, with the gas phase introduced at the bottom of the reactor. Slurry reactors can be treated as a two-phase system, by regarding the catalyst – liquid phase suspension, or 'slurry', as a pseudo-homogeneous phase[22].
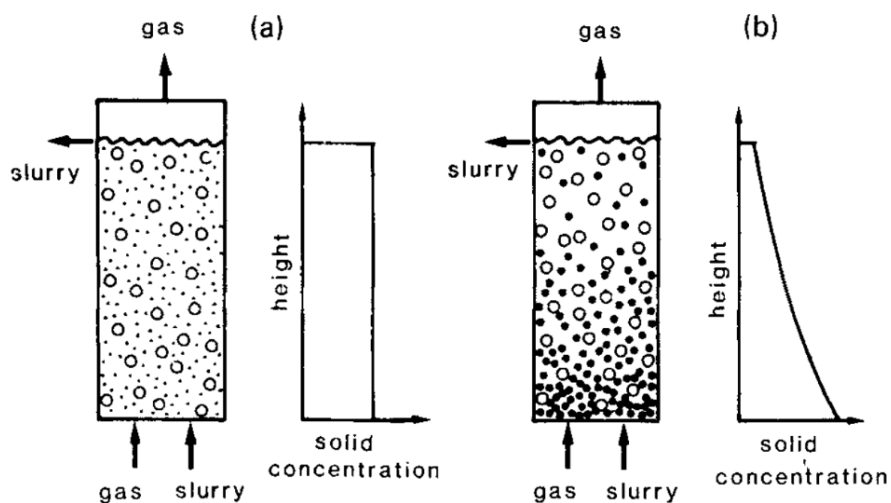
Figure 2.4 Illustration of (a) slurry reactor and (b) bubble column reactor[22]

Figure 2.4 illustrates the set-up and corresponding catalyst dispersion for a slurry and bubble column reactor. In both types of reactor, the slurry is agitated by turbulence induced by the rising gas bubbles but with a different flow regime. In a bubble column reactor, the agitation of the catalyst particles is dominated by gravity, resulting in the higher concentration of catalyst particles nearer the bottom of the reactor. For a slurry reactor however, the agitation is such that the particles are uniformly distributed throughout, creating a pseudo-homogeneous slurry of catalyst and liquid pollutants[22]. Similar to batch and bubble column reactors, the high liquid to catalyst ratio increases the potential for phenol polymerization, as observed by Levec *et al.*[17] in a slurry reactor.

The balance between the draft force acting on the catalyst by the gas and liquid flow and the net weight of the particles, resulting in uniform suspension, requires smaller catalyst particles than those typically used in bubble column reactors[23]. Smaller catalyst particles can lead to difficulty during separation from the effluent.

Slurry reactors have been used in the CWAO of wastewaters from Kraft bleaching plants, olive oil mills, textile and alcohol distillery industries[24].

2.2.2.3 Trickle bed reactor (TBR)

A trickle bed reactor (TBR) differs from the other continuous flow reactors previously discussed, in that the catalyst is confined to a bed which the reactants are passed over. The catalyst particles are packed into a cylindrical bed, typically within a column style reactor; the size of the catalyst particles is important to prevent backpressure build-up. The higher catalyst loading to volume of wastewater ratio, lower operational costs and effectiveness at high temperatures and pressures make TBRs preferable to slurry of bubble column reactors for CWAO[25].

A TBR can be operated co-currently, where both the wastewater and gas flow downwards through the catalyst bed, or counter-currently, where the gas phase is introduced and pumped upwards from the bottom of the reactor, against the downward flow of the wastewater, as illustrated in Figure 2.5.

Co-current

Wastewater
+
Air

Counter current

Wastewater

Catalyst Bed

Air
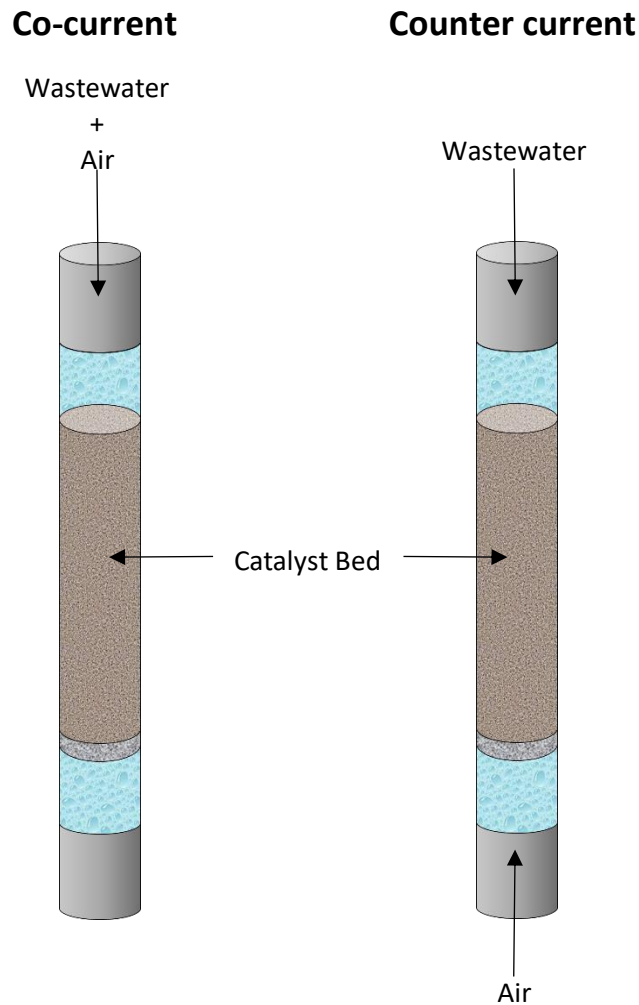
Figure 2.5 Illustration of co-current and counter current flow in a trickle bed reactor[26]

There are advantages and disadvantages in operating a TBR either counter currently or co-currently, with the appropriate choice dependent upon a number of factors. A TBR under counter current flow, sometimes referred to as a Packed Bubble Column (PBC), can give increased external catalyst wetting and may aid the dislodging of any sludge build-up on the catalyst[27]. The removal of build-up on the catalyst, will expose active sites that may have become inhibited, regenerating the catalyst surface and therefore increasing its lifetime. The agitation caused by the opposing gas flow, increases the mixing and contact time between the catalyst and wastewater, which in turn can increase the potential for higher catalytic activity. Longer reactant residence times, however, may be undesirable if there is a possibility of side reactions occurring the liquid phase, such as polymerisation[28]. Under counter current flow, the residence time of the liquid phase is higher and the residence time of the gas phase is lower, compared to co-current operation[27].

Therefore, since the polymerisation of phenol products is undesirable and the gas mass transfer rate impaired by a larger portion of liquid phase, counter-current flow may not be beneficial for the CWAO of phenol.

Comparatively, co-current flow ensures mixing of the liquid and gas phases before they reach the catalyst. It can also be more suitable for laboratory scale reactions, as often counter current reactors do not have the necessary pressure to ensure sufficient liquid – gas mixing on a small scale[25]. Co-current downward flow is often preferred due to the better mechanical stability of the bed, reduced flooding and lower operational costs of the liquid phase pumps compared with counter-current operations[29]. Co-current TBRs have shown success in the removal of organic pollutants, such as phenol, and a large portion of CWAO research in TBRs has been dedicated to co-current flow[30-33]. Maugans *et al.*[34] observed deactivation of Pt/TiO$_2$ for the oxidation of phenol in a batch reactor, whilst no deactivation was seen when in a co-current TBR.

Under a co-current trickle flow regime there is the possibility of liquid maldistribution, which may leave portions of the catalyst bed poorly irrigated (not all of the catalyst pellets may come into contact with the wastewater)[28]. The external wetting efficiency of the catalyst, that is, the fraction of the external area of catalyst wetted by the liquid flow, can give an indication of the extent of catalyst utilization[35]. For those operations in which the chemical reaction can only occur on the wetted surface of the catalyst, low external wetting efficiency decreases the potential reaction rate. Incomplete external wetting of the catalyst can arise from low liquid flow rates not providing a sufficient volume of wastewater to cover the catalyst particles in a continuous liquid film at all times. This is of concern, as liquid maldistribution may result in hot spots and reactor runaway[25].

Reactor runaway describes a process in which an increase in temperature within the reactor due to an exothermic reaction, causes a further increase in temperature due to an increase in reaction rate. The consequences of the resulting exponential heat growth can be disastrous, such as reactor rupture or explosion[36]. When the catalyst is poorly irrigated by the liquid phase, the spots where there is little contact with the liquid phase, heat transfer is hampered, which can lead to

unwanted highly exothermic side reactions. The increase in temperature can then cause vaporization of the liquid phase, further hampering heat transfer due to the lower heat capacity of the vapour. Such spots are known as 'hot spots' and can initiate reactor runway. Development of hot spots typically takes time and can be prevented by periodic flooding of the reactor with the liquid phase or quenching with water[37].

McManus *et al.*[38] reported the presence of hot spots within the catalyst bed when investigating α-methylstyrene hydrogenation. The hot spots were brought about by reaction heat generated in the pores of liquid filled catalyst pellets, with the lack of sufficient wetting of the surrounding pellets preventing efficient heat withdrawal. Increasing gas and liquid flow rates at high pressures can increase the contact efficiency between catalyst and reactants, but at the expense of contact time.

The probability of reactor runaway is reduced for CWAO due to the higher specific heat capacity of water compared with other common non-aqueous solvents. The higher specific heat capacity of water necessitates a greater amount of energy required to vaporize the reaction feed so hot spots are less likely to occur. The low concentration of reactants in the feed also reduces the possibility of runaway as it is unlikely that the resulting exotherm will be large for such low concentrations of reactant. When compared to processes such as hydrogenation, polymerization or petrochemical refining, where the highest possible concentration of hydrocarbons or organic reactants are used, the large amount of moles in the feed means there is a potential for a very large exothermic release. The higher concentration of organics associated with these processes increases the potential for highly exothermic reactions, fuelling reactor runaway[39]. The relatively low concentrations of phenol commonly found in wastewater streams (<5 g L^{-1})[40] make reactor runaway significantly less of a concern for CWAO of phenol.

Eftaxias *et al.*[33] investigated the CWAO of phenol over activated carbon in a TBR at both co-current and counter current flow, with higher phenol conversions observed for co-current downwards flow over a range of temperatures. They

proposed that under co-current regime, a large section of the external catalyst surface was either covered by an extremely thin liquid layer, or directly exposed to the gas phase. The higher gas-solid mass transfer rate compared to the gas transfer rate at the liquid-solid interface, suggested the 'dry' catalyst surface was always saturated with oxygen. Given the limiting reactant was oxygen in this case, it was concluded that the reduced wetting of the catalyst bed positively affected the catalyst performance and that under 'fully wetted' counter current flow the reaction is limited by gas-liquid mass transfer.

Another example of CWAO of phenolic compounds in co-current TBR conducted by Suarez-Ojeda et al.[40] showed that the extent of oxidation is highly influenced by the liquid flow rate, essentially the catalyst-wastewater contact time. Thus, lower liquid flow rates can promote catalyst activity by increasing catalyst – pollutant contact time and by reducing wettability of the catalyst bed. However, a balance must be found concerning partial wettability; if a large portion of the catalyst is not in contact with the wastewater, the efficiency and overall performance of the catalyst is reduced and the potential for hot spots within the catalyst bed increases.

The benefits of co-current flow in TBRs are further expressed by Dudukovic et al.[41]. Under a co-current regime, the liquid flow rate can be reduced more than in a counter current set-up, which allows for a higher flexibility regarding reactor operating conditions, and therefore more control over catalytic performance.

To summarise, the high catalyst to wastewater ratio in a TBR, can overcome the drawbacks of other reactors and batch processing. Although slurry and bubble column reactors provide enhanced mass transfer, the reduced potential for polymerisation of phenol products allows for longer catalyst lifetimes, making a TBR the appropriate choice for CWAO. Since counter-current flow is impractical on a smaller scale and has shown lower activity for phenol oxidation compared with co-current flow, a co-current regime is preferable for the CWAO of phenol.

2.2.3 Catalyst packing

The shape and size of catalyst particles are important parameters which must be considered, especially in packed bed reactors, as they can directly affect the flow of the wastewater. The larger the catalyst particles, the more inefficiently they fill a particular space, creating larger gaps between the particles. Larger gaps allow the liquid phase to flow through the catalyst with little hindrance. In contrast, smaller particles result in more efficient packing, offering more resistance to the liquid phase, increasing the catalyst-pollutant contact time[14]. Smaller particles also have less mass transfer limitations since a larger portion of the active sites will be more accessible to the pollutants.

If particle size is decreased further into powders, the liquid flow can become restricted enough to cause reactant hold-up, resulting in a pressure drop along the catalyst bed[28]. Issues regarding a pressure drop can cause increased energy expenditure, as higher pressures are needed to overcome the restriction[42]. Powdered catalysts are also more likely to be flushed through the reactor and require more complex bed supports.

Figure 2.6 demonstrates the packing of samples with the same composition and weight, but with a change in packing efficiency due to difference in particle size.
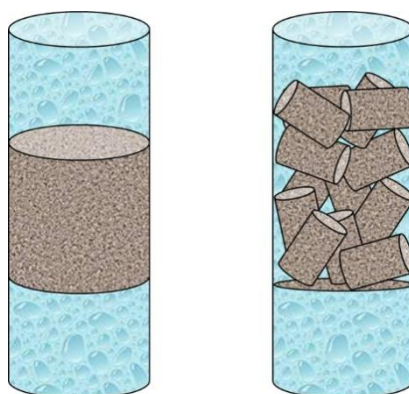
Figure 2.6 The packing efficiency in a catalyst bed by small particulates (left) and large particulates (right)[26]

A balance between particles size and packing efficiency must be reached. Catalyst particles should be small enough to allow sufficient contact time and mass transfer of reactants, but large enough for ease of flow of the liquid phase to avoid pressure drop related problems.

2.3 Catalysts for catalytic wet air oxidation (CWAO)

Numerous factors need to be considered when selecting an appropriate catalyst for a particular reaction; the right catalyst can diminish the severity of the reaction conditions as well as promoting complete oxidation of pollutants to H_2O and CO_2. Regarding CWAO, the choice of catalyst is predominately determined by its activity and stability under the acidic and oxidising environment in the reactor[43]. Other factors that can influence the decision are whether the active metal is prone to leaching or the surface area and thermal stability of the catalyst[44].

2.3.1 Current catalyst benchmark

Table 2.1 outlines a selection of catalysts explored in the literature for CWAO of phenol, including the concentration of pollutant, reactor type, operating temperature and pressure and percentage conversion achieved.

Table 2.1 Performance and operating conditions of catalysts investigated in the literature. ([Ph] = concentration of phenol, pO$_2$ = partial pressure of O$_2$, X$_{ph}$ = percentage phenol conversion achieved, TBR = trickle bed reactor, SR = slurry reactor, FBR = fixed bed reactor, SBR = spinning basket reactor)

Catalyst	[Ph] (g L^{-1})	Reactor	T (ºC)	pO$_2$ (bar)	X$_{ph}$ (%)	Ref.
CeO$_2$-TiO$_2$	1	batch	150	6.2	100	[12]
	1	TBR	140	7.3	91	
Pt/Al$_2$O$_3$	5	batch	175	25	95	[45]
MnO$_x$-CeO$_x$	5	SR	130	25	100	
Ru/TiO$_2$	1	TBR	210	10	98	[30]
Ru/CeO$_2$-Al$_2$O$_3$	5	TBR	140	7	30	[31]
Pd/C	1	TBR	240	10	91	[32]
Act. carbon	5	TBR	160	2	>99	[33]
CuO/alumina	5	TBR	140	9	40	[46]
NiO/alumina	5	TBR	140	9	10	
CuO/alumina	5	TBR	140	9	80	[16]
CuO	1	FBR	160	16	60	[47]
Mn$_x$-Ce$_x$-O$_x$	1	batch	110	5	85	[48]
CuO/C	2.2	SBR	160	36	>99	[49]
Pt/TiO$_2$	1	batch	160	10	85	[50]
Pt/TiO$_2$-CeO$_x$	1	batch	160	10	96	
Pt/TiO$_2$	1	batch	175	10	90	[51]
Pt/CeO$_2$	5	batch	170	8.4	100	[52]
Ru/TiO$_2$	1	batch	200	6.9	>99	[53]
Ru/TiO$_2$-CeO$_2$	2	batch	160	20	100	[54]
Pt/TiO$_2$-CeO$_2$	2	batch	160	20	100	
Ru/CBC	1	FBR	160	16.7	100	[55]
Pt/SiC	1	TBR	160	2.9	>99	[26]
Pt/CeO$_2$	2	batch	160	20	57	[56]

A large variety of solid catalyst compositions have been explored for phenol oxidation, typically they can be separated into two categories: (i) metal oxide catalysts and (ii) supported metal catalysts[57]. Metal oxides catalysts are frequently less expensive, but often show deactivation caused by leaching of metal ions. Comparatively, supported metal catalysts, especially those containing precious metals, are considerably more expensive and suffer from poisoning of the catalysts surface by the deposition of carbonaceous species.

Regarding CWAO, an effective catalyst needs to show high stability when exposed to the acidic and oxidising conditions, caused by the presence of short chain carboxylic acids as reaction intermediates in the incomplete oxidation of phenol[58]. Other factors catalysts must face during WAO include - (i) leaching of the active component, (ii) loss of surface area, (iii) poisoning of active sites by CO evolution, and (iv) deposition of organic or inorganic species on the catalyst surface[59].

Catalysts investigated in the literature and their effectiveness for CWAO are discussed in further detail throughout the remainder of this chapter.

2.3.2 Metal oxide catalysts

The mixing of metal oxides can enhance the activity of the individual oxide[57]. Yang *et al.*[12] observed a higher activity for CeO_2-TiO_2 than for either singular oxide, whilst Kochetkova *et al.*[60] observed greater activity and stability for CuO-CoO-TiO_2/Al_2O_3 compared with CuO/Al_2O_3, for phenol oxidation below 200 ⁰C. The catalytic activity of metal oxides during phenol oxidation have been observed in the following order[61]: $CuO > CoO > Cr_2O_3 > NiO > MnO_2 > Fe_2O_3 > Cd_2O_3 > ZnO > TiO_2 > Bi_2O_3$ under similar conditions.

Among metallic oxide catalysts, higher activities have been observed for those based on copper oxides for CWAO[46,62-64]. Despite initial high activity, many studies observed leaching of the copper into the wastewater[16,47,65-67]. Leaching of the copper from the solid catalyst resulted in the presence of copper cations in the

reaction media, which then contributed homogenously to the oxidation of phenol. Concentrations of <0.1 g L^{-1} copper were recorded in solution[58], increasing the toxicity of the wastewater[68] and therefore requiring the wastewater to undergo further treatment, not uncommon in homogenous processes.

Copper leaching was observed to be a function of the pH of the wastewater, with lower, more acidic wastewater notably increasing the concentration of copper ions in solution[58]. Phenol oxidation proceeds *via* the formation of short chain acids, and so low pH values are typical in the aqueous phase for CWAO of phenol[43]. The formation of oxalic acid as a reaction intermediate was shown to be of particular significance. Oxalic acid was able to precipitate the copper in solution and the resulting copper oxalate complex then deposited on the catalyst surface, which prevented further leaching. Although copper leaching was reduced, the catalytic activity also rapidly decreased, attributed to the removal of the homogenous contribution and the obscuring of active sites on the solid catalyst from the deposited complexes.

Overall, the leaching of the copper under the acidic conditions associated with the process, and the increase in water toxicity due to the presence of copper cations, prove CuO to be an ineffective and unstable catalyst for CWAO of phenol.

Another metal oxide studied for phenol oxidation is nickel oxide supported on alumina, however only 10 % conversion was achieved in a TBR at 140 $^{\circ}$C[46]. Similar to the copper catalysts, leaching of the active metal occurred with NiO detected in the off-stream.

Chen *et al.*[48] investigated Mn-Ce-O composite catalysts for the CWAO of phenol in a batch slurry reactor, with varying ratios of Mn and Ce. A ratio of 60:40 Mn:Ce was found to be the most active, achieving 85 % phenol conversion. Characterisation of the catalyst revealed two different active sites, one related to manganese oxide which was primarily responsible for oxidation, and the other ascribed to electron-rich ceria which efficiently activated adsorbed oxygen. The catalysts with higher Mn content also showed higher resistance to deactivation caused by carbonaceous deposits.

The majority of metal oxides studied in the literature were not robust enough to withstand the severe conditions of CWAO. Under a constant flow of hot air and stream of acidic wastewater, metal oxides are often subjected to leaching and thus further deteriorate the quality of the treated water.

2.3.3 Supported metal catalysts

Supported metal catalysts are composed of an active metal component, required to promote the catalytic reaction, and a support on which the active metal is dispersed. Both the support and active component contribute to the catalytic performance, including the catalyst lifetime, selectivity, activity towards phenol conversion and resistance to the high temperature acidic conditions of CWAO.

Supported metal catalysts, particularly those containing precious metals, have proved their effectiveness for CWAO over a wide range of organic pollutants[69]. They typically show higher activity and stability compared to metal oxide catalysts, and are less prone to deactivation caused by leaching of the active component[13,44].

2.3.3.1 Active metal components

Typically for CWAO, the choice of active metal component has generally been focused on platinum group metals (PGMs). PGMs have gained popularity due to a combination of high activity and stability; unlike metal oxide catalysts, noble metals have shown a higher resistance to leaching under the acidic conditions[24]. PGMs do however come with a higher price tag when compared with metal oxides and as a result their performance must superior in multiple aspects (catalyst lifetime, activity, selectivity etc.) to justify the additional expenditure.

PGMs are often discussed as a 'limited resource' with the ambition of designing catalysts which incorporate more highly abundant metals; however, their high value encourages development of recycling technologies to recover these precious metals from scrap material. Pyro- and hydrometallurgical methods are frequently used to recover PGMs from catalytic converters, although if the recycling is to be cost effective over 90 % of the metal must be recovered[70,71]. As recycling technologies continue to improve in terms of efficiency and cost, there is no reason to exclude such well-established metals from continued catalyst development. Palladium, platinum, ruthenium, iridium and rhodium have all proven their effectiveness for the CWAO of pollutants, including phenol[72], carboxylic acids[73] and nitrogen containing compounds[74]. Thus, despite their high cost, PGMs are still frequently used due to their higher catalytic activity and higher resistance to metal leaching for CWAO[24,54,69].

Trawczyński et al.[75] investigated noble metals Pd, Pt and Ru supported on carbon black material (CBC) for the CWAO of phenol in a trickle bed reactor. Catalytic activity was observed in the following order: Pt > Pd ≈ Ru. The trend in activity was attributed to differences in the adsorption capacity for organic molecules and the adsorption energy of oxygen on the different metals.

Platinum has repeatedly been shown to be the most active PGM in the abatement of organic wastewater pollutants[57]. Qin et al.[76] observed the trend Pt > Pd > Ru for catalytic activity, independent of whether the metals were supported on Al_2O_3 or activated carbon. Pt also displayed the highest selectivity towards CO_2 and total organic carbon (TOC) removal. When supported on TiO_2, Okitsu et al.[77] reported the trend Pt >> Pd > Ru > Rh for the decomposition of ρ-chlorophenol.

Platinum can exist in either metallic or oxide form during the reaction; when in the oxide form, PtO_2, can act as a catalyst by oxidising the pollutant, before reverting back to its metallic form[78]. This reaction cycle is signified by the following reaction equations, where the pollutant is represented as A:

$$Pt + O_2 \rightarrow PtO_2 \qquad \textit{Equation 2.2}$$

$$PtO_2 + A \rightarrow Pt + AO_2 \qquad \textit{Equation 2.3}$$
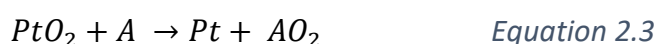
When investigating the effects of ceria loading on a Pt/TiO$_2$ catalyst, Rocha et al.[50] found that increasing the ceria content led to an increase in Pt^{2+} species, brought about by the presence of oxygen provided by CeO$_2$, causing the metallic Pt^0 to be oxidised to Pt^{2+}. Once the ceria content was increased to such an extent (10 wt. % ceria) that the surface platinum was exclusively in the oxide form, a significant decrease in phenol conversion was observed. For small additions of ceria (3 wt. %), however, a 10 % increase in phenol conversion was observed when compared with Pt/TiO$_2$ catalyst consisting of exclusively Pt^0. The addition of ceria also yielded an increase in the catalyst surface area, which was thought to be responsible for the increased activity observed and not necessarily the presence of Pt^{2+} species.

Monteros et al.[54] also reported similar findings with a decrease in catalytic activity observed when Pt-based catalysts were doped with ceria, independent of specific surface area. High phenol conversions were observed for Ru/TiO$_2$ and Pt/TiO$_2$ catalysts with varied amounts of CeO$_2$ doping. In the case of platinum, Pt/TiO$_2$-χ wt%-CeO$_2$ catalysts achieved higher phenol conversion with lower weight percentages of ceria (5 – 10 %), with complete phenol conversion also obtained in the absence of ceria. Whereas for ruthenium, Ru/TiO$_2$-χ wt%-CeO$_2$ catalysts achieved similar phenol conversion regardless of the amount of ceria (0 – 100 %). In both studies, Monteros and Rocha also saw an increase in the formation of polymers and accumulation of adsorbed species with increased ceria loading on the platinum catalysts. Gaálová et al.[80] proposed that the ceria increases the oxygen storage capacity (OSC) of the precious metal catalysts, and ceria doping improves the mass transfer of oxygen from the gaseous phase to the metallic active sites. Catalytic activity for CWAO, however, has been found to be independent of catalyst OSC[78,81], and it has been suggested that it is ceria's capacity to affect the number of Lewis acid sites on the catalyst surface, which phenol molecules can bind to, that is responsible for any variation in activity observed. Monteros et al.[54] saw a decrease in the total number of Lewis acid sites with ceria loading for the Pt-based catalysts, whilst the number of acid sites was independent of ceria loading for Ru-based catalysts, which is in accordance with

the catalytic activities observed. Figure 2.7 shows the proposed reaction mechanism:
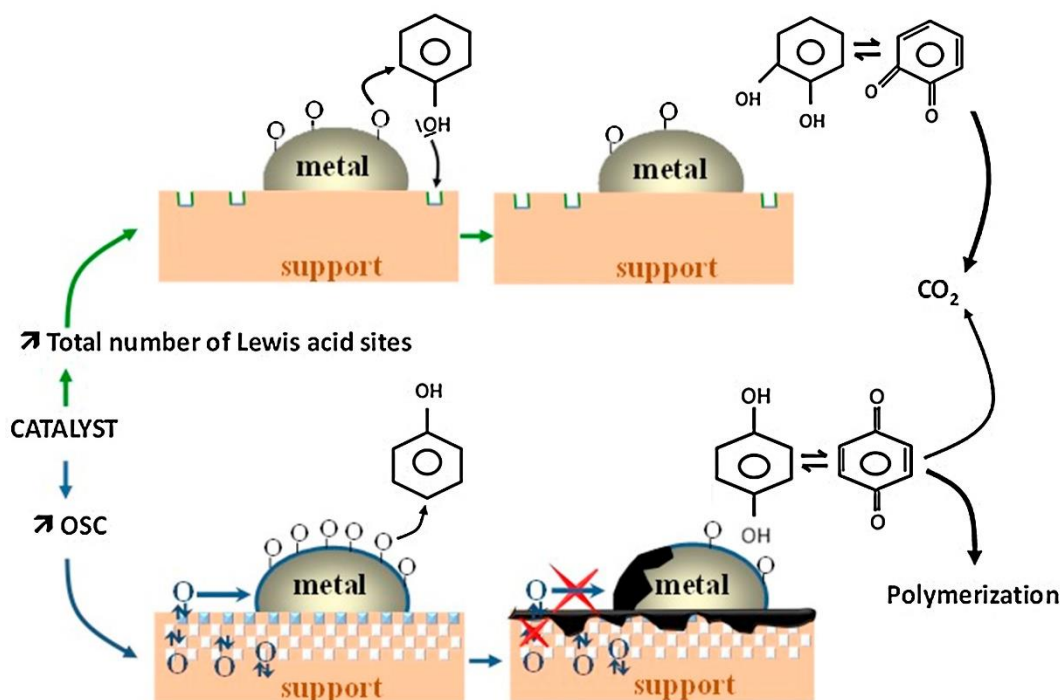
Figure 2.7 Proposed mechanism of phenol oxidation over ceria doped Ru and Pt/TiO₂ catalysts[54]

The reaction mechanism for phenol oxidation over a supported precious metal catalyst suggests that an increase in OSC favours oxidation of phenol in the *para* position. Oxidation in this orientation results in the formation of *para*-benzoquinone, which can promote polymerisation, and thus lead to catalyst poisoning *via* carbon deposition[13]. When the number of acid sites on the surface is increased, however, phenol oxidation in the *ortho* position becomes the most sterically preferred orientation, due the interaction between the phenol hydroxyl group and the acid site. Oxidation *via* the ortho position results in ortho-benzoquinone which inhibits polymerisation, lowering the potential for deactivation. Although small loadings of ceria (≤5 %) may slightly increase phenol conversion for platinum catalysts, the reduction of Lewis acid sites and resulting growth polymerisation reactions make ceria addition less desirable in Pt-based catalysts. An increase in catalytic activity is not always beneficial if catalyst lifetime is diminished This mechanism is supported by Lafaye *et al.*[78], who reported that an increase in OSC of Pt/CeO₂-TiO₂ lead to the formation of polymers which

poisoned the catalyst surface, whereas, increased Lewis acidity had a positive effect in orientating the reaction directly to CO_2.

Masende et al.[82] demonstrated that the activity of a Pt/graphite catalyst and the selectivity of the oxidation products are influenced by the extent of oxygen coverage on the platinum surface. A fully oxidised PtO_x surface resulted in a change in the selectivity of the reaction and favoured the formation of p-benzoquinone. p-benzoquinone was responsible for the polymer formation observed and also deactivation of the catalyst via obstruction of the active sites, further supporting the reaction mechanism in Figure 2.7.

Platinum has been established as intrinsically more active for phenol oxidation compared with ruthenium and more successful at promoting total oxidation, however, due to its lower cost, Ru is common among catalysts investigated for CWAO. On certain supports ruthenium has achieved higher or equal phenol conversions compared with platinum[53,76].

Cybulski et al.[55] reported total phenol conversion at 160 °C in a fixed bed reactor using a Ru/C catalyst. When compared with a Pt/C catalyst, the initial reaction rate of the ruthenium catalyst was equal to that of the platinum; only when the temperature was reduced to 140 °C did Pt/C show a superior initial reaction rate.

For the CWAO of acetic acid, Gaálová et al.[80] reported the initial activity of ruthenium to be independent of the support material, when comparing CeO_2 doped with multiple ratios of Zr and Pr oxide. Of note was the observation that the increased Ru particle sizes led to an increase in catalytic activity. Typically, smaller metal particles give rise to higher activity due to an increase in surface area, and therefore a larger portion of exposed metallic active sites. Gaálová et al. proposed that the larger particles were composed of large Ru^0 particles surrounded by Ru^{n+} species, which facilitated the production of superoxide radicals:

$$Ru^{3+} + O_2 \rightarrow Ru^{4+} + O_2^- \cdot \qquad \textit{Equation 2.4}$$
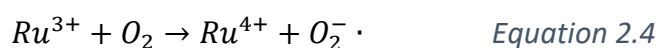
Ru^{3+} and Ru^{4+} are known for catalysing the production of superoxide radicals[83], which can result in increased activity as the formation of such radicals increases the oxidising potential of the catalyst[80]. Due to the partial oxidation of the larger Ru particles, oxygen transfer from the support to the metal active sites was no longer the rate limiting factor for CWAO of acetic acid.

In addition, when compared with equivalent platinum catalysts, ruthenium demonstrated a higher resistance to deposition of carbonaceous species under CWAO conditions[81].

To summarise, noble metal catalysts such as platinum and ruthenium, have shown to be very effective for CWAO of organic pollutants. They are better able to withstand the acidic and oxidising conditions associated with the process, which is why, despite their high cost, they are still predominately being investigated.

2.3.3.2 Catalysts supports

The primary role of a heterogeneous catalyst support is to disperse the active metal particles, allowing for a high metallic surface area. Regarding CWAO, an efficient catalyst support requires high thermal stability and resistance to low pH values, as due to the formation of intermediates the reaction media may become increasingly acidic.

Catalyst supports are typically characterised by high surface areas. The catalyst surface is an important factor in adsorption and desorption of reactants and products; therefore, the appropriate catalyst support can have a pronounced effect on catalytic performance[84]. A support may also aid catalysis by improving mass transfer of oxidants across the surface to the active sites[85].

The most commonly reported supports for catalysts for CWAO are γ-Al_2O_3, TiO_2, CeO_2, ZrO_2 and carbon materials[24,50]. The application of ceria as a support and its ability to facilitate oxygen transfer has previously been discussed[78]. Alumina (Al_2O_3) has also demonstrated proficiency as a catalyst support for phenol

abatement with a variety of active metals[86-88]. Typically, γ-Al$_2$O$_3$ is used, as opposed to α-Al$_2$O$_3$, due to its superior surface area[89]; a higher surface area is advantageous as it can lead to higher dispersion of the active metal. γ-alumina also has a higher degree of surface functionality, referring to surface hydroxyl groups which can beneficially influence the interaction of reactants with the catalyst[90,91]. For the CWAO of phenol, alumina showed a higher stability over 9 days in a TBR at 140 ^{o}C compared with a silica support, which proved very sensitive to the acidic reaction media[92].

Another frequently investigated support is TiO$_2$, which has been successfully utilized for CWAO with numerous active metals[93-95]. Pintar *et al.*[30] also observed over 40 % TOC removal in the presence of bare TiO$_2$ support at 240 ^{o}C in a TBR.

Activated carbon (AC) and carbon based materials have gained increasing popularity for CWAO due to their exceptional stability and resistance to leaching in acidic conditions[75]. The adsorptive properties of AC have also been extensively investigated, including its use in adsorption treatment methods for phenol removal[96,97]. Both phenol and oxygen adsorb strongly to AC[98], which can affect its catalytic performance if the surface becomes saturated with phenol without oxidation occurring.

AC has been successful in the CWAO of phenol oxidation without the presence of any active metal[99-101]. When tested in a trickle bed reactor, leaching of the active phase and deposition of carbonaceous species on the catalyst surface have been substantially reduced with an AC catalyst[14].

When compared to commercial a copper catalyst, AC achieved a higher phenol conversion at 140 ^{o}C and 9 bar O$_2$ in a TBR[99]. However, at higher temperatures (>500 ^{o}C), AC and carbon materials have shown a tendency to undergo combustion[102], resulting in mass loss of the catalyst. Combustion, and therefore catalyst loss, can be reduced by lowering the oxygen partial pressure and the reaction temperature, however, small percentages (<2 %) of loss of AC are still apparent under conditions as mild as 2 bar pressure[99] and 120 ^{o}C[75]. The

oxidation of phenol and carbon are competitive reactions, making AC a less suitable catalyst for CWAO[103].

A less explored catalyst support for CWAO is β-silicon carbide (β-SiC); SiC is an incredibly inert material with exceptional mechanical and thermal properties[104]. Therefore, SiC would be able to tolerate the acidic and oxidising conditions associated with the process, making it an excellent candidate. SiC has been successfully used in variety of catalyst applications, confirming its ability as a catalyst support material[105-107].

Compared with other conventional supports such as TiO_2 and γ-Al_2O_3, β-SiC has a much lower surface area (approximately 30 m^2 g^{-1})[108]. Whilst investigating catalyst deactivation by adsorption of polymers and intermediary by-products of phenol oxidation, Nousir *et al.*[56] found that the adsorption of such species is limited on low specific surface area catalysts. Assuming the active metal particle size remains the same, when the specific surface area decreases, the relative metal – support interface increases. The better metal – support interface led to better oxygen transfer, which increased phenol mineralization and reduced surface poisoning on $Pt/Ce_xZr_{1-x}O_2$ catalysts.   The lack of hydroxyl groups on the surface of SiC results in a relatively hydrophobic surface[109], which can also influence the mechanism of oxygen activation by the catalyst.

Davies *et al.*[26] demonstrated the ability of noble metals supported on β-SiC as successful catalysts in the CWAO of phenol, achieving >99 % conversion at 160 °C and 13.1 $bar_{(g)}$ pressure in a TBR. When compared to relatively hydrophilic conventional alumina catalysts, Pt/SiC showed superior phenol conversion. This led to the observation that the hydrophobic nature, and thus the wettability, of the support plays a fundamental role in the CWAO of phenol. This phenomenon was further demonstrated when a Pt/Al_2O_3 catalyst was subjected to a silane coating, reducing the hydroxyl functionality of the catalyst. When the hydrophobicity of the catalyst was increased, a >25 % increase in phenol conversion was observed at 120 °C and 13.1 $bar_{(g)}$[26].

The effect of surface wettability was further investigated in this study by comparison of SiC and alumina supports.

2.4 Hydrophobicity and CWAO

The effect of the hydrophobic nature of a catalyst on oxidation reactions has previously been seen in the literature[110]. Chuang *et al.*[111] observed the destruction of volatile organic compounds (VOCs) using a platinum catalyst supported on hydrophobic and hydrophilic material. The temperature ranges for the destruction of VOCs, shown in Table 2.2, were lower for the hydrophobic support in all cases.

Table 2.2 Summary of VOC destruction temperatures over a Pt catalyst supported on a hydrophilic and hydrophobic support carried out by Chuang et al.[111]

VOC compound	VOC destruction temperature range (^{o}C)	
	hydrophilic support	hydrophobic support
Methanol	150 – 250	30 - 80
Formaldehyde	232 – 621	60 – 80
Benzene, toluene and xylene	250 – 300	90 – 130

Conventionally heterogenous catalysts are hydrophilic in nature, causing the catalyst surface to be completely wetted during liquid phase reactions. When gaseous reactants are also present, as is the case for CWAO, the mass transfer of oxygen to the catalyst surface is limited to only one pathway, *via* dissolution in the liquid phase. Hence, elevated pressures and temperatures are required to increase the concentration of dissolved oxygen in the wastewater.

Tromans *et al.*[112] examined the temperature and pressure dependence of oxygen solubility in pure water. Figure 2.8 shows the concentration of dissolved oxygen as a function of temperature and oxygen partial pressure. Under atmospheric conditions, oxygen has a low solubility in water and the rate of transfer of oxygen from the gas phase towards the catalyst surface is commonly

cited as the rate limiting step for CWAO[54,78]. Many reactions carried out in TBRs are mass transfer limited, and oxidation reactions in particular are controlled by O_2 transport[37].
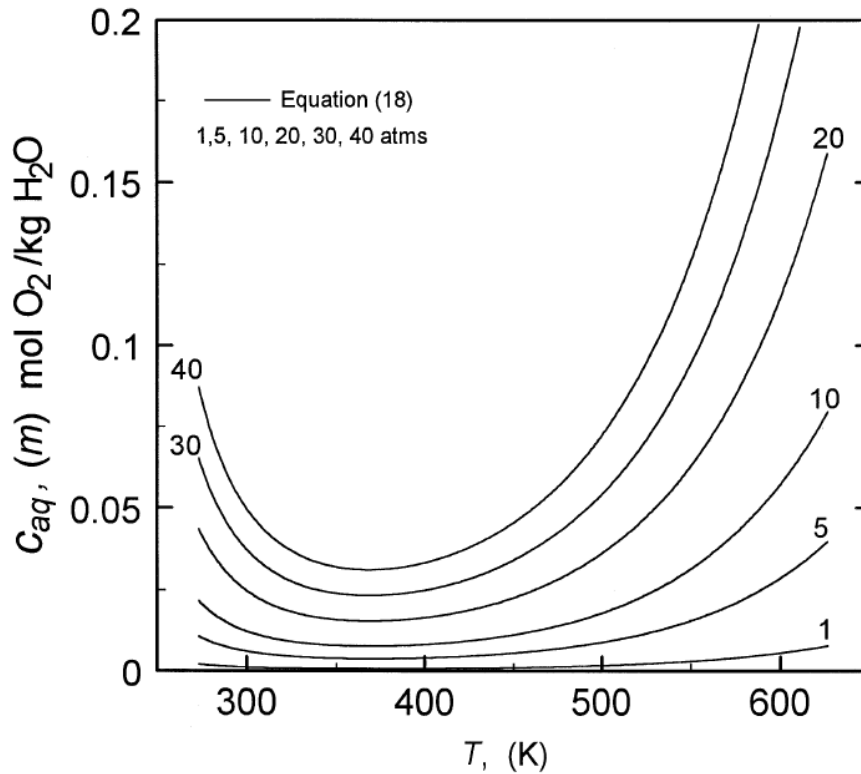
Figure 2.8 The effect of temperature on the molal solubility of O_2 (C_{aq}) as a function of the oxygen partial pressure (1 – 40 atms)[112]

Over the typical temperatures associated with CWAO (between 400 – 500 K), the concentration of dissolved oxygen does not increase significantly with temperature at low oxygen partial pressure. Only when pO_2 approaches 5 – 10 atms (which equates to approximately 23 – 47.5 bar pressure of air) does a change in temperature (within the active range for CWAO) have a pronounced effect on the concentration of dissolved oxygen.

Due to the importance of oxygen solubility for CWAO, it is necessary to define the relationship between gaseous and dissolved oxygen. Henry's law states that at a constant temperature, the amount of dissolved gas is directly proportional to its partial pressure in the gas phase, which is expressed in Equation 2.5[113]. An increase in pressure increases the solubility and conversely a decrease in pressure decreases solubility.

$$C_{aq} = k_H P_{gas}$$

Equation 2.5 Henry's law formula, where C_{aq} = concentration of dissolved gas, k_H = Henry's law constant and P_{gas} = partial pressure of gas

The proportionality factor, Henry's law constant, is dependent upon the nature of the gas and solvent at a specific temperature. Small values of k_H indicate high solubility, whereas high values indicate low solubility. Henry's law is applicable for most dilute aqueous systems at moderate temperatures and pressure, but does not hold true when gases are under extremely high pressures (>100 atm)[114,115].

Tromans *et al.*[112] presented Equation 2.6 to calculate the concentration of dissolved oxygen in water, extrapolated from Henry's Law and thermodynamic analysis of oxygen solubility in water. The equation describes the relationship between temperature, pressure and oxygen solubility over a broad range of conditions, including those typically encountered in CWAO operations (0 – 350 °C, <60 bar), without the requirement of multiple k_H values for a given temperature range

$$C_{aq} = P_{O_2}\, e\, xp\left(\frac{0.046T^2 + 203.35T\ln(\frac{T}{298}) - (299.378 + 0.092T)(T - 298) - 20.591 x10^3}{(8.3144)T}\right)$$

Equation 2.6 used to calculate the concentration of dissolved oxygen at a specific T and P, where C_{aq} = concentration of dissolved O_2, P_{O2} = partial pressure of oxygen, T = temperature

Whilst investigating the mass transfer of oxygen during the oxidation of formaldehyde, Lavelle *et al.*[116] found use of a hydrophobic catalyst support to have a significant effect on the mass transfer and chemical kinetics of the oxidation reaction. The presence of a 'surface gas envelope' was observed for a hydrophobic Pt/polydivinylbenzene catalyst when submerged in the liquid reaction media, which lead to the identification of two possible reaction pathways.

A. Intraparticle mass transfer steps

AR1. Liquid phase transfer of reductant to catalyst surface gas envelope

AO1. Oxidant transfer from bulk gas to bubble

Gas phase oxidant route

Liquid phase oxidant route

AO2a. Bubble transfer of oxidant to catalyst surface gas

AO2b. Oxidant dissolution

AO2c. Liquid phase transfer of oxidant to catalyst surface gas envelope

B. Intraparticle Gas Phase Mass Transfer Steps

(Gas phase transfer across surface gas envelope, pore diffusion, etc.)

C. Surface Reaction Steps

(Adsorption, chemical reaction, desorption)

Figure 2.9 Kinetic steps proposed by Lavelle et al.[116] for the oxidation of aqueous organic compounds over a hydrophobic solid catalyst

Figure 2.9 illustrates the reaction steps for the oxidation of aqueous organic compounds during CWAO over a hydrophobic catalyst. The reaction can proceed *via* two routes, one of which involves the disolution of oxygen (AO2b) followed by liquid phase transfer to the catalyst surface (AO2c) and the other through which gaseous oxygen is directly transferred to catalyst surface *via* a 'surface gas envelope' (AO2a).

When comparing the contribution of the possible oxygen transfer pathways in a Carberry-type batch reactor, the gas phase route was found to be more pronounced at high stirrer speeds. The percentage contribution of each oxygen transfer routes as a function of stirrer speed is displayed in Figure 2.10.
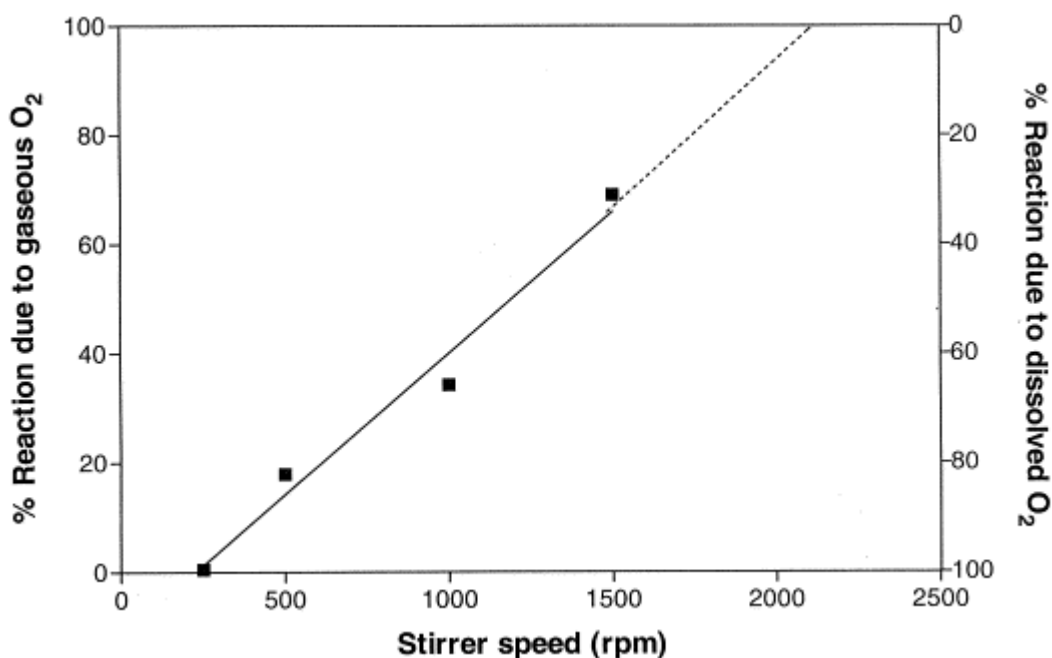
Figure 2.10 Contribution of oxygen mass transfer routes to the oxidation of formaldehyde carried out by Lavelle et al.[116]

At low stirrer speeds (< 1000 rpm), dissolved oxygen participated in the majority of the formaldehyde oxidation; this was linked to a positive relationship between stirrer rates and the gas – liquid interfacial area. When comparable reactions carried out by Chuang *et al.*[111] under similar conditions, a considerable decrease in the activation energy for formaldehyde oxidation was observed, 14 kJ mol^{-1} compared to 37.3 kJ mol^{-1}.

Support wettability was also shown to play a key role in the CWAO of phenol by Davies *et al.*[117] when investigating a comparatively hydrophilic Ru/Al$_2$O$_3$ catalyst and a relatively hydrophobic Pt/SiC catalyst. Alumina is regarded as hydrophilic due to its high degree of hydroxyl functionality[118]. When a water droplet comes into contact with such a surface, it will form dipole interactions with the hydroxyl groups, increasing the adhesion between the catalyst surface and water, often denoted by smaller contact angles[119]. SiC exhibits low surface hydroxyl functionality[109], and thus is comparatively hydrophobic.

The increased interaction between the aqueous phase and the alumina support results in increased wetting of the catalyst surface, which in turn limits the transfer of gaseous oxygen to the catalyst active sites, since oxygen must first be dissolved in the liquid phase in order to access the wetted catalyst surface[116]. A

hydrophobic material however, will only become partially wetted as the energy required to create a solid – gas interface is less than that required for a solid – liquid interface, for such materials[120].

When supported on both alumina and SiC, an enhanced phenol conversion was observed for the Pt/SiC catalyst compared to Pt/Al$_2$O$_3$, 97 % and 58 % conversion respectively, in a TBR at 140 °C and 13.1 bar$_{(g)}$[121]. When RuO$_2$ was the active component, however, a higher catalytic activity was observed for Ru/Al$_2$O$_3$ compared to Ru/SiC, achieving >40 % and >20 % phenol conversions respectively. This led to the suggestion than a metal – support synergy exists; when the active component is composed of metallic Pt a hydrophobic support is preferential, but for ionic RuO$_2$, a hydrophilic support is more effective.
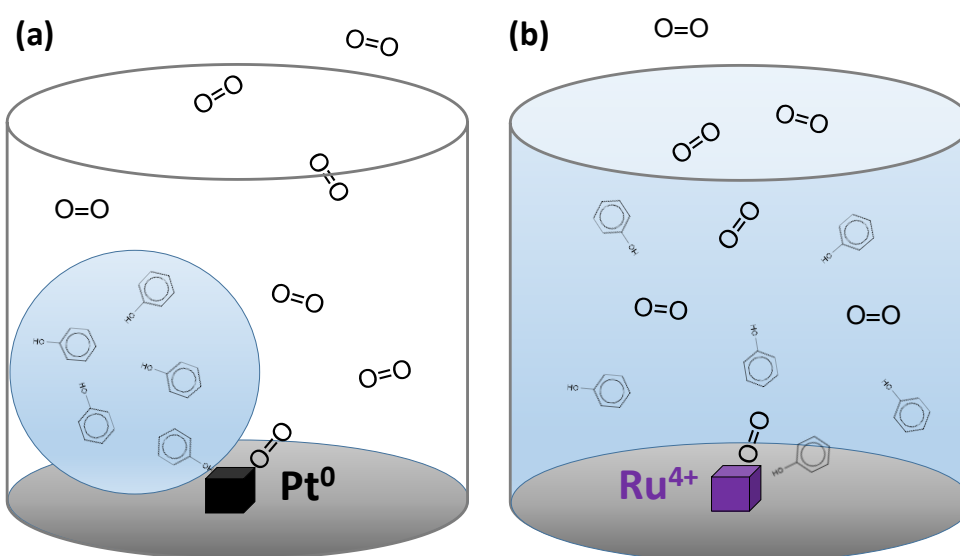
Figure 2.11 Proposed reaction pathways for the activation of phenol and O$_2$ on the active sites located inside the catalyst pore structures for (a) Pt dispersed on a partially wetter surface (hydrophobic support) and (b) RuO$_2$ dispersed on a fully wetted surface (hydrophilic support)[121]

During the CWAO of phenol, RuO$_2$ adsorbs both phenol and O$_2$ from the aqueous phase (Figure 2.11b), whereas Pt adsorbs O$_2$ directly from the gas phase (Figure 2.11a)[121]. The study showed the intrinsic activity of Pt/SiC to be greater than that of Ru/Al$_2$O$_3$, suggesting a hydrophobic catalyst support is beneficial to CWAO reactions.

High pressures are often utilized in CWAO processes to increase the concentration of dissolved oxygen and therefore promote oxidation. If an

alternative oxygen transfer route is available for hydrophobic catalysts, which does not require dissolved oxygen, such high pressures may not be necessary. Being able to conduct CWAO under ambient conditions and reduced operating pressures would offer economical, safety and environmental advantages on an industrial scale. It should also be considered that a hydrophobic catalyst may help prevent poisoning by reducing irreversibly bound liquid phase species during reaction.

2.5 Project aims

The primary aim of this project was to optimize the process of CWAO of phenol; by building on previous research an alternative range of catalyst compositions were investigated. The optimization of a platinum supported on silicon carbide catalyst was reviewed in terms of improved surface area and addition of a second active metal component. The nature and effect of a hydrophobic catalyst was explored, with the ultimate goal of achieving CWAO under ambient conditions. The effectiveness of Pt/SiC for the wet air oxidation of other common organic pollutants was also investigated.

2.6 References

(1)   Recoognizing the Best in Innovation: Breathrough Catalyst, R*&D Magazine*, Sept **2005**, 20.
(2)   Kolaczkowski, S. T.; Plucinski, P.; Beltran, F. J.; Rivas, F. J.; McLurgh, D. B. Wet air oxidation: a review of process technologies and aspects in reactor design. *Chemical Engineering Journal* **1999,** *73* (2), 143.
(3)   Lumen Learning: Introduction to Chemistry: The Effect of a Catalyst, **2019**.
(4)   Hocevar, S.; Batista, J.; Levec, J. Wet oxidation of phenol on Ce1-xCuxO2-delta catalyst. *Journal of Catalysis* **1999,** *184* (1), 39.
(5)   Lei, L. C.; Chen, G. H.; Hu, X. J.; Yue, P. L. Homogeneous catalytic wet-air oxidation for the treatment of textile wastewater. *Water Environment Research* **2000,** *72* (2), 147.

(6)   Bernardi, M.; Cretenot, D.; Deleris, S.; Descorme, C.; Chauzy, J.; Besson, M. Performances of soluble metallic salts in the catalytic wet air oxidation of sewage sludge. *Catalysis Today* **2010,** *157* (1-4), 420.

(7)   Rivas, F. J.; Kolaczkowski, S. T.; Beltran, F. J.; McLurgh, D. B. Hydrogen peroxide promoted wet air oxidation of phenol: influence of operating conditions and homogeneous metal catalysts. *Journal of Chemical Technology and Biotechnology* **1999,** *74* (5), 390.

(8)   Imamura, S. Catalytic and noncatalytic wet oxidation. *Industrial & Engineering Chemistry Research* **1999,** *38* (5), 1743.

(9)   Whyman, R.; Applied organometallic chemistry and catalysis. *Oxford University Press*, **2001**.

(10)   Mahajani, V. V.; Joshi, J. B.; Mishra, V. S.; Mahajani, V. V.; Joshi, J. B. Wet Air Oxidation. *Industrial & engineering chemistry research.* **1995,** *34* (1), 2.

(11)   Essential Chemical Industry Online, essentialchemicalindustry.org/processes/chemical-reactors.html, **2019**.

(12)   Yang, S. X.; Zhu, W. P.; Wang, J. B.; Chen, Z. X. Catalytic wet air oxidation of phenol over CeO_2-TiO_2 catalyst in the batch reactor and the packed-bed reactor. *Journal of Hazardous Materials* **2008,** *153* (3), 1248.

(13)   Levec, J.; Pintar, A. Catalytic wet-air oxidation processes: A review. *Catal. Today* **2007,** *124* (3-4), 172.

(14)   Stuber, F.; Polaert, I.; Delmas, H.; Font, J.; Fortuny, A.; Fabregat, A. Catalytic wet air oxidation of phenol using active carbon: performance of discontinuous and continuous reactors. *Journal of Chemical Technology and Biotechnology* **2001,** *76* (7), 743.

(15)   Pintar, A.; Levec, J. Catalytic-oxidation of organics in aqueous solutions 1. Kintetics of phenol oxidation. *Journal of Catalysis* **1992,** *135* (2), 345.

(16)   Alejandre, A.; Medina, F.; Fortuny, A.; Salagre, P.; Sueiras, J. E. Characterisation of copper catalysts and activity for the oxidation of phenol aqueous solutions. *Applied Catalysis B-Environmental* **1998,** *16* (1), 53.

(17)   Levec, J.; Pintar, A. Catalytic-oxidation od aqueous solutions of organics – an effective method for the removal of toxic pollutants from waste-waters. *Catalysis Today* **1995,** *24* (1-2), 51.

(18)   Pintar, A.; Levec, J. Catalytic liquid-phase oxidation of phenol aqueous solutions – A kintetic investigation. *Industrial & Engineering Chemistry Research* **1994,** *33* (12), 3070.

(19)   Abid, M. F.; Alwan, G. M.; Abdul-Ridha, L. A. Study on Catalytic Wet Air Oxidation Process for Phenol Degradation in Synthetic Wastewater Using Trickle Bed Reactor. *Arabian Journal for Science and Engineering* **2016,** *41* (7), 2659.

(20)   Kantarci, N.; Borak, F.; Ulgen, K. O. Bubble column reactors. *Process Biochemistry* **2005,** *40* (7), 2263.

(21)   Khadem-Hamedani, B.; Yaghmaei, S.; Fattahi, M.; Mashayekhan, S.; Hosseini-Ardali, S. M. Mathematical modeling of a slurry bubble column reactor for hydrodesulfurization of diesel fuel: Single- and two-bubble configurations. *Chemical Engineering Research & Design* **2015,** *100*, 362.

(22)   Tsutsumi, A.; Kim, Y. H.; Togawa, S.; Yoshida, K.; Classification of three-phase reactors. *Sadhana*, **1987**; Vol. 10.

(23)   A, B.; Van Swaaij, W. P. M.; Chemical Reactor Design and Technology: NATO ASI Series, Springer, Dordrecht, **1986**; Vol. 110.

(24)   Kim, K. H.; Ihm, S. K. Heterogeneous catalytic wet air oxidation of refractory organic pollutants in industrial wastewaters: A review. *Journal of Hazardous Materials* **2011,** *186* (1), 16.

(25)   AlDahhan, M. H.; Larachi, F.; Dudukovic, M. P.; Laurent, A. High-pressure trickle-bed reactors: A review. *Industrial & Engineering Chemistry Research* **1997,** *36* (8), 3292.

(26)   Davies, D.; Catalytic Wet Air Oxidation: Developing a Continuous Process: Cardiff University PhD Thesis, **2016**.

(27)   Pohorecki, R.; Bridgwater, J.; Molzahn, M.; Gani, R.; Gallegos, C.; Chemical engineering and chemical process technology: chemical reaction engineering. EOLSS Publishers/UNESCO: UK, **2010**; Vol. 3.

(28)   Dudukovic, M. P.; Larachi, F.; Mills, P. L. Multiphase reactors - revisited. *Chemical Engineering Science* **1999,** *54* (13-14), 1975.

(29)   Saroha, A. K.; Nandi, I. Pressure drop hysteresis in trickle bed reactors. *Chemical Engineering Science* **2008,** *63* (12), 3114.

(30)   Pintar, A.; Batista, J.; Tisler, T. Catalytic wet-air oxidation of aqueous solutions of formic acid, acetic acid and phenol in a continuous-flow trickle-bed reactor over Ru/TiO$_2$ catalysts. *Applied Catalysis B-Environmental* **2008,** *84* (1-2), 30.

(31)   Massa, P.; Ivorra, F.; Haure, P.; Cabello, F. M.; Fenoglio, R. Catalytic wet air oxidation of phenol aqueous solutions by 1% Ru/CeO$_2$-Al$_2$O$_3$ catalysts prepared by different methods. *Catalysis Communications* **2007,** *8* (3), 424.

(32)   Taboada, C. D.; Batista, J.; Pintar, A.; Levec, J. Preparation, characterization and catalytic properties of carbon nanofiber-supported Pt, Pd, Ru monometallic particles in aqueous-phase reactions. *Applied Catalysis B-Environmental* **2009,** *89* (3-4), 375.

(33)   Eftaxias, A.; Font, J.; Fortuny, A.; Fabregat, A.; Stuber, F. Kinetics of phenol oxidation in a trickle bed reactor over active carbon catalyst. *Journal of Chemical Technology and Biotechnology* **2005,** *80* (6), 677.

(34)   Maugans, C. B.; Akgerman, A. Catalytic wet oxidation of phenol in a trickle bed reactor over a Pt/TiO$_2$ catalyst. *Water Research* **2003,** *37* (2), 319.

(35)   Kundu, A.; Nigam, K. D. P.; Verma, R. P. Catalyst wetting characteristics in trickle-bed reactors. *Aiche Journal* **2003,** *49* (9), 2253.

(36)   Goossens, E.; Donker, R.; vandenBrink, F. Reactor runaway in pyrolysis gasoline hydrogenation. *Hydrotreatment and Hydrocracking of Oil Fractions* **1997,** *106*, 245.

(37)   Silveston, P. L.; Hanika, J. Challenges for the periodic operation of trickle-bed catalytic reactors. *Chemical Engineering Science* **2002,** *57* (16), 3373.

(38)   McManus, R. L.; Funk, G. A.; Harold, M. P.; Ng, K. M. Experimental strudy of reaction in trickle bed reactos with liquid maldistribution. *Industrial & Engineering Chemistry Research* **1993,** *32* (3), 570.

(39) Liu, S. H.; Shu, C. M.; Hou, H. Y. Applications of thermal hazard analyses on process safety assessments. *Journal of Loss Prevention in the Process Industries* **2015,** *33,* 59.

(40) Suarez-Ojeda, M. E.; Stuber, F.; Fortuny, A.; Fabregat, A.; Carrera, J.; Font, J. Catalytic wet air oxidation of substituted phenols using activated carbon as catalyst. *Applied Catalysis B-Environmental* **2005,** *58* (1-2), 105.

(41) Dudukovic, M. P.; Larachi, F.; Mills, P. L. Multiphase catalytic reactors: A perspective on current knowledge and future trends. *Catalysis Reviews-Science and Engineering* **2002,** *44* (1), 123.

(42) Ahmadi, S.; Sefidvash, F.; Study of pressure drop in fixed bed reactor using a computational fluid dynamics (CFD) code. *Chem Engineering*: Baha'i Institute, **2018**; Vol. 2.

(43) Besson, M.; Gallezot, P. Deactivation of metal catalysts in liquid phase organic reactions. *Catalysis Today* **2003,** *81* (4), 547.

(44) Luck, F. Wet air oxidation: past, present and future. *Catalysis Today* **1999,** *53* (1), 81.

(45) Hamoudi, S.; Larachi, F.; Sayari, A. Wet oxidation of phenolic solutions over heterogeneous catalysts: Degradation profile and catalyst behavior. *Journal of Catalysis* **1998,** *177* (2), 247.

(46) Alejandre, A.; Medina, F.; Salagre, P.; Fabregat, A.; Sueiras, J. E. Characterization and activity of copper and nickel catalysts for the oxidation of phenol aqueous solutions. *Applied Catalysis B-Environmental* **1998,** *18* (3-4), 307.

(47) Santos, A.; Yustos, P.; Quintanilla, A.; Rodriguez, S.; Garcia-Ochoa, F. Route of the catalytic oxidation of phenol in aqueous phase. *Applied Catalysis B-Environmental* **2002,** *39* (2), 97.

(48) Chen, H.; Sayari, A.; Adnot, A.; Larachi, F. Composition-activity effects of Mn-Ce-O composites on phenol catalytic wet oxidation. *Applied Catalysis B-Environmental* **2001,** *32* (3), 195.

(49) Alvarez, P. M.; McLurgh, D.; Plucinski, P. Copper oxide mounted on activated carbon as catalyst for wet air oxidation of aqueous phenol. 1. Kinetic and mechanistic approaches. *Industrial & Engineering Chemistry Research* **2002,** *41* (9), 2147.

(50) Lunagomez Rocha, M. A.; Del Angel, G.; Torres-Torres, G.; Cervantes, A.; Vazquez, A.; Arrieta, A.; Beltramini, J. N. Effect of the Pt oxidation state and Ce^{3+}/Ce^{4+} ratio on the Pt/TiO_2-CeO_2 catalysts in the phenol degradation by catalytic wet air oxidation (CWAO). *Catalysis Today* **2015,** *250,* 10.

(51) Maugans, C. B.; Akgerman, A. Catalytic wet oxidation of phenol over a Pt/TiO_2 catalyst. *Water Research* **1997,** *31* (12), 3116.

(52) Duprez, D.; Delanoe, F.; Barbier-Jr, J.; Isnard, P.; Blanchard, G. Catalytic oxidation of organic compounds in aqueous media. *Catalysis Today* **1996,** *29* (1-4), 317.

(53) Vaidya, P. D.; Mahajani, V. V. Insight into heterogeneous catalytic wet oxidation of phenol over a Ru/TiO_2 catalyst. *Chemical Engineering Journal* **2002,** *87* (3), 403.

(54)   Monteros, A. E. d. l.; Lafaye, G.; Cervantes, A.; Del Angel, G.; Barbier Jr, J.; Torres, G. Catalytic wet air oxidation of phenol over metal catalyst (Ru,Pt) supported on TiO$_2$–CeO$_2$ oxides. *Catalysis Today* **2015**, *258, Part 2*, 564.

(55)   Cybulski, A.; Trawczynski, J. Catalytic wet air oxidation of phenol over platinum and ruthenium catalysts. *Applied Catalysis B-Environmental* **2004,** *47* (1), 1.

(56)   Nousir, S.; Keav, S.; Barbier-Jr, J.; Bensitel, M.; Brahmi, R.; Duprez, D. Deactivation phenomena during catalytic wet air oxidation (CWAO) of phenol over platinum catalysts supported on ceria and ceria-zirconia mixed oxides. *Applied Catalysis B-Environmental* **2008,** *84* (3-4), 723.

(57)   Matatov-Meytal, Y. I.; Sheintuch, M. Catalytic abatement of water pollutants. *Industrial & Engineering Chemistry Research* **1998,** *37* (2), 309.

(58)   Santos, A.; Yustos, P.; Quintanilla, A.; Ruiz, G.; Garcia-Ochoa, F. Study of the copper leaching in the wet oxidation of phenol with CuO-based catalysts: Causes and effects. *Applied Catalysis B-Environmental* **2005,** *61* (3-4), 323.

(59)   Pintar, A. Catalytic processes for the purification of drinking water and industrial effluents. *Catalysis Today* **2003,** *77* (4), 451.

(60)   Kochetkova, R.; Shiverskaya, I.; Kochetkov, A.; Yu, A.; Panfilova, I.; Technological parameters of liquid phase oxidation of wastewater phenols. *Koks Khim.*, **1993**; Vol. 9.

(61)   Kochetkova, R. P.; Babikov, A. F.; Shpilevskaya, L. I.; Shiverskaya, I. P.; Eppel, S. A.; Shmidt, F. K. Liquid-phase catalytic oxidation of phenol. *Chemistry and Technology of Fuels and Oils* **1992,** *28* (3-4), 225.

(62)   Sadana, A.; Katzer, J. R. Involvement of free-radicals in aqueous-phase catalytic oxidation of phenol over copper oxide. *Journal of Catalysis* **1974,** *35* (1), 140.

(63)   Wu, Q.; Hu, X.; Yue, P. L.; Zhao, X. S.; Lu, G. Q. Copper/MCM-41 as catalyst for the wet oxidation of phenol. *Applied Catalysis B-Environmental* **2001,** *32* (3), 151.

(64)   Hocevar, S.; Krasovec, U. O.; Orel, B.; Arico, A. S.; Kim, H. CWO of phenol on two differently prepared CuO-CeO$_2$ catalysts. *Applied Catalysis B-Environmental* **2000,** *28* (2), 113.

(65)   Alvarez, P. M.; McLurgh, D.; Plucinski, P. Copper oxide mounted on activated carbon as catalyst for wet air oxidation of aqueous phenol. 2. Catalyst stability. *Industrial & Engineering Chemistry Research* **2002,** *41* (9), 2153.

(66)   Kim, S. K.; Kim, K. H.; Ihm, S. K. The characteristics of wet air oxidation of phenol over CuO$_x$/Al$_2$O$_3$ catalysts: Effect of copper loading. *Chemosphere* **2007,** *68* (2), 287.

(67)   Santos, A.; Yustos, P.; Durban, B.; Garcia-Ochoa, F. Catalytic wet oxidation of phenol: Kinetics of phenol uptake. *Environmental Science & Technology* **2001,** *35* (13), 2828.

(68)   Santos, A.; Yustos, P.; Quintanilla, A.; Garcia-Ochoa, F.; Casas, J. A.; Rodriguez, J. J. Evolution of toxicity upon wet catalytic oxidation of phenol. *Environmental Science & Technology* **2004,** *38* (1), 133.

(69) Luck, F. A review of industrial catalytic wet air oxidation processes. *Catalysis Today* **1996,** *27* (1-2), 195.

(70) Fornalczyk, A.; Cebulski, J.; Saternus, M.; Willner, J. Possibilites of platinum recovery from metal suppotred spent auto catalysts. *Metalurgija* **2014,** *53* (4), 609.

(71) Fornalczyk, A.; Saternus, M. Removal of platinum group metals from the used auto catalytic converter. *Metalurgija* **2009,** *48* (2), 133.

(72) Keav, S.; de los Monteros, A. E.; Barbier, J.; Duprez, D. Wet Air Oxidation of phenol over Pt and Ru catalysts supported on cerium-based oxides: Resistance to fouling and kinetic modelling. *Applied Catalysis B-Environmental* **2014,** *150*, 402.

(73) Barbier-Jr, J.; Delanoe, F.; Jabouille, F.; Duprez, D.; Blanchard, G.; Isnard, P. Total oxidation of acetic acid in aqueous solutions over noble metal catalysts. *Journal of Catalysis* **1998,** *177* (2), 378.

(74) Martín-Hernández, M.; Carrera, J.; Suárez-Ojeda, M. E.; Besson, M.; Descorme, C. Catalytic wet air oxidation of a high strength p-nitrophenol wastewater over Ru and Pt catalysts: Influence of the reaction conditions on biodegradability enhancement. *Applied Catalysis B: Environmental* **2012,** *123–124*, 141.

(75) Trawczynski, J. Noble metals supported on carbon black composites as catalysts for the wet-air oxidation of phenol. *Carbon* **2003,** *41* (8), 1515.

(76) Qin, J. Y.; Zhang, Q. L.; Chuang, K. T. Catalytic wet oxidation of p-chlorophenol over supported noble metal catalysts. *Applied Catalysis B-Environmental* **2001,** *29* (2), 115.

(77) Okitsu, K.; Higashi, K.; Nagata, Y.; Dohmaru, T.; Takenaka, N.; Bandow, H.; Maeda, Y. Decomposition of p-chlorophenol by wet oxidation in the presense of supported noble-metals catalysts. *Nippon Kagaku Kaishi* **1995,** (3), 208.

(78) Lafaye, G.; Barbier, J.; Duprez, D. Impact of cerium-based support oxides in catalytic wet air oxidation: Conflicting role of redox and acid-base properties. *Catalysis Today* **2015,** *253*, 89.

(79) Chen, I. P.; Lin, S. S.; Wang, C. H.; Chang, L.; Chang, J. S. Preparing and characterizing an optimal supported ceria catalyst for the catalytic wet air oxidation of phenol. *Applied Catalysis B-Environmental* **2004,** *50* (1), 49.

(80) Gaalova, J.; Barbier-Jr, J.; Rossignol, S. Ruthenium versus platinum on cerium materials in wet air oxidation of acetic acid. *Journal of Hazardous Materials* **2010,** *181* (1-3), 633.

(81) Mikulova, J.; Barbier-Jr, J.; Rossignol, S.; Mesnard, D.; Duprez, D.; Kappenstein, C. Wet air oxidation of acetic acid over platinum catalysts supported on cerium-based materials: Influence of metal and oxide crystallite size. *Journal of Catalysis* **2007,** *251* (1), 172.

(82) Masende, Z. P. G.; Kuster, B. F. M.; Ptasinski, K. J.; Janssen, F.; Katima, J. H. Y.; Schouten, J. C. Platinum catalysed wet oxidation of phenol in a stirred slurry reactor - The role of oxygen and phenol loads on reaction pathways. *Catalysis Today* **2003,** *79* (1-4), 357.

(83) Yang, S. X.; Feng, Y. J.; Wan, J. F.; Zhu, W. P.; Jiang, Z. P. Effect of CeO_2 addition on the structure and activity of RuO_2/gamma-Al_2O_3 catalyst. *Applied Surface Science* **2005,** *246* (1-3), 222.

(84) Pirkanniemi, K.; Sillanpaa, M. Heterogeneous water phase catalysis as an environmental application: a review. *Chemosphere* **2002,** *48* (10), 1047.

(85) Cooper, C.; Burch, R. An investigation of catalytic ozonation for the oxidation of halocarbons in drinking water preparation. *Water Research* **1999,** *33* (18), 3695.

(86) Zhang, Q. L.; Chuang, K. T. Alumina supported noble metal catalysts for destructive oxidation of organic pollutants in effluent from a softwood kraft pulp mill. *Industrial & Engineering Chemistry Research* **1998,** *37* (8), 3343.

(87) Kim, S. K.; Ihm, S. K. Nature of carbonaceous deposits on the alumina supported transition metal oxide catalysts in the wet air oxidation of phenol. *Topics in Catalysis* **2005,** *33* (1-4), 171.

(88) Zhang, Q. L.; Chuang, K. T. Kinetics of wet oxidation of black liquor over a Pt-Pd-Ce/alumina catalyst. *Applied Catalysis B-Environmental* **1998,** *17* (4), 321.

(89) Imamura, S.; Sasaki, H.; Shono, M.; Kanai, H. Structure of molybdenum supported on alpha-, gamma-, and chi-aluminas in relation to its epoxidation activity. *Journal of Catalysis* **1998,** *177* (1), 72.

(90) Heracleous, E.; Lemonidou, A. A. Reaction pathways of ethane oxidative and non-oxidative dehydrogenation on gamma-Al_2O_3 studied by temperature-programmed reaction (TP-reaction). *Catalysis Today* **2006,** *112* (1-4), 23.

(91) Weissman, J. G. Niobia-alumina supported hydroprocessing catalysts: Relationship between activity and support surface acidity. *Catalysis Today* **1996,** *28* (1-2), 159.

(92) Miro, C.; Alejandre, A.; Fortuny, A.; Bengoa, C.; Font, J.; Fabregat, A. Aqueous phase catalytic oxidation of phenol in a trickle bed reactor: Effect of the pH. *Water Research* **1999,** *33* (4), 1005.

(93) Masende, Z. P. G.; Kuster, B. F. M.; Ptasinski, K. J.; Janssen, F.; Katima, J. H. Y.; Schouten, J. C. Support and dispersion effects on activity of platinum catalysts during wet oxidation of organic wastes. *Topics in Catalysis* **2005,** *33* (1-4), 87.

(94) Kim, K. H.; Ihm, S. K. Characteristics of titania supported copper oxide catalysts for wet air oxidation of phenol. *Journal of Hazardous Materials* **2007,** *146* (3), 610.

(95) Béziat, J.-C.; Besson, M.; Gallezot, P.; Durécu, S. Catalytic Wet Air Oxidation on a Ru/TiO_2 Catalyst in a Trickle-Bed Reactor. *Industrial & Engineering Chemistry Research* **1999,** *38* (4), 1310.

(96) Mattson, J. S.; Mark, H. B.; Malbin, M. D.; Weber, W. J.; Crittend.Jc. Surface chemistry of active carbon – specific adsorption of phenols. *Journal of Colloid and Interface Science* **1969,** *31* (1), 116.

(97) Zogorski, J. S.; Faust, S. D.; Haas, J. H. Kinetics of adsorptin of phenols by granular activated carbon. *Journal of Colloid and Interface Science* **1976,** *55* (2), 329.

(98)   Prober, R.; Pyeha, J. J.; Kidon, W. E. Interaction of activated carbon with dissolved-oxygen. *Aiche Journal* **1975,** *21* (6), 1200.

(99)   Fortuny, A.; Miro, C.; Font, J.; Fabregat, A. Three-phase reactors for environmental remediation: catalytic wet oxidation of phenol using active carbon. *Catalysis Today* **1999,** *48* (1-4), 323.

(100)   Tukac, V.; Hanika, J. Catalytic wet oxidation of substituted phenols in the trickle bed reactor. *Journal of Chemical Technology and Biotechnology* **1998,** *71* (3), 262.

(101)   Tukac, V.; Hanika, J. Catalytic effect of active carbon black Chezacarb in wet oxidation of phenol. *Collection of Czechoslovak Chemical Communications* **1996,** *61* (7), 1010.

(102)   Rodriguez-Reinoso, F. The role of carbon materials in heterogeneous catalysis. *Carbon* **1998,** *36* (3), 159.

(103)   Fortuny, A.; Font, J.; Fabregat, A. Wet air oxidation of phenol using active carbon as catalyst. *Applied Catalysis B-Environmental* **1998,** *19* (3-4), 165.

(104)   Ledoux, M. J.; Pham-Huu, C. Silicon carbide - a novel catalyst support for heterogeneous catalysis. *Cattech* **2001,** *5* (4), 226.

(105)   Wei, Q. H.; Yang, G. H.; Yoneyama, Y.; Vitidsant, T.; Tsubaki, N. Designing a novel Ni-Al$_2$O$_3$-SiC catalyst with a stereo structure for the combined methane conversion process to effectively produce syngas. *Catalysis Today* **2016,** *265*, 36.

(106)   Tuler, F. E.; Portela, R.; Avila, P.; Bortolozzi, J. P.; Miro, E. E.; Milt, V. G. Development of sepiolite/SiC porous catalytic filters for diesel soot abatement. *Microporous and Mesoporous Materials* **2016,** *230*, 11.

(107)   Nhut, J. M.; Vieira, R.; Pesant, L.; Tessonnier, J. P.; Keller, N.; Ehret, G.; Pham-Huu, C.; Ledoux, M. J. Synthesis and catalytic uses of carbon and silicon carbide nanostructures. *Catalysis Today* **2002,** *76* (1), 11.

(108)   Moene, R.; Makkee, M.; Moulijn, J. A. High surface area silicon carbide as catalyst support characterization and stability. *Applied Catalysis a-General* **1998,** *167* (2), 321.

(109)   Guerfi, K.; Lagerge, S.; Meziani, M. J.; Nedellec, Y.; Chauveteau, G. Influence of the oxidation on the surface properties of silicon carbide. *Thermochimica Acta* **2005,** *434* (1-2), 140.

(110)   Chuang, K. T.; Cheng, S.; Tong, S. M. Removal and destruction of benzene, toluene, and xylene from waste-water by air stripping and catalytic-oxidation. *Industrial & Engineering Chemistry Research* **1992,** *31* (11), 2466.

(111)   Chuang, K. T.; Zhou, B.; Tong, S. M. Kinetics and mechanism of catalytic-oxidation of formaldehyde over hydrophobic catalysts. *Industrial & Engineering Chemistry Research* **1994,** *33* (7), 1680.

(112)   Tromans, D. Temperature and pressure dependent solubility of oxygen in water: a thermodynamic analysis. *Hydrometallurgy* **1998,** *48* (3), 327.

(113)   Sander, R. Compilation of Henry's law constants (version 4.0) for water as solvent. *Atmospheric Chemistry and Physics* **2015,** *15* (8), 4399.

(114)   Rosenberg, R. M.; Peticolas, W. L. Henry's law: A retrospective. *Journal of Chemical Education* **2004,** *81* (11), 1647.

(115)   David, M. D.; Fendinger, N. J.; Hand, V. C. Determination of Henry's law constants for organosilicones in acutal and simulated wastewater. *Environmental Science & Technology* **2000,** *34* (21), 4554.

(116)   Lavelle, K.; McMonagle, J. B. Mass transfer effects in the oxidation of aqueous organic compounds over a hydrophobic solid catalyst. *Chemical Engineering Science* **2001,** *56* (17), 5091.

(117)   Davies, D.; Golunski, S.; Johnston, P.; Lalev, G.; Taylor, S. H. Dominant Effect of Support Wettability on the Reaction Pathway for Catalytic Wet Air Oxidation over Pt and Ru Nanoparticle Catalysts. *Acs Catalysis* **2018,** *8* (4), 2730.

(118)   Digne, M.; Sautet, P.; Raybaud, P.; Euzen, P.; Toulhoat, H. Hydroxyl groups on gamma-alumina surfaces: A DFT study. *Journal of Catalysis* **2002,** *211* (1), 1.

(119)   Karim, A. M.; Rothstein, J. P.; Kavehpour, H. P. Experimental study of dynamic contact angles on rough hydrophobic surfaces. *Journal of Colloid and Interface Science* **2018,** *513*, 658.

(120)   Wu, J. C. S.; Chang, T. Y. VOC deep oxidation over Pt catalysts using hydrophobic supports. *Catalysis Today* **1998,** *44* (1-4), 111.

(121)   Saunders, K.; Davies, D.; Golunski, S.; Johnston, P.; Plucinski, P. Making the Most of Precious Metal Nanoparticles in the Purification of Industrial Wastewater by Catalytic Wet Air Oxidation Revealing synergy between platinum and catalyst support. *Johnson Matthey Technology Review* **2018,** *62* (4), 429.

Chapter 3

Experimental

3.1 Introduction

This chapter outlines the experimental methods used in this study, including catalyst preparation, characterization and activity testing. In order to be able to correlate catalytic activity with structure the catalysts were characterised using a range of both bulk and surface sensitive techniques. The principles behind these characterization methods are described, as well as experimental procedure.

3.2 List of materials and suppliers

Table 3.1 provides a list of the chemicals used throughout this study, including the purity of the material and supplier.

Table 3.1 List of materials used throughout this work

Substance	Purity	Supplier
$Pt(acac)_2$	minimum 48 % Pt	Alfa Aesar
$Ru(acac)_3$	≥ 97 %	Sigma Aldrich
$CeN_3O_8.6H_2O$	≥ 99.5 %	Alfa Aesar
Silicon carbide	---	Johnson Matthey
	Na ≥ 80 ppm	SiCAT
Alumina	---	Johnson Matthey
Phenol	≥ 99.9 %	Sigma Aldrich
Bisphenol A	≥ 99.9 %	Sigma Aldrich
Toluene	≥ 99.8 %	Sigma Aldrich
UHPLC water	≤ 0.0003 % impurity	Fischer Scientific
Methanol	≥ 99.9 %	Fischer Scientific
H_3PO_4	≥ 99.9 %	Sigma Aldrich

A range of metal precursors exist for platinum and ruthenium, the choice of which can affect the catalytic activity and properties of the resulting supported metal catalyst. For the low temperature water gas shift reaction over a Pt/TiO_2 catalyst, Iida et $al.$[1] found the catalytic activity decreased in the following order for the precursors used: $H_2PtCl_6.6H_2O \approx Pt(acac)_2 > [Pt(NH_3)_4]Cl_2 > [Pt(NH_3)_4](NO_3)_2$. Of the two precursors which lead to the highest catalytic activity, $H_2PtCl_6.H_2O$ was less desirable due to the presence of chlorine. Although chlorine is frequently used as a disinfectant in the water treatment industry, it is toxic to aquatic life and chlorinated water must be treated before release into the environment[2]. Chlorine in water courses can have negative impacts on the global environment and health[3,4], and to minimise the possibility of chlorine in the end stream of CWAO processes, $Pt(acac)_2$ was selected as the platinum precursor.

3.3 Catalyst preparation method

An extensive number of preparation methods are available for the synthesis of heterogeneous catalysts, each with their own advantages and disadvantages. One such preparation method is incipient wetness impregnation, which was used for the preparation of all the catalysts used in this study. Impregnation methods typically give rise to larger active metal particles on supported metal catalysts, compared with deposition-precipitation or sol immobilisation methods[5]. Although smaller metal particles are desirable for catalysis (as they allow for a higher percentage of exposed metal atoms, and thus potential active sites), the efficiency and minimal preparation steps required for impregnation make it a valuable tool for catalyst synthesis. Impregnation also does not require any complex or energy intensive steps (other than calcination)[6], making it a more economical and environmentally friendly method. Furthermore, impregnation allows for consistent replication of catalysts, which was important when relatively large quantities of the catalyst were required.

All catalysts were prepared by incipient wetness impregnation, followed by drying and finally, calcination. Impregnation was initiated by dissolving a metal

precursor in a minimum amount of solvent required to fill the pores, followed by addition of the support material. The solution is then left for a sufficient amount of time to ensure impregnation into the catalyst's pores, before being dried by rotary evaporation and calcined in static air. For the bimetallic catalysts, with the exception of the co-impregnated catalysts (where both active metal components were impregnated during the same step), the first metal would be impregnated, rotary evaporated, dried and calcined, before repeating the process with the second active metal component.

All of the precursors and catalyst supports were weighed separately on an analytical balance (4 d.p) to ensure the correct loading (weight percentage) of metal on the support. The catalysts were prepared in 10 g batches and the conditions kept as consistent as possible in order to maintain uniformity throughout batches.

3.3.1 Preparation of platinum catalysts

The same incipient wetness impregnation method was used to prepare all of the platinum catalysts, with a variety of silicon carbide supports.

The metal precursor, platinum acetylacetonate ($Pt(acac)_2$) (0.403 g), was dissolved in a minimum amount of toluene, approximately 30 mL for a 2 wt % (by mass) of platinum. The catalyst support (9.8 g) was then added to the dissolved precursor in a 250 mL round bottom flask and left for 24 hours at room temperature to impregnate.

After the initial impregnation step, the solvent was removed using a rotary evaporator equipped with a water bath, of which the temperature was set to 80 – 90 °C. The pressure was reduced gradually to 200 mbar until all of the solvent had been visually removed. The remaining solid was dried in an oven at 110 °C for a further 24 hours, to ensure any residual solvent had evaporated.

The final stage of the catalyst preparation involved calcination in a tube furnace under static air at 500 ^{o}C for 2 hours, with a ramp rate of 10 ^{o}C min^{-1}. During calcination the platinum precursor is reduced to platinum metal and oxides; the calcination temperature was chosen based on previous studies[7]. Once cooled, the catalysts were then ready for CWAO.

A portion of the catalysts required the support material to be of varying sizes, this was achieved by crushing the extrudates in a pestle and mortar, and sieving the particles to obtain the desired size ranges. The support was then subject to impregnation, as described above.

3.3.2 Preparation of ruthenium catalysts

The Ru/SiC catalysts were prepared in the same manner as the platinum catalysts, with ruthenium acetylacetonate (Ru(acac)$_3$) as the metal precursor.

For the comparatively hydrophilic catalyst, 2 % Ru/5 % ceria/alumina, the support material first had to be prepared by crushing the 3 mm alumina pellets in a pestle and mortar and sieved to achieve a particle size range between 0.425 – 0.6 mm.

The alumina support (9.3 g) was then added to a solution of cerium (III) nitrate hexahydrate (1.262 g) dissolved in a minimum amount of HPLC purity water and left for 24 hours at room temperature to impregnate. The solution was dried by rotary evaporation, followed by 24 hours at 110 ^{o}C to evaporate any residual water. The catalyst was then calcined under static air at 500 ^{o}C for 2 hours, with an initial ramp rate of 10 ^{o}C min^{-1}.

Once cooled, the method was repeated for ruthenium impregnation. The metal precursor Ru(acac)$_3$ (0.788 g) was dissolved in toluene (≈30 mL), the ceria/alumina added and allowed to impregnate for 24 hours, after which the solvent was evaporated by rotary evaporation. After drying for 24 hours at 110 ^{o}C the catalyst was calcined again under the same conditions.

3.3.3 Preparation of bi-metallic catalysts

For the preparation of ruthenium and platinum bi-metallic catalysts, the first metal would be impregnated, rotary evaporated, dried and calcined following the procedure described above and then the sequence repeated for the second metal.

For co-impregnation, both metal precursors were simultaneously dissolved in toluene, before impregnation onto the support, rotary evaporation, drying and finally calcination.

3.4 Catalyst characterisation techniques

3.4.1 Powder x-ray diffraction (XRD)

As the properties of a material are governed by its structure, powder x-ray diffraction is a key analytical technique used for phase identification of crystalline materials and can provide information on crystallite size.

A beam of incident x-rays is directed onto a powdered crystallite sample and the resulting diffraction angle of the photons is measured. The diffraction angle of the x-ray beam is dependent upon lattice spacing of the material and can be calculated using Bragg's law[8]:

$$n\lambda = 2dsin\theta$$

Equation 3.1, where λ = wavelength of incident x-rays (m), d = lattice spacing (m), θ = angle of diffraction, n = integer

Diffraction only occurs if the angle between the incident beam and diffracted beam is a function of 2θ[9]. When the x-rays interact with the surface, they are partially diffracted; the x-rays that are not initially diffracted pass through to the next layer of atoms in the lattice and are partially diffracted again, as illustrated in Figure 3.1[10].
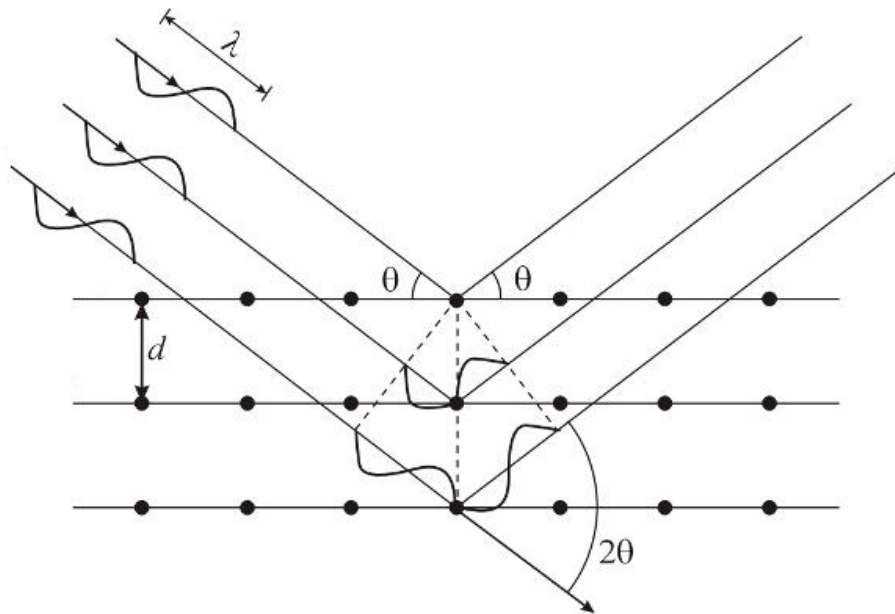
Figure 3.1 X-ray diffraction through a solid[10]

The XRD diffraction pattern plots the intensity of the diffracted radiation against the angle of the detector. The peaks in the XRD pattern are directly related to the atomic lattice spacing (d), which along with the diffraction angle can be used to identify the crystal structure of the sample by comparison with a reference database.

The average crystallite size of the powder can also be determined using the Scherrer equation. Smaller crystallites produce broader peaks in the XRD diffraction pattern due to fewer repeating lattice planes. Essentially the smaller a crystallite is, the broader the angle of diffracted x-rays[11]. It is therefore possible to calculate the average size from the peak width at half maximum (FWHM) using the Scherrer equation[12]:

$$D = \frac{K\lambda}{\beta cos\theta}$$

Equation 3.2, where D = average crystallite size (nm), K = Scherrer constant,
λ = wavelength of x-rays (nm), θ = angle of diffraction, β = peak width at FWHM

The average crystallite size can help give an insight into the distribution of active nanoparticles, however the Scherrer equation does come with a large degree of error. For analysis to be meaningful, the peak width must be purely the result of the material itself and free from effects that cause peak broadening, such

as dislocations, stacking faults, micro-strain within the sample and instrumental broadening[13]. Typically, the average crystallite size calculated from Scherrer equation is overestimated by 15 % for crystallite sizes up to 100 nm[14].

Despite the error in crystallite size measurement, XRD is a useful tool in the characterisation of heterogeneous catalysis and allows for the determination of structural composition.

Experimental

A PANanalytical X'pert PRO diffractometer with a CuKα radiation source working at 40 KeV and 40 mA was used to characterise the catalysts. The samples were ground into a powder using a pestle and mortar and packed into a sample holder. X'Pert Data Collector software was used to analyse the diffraction patterns, and phase identification was carried out using the International Centre Diffraction Data (ICDD) database. The crystallite sizes were determined by the X'Pert software using the Scherrer equation.

3.4.2 Nitrogen physisorption using Brunauer Emmet Teller (BET) method

The surface area of a catalyst is closely linked to catalytic performance; the higher the surface area, the higher the potential of exposed active sites and the higher potential activity. Brunauer Emmett Teller (BET) surface area analysis provides specific surface area evaluation of materials using the principle of physisorption of nitrogen gas on the surface of the catalyst at -196 °C, measured as a function of relative pressure. Essentially, the higher the surface area of a material, the more gas adsorbed and vice versa. A flow of nitrogen gas is passed over the sample at varying pressures and the adsorption capability calculated using the BET adsorption isotherm[15]:

$$\frac{P}{V_a(P_0 - P)} = \frac{1}{V_m C} + \frac{(C-1)}{V_m C} \; x \; \frac{P}{P_0}$$

Equation 3.3, where P = pressure, P_0 = saturation pressure, V_a = volume of gas (N_2) adsorbed,
Vm = volume of monolayer, C = multi-layer adsorption parameter

Which in turn allows for the calculation of surface area:

$$s. a. = \frac{V_m \sigma N_a}{mv}$$

Equation 3.4, where σ = molecular area of N_2 (0.162 nm^2), N_a = Avogadro's number,
m = mass of sample, v = molar volume of gas

Firstly, before the BET surface areas can be measured, the samples must first be 'degassed' to remove any gases or vapours that may already be physically adsorbed onto the surface. If any adsorbed gases are present on the surface and the material is not degassed, this would have a negative effect on the final specific surface area value. Once the surface is free of any adsorbed species the sample is cooled to cryogenic temperatures using liquid nitrogen and then exposed to an inert gas at a chosen number of pressure points, in the case of this study a 5-point method with nitrogen gas was used. Typically, for a Type II isotherm (Figure 3.2), as the pressure is increased the number of N_2 molecules physiosorbed to the surface also increases, until the saturation pressure, P_0 is reached. The saturation pressure is the pressure at which the catalyst surface has become fully saturated with N_2 and no further adsorption occurs. The volume of N_2 adsorbed by the material is measured at each pressure point and plotted against P/P_0 to give the BET isotherm, from which the surface area can be calculated.
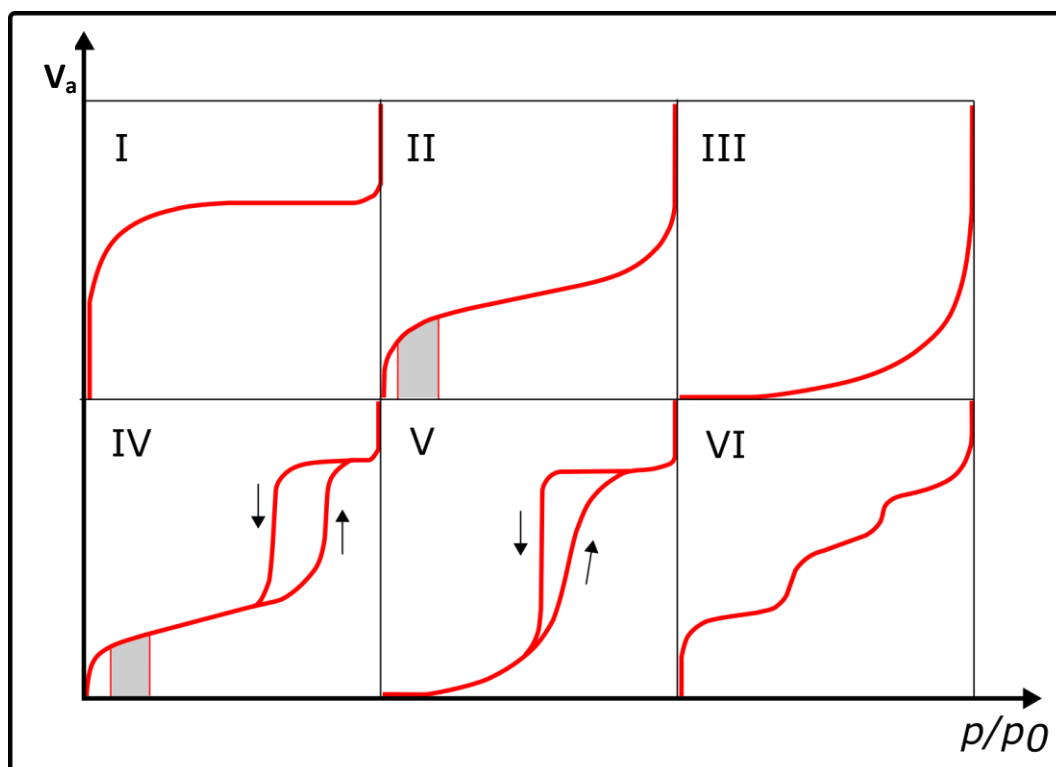
Figure 3.2 Typical BET adsorption isotherms[16]

The majority of physisorption isotherms can be grouped into six categories, as shown in Figure 3.2[16]. Type I isotherms are typical of microporous solids with relatively low external surface area and indicative of monolayer only adsorption[17,18]. Type II represents multi-layer adsorption, further adsorption after the monolayer; such isotherms are characteristic of samples with a large pore size distribution[17]. The shaded area underneath the curve represents when the monolayer saturation point is reached and multi-layer adsorption begins[17]. Type III isotherms are not commonly observed for N_2 adsorption on catalysts; they are typical of materials with an indistinct monolayer, shown by the convex curve and lack of saturation point on the isotherms[17,19]. Type IV isotherms are typical of mesoporous materials and follow an initial path similar to Type II multi-layer adsorption, but with finite multi-layers, indicating complete filling of pores[18]. Type V is similar to Type III isotherms and are also uncommon, they indicate weak adsorbent − adsorbate interactions[17]. Finally, Type VI isotherms represents stepwise multi-layer adsorption characteristic of uniform non-porous materials. The sharpness of the distinct layers for Type VI is dependent upon the temperature of analysis[17].

Experimental

The BET surface area of the catalysts was determined *via* a 5-point nitrogen adsorption method using a Quantochrome NOVA 2200e Surface Area and Pore Size Analyser instrument. Approximately 50 mg of catalyst was initially pre-treated by degassing under vacuum at 150 °C for a minimum of 3 hours. The samples were kept at cryogenic temperatures under liquid nitrogen for the duration of the analysis.

BET was not able to establish the pore volume of the samples, therefore helium pycnometry was carried out using a Micrometrics AccuPyc II 1340 Gas Pycnometer to gain an insight into the porosity of the samples. Helium pyconmetry relies on the same principals of adsorption as BET with helium gas used as the adsorbate; helium can penetrate further into the catalyst pores due to its smaller size. Oxidation reactions can rely heavily on mass transfer; thus, it is important to establish any contributions porosity and surface area may have on CWAO.

3.4.3 Thermogravimetric analysis (TGA)

Thermogravimetric analysis (TGA) is an analytical technique in which the mass of a material is continuously monitored as a function of temperature and time[20]. A sample is subjected to elevated temperatures under a controlled atmosphere, and the resulting thermogravimetric (TG) curve shows the percentage mass change of the sample against temperature[21].
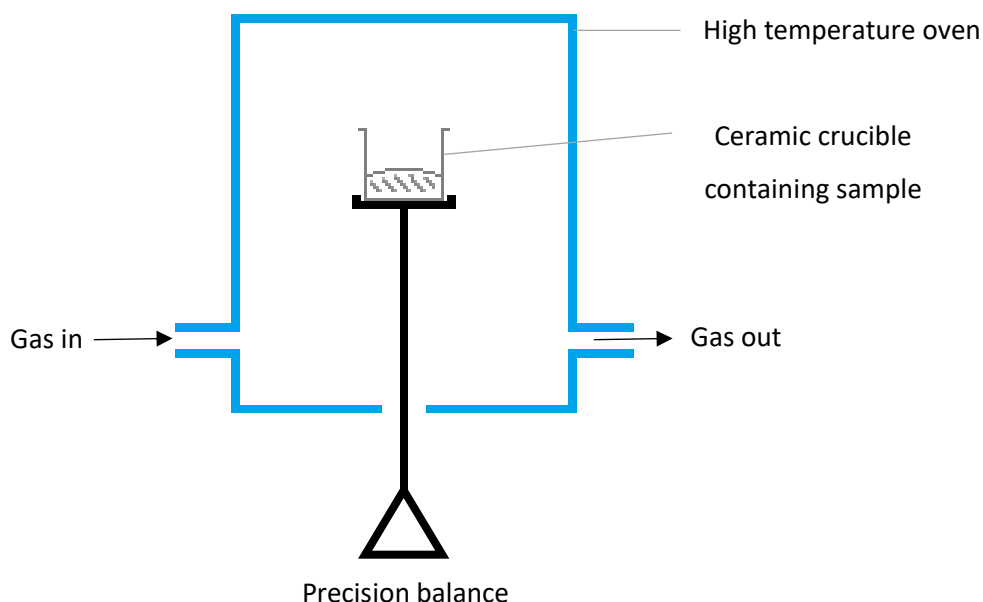
Figure 3.3 Illustration of typical TGA instrument

Figure 3.3 illustrates a typical set up of a TGA instrument, consisting of a top-loading crucible supported on a precision mass balance, surrounded by a high temperature furnace. The rate at which the temperature is increased, the maximum temperature, the gas flow rate and the duration between mass measurements are all parameters that can be varied.

TGA can provide important information on both fresh and post-reaction catalysts. TGA can help determine appropriate calcination conditions by monitoring the temperature at which metal precursors decompose, as well as evaluating the thermal stability of a catalyst in an oxidative environment, similar to the conditions experienced during CWAO. TGA of used catalysts can reveal possible changes that may have occurred during the reaction, such as adsorption of certain species that may lead to catalyst deactivation. Carbon impurities would be oxidised to CO_2 during heating under an oxidising atmosphere, resulting in a decrease in mass which would be shown in the TG curve.

TGA was further used to establish the relative hydrophobicity of the catalysts in this study, by monitoring the loss of adsorbed water as well as the temperature and rate at which the water was evaporated.

Experimental

TGA was carried out using a Perkin Elmer 400 thermogravimetric analyser, with approximately 30 – 50 mg of sample. The sample was loaded into a ceramic crucible and heated from 30 – 900 °C at 10 °C min^{-1} under 20 mL min^{-1} of flowing air. The sample mass, temperature and time were recorded using *Pyris* software linked to the instrument.

3.4.4 Temperature programmed reduction (TPR)

Temperature programmed reduction (TPR) is a widely used characterisation technique for determining the reduction potential (reducibility) of solids and catalysts[22,23].

Samples are exposed to a flow of a reducing gas mixture, typically hydrogen in an inert gas such as argon, at increasing temperatures. The concentration of hydrogen consumed by the sample is measured *via* a thermal conductivity detector (TCD)[24] and can be used to calculate reduction potential of a catalyst. By comparison with other reduction profiles characteristic to certain compounds, redox properties and oxidation states can be determined. The temperature at which a peak occurs, along with the shape and size of the peak can reveal information on the chemical nature, environment and quantity of the reducible species[25]. Compounds present on the surface can reduce at different temperatures than those in the catalyst bulk.

The redox properties of a catalyst can influence its activity; Pt^0 has been shown to be the active metal component (compared to Pt^{2+}) for CWAO[26,27]. Therefore, TPR is a crucial technique for evaluation of the oxidation states of the active metal component for comparison with catalyst performance.

Experimental

TPR was carried out using a Quantochrome ChemBET TPR/TPD Chemisorption Analyser with approximately 50 mg of catalyst sample placed in a U-tube between small amounts of quartz wool. The catalysts were subject to pre-treatment in flowing 5 % helium/argon (flow rate 14 cm^3 min^{-1}) at 110 °C for 45 minutes in order to remove any weakly adsorbed species which could interfere with the analysis.

After pre-treatment, the catalysts were subjected to a flow of 5 % hydrogen/argon at a flow rate of 14 cm^3 min^{-1}, between 40 – 800 °C using a ramp rate of 15 °C min^{-1}. The hydrogen consumption was measured with a TCD and the data plotted as a function of temperature using TPRWin software.

3.4.5 X-ray photoelectron spectroscopy (XPS)

X-ray photoelectron spectroscopy (XPS) is a surface sensitive technique used for quantitative and qualitative analysis of the elemental composition on the surface of a solid sample. The elemental composition, empirical formula, chemical and electronic states of a catalyst can all be determined. Although XPS is primarily a surface sensitive technique, depending on experimental parameters, the first 20 atomic layers may be probed[19,28].

A sample is subjected to x-ray radiation, ionising the compound, exciting the core electrons, which are then detected by the XPS instrument. The ejected electrons energies can be determined using the following equation based on the energy of the incident x-rays[29,30]:

$$h v = \frac{1}{2} m_e v^2 + I_i$$

Equation 3.5, where h = Plank's constant (6.626 x 10^{-34} m^2 kg s^{-1}), v = incident x-ray frequency (s^{-1}), m$_e$ = mass of an electron (9.109 x 10^{-31} kg), v = velocity (m s^{-1}), I$_i$ = ionisation energy of an electron from orbital I (m^2 kg s^{-2})

The energy of the emitted electron is characteristic of the element it originated from and the relative peak intensities in the XPS spectrum can be used to quantify the elements as a percentage of the surface measured and provide information on their oxidation states.

Experimental

XPS analysis was performed using a Thermo Fischer Scientific K-alpha+ spectrometer. The samples were adhered onto the sample holder by double sided scotch tape and analysed using a 72 W micro-focused monochromatic A1 x-ray source over a 400 μm area. CasaXPS software was used to analyse the spectra; peaks were fitted to Gaussian Lorentzian curves with Shirley backgrounds.

3.4.6 Scanning electron microscopy (SEM) and energy dispersive x-ray (EDX) spectroscopy

Scanning electron microscopy (SEM) is a surface analytical technique which produces high-resolution images of surface topography of a solid material. Coupled with energy dispersive x-rays spectroscopy (EDX), it is possible to determine the elemental composition and average size of metal particles present of the surface[31]. The schematic of a typical SEM instrument is illustrated in Figure 3.4.
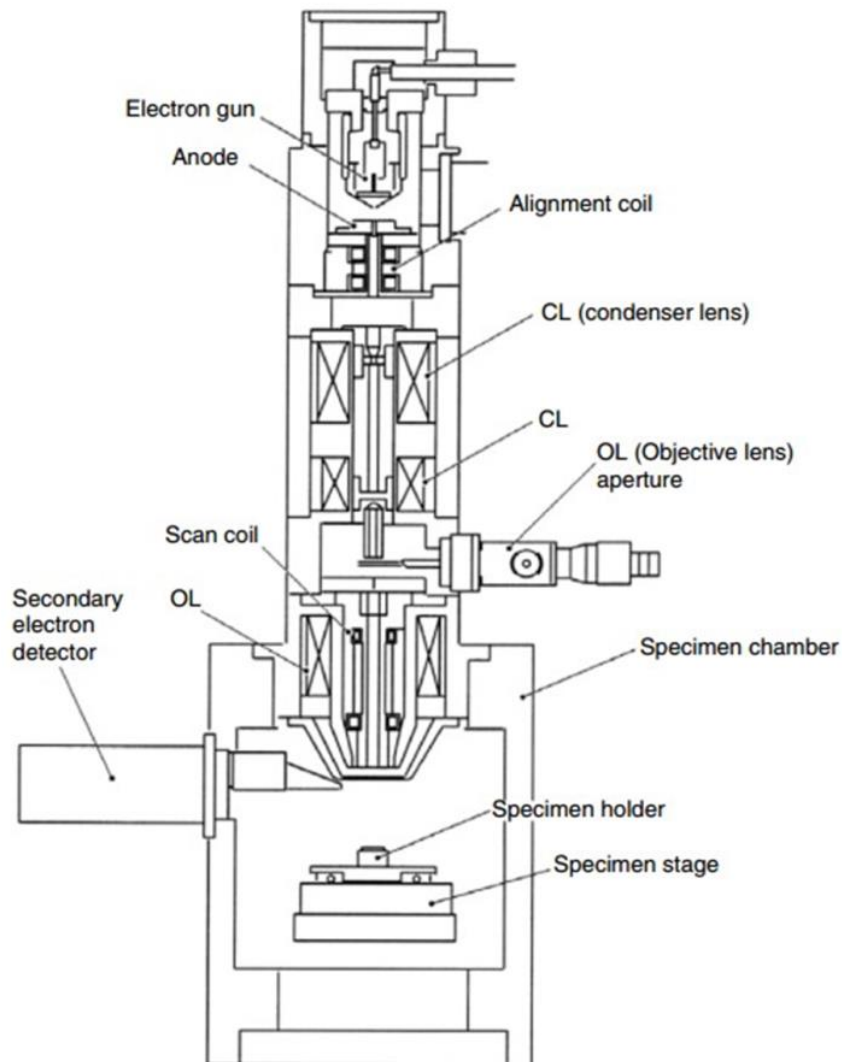
Figure 3.4 Schematic of a typical SEM instrument[32]

A scanning electron beam, produced *via* application of voltage to a tungsten filament, is focused through condenser lenses onto the sample[33]. When the primary electron beam interacts with the sample, the resultant back-scattered or secondary electrons are detected to produce an image of the surface. The intensity of the secondary electrons is governed by the surface topography of the sample and so an image can be constructed by measuring secondary electron intensity as a function of position of the scanning primary electron beam. The contrast in the image represents the topography of the sample, as backscattered electrons typically come from atoms further within the bulk of the sample. Heavier elements (with larger atoms) are better at scattering the electron beam and thus the intensity of the backscattered electrons can be correlated to the atomic number of the element. This also gives rise to heavy metals appearing brighter in

SEM images[33]. SEM/EDX analysis is conducted under vacuum and typically instruments have resolutions up to 5 nm.

Experimental

Three different SEM instruments were used throughout the study, a Hitachi TM3030Plus Tabletop Microscope, a Carl Zero Supra SEM microscope 35VP and a Tescan MAIA3 Triglav FEG-SEM. In each case the samples were mounted on carbon adhesive discs, and images captured at varying magnifications. The chemical composition of the samples was measured using the equipped EDX analysers.

A minimum of 10 images were captured per sample, at various positions along the material's surface and at different magnifications to provide a better representation of the sample.

For samples which required analysis of a cross-section of the catalyst pellet, the pellets were sliced width-wise using a scalpel and mounted face up on the carbon adhesive discs. These catalysts were also ground to a powder using a pestle and mortar and subject to EDX analysis.

3.5 Catalyst activity testing for CWAO of phenol

The catalysts were tested for the catalytic wet air oxidation of phenol in a continuous flow trickle bed reactor with real-time analysis of the end stream by high performance liquid chromatography (HPLC). The complete oxidation of phenol to CO_2 and H_2O follows a complex reaction pathway, proceeding through a variety of intermediates; HPLC analysis allows for the detection of these intermediates and so partial oxidation of phenol can also be monitored.

3.5.1 Trickle bed reactor (TBR)

Figure 3.5 illustrates the trickle bed reactor set-up, with the essential components for CWAO labelled; below is an accompanying description of how the contaminated wastewater was processed through the reactor. The majority of the reactor components were connected by 9 mm diameter stainless-steel tubing.
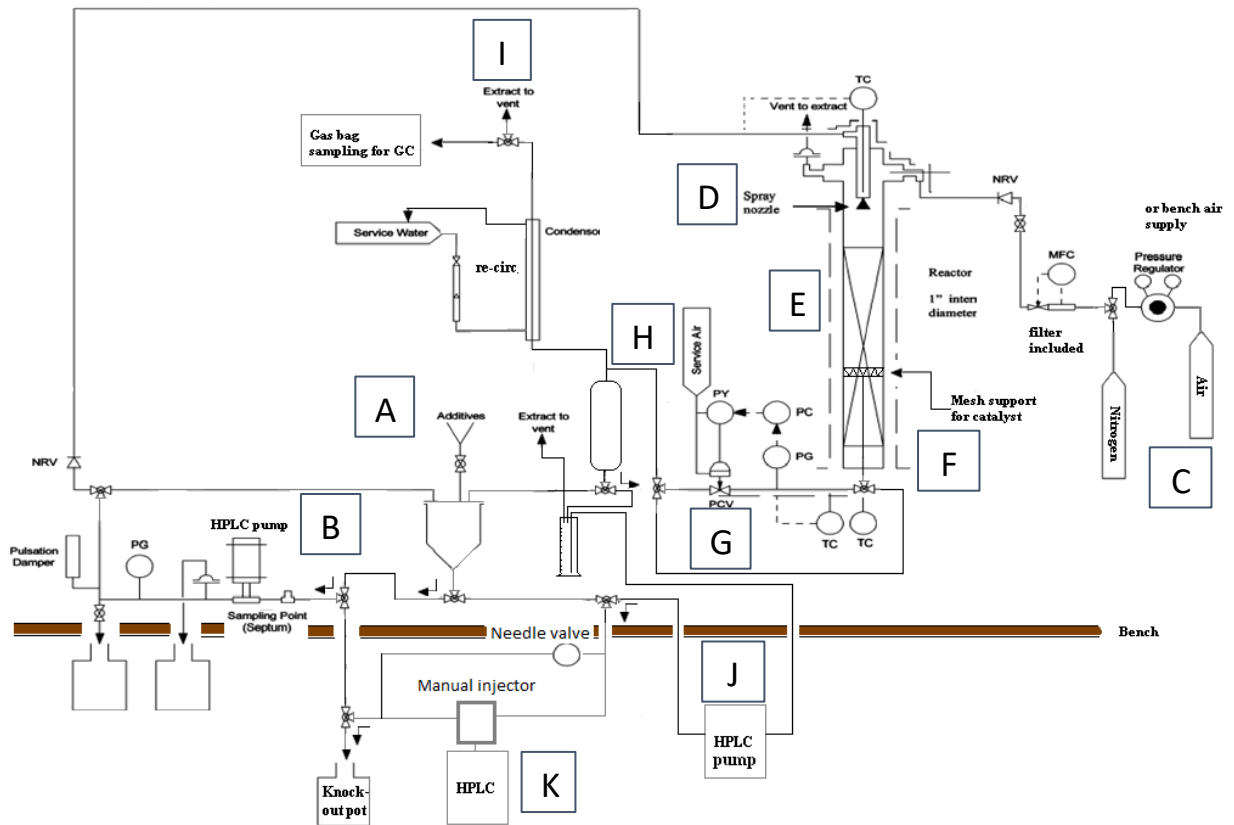
Figure 3.5 Trickle bed reactor (TBR) schematic for CWAO of phenol

A – phenol solution inlet

B – HPLC pump 1

C – compressed air supply

D – spray nozzle

E – reactor containing catalyst bed

F – furnace

G – pneumatic actuator

H – gas- liquid separation

I – gas phase vent

J – HPLC pump 2

K – HPLC instrument

An aqueous phenol solution was prepared by dissolving phenol (2.5 g) in a 2.5 L Winchester bottle of HPLC purity water to give a concentration of 1 g L^{-1}. Each time a new phenol solution was prepared its precise concentration ($\pm$ 0.01 mg L^{-1}) was measured using HPLC and used to calculate total phenol conversion achieved by the various catalysts. This concentration was chosen as benchmark for toxic organic wastewater in previous CWAO studies and is realistic of the concentrations typically found in phenolic wastewaters[7].

The aqueous phenol solution was fed into the additives pot (A) and HPLC pump 1 (B) was responsible for delivering the liquid phase to the catalyst bed at a chosen flow rate. The gas phase (compressed air) was stored in a pressurised cylinder (C) and delivered by a mass flow controller (MFC) connected to a control box, which allowed for a specific flow rate to be set. Both the liquid and gas phases were dispersed using a spray nozzle (D) and allowed to flow co-currently together through the catalyst bed (E).

The catalytic reactor (E) was a removable 10 cm length of stainless-steel tubing (9 mm inner diameter), which could be detached and filled with a desired catalyst. A wire mesh and quartz wool were placed inside to keep the packed bed of catalyst securely in place. The catalytic reactor was surrounded by a furnace (F) connected to the same control box as the MFCs from which the reaction temperature could be set. Multiple thermocouples were placed both inside the stainless-steel tubing and within the furnace to monitor the catalyst temperature and furnace temperature. Glass wool and insulating tapes were placed around tubing to reduce heat loss.

A pneumatic actuator (G) controlled the reaction pressure whilst also maintaining a continuous process. The actuator was linked to the control box where the reaction pressure could be set; a secondary supply of compressed air was necessary to keep the spring-loaded valve open enough to maintain reaction pressure whilst also maintaining the continuous flow.

Once the liquid and gas phases had trickled through the catalyst bed (E) and flowed past the pneumatic actuator (G) the two phases were separated by a

sealed measuring cylinder (H). The measuring cylinder collected the liquid phase and allowed for additional monitoring of the liquid flow rate. The gas phase was vented off through plastic tubing into a fume cupboard (I).

HPLC pump 2 (J) fed the collected liquid phase through another line, fitted with an inlet filter, to the HPLC instrument where analysis of the outlet stream took place, before collecting in a knock out pot (K) to be safely disposed of.

3.5.1.1 Standard reactor conditions

To accurately compare the catalytic activities, reactor conditions were kept as consistent as possible. The reactor conditions were modelled after those described by Fortuny *et al.*[34] and optimized by Davies *et al.*[7] to allow for comparison to results found in the literature. Table 3.2 lists the typical conditions used in this study.

Table 3.2 Reactor conditions used for the CWAO of phenol

Variable	
Temperature	$80 - 160\ ^{\circ}C$
Pressure	$0 - 13.1\ bar_{(g)}$
Liquid flow rate	$1.1\ mL\ min^{-1}$
Gas phase flow rate	$144\ mL\ min^{-1}$
Phenol concentration	$1\ g\ L^{-1}$
Catalyst mass	$8\ g$

3.5.2 Liquid phase analysis by high performance liquid chromatography (HPLC)

High performance liquid chromatography (HPLC) and UV visible detection were used to analyse the off stream, and measure the concentration of phenol oxidised during the reaction. HPLC is responsible for separating the compounds present in the liquid phase, whilst UV-vis identifies and quantifies these

compounds. The reactor effluent was continuously fed through a sample loop within the HPLC instrument, where analysis injections were periodically taken.

A mobile phase carries the sample at high pressure through a column containing chromatographic packing material (the stationary phase). As samples pass through the column, they interact with the stationary phase; this interaction dictates the retention time of different compounds. For example, a polar sample would have a strong affinity to a polar stationary phase, resulting in a longer retention time than a non-polar sample passing through the same column. The time taken to elute through the column (the retention time) allows for separation of different species in the analyte, which can then be identified by UV-vis detection. Depending on the analyte, the stationary and mobile phases can be tailored for detection of specific compounds based on the degree of interaction.

A reverse phase (C18-Shim-pack XR-ODS: 3 mm diameter, 50 mm length) packed bed column was used to separate products, with a methanol based mobile phase. The reverse phase column refers to a hydrophobic stationary phase as opposed to a typical hydrophilic column. In contrast, the mobile phase was hydrophilic, which allowed for faster elution of hydrophilic compounds. A gradient flow method was used for the mobile phase, an initial concentration of 4.7 % MeOH in H_2O, was linearly increased between 4 – 8 minutes (17 minutes total analysis time) to 60 % MeOH in H_2O. Gradient flow of the mobile phase allowed for further flexibility regarding compound separation as well as optimization of the analysis time. Small amounts of phosphoric acid (0.22 vol% H_3PO_4) was also included in the mobile phase to reduce peak tailing and ensure the stationary phase remained protonated after organic acids passed through the column. A constant temperature of 30 ^{o}C was maintained throughout the HPLC instrument to ensure consistent separation.

Once separated, a dual wavelength UV detector identified the products in order of elution. The detector used the varying UV absorptions to quantify the products. Based on the phenol oxidation pathways discussed in Chapter 1, the HPLC analysis was designed for the detection of nine of the most common intermediates. Each of these intermediates, as well as phenol, were calibrated

from standards at different known concentrations - the resulting calibration curves can be found in the Appendix. Figure 3.6 shows a typical HPLC chromatogram from the CWAO experiments showing the observed products; the concentration of phenol is represented by the peak at a retention time of 10.8 minutes.
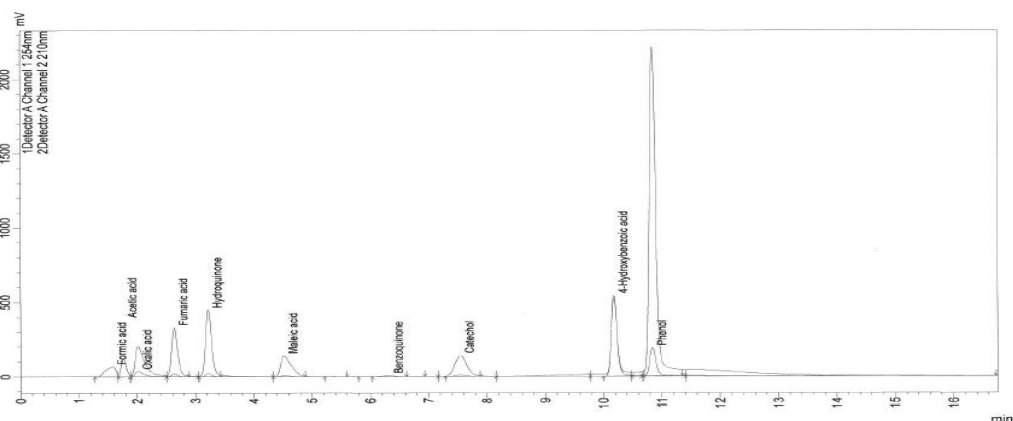
Figure 3.6 A typical chromatogram of phenol and its partial oxidation products for CWAO

HPLC analysis of the wastewater took 17 minutes and the resulting chromatogram after each measurement was used to calculate the phenol conversion achieved by the catalysts.

3.6 Catalyst activity testing for CWAO of bisphenol A (BPA)

For the investigation into CWAO of BPA (Chapter 6), the activity testing was carried out at the National Institute of Chemistry in Ljubljana, Slovenia, using a PID Microactivity trickle bed reactor. Analysis of the end stream was conducted by HPLC and Total Organic Carbon measurements (TOC).

3.6.1 Trickle bed reactor (TBR)

Catalyst activity testing was conducted in a PID Eng&Tech Mircoactivity Reference unit, an automated, fixed bed, continuous-flow trickle bed reactor.

Liquid and gaseous flows were introduced into the hot box system concurrently, where both phases were preheated separately before introduction into the reactor unit containing the catalyst bed. The reactor schematic is illustrated in Figure 3.7.
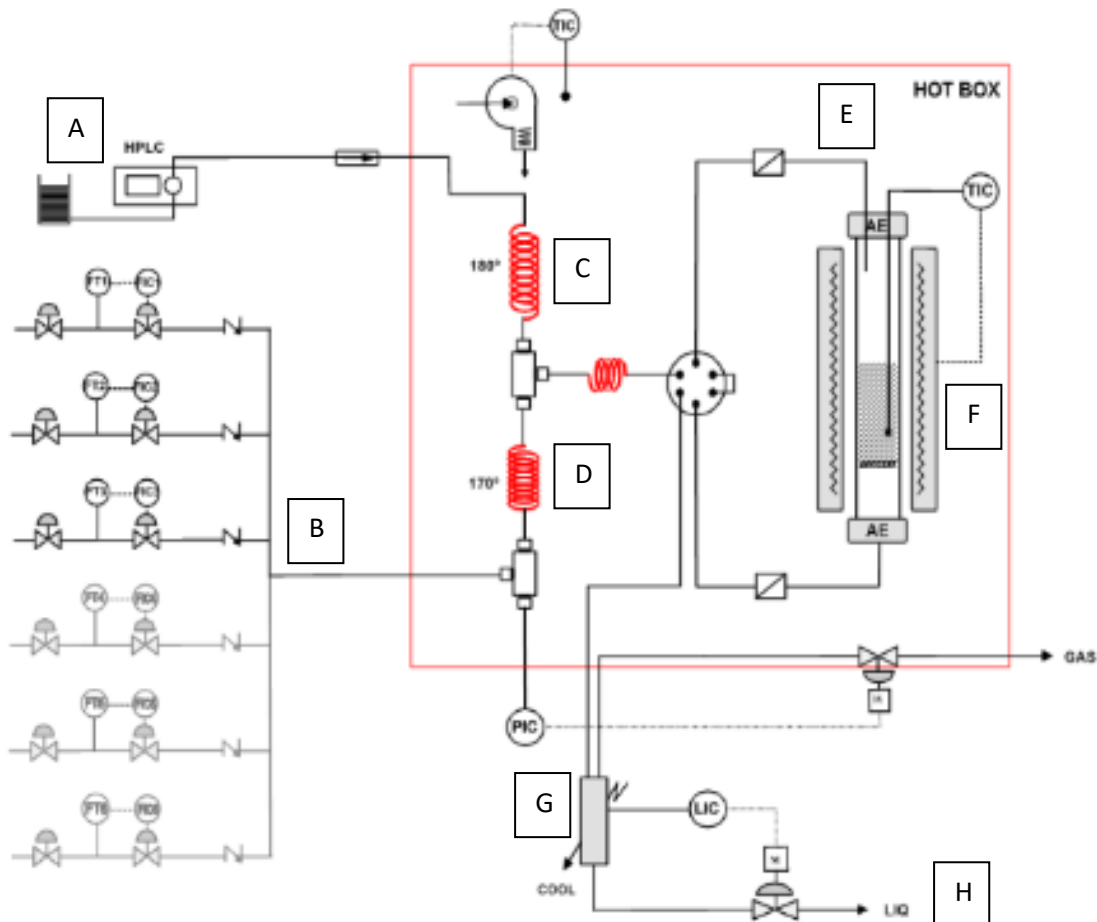
Figure 3.7 TBR schematic for CWAO of BPA

A – BPA solution and HPLC pump   E – gas - liquid inlet

B – mass flow controllers   F – catalyst bed

C – liquid phase pre-heating   G – gas - liquid separation

D – gas phase pre-heating   H – liquid phase collection

The TBR schematic illustrates the rig design, whereby the aqueous BPA solution was fed into the reactor *via* a Gilson 307 HPLC pump at a desired flow rate (A). To replicate compressed air, a gas mix of 20.8 % oxygen and 79.2 % nitrogen was introduced into the reactor *via* Bronkhorst EL-FLOW mass-flow controllers (B). The gas and liquid phases were heated separately in the hot box (C & D), before introduction to the reactor (E). The catalyst bed was held in place by a removable

2 μm Hastelloy porous plate contained in a stainless-steel tube of dimensions 305 mm x 9 mm (inner diameter) (F). The gas and liquid phase were flowed co-currently over the catalyst and then separated (G). Liquid phase samples were collected periodically throughout the experiments by an ADVANTEC CHF122SC fraction collector and analysed using HPLC and UV detection (H).

Unless otherwise stated, the standard operating conditions for catalyst activity studies are outlined in Table 3.3.

Table 3.3 Standard operating conditions used for CWAO of BPA

Variable	
Reactor temperature (^{o}C)	60
Hot box for liquid and gas pre-heating temperature (^{o}C)	40
Reactor pressure (bar$_{(g)}$)	7
Initial BPA concentration (mg L^{-1})	60
Mass of catalyst (g)	2
Liquid flow rate (mL min^{-1})	2
Gas flow rate (mL min^{-1})	120

3.6.2 High performance liquid chromatography (HPLC)

The reactor effluent was periodically collected and the BPA content analysed by high performance liquid chromatography (HPLC) separation followed by ultraviolet (UV) detection. A Thermoscientific SCM 1000 HPLC with a C18 (4.6 mm diameter and 100 mm length) reversed phase column was responsible for separating the eluted products along with a mobile phase consisting of 70 % methanol in water, pumped at a rate of 0.5 mL min^{-1}. Once separated, any BPA present in the sample was detected and quantified by UV detection, Figure 3.8 shows a typical chromatogram, with the retention time of BPA at 6 minutes.
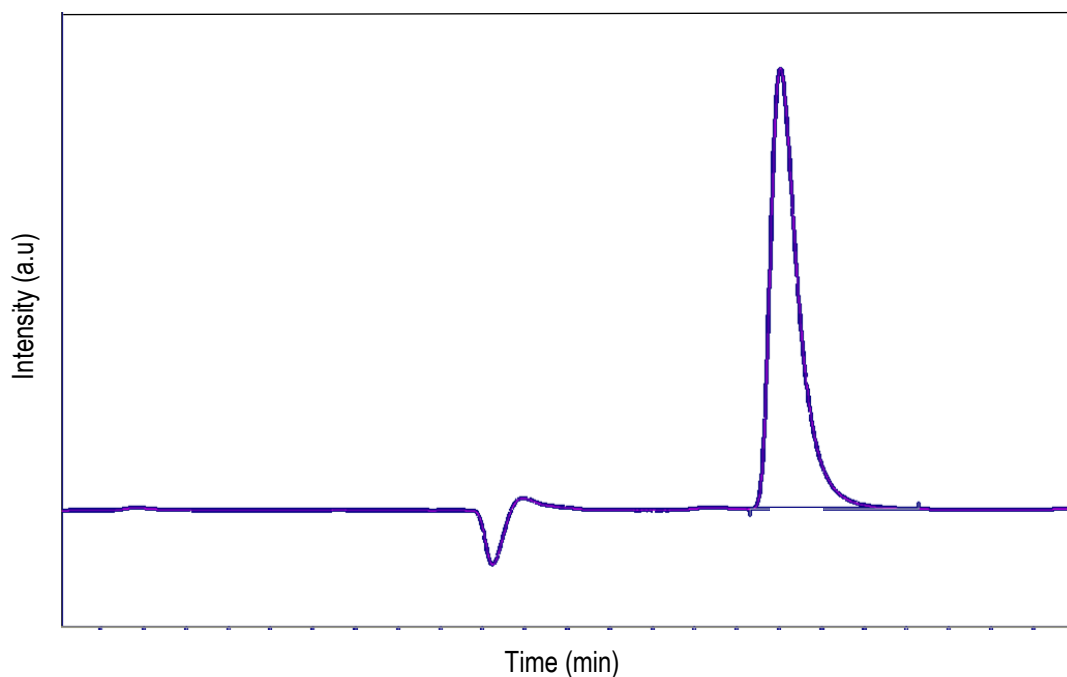
Figure 3.8 A typical HPLC chromatogram of bisphenol A

Under the reactor set up for CWAO of BPA, it unfortunately wasn't possible to measure the concentrations of common oxidation intermediates by HPLC, and so the total organic carbon (TOC) content of the off stream was used as a measure of complete oxidation.

3.6.3 Total organic carbon (TOC) measurements

The extent of mineralization of BPA was determined by measure of the total organic carbon (TOC) content of the effluent. The TOC content is a measure of the concentration of organic molecules present in wastewater and is commonly used as a non-specific indicator of water quality[35].

TOC analysis was carried out using a Teledyne Tekmer Torch TOC analyser, equipped with a high pressure NDIR detector. Before any TOC evaluations took place, the instrument was calibrated with 18.2 MΩ HPLC purity water, likewise used in the synthesis of the aqueous BPA solution.

3.7 References

(1)   Iida, H.; Kondo, K.; Igarashi, A. Effect of Pt precursors on catalytic activity of Pt/TiO$_2$ (rutile) for water gas shift reaction at low-temperature. *Catalysis Communications* **2006,** *7* (4), 240.

(2)   Ferraris, M.; Chiesara, E.; Radice, S.; Giovara, A.; Frigerio, S.; Fumagalli, R.; Marabini, L. Study of potential toxic effects on rainbow trout hepatocytes of surface water treated with chlorine or alternative disinfectants. *Chemosphere* **2005,** *60* (1), 65.

(3)   Tundo, P.; He, L.-N.; Lokteva, E.; Mota, C.; Chemistry beyond chlroine. *Springer Nature*, **2016**. 3 - 605

(4)   Tundo, P. Chlorine-free synthesis: An overview. *Pure and Applied Chemistry* **2012,** *84* (3), 411.

(5)   Campanati, M.; Fornasari, G.; Vaccari, A. Fundamentals in the preparation of heterogeneous catalysts. *Catalysis Today* **2003,** *77* (4), 299.

(6)   Schwarz, J. A.; Contescu, C.; Contescu, A. Methods for preparation of catalytic materials. *Chemical Reviews* **1995,** *95* (3), 477.

(7)   Davies, D.; Catalytic Wet Air Oxidation: Developing a Continuous Process: Cardiff University PhD Thesis, **2016**.

(8)   Jauncey, G. E. M. The scattering of X-rays and Braggs law. *Proceedings of the National Academy of Sciences of the United States of America* **1924,** *10*, 57.

(9)   Warren, B. E.; X-ray Diffraction. *Addison-Wesley Pub*, **1969**.

(10)   Ku Leuven; X-ray diffraction, *Institute for nuclear and radiation physics*, **2019**.

(11)   Uvarov, V.; Popov, I. Metrological characterization of X-ray diffraction methods at different acquisition geometries for determination of crystallite size in nano-scale materials. *Materials Characterization* **2013,** *85*, 111.

(12)   Dagostino, A. T. Determination of thin metal-film thickness by x-ray-diffractometry using the scherrer equation, atomic-absorption analysis and transmission reflection visible spectroscopy. *Analytica Chimica Acta* **1992,** *262* (2), 269.

(13)   Chung, F. H; Industrial applications of x-ray-diffraction. *American Laboratory* **1989,** *21* (2), 144.

(14)   Hargreaves, J. S. J. Some considerations related to the use of the Scherrer equation in powder X-ray diffraction as applied to heterogeneous catalysts. *Catalysis Structure & Reactivity* **2016,** *2* (1-4), 33.

(15)   Brunauer, S.; Emmett, P. H.; Teller, E. Adsorption of gases in multimolecular layers. *Journal of the American Chemical Society* **1938,** *60*, 309.

(16)   Connelly, A.; BET surface area, Laboratory Techniques, Science, **2017**.

(17)   Sing, K. S. W. Reporting physisorption data for gas solid systems - with special reference to the determination of surface-area and porosity. *Pure and Applied Chemistry* **1982,** *54* (11), 2201.

(18)   Chorkendorff , I.; Niemantsverdriet, J. W.; Concepts of modern catalysis and kinetics, 1st ed.; *Wiley*, **2003**.

(19) Carter, J.; Gold catalysis for the low temperature water gas shift reaction. Cardiff University, **2016**.

(20) Fang, H. L.; DaCosta, H. F. M. Urea thermolsis and NOx reduction with and without SCR catalysts. *Applied Catalysis B-Environmental* **2003,** *46* (1), 17.

(21) Mendham, J.; Denney, R. C.; Barnes, J. D.; Thomas, M.; Vogel's textbook of quantiative chemical analysis, 6th ed. *Prentice Hall*, **2000**.

(22) Reiche, M.; Baiker, A. Characterization by temperature programmed reduction. *Catalysis Today* **2000,** *56* (4), 347

(23) Koopman, P. G. J.; Kieboom, A. P. G.; Vanbekkum, H.; Characterization of ruthenium catalysts as studied by temperature programmed reduction. *Journal of Catalysis* **1981,** *69* (1), 172.

(24) Hurst, N. W.; Gentry, S. J.; Jones, A.; McNicol, B. D. Temperature programmed reduction. *Catalysis Reviews-Science and Engineering* **1982,** *24* (2), 233.

(25) Gerhard, E.; Knözinger, H.; Weitkamp, J.; Handbook of heterogenous catalysis, 2nd ed.; *Wiley*, **2008**; Vol. 1.

(26) Lin, K.-J. a. Y. S.-P. The effect of organic pollution on the abundance and distribution of aquatic oligochaetes in an urban water basin, Taiwan. *Hydrobiologia* **2008,** *596*, 213.

(27) Cybulski, A.; Trawczyński, J. Catalytic wet air oxidation of phenol over platinum and ruthenium catalysts. *Appl. Catal. B: Environmental* **2004** *47*, 1

(28) Rothenberg, G.; Catalysis: concepts and green applications, 1st ed.; *Wiley*, **2008**.

(29) Turner, D. W.; Aljobory, M. I. Determination of ionization potentials by photoelectron energy measurement. *Journal of Chemical Physics* **1962,** *37* (12), 3007.

(30) Biesinger, M. C.; Payne, B. P.; Grosvenor, A. P.; Lau, L. W. M.; Gerson, A. R.; Smart, R. S. Resolving surface chemical states in XPS analysis of first row transition metals, oxides and hydroxides: Cr, Mn, Fe, Co and Ni. *Applied Surface Science* **2011,** *257* (7), 2717.

(31) Spoto, G.; Gribov, E. N.; Ricchiardi, G.; Damin, A.; Scarano, D.; Bordiga, S.; Lamberti, C.; Zecchina, A. Carbon monoxide MgO from dispersed solids to single crystals: a review and new advances. *Progress in Surface Science* **2004,** *76* (3-5), 71.

(32) Tursunov, O.; Dobrowolski , J.; Klima , K.; Kordon, B.; Ryczkowski, J.; The Influence of Laser Biotechnology on Energetic Value and Chemical Parameters of Rose Multiflora Biomass and Role of Catalysts for bio-energy production from Biomass, *World Journal of Environmental Engineering*, **2015**; 3 (2).

(33) Bogner, A.; Jouneau, P. H.; Thollet, G.; Basset, D.; Gauthier, C. A history of scanning electron microscopy developments: Towards "wet-STEM" imaging. *Micron* **2007,** *38* (4), 390.

(34) Suarez-Ojeda, M. E.; Stuber, F.; Fortuny, A.; Fabregat, A.; Carrera, J.; Font, J. Catalytic wet air oxidation of substituted phenols using activated carbon as catalyst. *Applied Catalysis B-Environmental* **2005,** *58* (1-2), 105.

(35)   Ouyang, Y.; Evaluation of river water quality monitoring stations by principal component analysis. *Water Research* **2005,** *39* (12), 2621.

Chapter 4

Addition of ruthenium to platinum catalysts for CWAO of phenol

4.1 Introduction

From previous studies within the group, platinum supported on silicon carbide has proven to be a promising catalyst for CWAO of phenol[1]. SiC is a very inert support material, with a high hardness of 2800 kg mm^{-2} [2], which makes SiC more able to tolerate the harsh acidic and oxidising conditions within the reactor[3], when compared to conventional heterogenous supports, such as alumina (Al_2O_3) or titania (TiO_2).

The underlying causes for the increased activity seen for SiC catalysts is thought to be the reduced wettability of the support material. The hydrophobic support leads to the adsorption of oxygen directly from the gas phase onto the catalyst surface through air bubbles located within pores. A degree of hydrophilicity is also required to allow the contaminated aqueous phase to come into contact with the catalyst, and thus the active sites. It is thought that the platinum particles provide access and are capable of adsorbing phenol from the aqueous phase[4].

Being of limited resource, platinum group metals (PGMs) often come with a high price tag[5]. Due to a variety of industrial and jewellery applications, platinum is in higher demand than other PGMs, such as ruthenium, and as such is considerably more expensive. The estimated cost for platinum is 3 – 4 times that of ruthenium[6]. Studies have shown supported ruthenium catalysts to also be active for CWAO[7-9], it would therefore be beneficial if the higher activities

associated with platinum could also be combined with the relatively lower cost of ruthenium.

Bi-metallic platinum and ruthenium catalysts were prepared *via* incipient wetness impregnation with a fixed metal loading of 2 % by mass. With the exception of the co-impregnated catalyst, where both metals were impregnated simultaneously, the bi-metallic catalysts were impregnated and calcined with the initial metal and then impregnated and calcinated again with the second metal. The β-SiC support material was ground using a pestle and mortar and sieved to achieve a size range between 450 – 600 μm granules. The catalysts tested in this study are outlined in Table 4.1.

Table 4.1 Description of the Ru and Pt mono and bimetallic SiC catalysts used in this study

Catalyst	Description
2% Pt/SiC	Pt impregnated on SiC (450 – 600 μm) Calcined at 500 °C
1% Ru/1% Pt/SiC	Prepared by post-impregnation of ruthenium on 1% Pt/SiC (450 – 600 μm) Calcined at 500 °C
1% Pt/1% Ru/SiC	Prepared by post-impregnation of platinum on 1% Ru/SiC (450 – 600 μm) Calcined at 500 °C
1% Pt + 1% Ru/SiC	Prepared by simultaneous impregnation of platinum and ruthenium on SiC (450 – 600 μm) Calcined at 500 °C
2% Ru/SiC	Ru impregnated on SiC (450 – 600 μm) Calcined at 500 °C

4.2 Pre-reaction catalyst characterisation

To gain further understanding of the catalyst structure and allow correlation with activity, a variety of characterisation techniques were used to build a full picture of each catalyst.

4.2.1 Powder x-ray diffraction (XRD)

Powder x-ray diffraction (XRD) was used to characterise the crystallinity of the catalysts and in particular provide information on the phase of the active metal component. Figure 4.1 shows the diffraction profile of the silicon carbide supported catalysts.
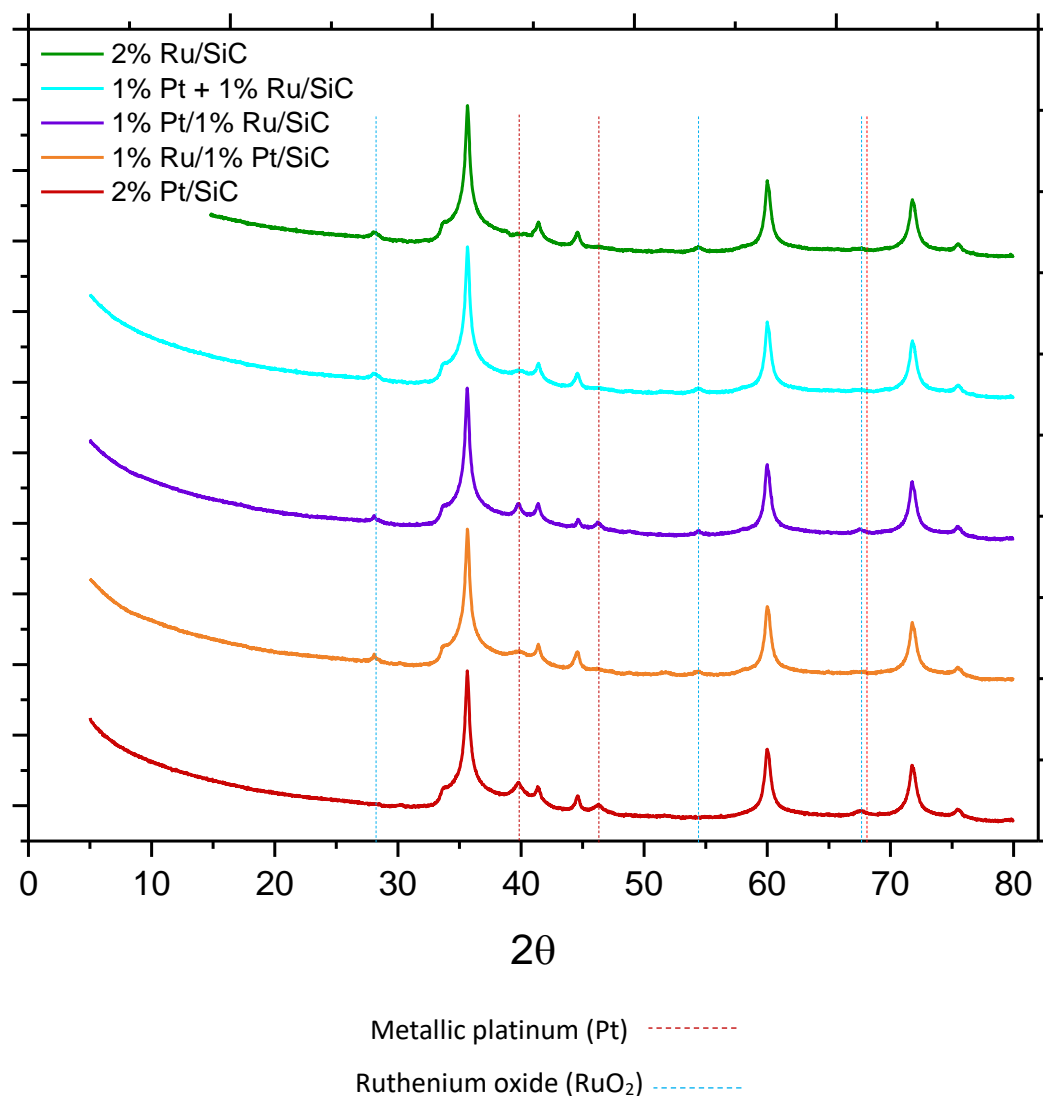
Figure 4.1 Powder XRD patterns for the Pt and Ru bi-metallic SiC catalysts

The most noticeable peaks were observed at 35.5°, 41.5°, 60°, 72° and 75.5° for all the catalysts and are indicative of β-silicon carbide[10]. The remainder of the peaks concur with the active metals, ruthenium and platinum. Due to the lower loadings for the bi-metallic catalysts and overlapping with the larger SiC peaks, some of these peaks are harder to distinguish.

Metallic platinum has been shown to be more active than platinum oxide for CWAO of phenol[11-15] and the peaks occurring at 40°, 46° and 67.5° for all but 2% Ru/SiC catalyst are characteristic of metallic platinum[16]. Indicated by the dotted red lines, these peaks are most noticeable for the 2% Pt/SiC catalyst. No peaks associated with ionic platinum were observed in the diffraction patterns, suggesting all the platinum detected by XRD analysis exists as metallic Pt.

Ruthenium oxide peaks, indicated by the dotted blue lines, are observed at 29°, 54° and 67° for all the ruthenium containing catalysts, with no peaks observed for metallic ruthenium[17,18].

When pure SiC was analysed using XRD, no platinum or ruthenium oxide peaks were present, confirming the successful impregnation of the metals on the support.

4.2.2 Surface area studies

The Brunauer Emmett Teller (BET) method was used to determine the surface area of the catalysts. Since they are all supported on the same silicon carbide support, similar surface area values are expected, the results can be seen in Table 4.2.

Table 4.2 Surface area values determined using N_2 adsorption and BET theory of the Pt and Ru bi-metallic catalysts supported on SiC

Catalyst	Surface area ($m^2\ g^{-1}$)
2% Pt/SiC	25.4
1% Ru/1% Pt/SiC	24.1
1% Pt /1% Ru/SiC	26.5
1% Ru + 1% Pt/SiC	27.7
2% Ru/SiC	24.5
SiC support	26.3

β-SiC is notorious for having a low specific surface area[19] and commercially available β-SiC typically has surface areas of approximately $25 - 30\ m^2\ g^{-1}$ [20,21]. The range of surface areas exhibited by the catalysts are in agreement with this typical value.

The surface area values are within $\pm3.6\ m^2\ g^{-1}$ of each other. Given the $2 - 5\ \%$ error associated with the BET method, it can be assumed that the addition of

ruthenium *via* primary or secondary step impregnation had little effect on the catalyst surface area.

When compared with the support material, typically a decrease in specific surface area is observed for some supported metal catalysts, due to the active metal blocking the micropores of the porous support[22]. SiC has an ordered, highly crystalline structure, as observed in the XRD pattern as large, sharp peaks, which is known to have low porosity. The low porosity of SiC means that impregnated particles are less likely to have a significant effect on the surface area.

The BET results in Table 4.2 show small deviations in the surface area of the catalysts compared with the SiC support material, however these differences may not be considered significant due to the inherent error of the method. It is worth noting that these values are an average taken from measurement of 2 – 3 samples. When also factoring in any potential instrumental or human error, this could explain the minor differences observed in the surface area between the catalysts and the support material.

4.2.3 Thermogravimetric analysis (TGA)

Thermogravimetric analysis (TGA) measures the mass of a sample as a function of temperature and can give an indication as to whether the catalysts may undergo any mass related changes during the reaction. TGA can evaluate the thermal stability of catalysts under an oxidative environment at elevated temperatures similar to the environment in CWAO. The TGA profiles for the bi-metallic and mono-metallic catalysts are shown in Figure 4.2.
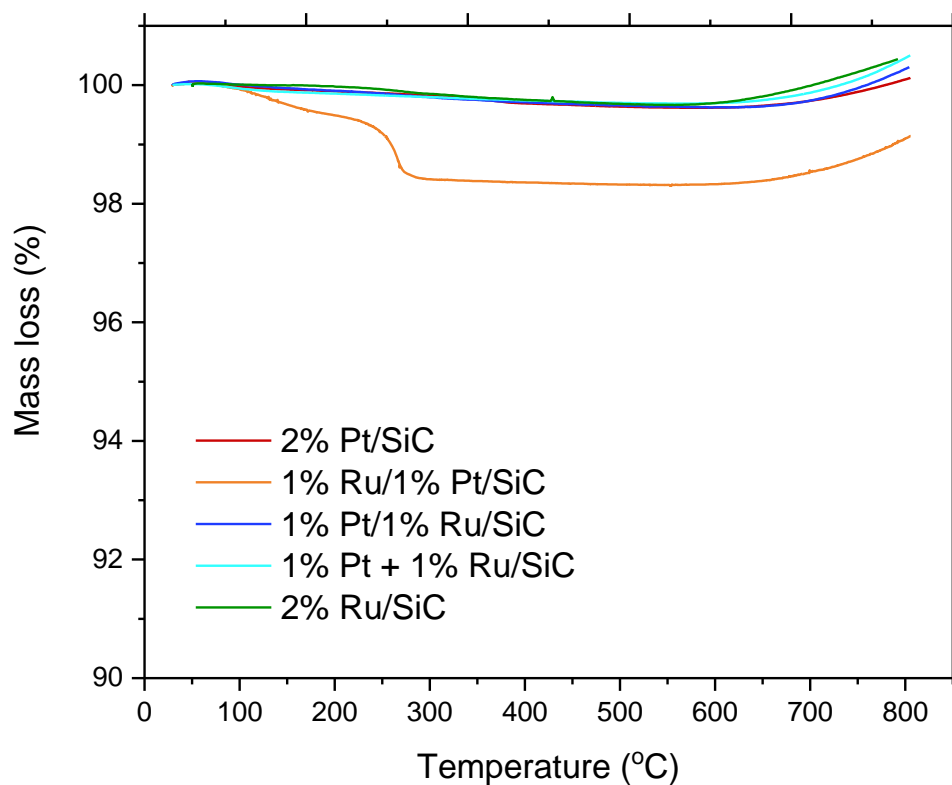
Figure 4.2 TGA profiles for the bi-metallic and mono-metallic SiC catalysts

Once calcined at 500 °C, the majority of the catalysts, with the exception of 1% Ru/1% Pt/SiC, showed less than a 0.75 % mass change up to temperatures of 800 °C. When the temperature increases beyond 600 °C, a mass gain is observed for all the catalysts, this is caused by buoyancy effects within the TGA instrument. As the temperature increases, the density of the gas surrounding the crucible decreases and thus experiences a less 'buoyant lift', resulting in an apparent mass gain in the TGA profile.

1% Ru/1% Pt/SiC exhibited a 2 % mass change between 100 – 270 °C, the TGA profile, along with the first derivative, which represents the rate at which the mass change has occurred, is present in Figure 4.3.
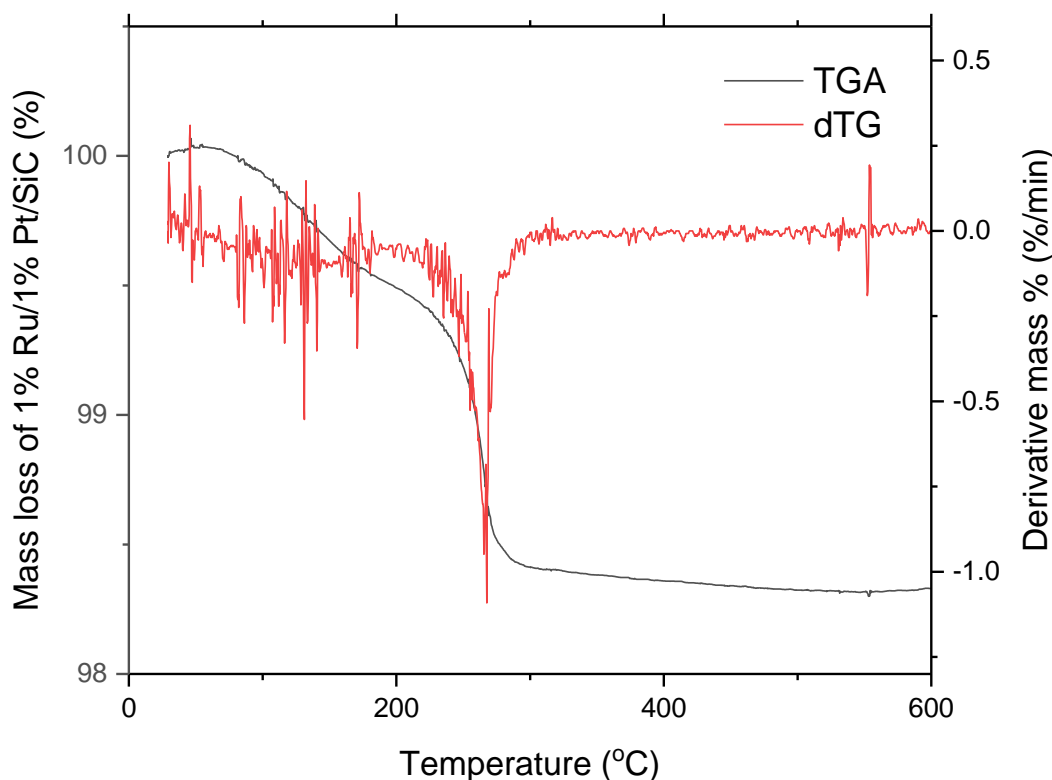
Figure 4.3 TGA profile and 1st mass derivative (dTG) for 1% Ru/1% Pt/SiC

The mass loss observed for the ruthenium post-impregnated on Pt/SiC catalyst occurs in two steps, and the respective peaks on the dTG profile are centred at 130 °C and 265 °C. Any mass loss attributed to the removal of any residual solvent would be expected to occur below 110 °C[23], therefore the mass loss observed for 1% Ru/1% Pt/SiC is likely caused by remaining metal precursor not fully decomposing during calcination. Since the platinum precursor underwent two calcination steps during catalyst preparation, the mass loss is more likely caused by decomposition of the ruthenium precursor, Ru(acac)$_3$. The degradation of Ru(acac)$_3$ has been reported to occur between 200 – 320 °C, under oxidative atmospheres[24]. When part of a supported metal catalyst however, the thermolysis of Ru(acac)$_3$ can proceed *via* a more complex pathway compared to that of pure Ru(acac)$_3$. When supported on Al$_2$O$_3$ and SiO$_2$, the decomposition of Ru(acac)$_3$, occurred in two steps, resulting in two peaks on the dTG profile, much like what is observed for 1% Ru/1% Pt/SiC[25].

Ruthenium is octahedrally coordinated in Ru(acac)$_3$, by six oxygen atoms, and as such the acetylacetonate (acac) ligands are not necessarily all equivalent with respect to their orientation to the support surface. The ligands which are

oriented towards the support, and thus, involved in hydrogen bonding with surface hydroxyl groups, can undergo a proton-assisted mechanism of thermolysis below 200 °C[26]. The acetylacetonate ligands, which do not interact with the surface hydroxyls, undergo thermal destruction at a higher temperature, centred around 270 °C. Plyuto *et al.*[25] observed an increase in proton-assisted thermolysis, when reducing the loading of ruthenium, due to the increased proportion of Ru(acac)$_3$ which can interact with the support.

4.2.4 Scanning electron microscopy (SEM)

Scanning electron microscopy (SEM) was used to visually analyse the surface of the catalysts and provide approximate information on active metal particle shape and size.

4.2.4.1 Microscopy studies of 2% Pt/SiC

As discussed in Chapter 3, the bright spots on SEM images indicate the presence of heavier elements, in this case platinum. Figure 4.4 shows SEM images of 2% Pt/SiC.
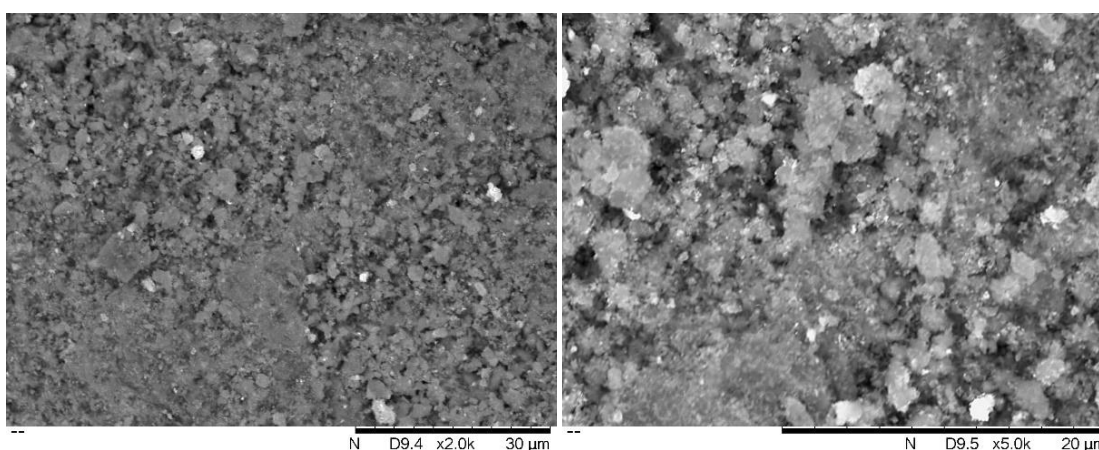
Figure 4.4 SEM images of 2% Pt/SiC at 2k and 5k magnification

The SEM images show the presence of large platinum particles ranging from 5 µm – 800 nm. The particle size range achieved here is on the larger end of

the scale for what is typically sought after for supported metal catalysts; smaller platinum particles (>100 nm) are desirable due to the increase in exposed metal atoms and thus, the number of potential active sites. Catalysts prepared by impregnation methods typically give rise to larger metal particles than other catalyst preparation methods[27], and the platinum particle size range of Pt/SiC is within those seen in the literature. When supported on TiO_2, platinum particles have been observed in an array of sizes, ranging from 450 μm − 0.35 nm[14,28-30]. Although smaller metal particles are preferable, the size does not necessarily dictate how active the catalyst will be for CWAO.

By use of EDX mapping it is possible to ascertain the elemental composition. The EDX mapping of 2% Pt/SiC is displayed in Figure 4.5.
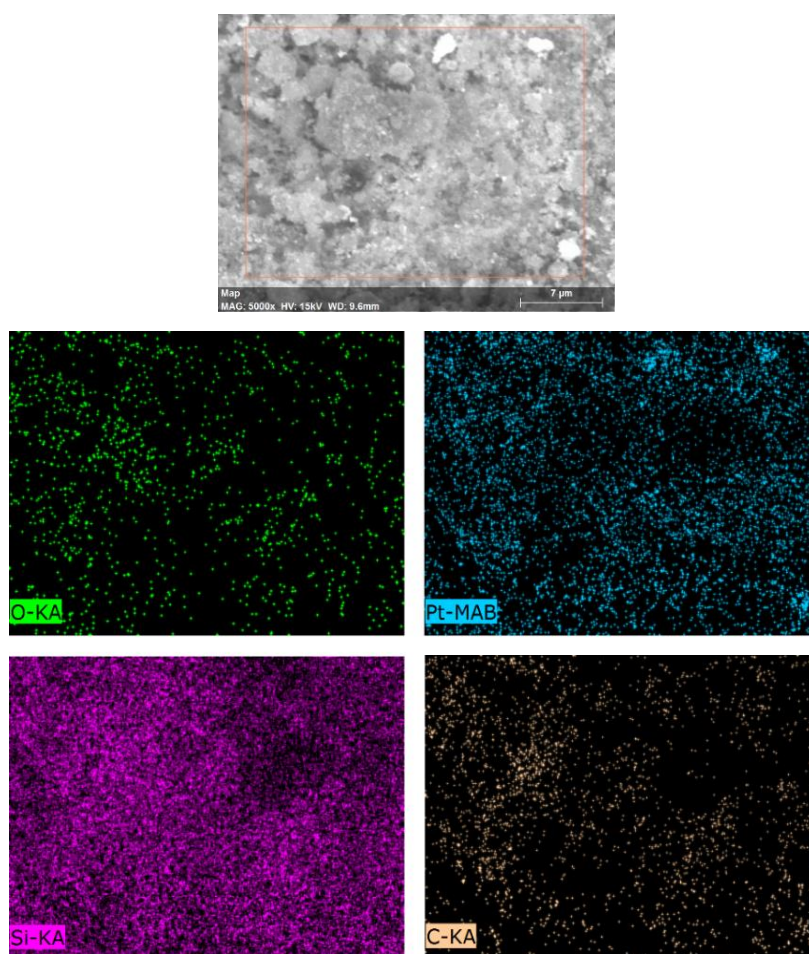
Figure 4.5 EDX mapping of 2% Pt/SiC

The elemental composition consisted of oxygen, platinum, silicon and carbon. The platinum appears well distributed across the surface, which is in agreement with the SEM images. The oxygen appears absent in the spots where

the platinum is more concentrated, suggesting the platinum exists in the metallic form, as confirmed by the XRD pattern. The oxygen present on the surface is likely chemisorbed oxygen or from SiO_2 amongst the SiC support. In the presence of oxygen, the outer layer of SiC can undergo passive or active oxidation to SiO_2, although this reaction is negligible unless operating at temperatures exceeding 600 °C for extended periods of time[31,32]. SiO_2 has an amorphous structure and will therefore not display any sharp reflections in the XRD, typically SiO_2 gives a very broad signal around 25° [33]. For diffraction to take place long range order is necessary, some surface layers of SiO_2 may not have long range order, and will therefore be invisible by diffraction.

4.2.4.2 Microscopy studies of 1% Ru/1% Pt/SiC

Since ruthenium is post-impregnated on Pt/SiC for this catalyst, the bright spots in the SEM images could indicate either ruthenium or platinum.
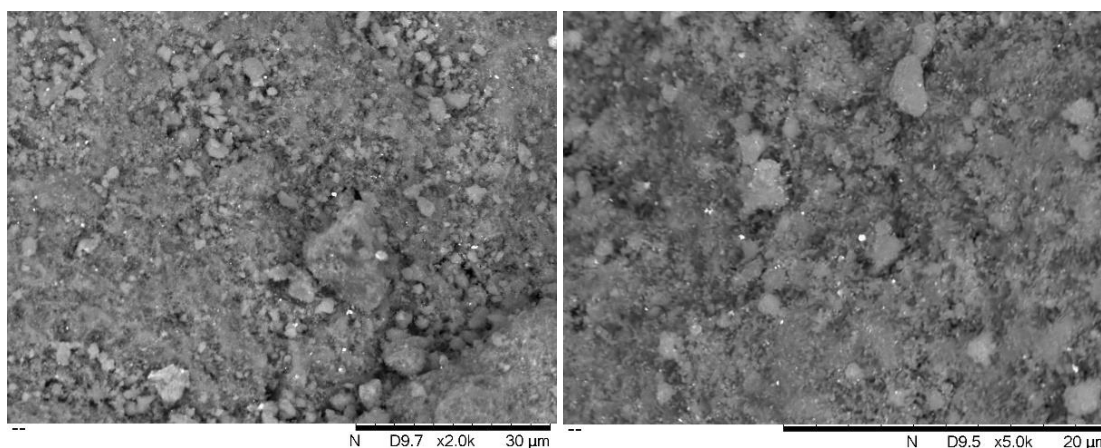
Figure 4.6 SEM images of 1% Ru/1% Pt/SiC at 2k and 5k magnification

The SEM images of 1% Ru/1% Pt/SiC (Figure 4.6) are not dissimilar to those of 2%Pt/SiC, however the metallic particles appear smaller with the largest of the particles being approximately 1 μm in size. As with platinum, when supported on TiO_2, ruthenium has also been observed in an array of particle sizes, ranging between 3 nm – 40 μm[34-36].
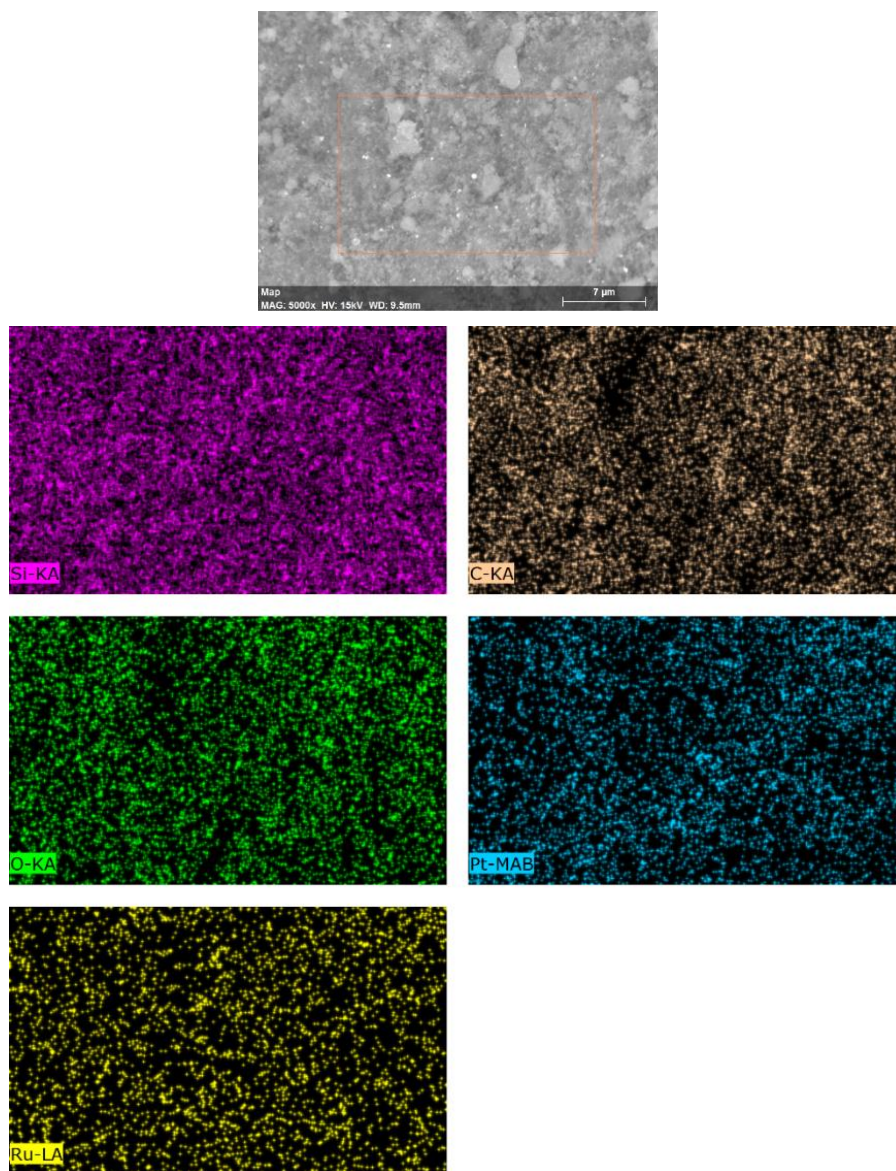
Figure 4.7 EDX mapping of 1% Ru/1% Pt/SiC

The EDX mapping of the catalyst (Figure 4.7) shows a high distribution of ruthenium; an increase in oxygen content is also observed compared with 2% Pt/SiC. The active ruthenium component was shown by XRD to be RuO_2, thus it is likely to be a contributing factor for the higher percentage of oxygen observed. Comparison of the Ru and Pt mapping show overlapping between the two metals, which could potentially indicate the formation of some bi-metallic particles.

Bi-metallic particles can exist in a variety of different architectures, such as alloys, core – shell and monometallic mixtures. These different configurations can give rise to different properties and bi-metallic particles of the same size, shape and composition can exhibit significant differences in catalyst activity[37]. Figure 4.8

displays a graphical representation of alloy, core – shell and monometallic architectures for a Pt – Ru bimetallic catalyst[38].
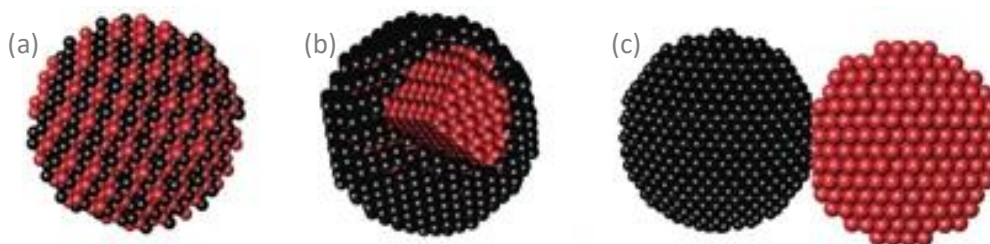
Figure 4.8 Graphical representation of different bimetallic architectures, where Pt is black and Ru is red (a) PtRu alloy (b) Ru core - Pt shell (c) linked monometallic nanoparticles[38]

When developing catalysts for the CO PrOX reaction, Alayoglu *et al.*[38] found Ru core – Pt shell nanoparticles to be both more active and more selective than their alloy or monometallic counterparts, towards CO oxidation. The core – shell architecture allowed for enhanced catalytic activity through a combination of increased availability of CO-free Pt surface sites and a hydrogen assisted O_2 dissociation mechanism which led to an accelerated reaction rate.

Bimetallic alloy particles can also improve catalysed oxidation reactions, in which the more oxophilic metal can act as an oxygen activator, which then facilitates oxidation of an adsorbed reactant on the neighbouring, less oxophilic metal centre[39,40].

The composition and architecture of bimetallic particles are important parameters which can markedly affect the catalytic performance of bi-metallic catalysts[41,42] and although it is not possible to ascertain the architecture of these bi-metallic particles through SEM, techniques such as high-resolution transmission electron microscopy (HRTEM) and Fourier transform infrared spectroscopy (FTIR) of probe molecules can help provide further insight.

Although HRTEM images of differing bimetallic architectures can appear almost identical, with the use of EDX line scans it is possible to differentiate between them. In the case of core – shell particles, the EDX line scans will show a higher distribution of metal towards the centre for the core metal, and higher distribution towards the edge of the particle for the outer shell metal. For bimetallic alloy particles, the EDX line scans will show a Gaussian distribution of

both metals for a random (alloy) arrangement, whereas monometallic particles will be easily distinguished from the presence of only one metal.

FTIR CO probe experiments can also aid in the identification of bimetallic architectures. For alloy and monometallic mixtures, two peaks corresponding to the presence of CO adsorbed on both metals would be expected, whereas for core – shell structures only a single peak would be observed, due to the presence of only one metal on the outer surface of the bimetallic particle.

Characterisation techniques such as temperature programmed reduction (TPR) and x-ray photoelectron spectroscopy (XPS) can also provide further insight. Upon alloying, the reduction temperature of a metal can be shifted from that of a single metal, which could be made apparent through TPR. XPS analysis may also reveal changes in binding energies of certain metals when part of bi-metallic particles. Unfortunately, these techniques were unavailable during the course of this research and consequently, it is not possible to definitively confirm the existence of bi-metallic particles in these catalysts. Although the EDX mapping may show overlapping of the two metals, this could be the result of one metal sat upon the other, not necessarily as part of a mixed metal particle, which would require further analysis to verify.

4.2.4.3 Microscopy studies of 1% Pt/1% Ru/SiC
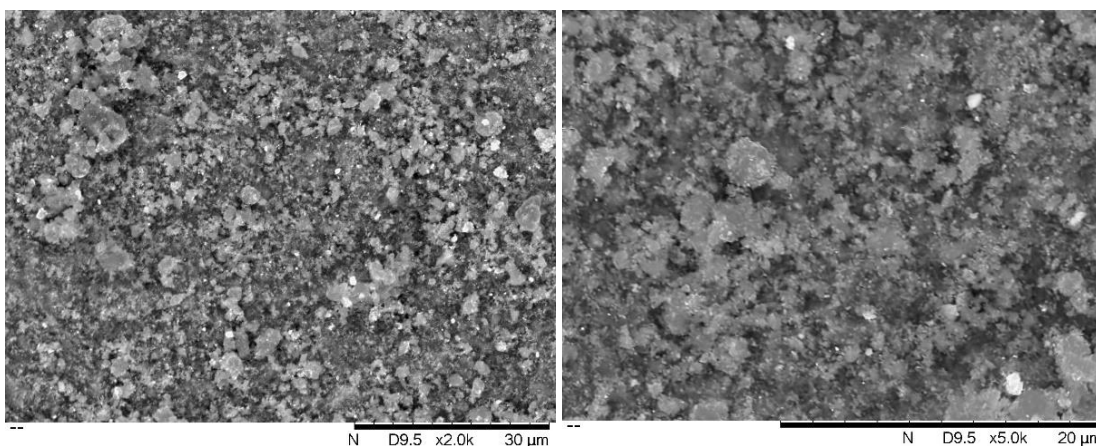
Figure 4.9 SEM images of 1% Pt/1% Ru/SiC at 2k and 5k magnification

The SEM images of 1% Pt/1% Ru/SiC (Figure 4.9) are similar to those seen for the previous catalysts. The particles are marginally larger than those for 1% Ru/1% Pt/SiC, but still well distributed over the surface.
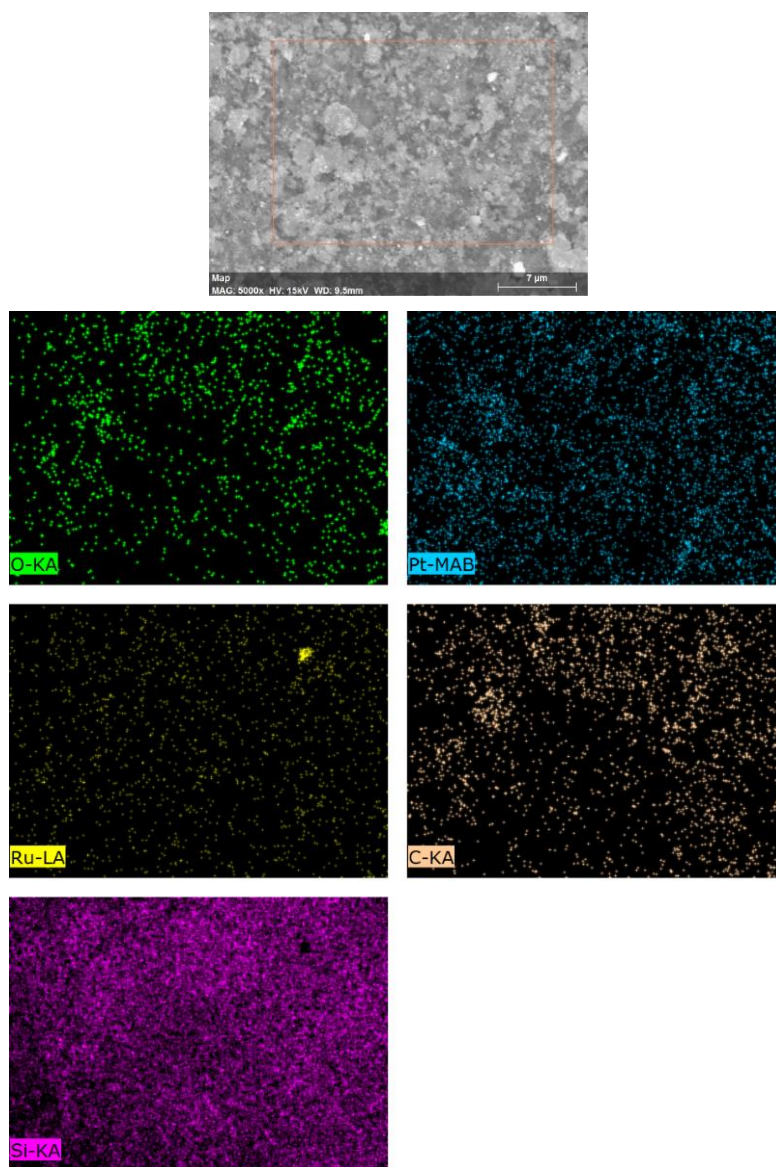
Figure 4.10 EDX mapping of 1% Pt/1% Ru/SiC

The EDX mapping of the catalyst (Figure 4.10) shows some larger ruthenium particles overlapping with platinum, suggesting the potential presence of bi-metallic particles. The mapping of ruthenium is much less distinctive than that of the 1% Ru/1% Pt/SiC, this could be the result of a platinum surface layer or Ru core – Pt shell particles. In either case, this would require further analytical techniques to confirm, some of which were discussed in the previous section.

4.2.4.4 Microscopy studies of 1% Pt + 1% Ru/SiC
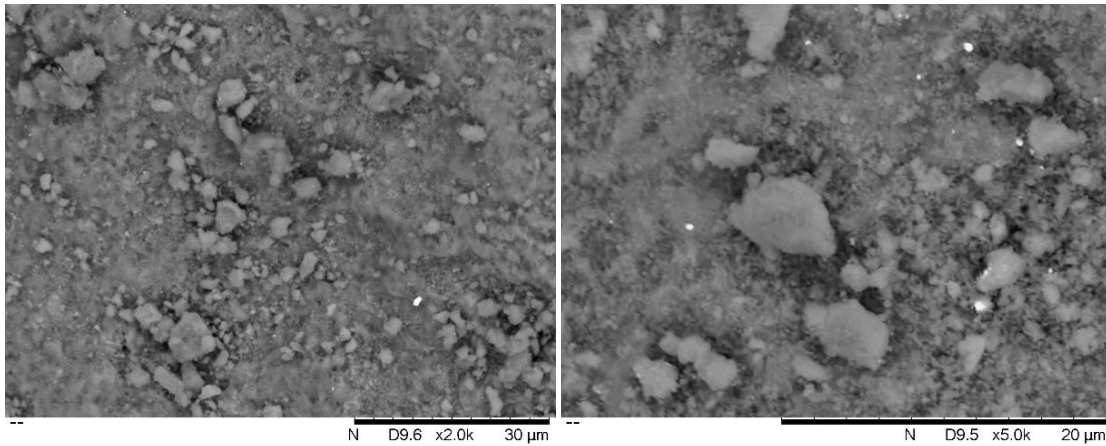
Figure 4.11 SEM images of 1% Pt + 1% Ru/SiC at 2k and 5k magnification

The SEM images for the simultaneous impregnation of Ru and Pt (1% Pt + 1% Ru/SiC) (Figure 4.11) catalyst shows fewer bright spots than the previous two bi-metallic catalysts. The co-impregnation could potentially allow for an increase in bi-metallic particles and thus produce a catalyst with less exclusively platinum or ruthenium particles.
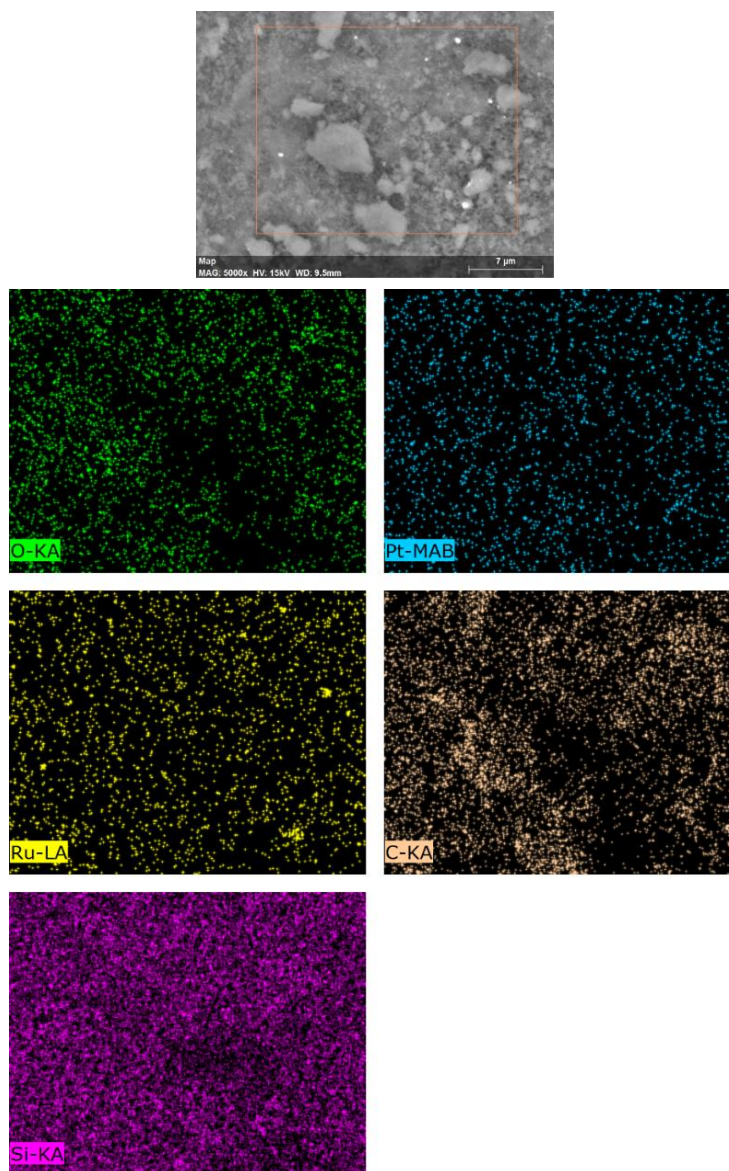
Figure 4.12 EDX mapping of 1% Pt + 1% Ru/SiC

The EDX mapping (Figure 4.12) shows independent ruthenium particles, larger than those observed for platinum. Compared with Pt, larger ruthenium particles are observed for all the bi-metallic catalysts, suggesting their presence is not influenced by the order of impregnation during catalyst preparation. Both metals show high distribution over the surface.

4.2.4.5 Microscopy studies of 2% Ru/SiC
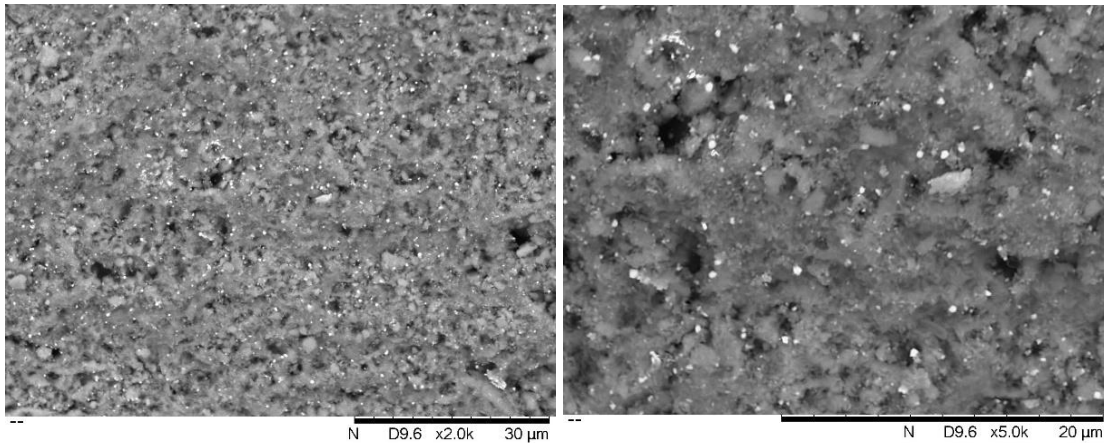
Figure 4.13 SEM images of 2% Ru/SiC at 2k and 5k magnification

SEM images of 2% Ru/SiC (Figure 4.13) show well dispersed metal particles of sizes less than 1 μm, smaller than those seen for the exclusively platinum catalyst.
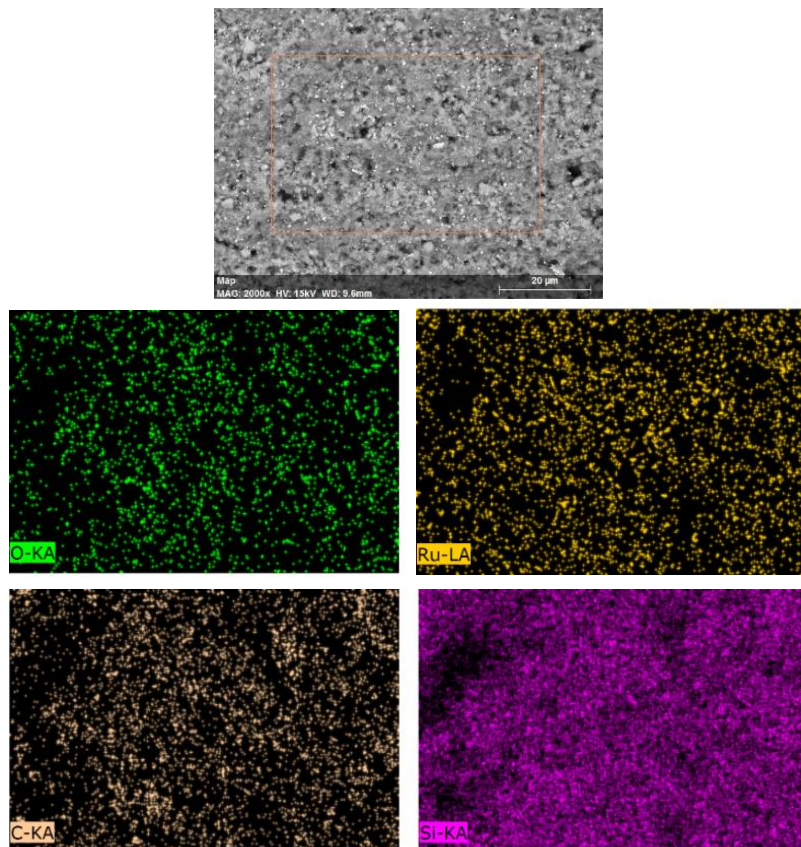
Figure 4.14 EDX mapping of 2% Ru/SiC

The EDX mapping of the Ru catalyst (Figure 4.14) confirms the high Ru dispersion, coupled with a high oxygen dispersion, which is attributed to ruthenium being in the oxidised form, confirmed by the XRD analysis.

4.2.5 Energy dispersive x-ray spectroscopy (EDX)

Energy dispersive x-ray (EDX) spectroscopy also allowed for quantification of the weight percentage of each element present within the sample. The SEM images could not distinguish between the different metals and so EDX was used to quantify the weight percentages of Ru and Pt. The weight percentages were measured at a minimum of 5 points throughout the samples and the average values are shown in Table 4.3.

Table 4.3 Average EDX atomic weight percentages of Ru and Pt SiC catalysts

Catalyst	Pt	Ru	Si	C	O
2% Pt/SiC	9.98		54.86	29.74	5.38
1% Ru/1% Pt/SiC	2.77	1.14	48.98	37.71	9.31
1% Pt /1% Ru/SiC	7.39	0.79	63.84	23.26	4.51
1% Ru + 1% Pt/SiC	0.46	0.61	56.97	35.29	6.53
2% Ru/SiC		3.36	54.63	35.07	6.74

Since the catalysts are primarily comprised of silicon carbide support, it is not unsurprising that the EDX shows the highest weight percentage for Si and C.

The platinum weight percentage for the Pt/SiC catalyst is inflated when compared with the 2 % nominal metal loading, suggesting that the majority of the platinum exists on the external surface of the SiC support pellet, and is not as distributed throughout the bulk of the support. The high weight percentage of metal on the external surface of the support was to be expected given the chosen impregnation method used for catalyst preparation, whereby the metal is added onto the SiC support as opposed to methods such as co-precipitation. Metallic active sites are more accessible to passing phenol molecules when on the surface of a catalyst, rather than embedded within the pores. Therefore, platinum is more effective on the surface of the support, as this can reduce mass transfer limitations and promote oxidation.

For the Ru post-impregnated on Pt/SiC catalyst, there is a higher weight percentage of platinum compared with ruthenium. The same trend is observed when the sequence of impregnation steps is reversed, with Pt post-impregnated on Ru/SiC, but with a larger difference between the metal weight percentages. Differences between the nominal and measured metal loadings could be a result of nonrepresentative sampling, where the sampling occurred at points which were not representative of the overall catalyst, in which case additional sampling is necessary to achieve a more accurate depiction of the catalyst. Disparities in the absolute metal content of the catalysts compared with the nominal loading can also result in lower measured weight percentages, techniques such as inductively coupled plasma mass spectrometry (ICP-MS) can help determine the absolute metal loading.

Further on in Chapter 5, a more detailed analysis of the metal loading on the external and internal surfaces of the SiC pellet has been carried out, confirming the measured metal loading to be similar to the nominal loading when the whole catalyst pellet is considered.

Small weight percentages (<0.08 %) of sodium were also observed in the EDX analysis. Commercial supports often contain trace impurities[43], however analysis of the pure SiC support revealed negligible amounts of sodium. More likely, sodium came about within the impregnation process and addition of the metal precursors, through factors such impurities in other chemicals or unclean or contaminated glass wear.

4.3 Catalyst activity studies

In previous studies, 2% Pt/SiC achieved nearly 100 % phenol conversion in the same trickle bed reactor at 160 °C and 13.1 bar$_{(g)}$[1]. When conversions reach 100 % it is not possible to gain a true comparison of catalytic activity, as only a portion of the active sites may be contributing to oxidation at any given time. Furthermore, any deactivation of the active sites may not show in terms of

decreased activity if only a fraction are required to achieve complete conversion. For this reason, and given the hypothesis that a hydrophobic catalyst wouldn't be as reliant on high operating pressures due to the ability to adsorb oxygen directly from the gas phase, the operating pressure was reduced to 7 bar$_{(g)}$.

The phenol conversion as a function of time at 160 °C and 7 bar$_{(g)}$ for the Pt and Ru catalysts is shown in Figure 4.15.
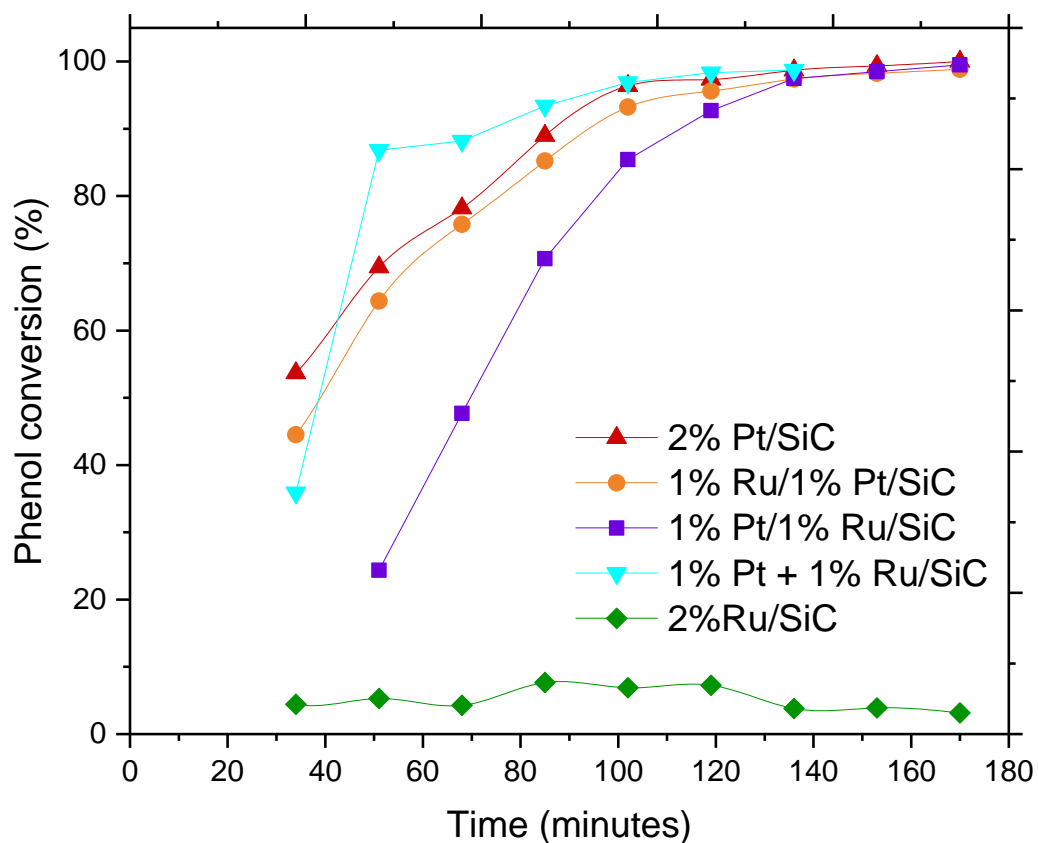
Figure 4.15 Phenol conversions as a function of time for Ru and Pt supported on SiC catalysts at 7 bar$_{(g)}$ and 160 °C

Even at the reduced pressure, with the exception of 2% Ru/SiC, the catalysts achieved greater than 98 % conversion during the 180 minute testing period. The vast majority of the heterogeneous catalysts reviewed in Chapter 2 required oxygen partial pressures greater than 5 bar$_{(g)}$, whereas the platinum containing SiC based catalysts are able to achieve almost complete phenol conversion with an oxygen partial pressure of less than 1.5 bar$_{(g)}$. The 2% Pt/SiC catalyst took between 100 – 120 minutes before stabilising at full conversion. When Pt/SiC was post-impregnated with ruthenium (1% Ru/1% Pt/SiC), the

catalyst exhibited an induction profile resembling 2% Pt/SiC, but with a slightly longer stabilization period of 150 minutes. When the sequence of impregnation steps was reversed, with platinum post-impregnated on Ru/SiC (1% Pt/1% Ru/SiC), the induction period increased to 170 minutes. When ruthenium and platinum were co-impregnated on SiC (1% Pt + 1% Ru/SiC), an induction period of 100 – 120 minutes was observed, similar to 2% Pt/SiC, however, the phenol conversion exceeded the exclusively platinum catalyst during this induction period.

The rate of phenol conversion during the first half of the induction period is increased when co-impregnated with platinum and ruthenium, although this does not reduce the total precious metal loading, an initial rate increase can be beneficial to the start-up of a CWAO reactor. In practice, during reactor start-up, the exit feed would be fed back into the reactor until conditions allowed for 100 % conversion and the wastewater could be safely released; if the time taken for the catalyst to reach complete conversion is reduced it can help optimise reactor start-up and improve process economics.

Pollutant conversion – time profiles such as these, consisting of slow conversion rates during the initial induction period before transition to a steady state or total degradation of contaminants, are not uncommon in CWAO processes and other free radical based catalytic oxidation mechanisms[12,44-46]. Langmuir – Hinshelwood type rate equations have been used to describe induction periods, which account for the adsorption of both phenol and dissociation of oxygen, as well as the surface reactions which govern the reaction rate[44,47,48]. The presence of certain reaction intermediates has also been thought to be responsible and the induction period is often attributed to the necessary time required to achieve a critical concentration of organic radicals[49].

Hydroquinone, a reaction intermediate for phenol oxidation, can be utilized as a free radical initiator. Since WAO proceeds through a free radical mechanism, any such compounds able to act as free radical initiators will affect the reaction rate. Vaidya *et al.*[50] observed enhanced initial reaction rates upon the addition of trace amounts of hydroquinone and proposed that the presence of

hydroquinone during liquid phenol oxidation, results in the formation of hydroxyl and perhydroxyl radicals which in turn influence the rate of oxidation. Under excess oxygen conditions, once formed, hydroquinone is rapidly oxidised to ρ-benzoquinone and hydrogen peroxide, before further oxidation to carbon dioxide and other low molecular weight products[47]. The oxidation reaction of hydroquinone is outlined in Figure 4.16.
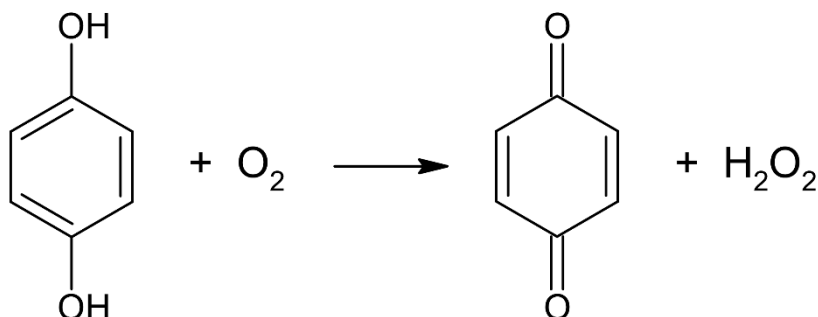
Figure 4.16 Oxidation of hydroquinone

Catechol, another reaction intermediate of phenol oxidation, will also undergo rapid oxidation in oxygen rich conditions, resulting in σ-benzoquinone and hydrogen peroxide[51]. The resulting production of hydrogen peroxide, from either intermediate, leads to the formation of hydroxyl and perhydroxyl radicals[52], as shown by Equations 4.1 and 4.2 respectively.

$$H_2O_2 \rightarrow 2OH \cdot \qquad\qquad \textit{Equation 4.1}$$

$$H_2O_2 + O_2 \rightarrow 2HO_2 \cdot \qquad\qquad \textit{Equation 4.2}$$

By observing reaction rates under oxygen rich and inert nitrogen atmospheres, Kolaczkowski *et al.*[52] established the production of hydroxyl radicals (Equation 4.1) to be the principal path for hydrogen peroxide decomposition under CWAO conditions and primarily responsible for radical formation. These hydroxyl radicals then participate in the oxidation reaction, oxidising other phenol molecules, creating further radicals, thus increasing the reaction rate. This autocatalytic behaviour is responsible for the induction period and the reaction approaches a steady state as the production and destruction of these radicals reaches equilibrium.

The difference in the induction periods for the platinum containing catalysts could therefore be a result of each catalysts ability to quickly oxidise phenol, allowing for the increased production of radicals. The similar conversion – time profiles for 2%Pt/SiC and 1% Ru/1%Pt/SiC (Ru post-impregnated on Pt/SiC), suggest similar catalytic behaviour, with the presence of ruthenium causing a slight elongation in the induction time. The catalyst with the longest induction period, Pt post-impregnated on Ru/SiC (1%Pt/1%Ru/SiC), was shown by SEM to have larger metal particles on average in comparison to the other catalysts. This increase in metallic particle size results in a reduced metallic surface area, thus a reduced number of potential active sites on the surface. Fewer active sites on the surface, where they are more accessible to the reactants, could result in a longer induction period (as seen in Figure 4.13) as the generation of the critical number of radicals would be more gradual.

For the 2% Ru/SiC a stable phenol conversion between 3 – 7 % was observed with no apparent induction period. The low activity achieved for this catalyst further indicates platinum to be the primary active metal for the CWAO of phenol, but partial substitution with ruthenium can maintain, and in the case of co-impregnation (1% Pt + 1% Ru/SiC), marginally exceed the activity of Pt/SiC under these conditions.

4.3.1 Catalyst selectivity

Catalyst selectivity is also an important parameter, even if 100 % conversion is achieved, the ability to direct a reaction towards a particular product can greatly affect the overall catalytic performance. In terms of CWAO, the ability to direct a reaction to complete oxidation to CO_2 and H_2O is the target. Incomplete oxidation of contaminants in wastewater requires that wastewater to undergo further treatment before it can be safely released into the environment, increasing the complexity of the purification process.

The selectivity of the catalysts was assessed by monitoring the concentration of partial oxidation products produced during the reaction. The concentrations of formic acid, acetic acid, oxalic acid, fumaric acid, hydroquinone, maleic acid, benzoquinone, catechol and 4-hydroxylbenzoic acid present in the off-stream were all measured by HPLC. For the Ru and Pt/SiC catalysts only the presence of formic, acetic, oxalic, maleic acids as well as benzoquinone were detected in the treated wastewater. Figure 4.17 contains graphs displaying the concentration of these intermediates as a function of time for the CWAO of phenol (for which the phenol conversion rates are shown in Figure 4.15).
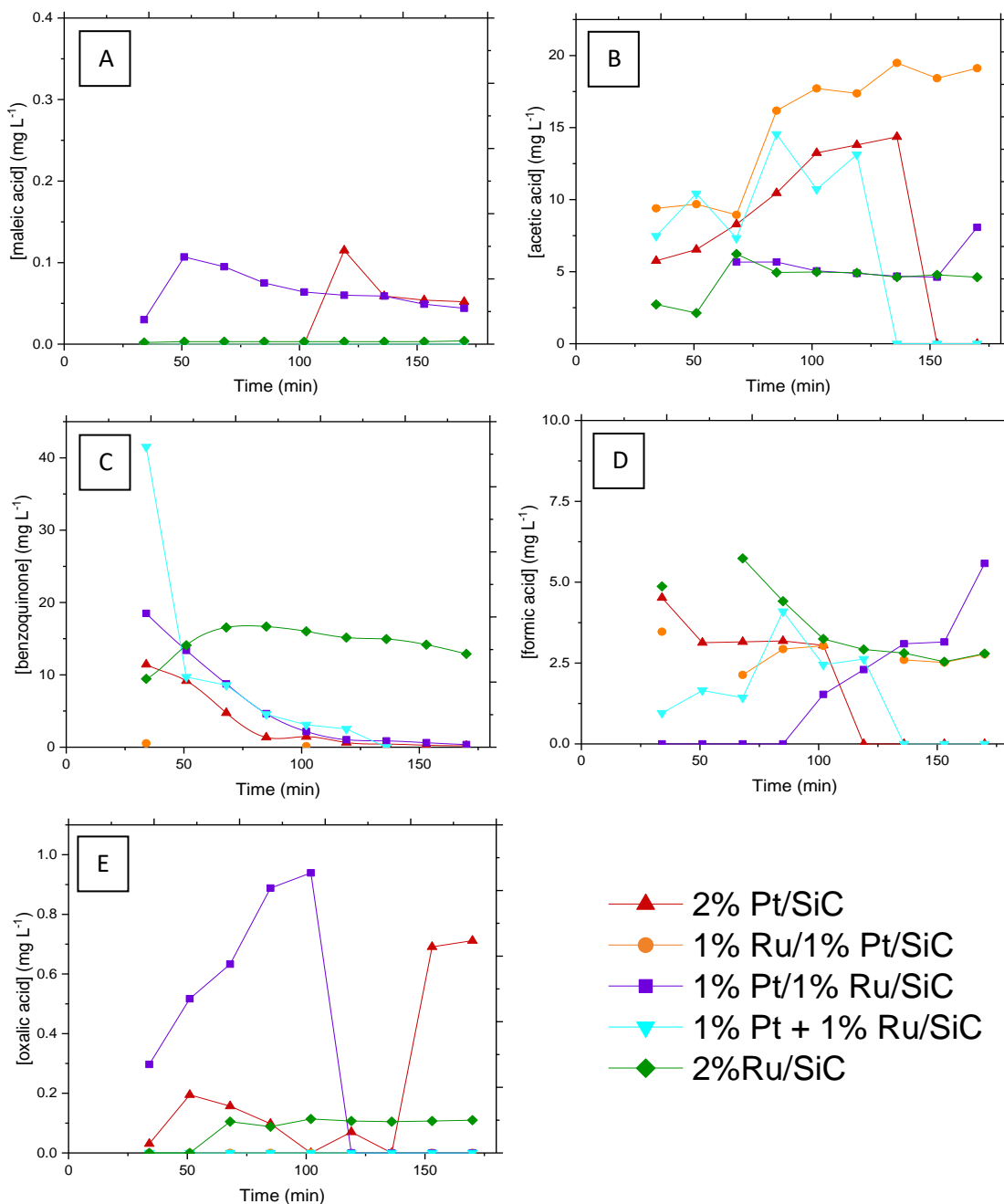
Figure 4.17 Concentration of partial oxidation products (A) maleic acid (B) acetic acid (C) benzoquinone (D) formic acid and (E) oxalic acid as a function of time for the Pt and Ru bi-metallic SiC catalysts for the CWAO of phenol at 160 °C and 7 bar(g)

Given the numerous reaction intermediates associated with phenol oxidation and to help better relate this data to the overall reaction mechanism, the reaction schematic proposed by Devlin *et al.*[53] (discussed in Chapter 1) is presented in Figure 4.18. The partial oxidation products detected in the end stream have been highlighted in red.
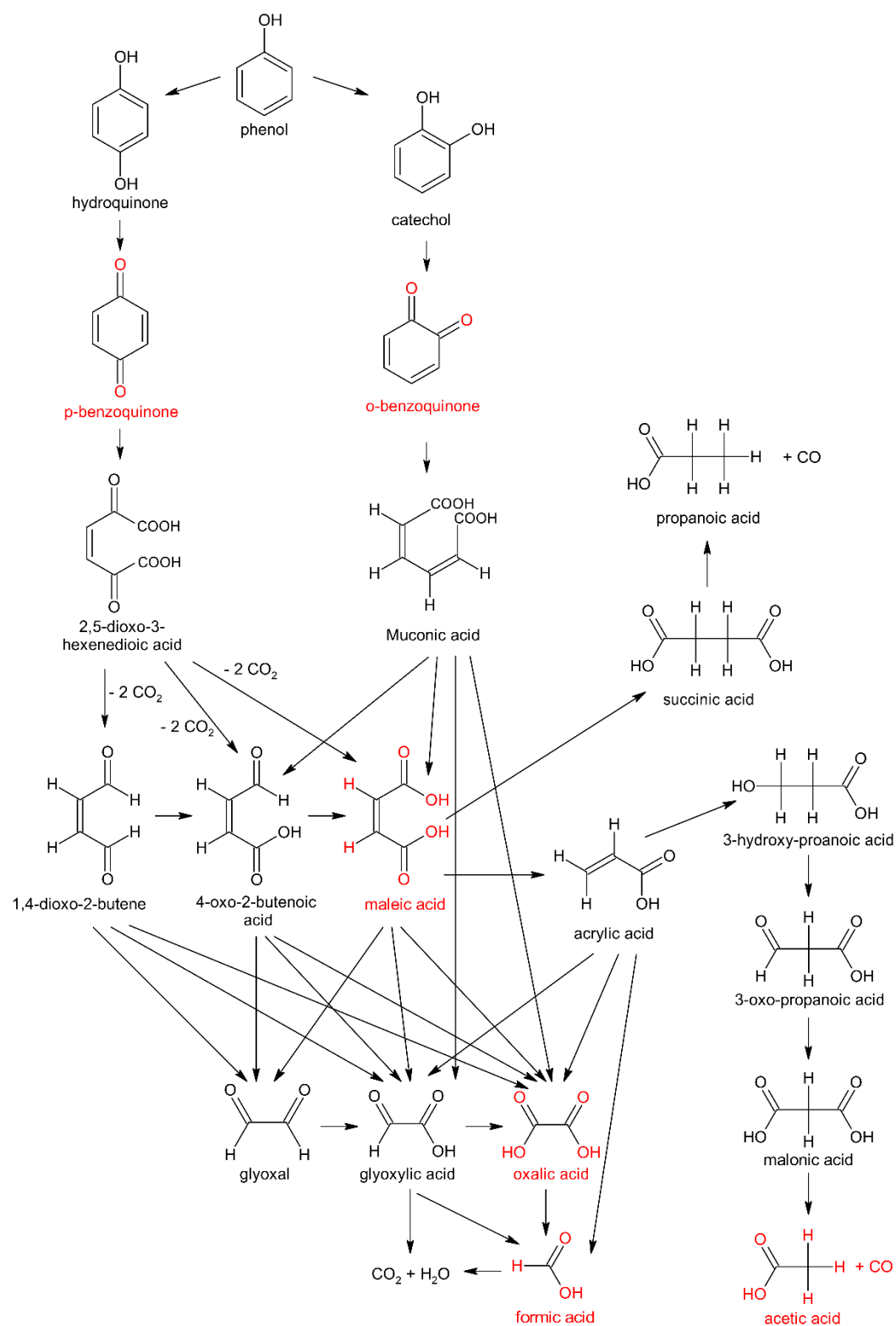
Figure 4.18 Phenol oxidation pathways proposed by Devlin et al.[53], with the intermediates present in the end stream highlighted in red.

Neither hydroquinone or catechol were detected in the treated wastewater, making it difficult to assess which pathway the oxidation reaction

initially took. The absence of these compounds is not unsurprising as once (if) formed, they would be readily oxidised to the corresponding *para* or *ortho* benzoquinone[44,47].

The oxidation product observed in the highest concentrations was benzoquinone (Figure 4.17 C). The platinum containing catalysts exhibited high initial benzoquinone concentration followed by a decrease to less than 1 mg L^{-1} as the reaction approached a steady state. The exclusively ruthenium catalyst displayed almost consistent benzoquinone concentration of approximately 10 mg L^{-1} throughout. Although the analysis method was unable to differentiate between the structural isomers, ρ- and σ-benzoquinone, the selectivity of the oxidation product can be influenced by the extent of oxygen coverage on the platinum surface[13]. For Pt/SiC, where the platinum exists in the metallic state, oxidation is more likely to occur in the *ortho* position, resulting in σ-benzoquinone.

It is unclear what effect the addition of RuO_2, (post, pre, or co impregnated) had on the preferred oxidation orientation; oxidation in the *para* position can result in polymerisation, which can lead to molecules such as 4-hydroxybenzoic acid[54]. No 4-hydroxybenzoic acid was present in the treated water for any of the catalysts, however, this does not necessarily confirm oxidation through the *ortho* position as the low liquid to catalyst ratio in trickle bed reactors will also decrease the potential for polymerisation[55] and oxidation in either orientation can still progress to CO_2 and H_2O.

Maleic acid (Figure 4.17A) was the intermediate present in the lowest concentrations; only the Pt/SiC and Ru post-impregnated on Pt/SiC catalysts observed concentrations of maleic acid greater than 0.1 mg L^{-1}. The 1% Pt/1% Ru/SiC catalyst showed a gradually decreasing amount of maleic acid as the reaction approached steady state regarding phenol conversion, whilst the Pt/SiC only showed the presence of maleic acid after 100 minutes, before also decreasing. The presence of two reactive centres (– COOH group and C – C double bond) in maleic acid is responsible for the higher reactivity with oxygen compared with other short chain acid intermediates[56], which can account for the relatively lower concentrations observed for maleic acid, compared to oxalic, formic and

acetic acids. The absence of fumaric acid, the trans isomer of maleic acid, can be attributed to the low concentration or lack of maleic acid in the treated wastewater[57].

Maleic acid can be the result of either benzoquinone isomer and is a crucial intermediate in phenol oxidation. The continued oxidation of maleic acid can proceed through a number of pathways and intermediates, namely, oxalic and acrylic acids. Oxidation to oxalic acid is preferred over oxidation to acrylic acid, as acrylic acid subsequently degrades to acetic acid, a highly refractory end product[58]. Given the presence of formic and acetic acids in the reaction media for all the catalysts, the oxidation of maleic acid must therefore proceed *via* both oxalic and acrylic acid pathways.

Oxalic acid (Figure 4.17 E) is present in low concentrations of <1 mg L^{-1}, thus, despite the rapid increase and decrease in concentrations observed for 1% Pt/1% Ru/SiC and Pt/SiC, the amount of the acid present in the end stream is still very minimal. For the Pt post-impregnated on Ru/SiC catalyst, the concentration of oxalic acid diminishes as the reaction reaches steady state, and is accompanied by an increase in formic acid (Figure 4.17 D) once at steady state. The increase in formic acid suggests that once at steady state, any oxalic acid is being further oxidised to formic acid. The exclusively Pt catalyst displays a slightly different trend, with an increase in oxalic acid concentration near the end of the reaction period. As the concentration of oxalic acid increases for Pt/SiC, the formic acid concentration decreases. Although it is possible for formic acid to be a product of the oxidation of glyoxylic and acrylic acids, the increase or decrease in oxalic acid concentration accompanied by a decrease or increase in formic acid respectively, suggests formic acid is likely the product of oxalic acid oxidation.

The catalysts all displayed similar concentrations of formic acid (Figure 4.17 D) at approximately 3 mg L^{-1}. After 120 – 130 minutes, once the reaction had reached steady state, the Pt/SiC and Ru + Pt/SiC co-impregnated catalysts showed a complete reduction in formic acid concentration, suggesting total oxidation of phenol *via* formic acid, resulting in the desired end products CO_2 and H_2O.

Acetic acid is often cited as the most difficult to oxidise intermediate in the phenol oxidation pathway and is frequently the major compound formed during CWAO of various organics[59-62]. Acetic acid (Figure 4.17 B) was observed in higher concentrations, <20 mg L^{-1}, compared with the other short chain carboxylic acids present. The Ru post-impregnated on Pt/SiC catalyst showed a steady accumulation of acetic acid as the reaction proceeded, whereas Ru/SiC and Pt post-impregnated on Ru/SiC displayed consistent concentration of approximately 5 mg L^{-1} throughout the reaction. Similarly to formic acid, Pt/SiC and the Pt + Ru co-impregnated catalyst exhibited a complete reduction in acetic acid concentration once the reaction reached steady state. Acetic acid can further decompose to CO_2 directly or *via* formic acid[63]; given no increase in formic acid was observed for either catalyst after the reaction reached steady state, it is likely the acetic acid was fully oxidised to CO_2. Given the presence of acetic acid in the end stream, the oxidation pathway would have likely proceeded *via* acrylic acid, which although not measured here, has been observed in the end stream of other CWAO operations[64,65].

Of the reaction intermediates detected, the majority were present in very low concentrations, and were in agreement with those proposed by Delvin *et al.*[53]. Although it was not possible to determine the initial reaction pathway, due to the lack of distinction between the benzoquinone isomers, the CWAO of phenol proceeded through maleic acid to acrylic and acetic acid, and *via* oxalic to formic acid. For the Pt/SiC and Pt + Ru co-impregnated catalyst, a diminish in the majority of partial oxidation products occurred once the reaction reached steady state. Any intermediates remaining in the end stream will require further treatment, therefore their identification is paramount so the appropriate treatment method, if necessary, can be selected. Knowledge of the reaction pathway can also aid future development of catalysts towards the complete destruction of phenol, or perhaps preferential production of a particular product.

To help correlate the production of the partial oxidation products with the phenol conversions achieved by the catalysts, the selectivity of the catalysts towards CO_2 was calculated. Since it was not possible to directly measure the

concentration of CO_2 during the reaction, instead the reaction intermediates measured by HPLC were used to calculate the selectivity. By calculating selectivity in this manor, a number of assumptions are being made, which must be considered. As the concentration of CO_2 was not being measured, it is assumed that no other intermediates are present in the end stream, and all carbon unaccounted for was CO_2.

The more common partial oxidation products were measured by HPLC analysis, however, not all of them were. Succinic acid, for example, has been observed in trace amounts during phenol oxidation[66]. Although unlikely to be present, as production would require the hydrogenation of the carbon – carbon double bonds in maleic acid, which would not be expected to occur to a significant degree under the oxidizing conditions of CWAO[53], the absence of this compound cannot be definitively confirmed since its concentration was not measured. The concentration of acrylic acid, another previously observed reaction intermediate, was also not measured. Consequently, the assumption that all carbon unaccounted for was CO_2, may result in an inflated selectivity value for the catalysts. Other intermediates, such as muconic acid or 2,5-dioxo-3-hexenedioic acid are expected to be too short lived to isolate[64].

The selectivity (at time t) for each of the catalysts was calculated using Equation 4.3, and then plotted as a function of time (Figure 4.19).

$$S_p = \left(1 - \frac{\sum \frac{n_s}{M}}{n_0 - n_t} \right) x \ 100$$

Equation 4.3, where S_p = selectivity of product p at time t (%), n_s = concentration of partial oxidation product at time t (moles), n_0 = concentration of phenol at time = 0 (moles), n_t = concentration of phenol at time t (moles), M = Molar ratio of moles of product/moles of substrate

and the term $\sum \frac{n_s}{M}$ calculates the moles of phenol partially oxidised to form reaction intermediates.
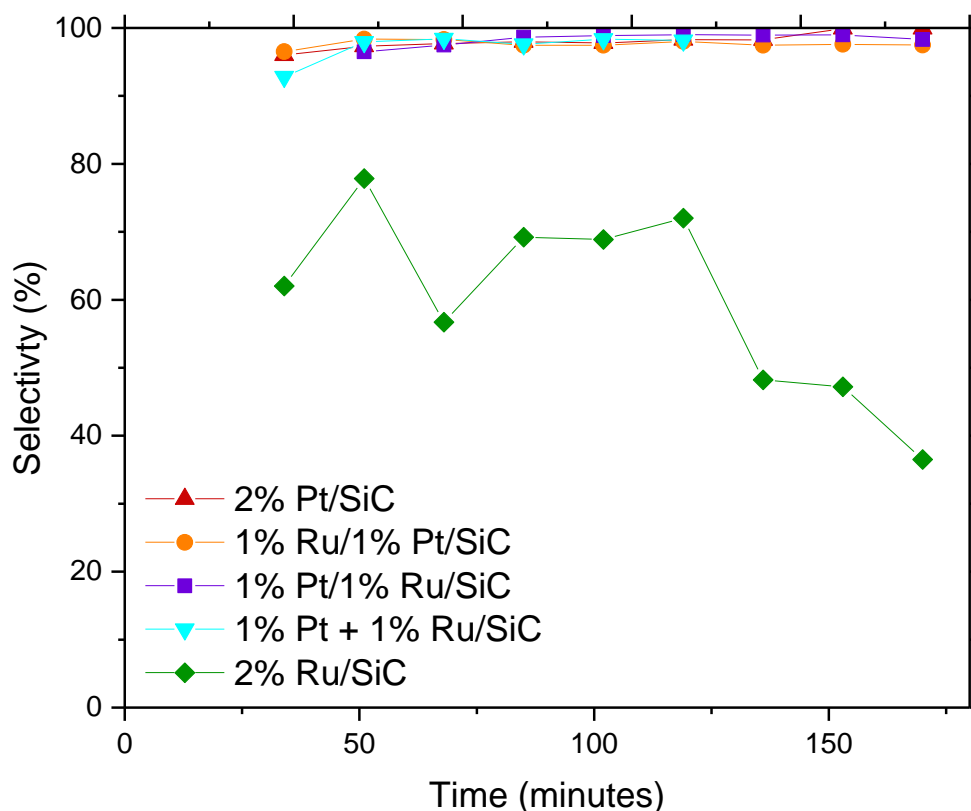
Figure 4.19 Selectivity as a function of time for the Ru and Pt SiC catalysts for CWAO of phenol at 160 °C and 7 bar$_{(g)}$

All the platinum containing catalysts exhibited high selectivity towards CO_2, with 2% Pt/SiC achieving the highest selectivity of 99.9 % after 150 minutes. The remaining platinum catalysts achieved selectivity values within 2 % of this after 170 minutes, whilst the exclusively ruthenium catalyst achieved a selectivity between 36.5 – 77.8 %, which gradually decreased as the reaction proceeded. The co-impregnated catalyst showed the highest reaction rate for phenol oxidation during the first 100 minutes, this was accompanied by a decrease in initial selectivity (92.8 %) when compared to the other Pt containing SiC catalysts.

As the majority of the catalysts achieved near 100 % selectivity, it is hard to assign a trend and definitively correlate the activity with selectivity. The high selectivity of the platinum catalysts (even during the induction period) does further prove them to be promising catalysts for CWAO of phenol. The lower activity observed for the exclusively ruthenium catalyst, accompanied by its lower selectivity, suggests platinum to be the more active metal for CWAO, when supported on SiC. Since the catalysts are operating at near 100 % conversion, only a portion of the active sites may be contributing to oxidation at any given time,

thus it is possible platinum largely is responsible for the high activities observed and the addition of ruthenium had little impact on catalytic activity. Partial substitution of Pt with Ru, however, can considerably lower costs, and maintain high catalytic performance under these conditions, and can therefore be applied to further optimize the SiC catalysts.

4.4 Post-reaction catalyst characterisation

Characterisation of the catalysts was repeated post-reaction to determine whether the catalysts underwent any chemical or physical changes during CWAO testing.

4.4.1 Powder x-ray diffraction (XRD)

Analysis of the catalysts post-reaction by XRD can reveal any phase changes the active metals may have undergone during CWAO. Catalyst deactivation caused by leaching or oxidising of the active metal has been shown for CWAO[3,67,68], XRD analysis of the used catalysts, displayed in Figure 4.20, may provide evidence of this.
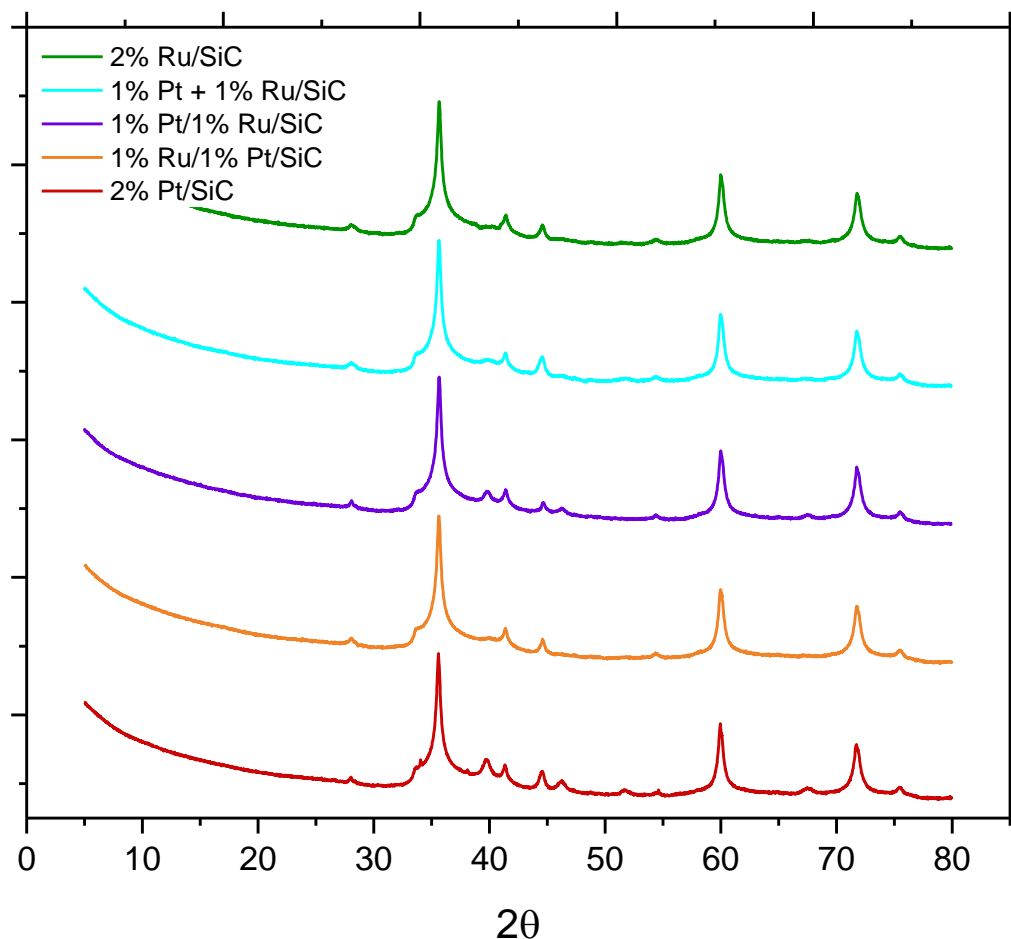
Figure 4.20 Powder XRD patterns for Ru and Pt bi-metallic SiC catalysts post-reaction

The XRD patterns of the post-reaction catalysts are similar to their pre-reaction counterparts, with no significant reduction in peak size observed for the peaks corresponding to RuO_2 and Pt. Post-reaction XRD analysis also revealed no new peaks, indicating no oxidation of the platinum or reduction of RuO_2 occurred during CWAO.

4.4.2 Thermogravimetric analysis (TGA)

TGA of post-reaction catalysts can identify any carbonaceous deposits that may have accumulated on the catalyst surface. Any carbon impurities adsorbed on the catalyst would be oxidised and identified by a mass loss in the TGA profile. The TGA profiles for the post-reaction catalysts are presented in Figure 4.21.
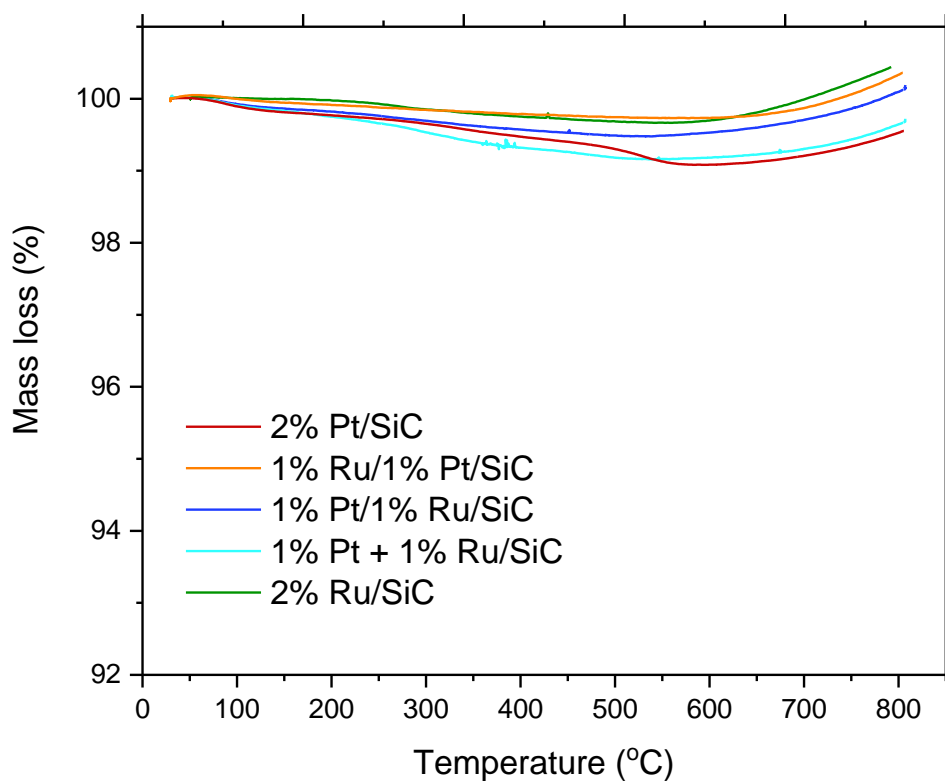
Figure 4.21 TGA analysis of Ru and Pt SiC catalysts post-reaction

The primary cause of deactivation for CWAO frequently reported in the literature is the deposition of carbonaceous species on the catalyst surface inhibiting access of pollutants to the catalyst active sites[69]. Any mass loss observed below 150 °C is characteristic of water, whilst mass loss occurring between 200 – 500 °C can be attributed to adsorbed carboxylic acid groups[70]. Catalyst deactivation caused by strong adsorption of acetic and formic acid has been previously reported for CWAO[71], both of which were observed in the treated wastewater for all the catalysts. Less than 1 % mass loss occurred for all the catalysts up to 600 °C, when compared to the 0.5 % mass loss observed for the pre-reaction catalysts, this indicates a very slow build-up of carbon deposits during the 3 hours of testing.

4.5 Conclusion

Substitution of platinum by ruthenium for SiC catalysts was investigated for CWAO of phenol. The XRD revealed the active metal components to be RuO_2

and Pt^0, whilst SEM-EDX showed high distribution of both metals on the SiC surface.

Thrifting of the metal loading by partial substitution of platinum with ruthenium showed minimal reduction in selectivity and activity towards phenol conversion at 160 °C and 7 bar$_{(g)}$. When fully substituted by ruthenium, the activity dropped below 7 % conversion, indicating that when supported on silicon carbide, platinum is a more active metal for CWAO of phenol than ruthenium.

During the induction period, the selectivity towards CO_2 was greater than 92.8 % for all the platinum containing catalysts, with measurable concentrations of carboxylic acids and benzoquinone detected in the off stream of the reactor. The exclusively platinum catalyst exhibited the highest selectivity of 99.9 %. All the catalysts impregnated with platinum achieved a selectivity >97 %, whilst the exclusively ruthenium catalyst achieved the lowest selectivity of <77.8 %.

No catalyst deactivation was seen during the period of testing, and post-reaction analysis by XRD and TGA showed no significant changes when compared to the pre-reaction counterparts.

4.6 References

(1)   Davies, D.; Catalytic Wet Air Oxidation: Developing a Continuous Process: Cardiff University PhD Thesis, **2016**.
(2)   Ledoux, M. J.; Pham-Huu, C. Silicon carbide - a novel catalyst support for heterogeneous catalysis. *Cattech* **2001**, *5* (4), 226.
(3)   Besson, M.; Gallezot, P. Deactivation of metal catalysts in liquid phase organic reactions. *Catalysis Today* **2003**, *81* (4), 547.
(4)   Saunders, K.; Davies, D.; Golunski, S.; Johnston, P.; Plucinski, P. Making the Most of Precious Metal Nanoparticles in the Purification of Industrial Wastewater by Catalytic Wet Air Oxidation Revealing synergy between platinum and catalyst support. *Johnson Matthey Technology Review* **2018,** *62* (4), 429.
(5)   Das, N.; Recovery of precious metals through biosorption - A review. *Hydrometallurgy* **2010,** *103* (1-4), 180.
(6)   Matthey, J. http://www.platinum.matthey.com/prices, Aug - Sept 2019.

(7)   Gallezot, P.; Chaumet, S.; Perrard, A.; Isnard, P. Catalytic wet air oxidation of acetic acid on carbon-supported ruthenium catalysts. *Journal of Catalysis* **1997,** *168* (1), 104.

(8)   Garcia, J.; Gomes, H. T.; Serf, P.; Kalck, P.; Figueiredo, J. L.; Faria, J. L. Carbon nanotube supported ruthenium catalysts for the treatment of high strength wastewater with aniline using wet air oxidation. *Carbon* **2006,** *44* (12), 2384.

(9)   Beziat, J. C.; Besson, M.; Gallezot, P.; Durecu, S. Catalytic wet air oxidation of carboxylic acids on TiO($_2$)-supported ruthenium catalysts. *Journal of Catalysis* **1999,** *182* (1), 129.

(10)   Wang, F.-L. a. Z. L.-Y. a. Z. Y.-F. SiC Nanowires Synthesized by Rapidly Heating a Mixture of SiO and Arc-Discharge Plasma Pretreated Carbon Black. *Nanoscale research letters* **2008,** *4*, 153.

(11)   Lunagomez Rocha, M. A.; Del Angel, G.; Torres-Torres, G.; Cervantes, A.; Vazquez, A.; Arrieta, A.; Beltramini, J. N. Effect of the Pt oxidation state and Ce^{3+}/Ce^{4+} ratio on the Pt/TiO_2-CeO_2 catalysts in the phenol degradation by catalytic wet air oxidation (CWAO). *Catalysis Today* **2015,** *250*, 10.

(12)   Monteros, A. E. d. l.; Lafaye, G.; Cervantes, A.; Del Angel, G.; Barbier Jr, J.; Torres, G. Catalytic wet air oxidation of phenol over metal catalyst (Ru,Pt) supported on TiO_2–CeO_2 oxides. *Catalysis Today* **2015,** *258, Part 2*, 564.

(13)   Masende, Z. P. G.; Kuster, B. F. M.; Ptasinski, K. J.; Janssen, F.; Katima, J. H. Y.; Schouten, J. C. Platinum catalysed wet oxidation of phenol in a stirred slurry reactor - The role of oxygen and phenol loads on reaction pathways. *Catalysis Today* **2003,** *79* (1-4), 357.

(14)   Chen, L.; Xu, Z. W.; He, C.; Wang, Y. G.; Liang, Z. Y.; Zhao, Q. X.; Lu, Q. Gas-phase total oxidation of nitric oxide using hydrogen peroxide vapor over Pt/TiO_2. *Applied Surface Science* **2018,** *457*, 821.

(15)   Milone, C.; Fazio, A.; Pistone, A.; Galvagno, S. Catalytic wet air oxidation of p-coumaric acid on CeO_2, platinum and gold supported on CeO_2 catalysts. *Applied Catalysis B-Environmental* **2006,** *68* (1-2), 28.

(16)   Hyde, T.; Crystallite size of supported platinum catalysts by XRD. *Johnson Matthey Technology Review: Platinum Metal Reviews*, **2008**; Vol. 52.

(17)   Joo, S. H.; Park, J. Y.; Renzas, J. R.; Butcher, D. R.; Huang, W. Y.; Somorjai, G. A. Size Effect of Ruthenium Nanoparticles in Catalytic Carbon Monoxide Oxidation. *Nano Letters* **2010,** *10* (7), 2709.

(18)   Ramani, M.; Synthesis and Characterization of Hydrous Ruthenium Oxide-Carbon Supercapacitors. *Journal of The Electrochemical Society - J Electrochem Soc.* **2001,** *148*.

(19)   Meng, G. W.; Cui, Z.; Zhang, L. D.; Phillipp, F. Growth and characterization of nanostructured beta-SiC *via* carbothermal reduction of SiO_2 xerogels containing carbon nanoparticles. *Journal of Crystal Growth* **2000,** *209* (4), 801.

(20)   Krawiec, P.; Kaskel, S. Thermal stability of high surface area silicon carbide materials. *Journal of Solid State Chemistry* **2006,** *179* (8), 2281.

(21)   Moene, R.; Makkee, M.; Moulijn, J. A. High surface area silicon carbide as catalyst support characterization and stability. *Applied Catalysis a-General* **1998,** *167* (2), 321.

(22)   Moradi, S. E.; Amirmahmoodi, S.; Baniamerian, M. J. Hydrogen adsorption in metal-doped highly ordered mesoporous carbon molecular sieve. *Journal of Alloys and Compounds* **2010,** *498* (2), 168.

(23)   Goodwin, R. D.; Toluene thermophysical properties from 178-K to 800-K at pressures to 1000-bar. *Journal of Physical and Chemical Reference Data* **1989,** *18* (4), 1565.

(24)   Gaur, R.; Mishra, L.; Siddiqi, M. A.; Atakan, B. Ruthenium complexes as precursors for chemical vapor-deposition (CVD). *Rsc Advances* **2014,** *4* (64), 33785.

(25)   Plyuto, Y. V.; Babich, I. V.; Sharanda, L. F.; de Wit, A. M.; Mol, J. C. Thermolysis of Ru(acac)($_3$) supported on silica and alumina. *Thermochimica Acta* **1999,** *335* (1-2), 87.

(26)   Kenvin, J. C.; White, M. G.; Mitchell, M. B.; Preparation and characterization of supported mononuclear metal-complexes as model catalysts. *Langmuir* **1991,** *7* (6), 1198.

(27)   Campanati, M.; Fornasari, G.; Vaccari, A. Fundamentals in the preparation of heterogeneous catalysts. *Catalysis Today* **2003,** *77* (4), 299.

(28)   Maugans, C. B.; Akgerman, A. Catalytic wet oxidation of phenol in a trickle bed reactor over a Pt/TiO$_2$ catalyst. *Water Research* **2003,** *37* (2), 319.

(29)   Maugans, C. B.; Akgerman, A. Catalytic wet oxidation of phenol over a Pt/TiO$_2$ catalyst. *Water Research* **1997,** *31* (12), 3116.

(30)   Bernardi, M.; Le Du, M.; Dodouche, I.; Descorme, C.; Deleris, S.; Blanchet, E.; Besson, M. Selective removal of the ammonium-nitrogen in ammonium acetate aqueous solutions by catalytic wet air oxidation over supported Pt catalysts. *Applied Catalysis B-Environmental* **2012,** *128*, 64.

(31)   Roy, J.; Chandra, S.; Das, S.; Maitra, S.; Oxidation behaviour of silicon carbide - a review. *Reviews on Advanced Materials Science* **2014,** *38* (1), 29.

(32)   Narushima, T.; Goto, T.; Hirai, T.; Iguchi, Y. High-temperature oxidation of silicon carbide and silicon nitride. *Materials Transactions Jim* **1997,** *38* (10), 821.

(33)   Poulsen, H. F.; Neuefeind, J.; Neumann, H. B.; Schneider, J. R.; Zeidler, M. D. Amorphous silica studied by high-energy x-ray-diffraction. *Nuclear Instruments & Methods in Physics Research Section B-Beam Interactions with Materials and Atoms* **1995,** *97* (1-4), 162.

(34)   Hamzah, N.; Nordin, N. M.; Nadzri, A. H. A.; Nik, Y. A.; Kassim, M. B.; Yarmo, M. A. Enhanced activity of Ru/TiO$_2$ catalyst using bisupport, bentonite-TiO$_2$ for hydrogenolysis of glycerol in aqueous media. *Applied Catalysis a-General* **2012,** *419*, 133.

(35)   Vaidya, P. D.; Mahajani, V. V. Insight into heterogeneous catalytic wet oxidation of phenol over a Ru/TiO$_2$ catalyst. *Chemical Engineering Journal* **2002,** *87* (3), 403.

(36)   Wang, J.; Liu, X. L.; Zeng, J. L.; Zhu, T. Y. Catalytic oxidation of trichloroethylene over TiO_2 supported ruthenium catalysts. *Catalysis Communications* **2016,** *76*, 13.

(37)   Alayoglu, S.; Zavalij, P.; Eichhorn, B.; Wang, Q.; Frenkel, A. I.; Chupas, P. Structural and Architectural Evaluation of Bimetallic Nanoparticles: A Case Study of Pt-Ru Core-Shell and Alloy Nanoparticles. *Acs Nano* **2009,** *3* (10), 3127.

(38)   Alayoglu, S.; Nilekar, A. U.; Mavrikakis, M.; Eichhorn, B. Ru-Pt core-shell nanoparticles for preferential oxidation of carbon monoxide in hydrogen. *Nature Materials* **2008,** *7* (4), 333.

(39)   Brankovic, S. R.; Wang, J. X.; Adzic, R. R. Pt submonolayers on Ru nanoparticles - A novel low Pt loading, high CO tolerance fuel cell electrocatalyst. *Electrochemical and Solid State Letters* **2001,** *4* (12), A217.

(40)   Diemant, T.; Hager, T.; Hoster, H. E.; Rauscher, H.; Behm, R. J. Hydrogen adsorption and coadsorption with CO on well-defined bimetallic PtRu surfaces - a model study on the CO tolerance of bimetallic PtRu anode catalysts in low temperature polymer electrolyte fuel cells. *Surface Science* **2003,** *541* (1-3), 137.

(41)   Alayoglu, S.; Eichhorn, B. Rh-Pt Bimetallic Catalysts: Synthesis, Characterization, and Catalysis of Core-Shell, Alloy, and Monometallic Nanoparticles. *Journal of the American Chemical Society* **2008,** *130* (51), 17479.

(42)   Zhou, S. H.; Varughese, B.; Eichhorn, B.; Jackson, G.; McIlwrath, K. Pt-Cu core-shell and alloy nanoparticles for heterogeneous NOx, reduction: Anomalous stability and reactivity of a core-shell nanostructure. *Angewandte Chemie-International Edition* **2005,** *44* (29), 4539.

(43)   Asundi, A. S.; Hoffman, A. S.; Nathan, S. S.; Boubnov, A.; Bare, S. R.; Bent, S. F. Impurity Control in Catalyst Design: The Role of Sodium in Promoting and Stabilizing Co and Co_2C for Syngas Conversion. *Chemcatchem* **2021,** *13* (4), 1186.

(44)   Sadana, A.; Katzer, J. R. Catalytic-oxidation of phenol in aqueous-solution over copper oxide. *Industrial & Engineering Chemistry Fundamentals* **1974,** *13* (2), 127.

(45)   Mukherjee, A.; Graydon, W. F. Heterogeneous catalytic oxidation of Tetralin. *The Journal of Physical Chemistry* **1967,** *71* (13), 4232.

(46)   Sadana, A.; Katzer, J. R. Involvement of free-radicals in aqueous-phase catalytic-oxidation of phenol over copper oxide. *Journal of Catalysis* **1974,** *35* (1), 140.

(47)   Pintar, A.; Levec, J. Catalytic liquid-phase oxidation of phenol aqueous-solutions - a kinetic investigation. *Industrial & Engineering Chemistry Research* **1994,** *33* (12), 3070.

(48)   Vreugdenhil, A. D. Mechanism of the silver-on-silica catalyzed oxidation of cumene in the liquid phase. *Journal of Catalysis* **1973,** *28* (3), 493

(49)   Luna, A. J.; Rojas, L. O. A.; Melo, D. M. A.; Benachour, M.; de Sousa, J. F. Total catalytic wet oxidation of phenol and its chlorinated derivates with MnO_2/CeO_2 catalyst in a slurry reactor. *Brazilian Journal of Chemical Engineering* **2009,** *26* (3), 493.

(50)   Vaidya, P. D.; Mahajani, V. V. Insight into sub-critical wet oxidation of phenol. *Advances in Environmental Research* **2002,** *6* (4), 429.

(51)   Yang, J.; Stuart, M. A. C.; Kamperman, M. Jack of all trades: versatile catechol crosslinking mechanisms. *Chemical Society Reviews* **2014,** *43* (24), 8271.

(52)   Kolaczkowski, S. T.; Beltran, F. J.; McLurgh, D. B.; Rivas, F. J. Wet air oxidation of phenol: Factors that may influence global kinetics. *Process Safety and Environmental Protection* **1997,** *75* (B4), 257.

(53)   Devlin, H. R.; Harris, I. J. Mechanism of the oxidation of aqueous phenol with dissolved-oxygen. *Industrial & Engineering Chemistry Fundamentals* **1984,** *23* (4), 387.

(54)   Alejandre, A.; Medina, F.; Fortuny, A.; Salagre, P.; Sueiras, J. E. Characterisation of copper catalysts and activity for the oxidation of phenol aqueous solutions. *Applied Catalysis B-Environmental* **1998,** *16* (1), 53.

(55)   Pintar, A.; Levec, J. Catalytic-oxidation of organics in aqueous-solutions .1. kinetics of phenol oxidation. *Journal of Catalysis* **1992,** *135* (2), 345.

(56)   Shende, R. V.; Levec, J. Subcritical aqueous-phase oxidation kinetics of acrylic, maleic, fumaric, and muconic acids. *Industrial & Engineering Chemistry Research* **2000,** *39* (1), 40.

(57)   Santos, A.; Yustos, P.; Quintanilla, A.; Rodriguez, S.; Garcia-Ochoa, F. Route of the catalytic oxidation of phenol in aqueous phase. *Applied Catalysis B-Environmental* **2002,** *39* (2), 97.

(58)   Gallezot, P.; Laurain, N.; Isnard, P. Catalytic wet-air oxidation of carboxylic acids on carbon-supported platinum catalysts. *Applied Catalysis B-Environmental* **1996,** *9* (1-4), L11.

(59)   Mikulova, J.; Barbier-Jr, J.; Rossignol, S.; Mesnard, D.; Duprez, D.; Kappenstein, C. Wet air oxidation of acetic acid over platinum catalysts supported on cerium-based materials: Influence of metal and oxide crystallite size. *Journal of Catalysis* **2007,** *251* (1), 172.

(60)   Oliviero, L.; Barbier, J.; Duprez, D.; Wahyu, H.; Ponton, J. W.; Metcalfe, I. S.; Mantzavinos, D. Wet air oxidation of aqueous solutions of maleic acid over Ru/CeO$_2$ catalysts. *Applied Catalysis B-Environmental* **2001,** *35* (1), 1.

(61)   Shende, R. V.; Levec, J. Wet oxidation kinetics of refractory low molecular mass carboxylic acids. *Industrial & Engineering Chemistry Research* **1999,** *38* (10), 3830.

(62)   Luck, F. A review of industrial catalytic wet air oxidation processes. *Catalysis Today* **1996,** *27* (1-2), 195.

(63)   Mantzavinos, D.; Hellenbrand, R.; Livingston, A. G.; Metcalfe, I. S. Catalytic wet air oxidation of polyethylene glycol. *Applied Catalysis B-Environmental* **1996,** *11* (1), 99.

(64)   Béziat, J.-C.; Besson, M.; Gallezot, P.; Durécu, S. Catalytic Wet Air Oxidation on a Ru/TiO$_2$ Catalyst in a Trickle-Bed Reactor. *Industrial & Engineering Chemistry Research* **1999,** *38* (4), 1310.

(65)   Shende, R. V.; Mahajani, V. V. Kinetics of wet air oxidation of glyoxalic acid and oxalic-acid. *Industrial & Engineering Chemistry Research* **1994,** *33* (12), 3125.

(66) Krajnc, M.; Levec, J. On the kinetics of phenol oxidation in supercritical water. *Aiche Journal* **1996**, 42 (7).

(67) Kim, K. H.; Ihm, S. K. Heterogeneous catalytic wet air oxidation of refractory organic pollutants in industrial wastewaters: A review. *Journal of Hazardous Materials* **2011,** *186* (1), 16.

(68) Kouraichi, R.; Delgado, J. J.; Lopez-Castro, J. D.; Stitou, M.; Rodriguez-Izquierdo, J. M.; Cauqui, M. A. Deactivation of Pt/MnO$_x$-CeO$_2$ catalysts for the catalytic wet oxidation of phenol: Formation of carbonaceous deposits and leaching of manganese. *Catalysis Today* **2010,** *154* (3-4), 195.

(69) Keav, S.; de los Monteros, A. E.; Barbier, J.; Duprez, D. Wet Air Oxidation of phenol over Pt and Ru catalysts supported on cerium-based oxides: Resistance to fouling and kinetic modelling. *Applied Catalysis B-Environmental* **2014,** *150*, 402.

(70) Santiago, M.; Stuber, F.; Fortuny, A.; Fabregat, A.; Font, J. Modified activated carbons for catalytic wet air oxidation of phenol. *Carbon* **2005,** *43* (10), 2134.

(71) Pintar, A.; Batista, J.; Tisler, T. Catalytic wet-air oxidation of aqueous solutions of formic acid, acetic acid and phenol in a continuous-flow trickle-bed reactor over Ru/TiO$_2$ catalysts. *Applied Catalysis B-Environmental* **2008,** *84* (1-2), 30.

Chapter 5

Effect of surface area on silicon carbide catalysts for CWAO of phenol

5.1 Introduction

As previously seen, Pt/SiC has been shown to be a very effective catalyst for the CWAO of phenol, this is believed to be because of SiC's hydrophobic nature, with 2 % Pt/SiC achieving 100 % phenol conversion at 7 bar$_{(g)}$ and 160 ^{o}C. It is proposed that the hydrophobic nature of SiC allows for a secondary oxidation mechanism, not reliant on the kinetically difficult step of oxygen dissolution, as discussed in Chapter 2.

Silicon carbide has an ordered, highly crystalline structure, as indicated by the large, sharp peaks seen in the XRD, and has a notoriously low surface area. Typically, commercially available β-SiC has a surface area of less than 30 m^2 g^{-1}, which greatly affects its desirability as an industrial catalyst support. Surface area can play a major role in catalytic activity, and increasing the surface area of a catalyst has been directly linked to increased activity on multiple occasions[1,2]. Often, if the surface area of the support is increased, the dispersion of the metal nano-particles is increased, thus the number of exposed metal atoms, which are typically the active sites, is increased, allowing the catalyst to achieve higher activity. To make SiC more industrially viable, a higher surface area is necessary. Three β-SiC supports were obtained from SICAT™, with varying nominal surface areas, SiC1 – 25 m^2 g^{-1}, SiC4 – 30 m^2 g^{-1}, and a TiC-SiC composite – 90 m^2 g^{-1}. A sacrifice was made in SiC's crushing strength with increased surface area, but for the purposes of CWAO it is more than adequate. A catalyst containing 2 % platinum was prepared *via* incipient wetness impregnation for each SiC support.

To be able to effectively compare these catalyst supports, a hydrophilic catalyst, 2 % Ru/5 % ceria/alumina, proven to be effective for phenol oxidation[3], was also prepared and tested, alongside the silicon carbide based catalysts.

Due to the similar nature of the catalysts, a shorthand key was used to help clearly distinguish between them, which is outlined in Table 5.1.

Table 5.1 A shorthand key used to distinguish between the catalysts used in this chapter

Code	Active component(s)	Support
K7	2 % Platinum	Silicon carbide - 1.6 mm Trilobe extrudate, 25 m^{2}g^{-1} nominal surface area, Calcined at 500 $^{\circ}$C
K8	2 % Platinum	Silicon carbide - 1.6 mm Trilobe extrudate, 30 m^{2}g^{-1} nominal surface area, Calcined at 500 $^{\circ}$C
K9	2 % Platinum	Silicon carbide and titanium carbide composite - 1.6 mm Trilobe extrudate, 90 m^{2}g^{-1} nominal surface area, Calcined at 500 $^{\circ}$C
K10	2 % Ruthenium, 5 % ceria	Alumina – 450 – 600 µm granules, Calcined at 500 $^{\circ}$C

5.2 Pre-reaction catalyst characterisation

A variety of characterisation techniques were employed to investigate catalyst structure and composition, which can then allow correlations to be made with activity towards CWAO. A combination of bulk and surface sensitive techniques were used to investigate how the catalysts might behave in terms of promoting oxidation.

5.2.1 Powder X-ray diffraction (XRD)

XRD analyses the bulk composition of the catalysts; the resultant diffraction angles of the peaks are characteristic of specific crystal structure, allowing the components of each catalyst to be identified through comparison with a reference database. Figure 5.1 shows the diffraction profiles for catalysts K7, K8 and K9.

Metallic platinum (Pt) ----------

Platinum oxide (PtO$_2$) ----------
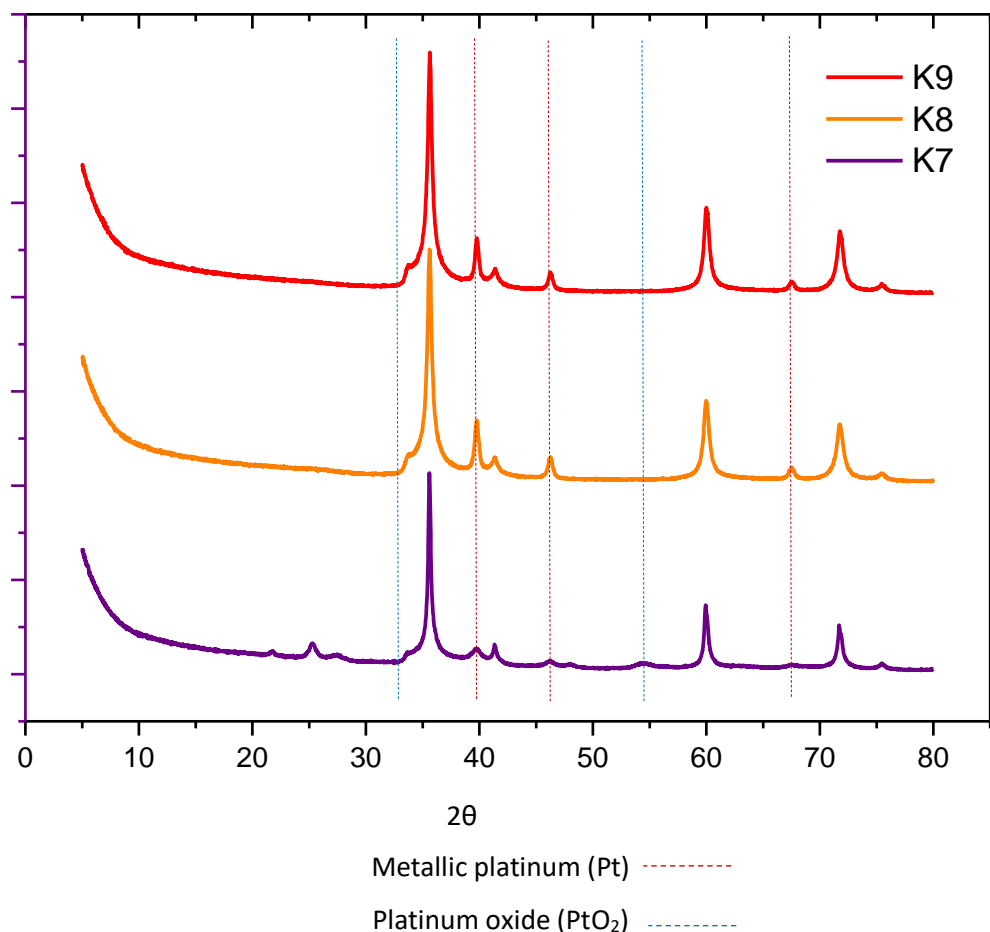
Figure 5.1 Powder XRD patterns of catalysts K7, K8 and K9

The diffraction patterns for the Pt/SiC catalysts are, as expected, very similar, with the majority of the peaks attributed to SiC. The large, sharp peaks present at 35.5°, 41.5°, 60°, 72° and 75.5° all concur with β-silicon carbide[4]. The titanium carbide peaks expected for K9 occur in almost identical positions to SiC, making them indistinguishable from the aforementioned SiC peaks[5]. The most noticeable difference between the catalysts are the peaks, which are characteristic of metallic platinum[6], occurring at 40°, 46° and 67.5°, indicated by

the dotted red lines in Figure 5.1. These metallic platinum peaks are significantly smaller for K7 than the equivalent peaks for K8 and K9. Further analysis of XRD pattern shows the presence of platinum oxide $(PtO_2)[7]$ for K7, indicated by the dotted blue lines at 33.5° and 54.5°, these peaks are absent for K8 and K9.

Both metallic platinum and platinum oxide have proven to be active for the CWAO of phenol, however, lower catalytic activity has been observed for PtO_2 compared with metallic Pt on identical supports[3]. Platinum oxide may also promote oxidation at the less favourable para position, which can increase the potential for polymerisation of the reaction products[8-11]. The reduction in loading for metallic Pt, as some Pt forms PtO_2, could negatively impact the catalytic activity of K7, when compared with K8 and K9.
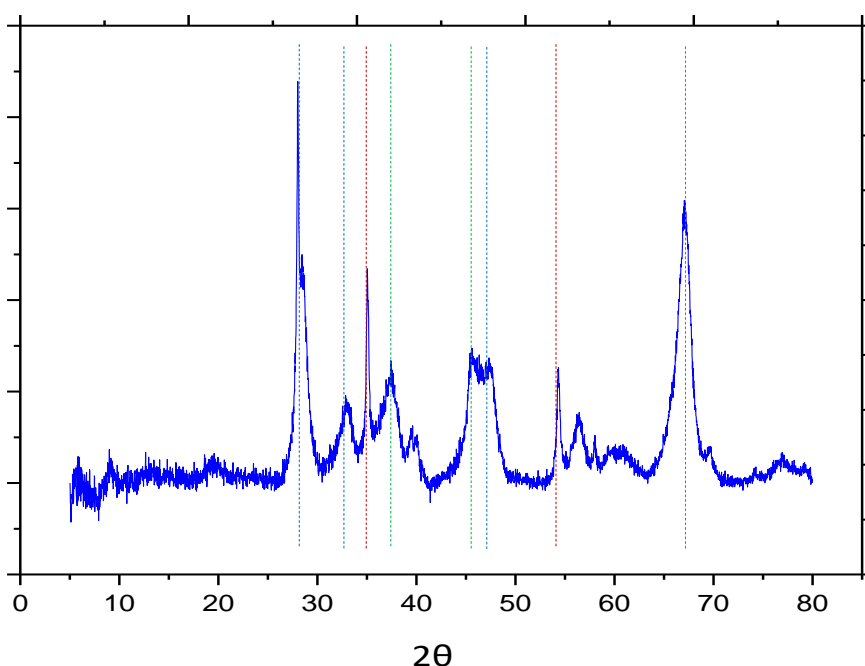
Figure 5.2 Powder XRD pattern of catalyst K10

Ruthenium Oxide (RuO_2) ----------

Ceria ----------

Alumina ----------

The XRD pattern for K10 (Ru/ceria/alumina), displayed in Figure 5.2, showed the presence of ruthenium oxide, RuO_2, at 35°, 47.5° and 54° (indicated by the dotted red lines) with no peaks characteristic of metallic Ru occurring at 45°, 48°, 50° and 52° [12,13]. While some of the peaks for metallic Ru would overlap with those for RuO_2, the lack of peaks seen at 50° and 52° are an indication that

metallic Ru is unlikely to be present. XRD considers the bulk of the sample and identification of small nanoparticles are not visible, and so small particles of metallic Ru on the surface may not have been detected, this also applies for surface PtO_2 regarding K7 – 9[14]. The combination of this and the background noise mean that the absence of metallic Ru cannot necessarily be confirmed through XRD data alone. Techniques such as x-ray photoelectron spectroscopy, however, can help identify surface species and determine the surface oxidation state of the metal.

The remainder of the peaks can be attributed to ceria at 28°, 33° and 47.5° and alumina occurring at 37.5°, 45.5° and 67°, indicated by the blue and green lines respectively. These values are supported by those in the literature[15,16].

By use of the Scherrer[17] equation, it is possible to estimate the average crystallite size of the active metal for each catalyst. The results can be seen in Table 5.2.

Table 5.2 Average platinum crystallite size for catalysts K7, K8 and K9 and average ruthenium crystallite size for K10

Catalyst	K7	K8	K9	K10
Average crystallite diameter (nm)	13.5	18.7	18.6	25.6

Smaller crystallites are preferable as it implies a higher surface area of exposed metal atoms, leading to more available active sites. K8 and K9 show similar platinum crystallite size of approximately 18 nm, with the estimate for K7 around 13 nm; the ruthenium crystallite size for K10 was the largest at 25 nm. These results are in accordance with those seen in the literature, when supported on TiO_2, an average platinum crystallite size of 16 nm was observed[18]. Calculation of the crystallite size is a useful characterisation tool in catalysis, however, it is important to consider the associated error with the Scherrer equation and note that is largely an estimate of crystallite size. The Scherrer equation operates on the assumption that only the grain size is responsible for peak broadening and for analysis to be meaningful, the peak width must be purely that pertaining to the

material and free from effects such as instrumental broadening[19]. Defects, dislocations or micro-strain in the sample, brought about by catalyst preparation, can also cause discrepancies in the XRD pattern, and thus estimated crystallite size[20]. Typically, when in the regime of <100 nm, a deviation of approximately 15 % can be expected when calculating crystallite size *via* the Scherrer equation[21].

5.2.2 Surface area and pore volume studies

Nitrogen adsorption using the BET method was used to measure the surface area of the various catalysts, whilst a helium pycnometer was utilized to analyse the pore volume, the results of which are presented in Table 5.3.

Table 5.3 Surface areas ($m^2 g^{-1}$) determined using BET nitrogen adsorption of catalysts K7, K8, K9 and K10 and pore volumes ($cm^3 g^{-1}$) determined using helium pycnometry of catalyst supports (before calcination) and catalysts (after calcination) at 500 ^oC

Catalyst	Catalyst surface area ($m^2 g^{-1}$)	Nominal surface area ($m^2 g^{-1}$)	Catalyst pore volume ($cm^3 g^{-1}$)	Support pore volume before calcination ($cm^3 g^{-1}$)
K7	29	25	0.3	0.3
K8	35	30	0.3	0.3
K9	34	90	0.3	0.3
K10	110	-	0.5	0.5

Upon characterisation of the catalysts by BET, it became apparent that the calcination step during catalyst preparation had adversely affected the surface area of K9. K7 and K8 both exhibited surfaces areas slightly higher than the nominal values specified by the supplier. The alumina chosen for K10 consisted of high surface area γ-alumina, so this larger surface area was as expected.

The pore volume of the catalysts and uncalcined supports was also measured using helium pycnometry, but no apparent change in pore volume was observed between the supports and their corresponding catalysts. As previously mentioned in Chapter 4, SiC is known to have low porosity and thus, the

impregnation of metal particles is less likely to have a significant effect on the surface area and pore volume. The alumina support for K10 shows an increase in porosity compared with SiC and similar pore volume values for γ-alumina are established in the literature[22,23]. Song *et al.*[24] observed no variations in pore volume or pore size when platinum was impregnated on to TiO_2, suggesting that the insertion of the metal particles did not significantly modify the textural properties of the support

To confirm the calcination process was responsible for the loss of surface area observed for K9, the SiC-TiC support underwent heat treatment for 2 hours at 300 °C, 400 °C and 500 °C. The resulting surface areas measurements, determined using the BET method, are shown in Table 5.4 and compared to the pre-calcined support.

Table 5.4 Surface areas in $m^2 g^{-1}$ determined using BET nitrogen adsorption of K9, SiC-TiC support calcined between 300 – 500 °C

	Surface area ($m^2 g^{-1}$)
K9 SiC-TiC support, uncalcined	98
K9 SiC-TiC support, calcined at 300°c	32
K9 SiC-TiC support, calcined at 400°c	31
K9 SiC-TiC support, calcined at 500°c	33

Even at temperatures as low as 300 °C, the large loss in surface area is still observed. Further analysis of SiC-TiC is required to help determine the cause of this surface area change. Although not necessarily the determining factor for an effective catalyst, increasing the surface area has been shown to have a positive effect on catalyst activity for CWAO[25]. With this in mind we would expect K10 to be a well performing catalyst, however there are several other physiochemical properties such as crystalline structure and hydrophobicity to be considered.

5.2.3 Thermogravimetric analysis (TGA)

TGA is a technique that monitors the mass loss of a catalyst as a function of temperature. It can be used as an indication of thermal stability, as well as showing the temperature range for the decomposition of metal precursors when deciding on an appropriate calcination temperature.

To obtain a better understanding of the surface area loss observed for K9, the pure support, along with the supports for K7 and K8 were subject to TGA analysis, the results of which are presented in Figure 5.3.

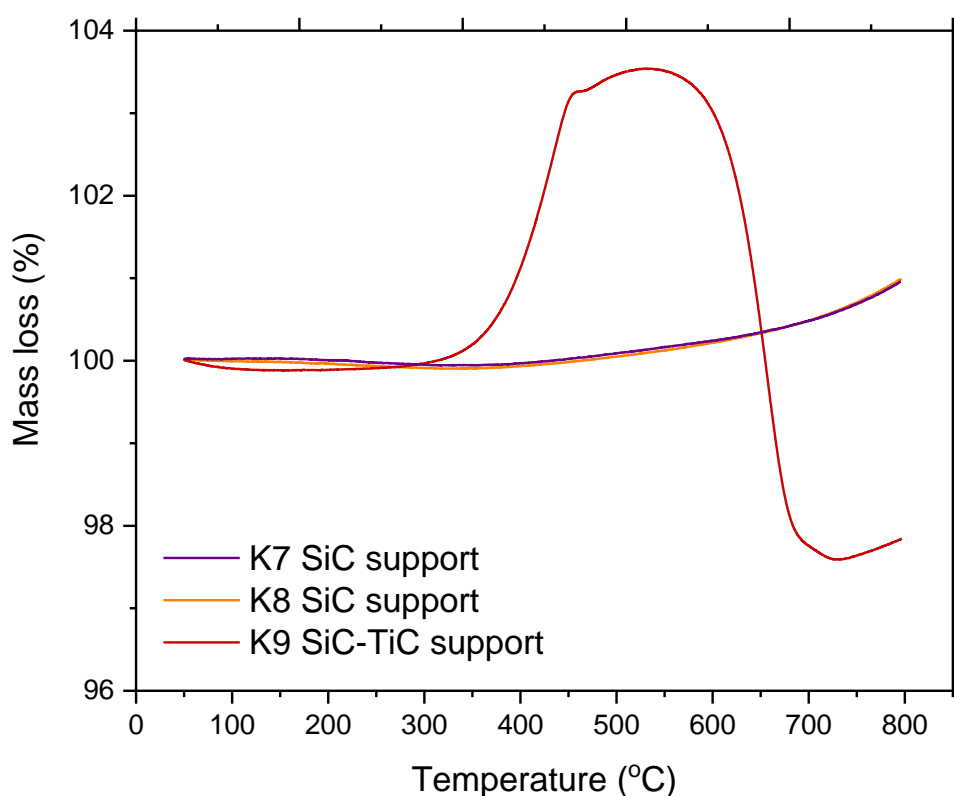*Figure 5.3 TGA profile of SiC and SiC-TiC supports*

It is apparent from the TGA profile that the SiC-TiC support undergoes a significant mass change above 300 °C, most likely responsible for the loss of surface area observed for K9 during calcination. The first derivative (dTG), which represents the rate at which the mass change has occurred, is presented in Figure 5.4 for the TGA profile of SiC-TiC.
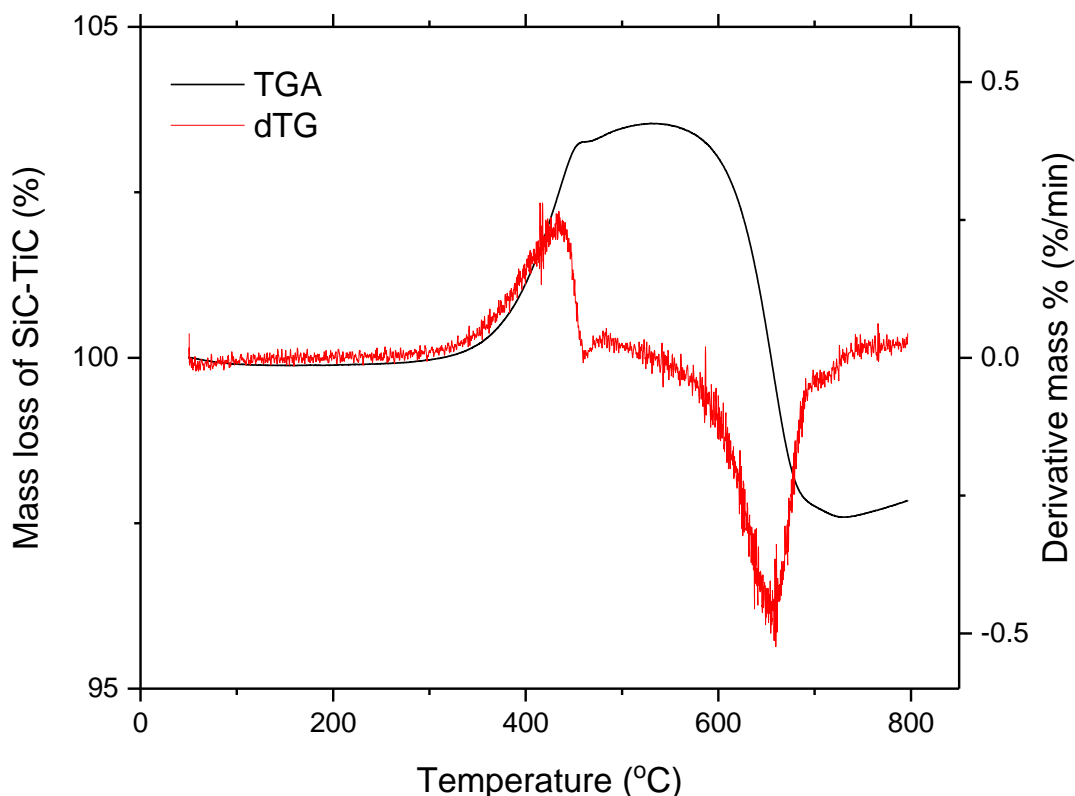
Figure 5.4 TGA profile and 1st mass derivative (dTG) of K9 SiC-TiC support

The TGA and dTG profiles of SiC-TiC reveal an initial mass increase of 3.5 % centred around 415 °C, followed by a 2.5 % mass decrease centred around 660 °C. Moene *et al.*[26] reported partial conversion of SiC to SiO$_2$ at elevated temperatures (800 °C) under air, whilst no conversion was seen under reducing N$_2$ atmosphere. The rate of oxidation was increased with the higher surface area silicon carbide samples, with a 60 – 70 % conversion to SiO$_2$ observed after 10 hours at 1000 °C. The passive oxidation of SiC was accompanied by a loss in surface area, much like what is observed here for K9, however due the low temperature at which the mass change occurs, it is unlikely that the production of SiO$_2$ is the primary cause[27]. The K7 and K8 SiC supports also show no such mass change.

Whilst investigating the oxidation of polycrystalline Ti$_3$SiC$_2$ composites between 700 – 1200 °C, Ji *et al.*[28] observed the presence of TiO$_2$ at the lowest temperature studied (700 °C), whilst the oxidation of SiC to SiO$_2$ was not observed until temperatures exceeded 900 °C. Barsoum *et al.*[29] also observed the formation of a surface oxide layer for Ti$_3$SiC$_2$ composites during heat treatment. SiO$_2$ was only

seen at temperatures above 900 $^{\circ}$C on the inner layer of the sample, whilst TiO_2 was observed on the surface at temperatures below this.

The oxidation of TiC to TiO_2 has been observed at 400 $^{\circ}$C, under atmospheric pressure[30,31], which is in line with the temperature the mass change occurs for the K9 support. Bellucci *et al.*[32] observed the partial substitution of TiC with oxygen, forming a TiC_xO_y phase, which also resulted in a reduction of surface area. Furthermore, the production of CO_2 was observed, which may account for the mass loss observed at 660 $^{\circ}$C. This suggests the oxidation of TiC to TiO_2 occurred during calcination and further explains the absence of a surface area loss observed for K7 and K8, as no TiC is present in these supports. Additional characterisation of K9 is necessary to confirm this.

To confirm the SiC-TiC support would not undergo any further mass related changes after catalyst preparation, the calcined catalysts were also subject to TGA analysis, the results of which are presented in Figure 5.5.
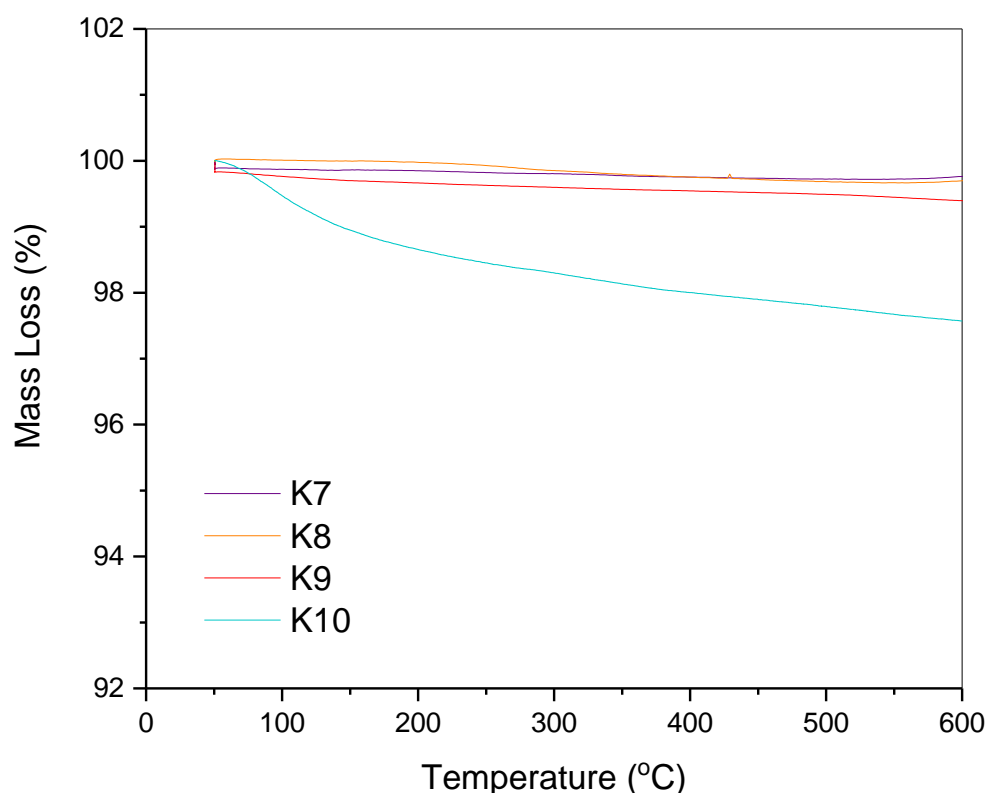
Figure 5.5 TGA profile of K7, K8, K9 and K10 fresh catalysts

Once calcined the SiC catalysts show no further significant mass changes up to 600 $^{\circ}$C. K10 shows approximately a 2 % mass loss, which the derivative

reveals to be centred around 80 °C. Mass loss observed below 150 °C is characteristic of water evaporating from the surface and given the use of water as a solvent during the preparation for K10, this is most likely the cause for the observable mass loss.

TGA can also provide an insight into the relative hydrophobicity or hydrophilicity of a solid. A hydrophilic catalyst will adsorb more water, which would be reflected in the TGA by a more prominent water loss curve. Alumina is regarded as hydrophilic due to its high degree of surface hydroxyl functionality[33]. When a water droplet comes into contact with such a surface it will form dipole interactions with the hydroxyl groups, increasing the adhesion between the catalyst surface and water, resulting in smaller contact angles[34]. SiC exhibits low surface hydroxyl functionality[3] and thus is considered hydrophobic. The preparation of K10 involves a 24 hour impregnation period where the alumina support is submerged in water; to allow for an accurate comparison, K9 was also subjected to the same immersion period and then dried in an identical manner as K10. The TGA and dTG profiles for K9 and K10 are shown in Figure 5.6 and 5.7 respectively.

Figure 5.6 TGA profile of K9, after 24 hour submersion in water with 1ˢᵗ derivative of mass loss
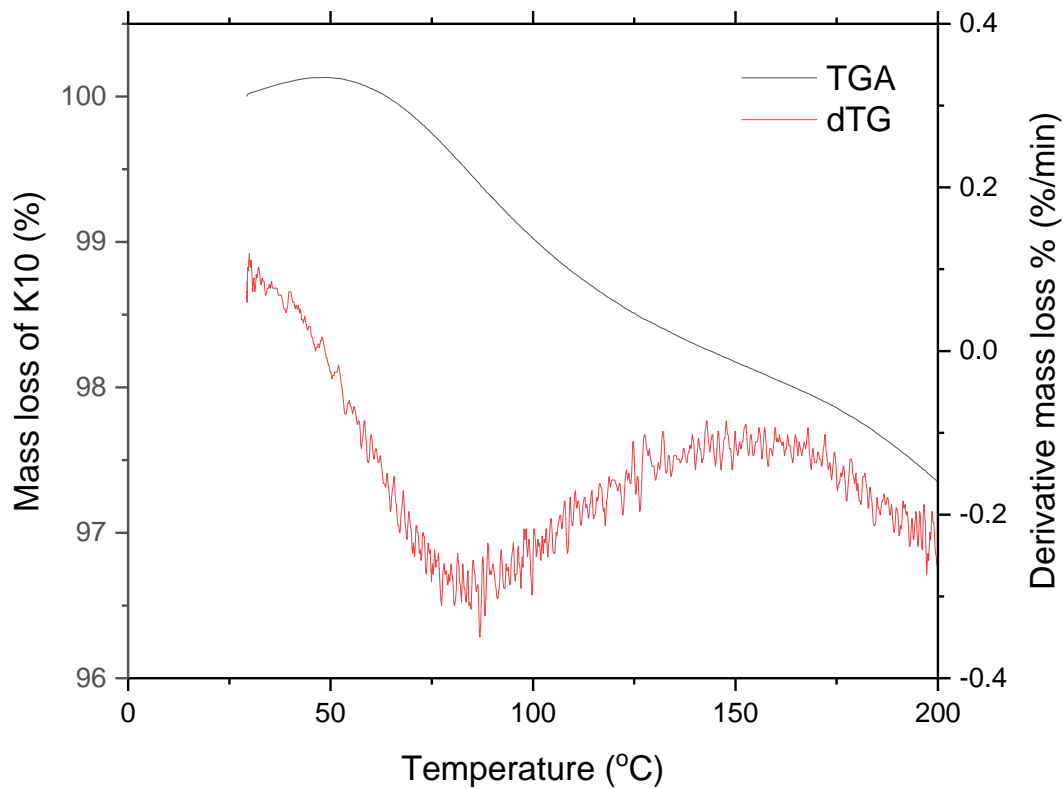
Figure 5.7 TGA profile of K10, after 24 hour submersion in water with 1ˢᵗ derivative of mass loss

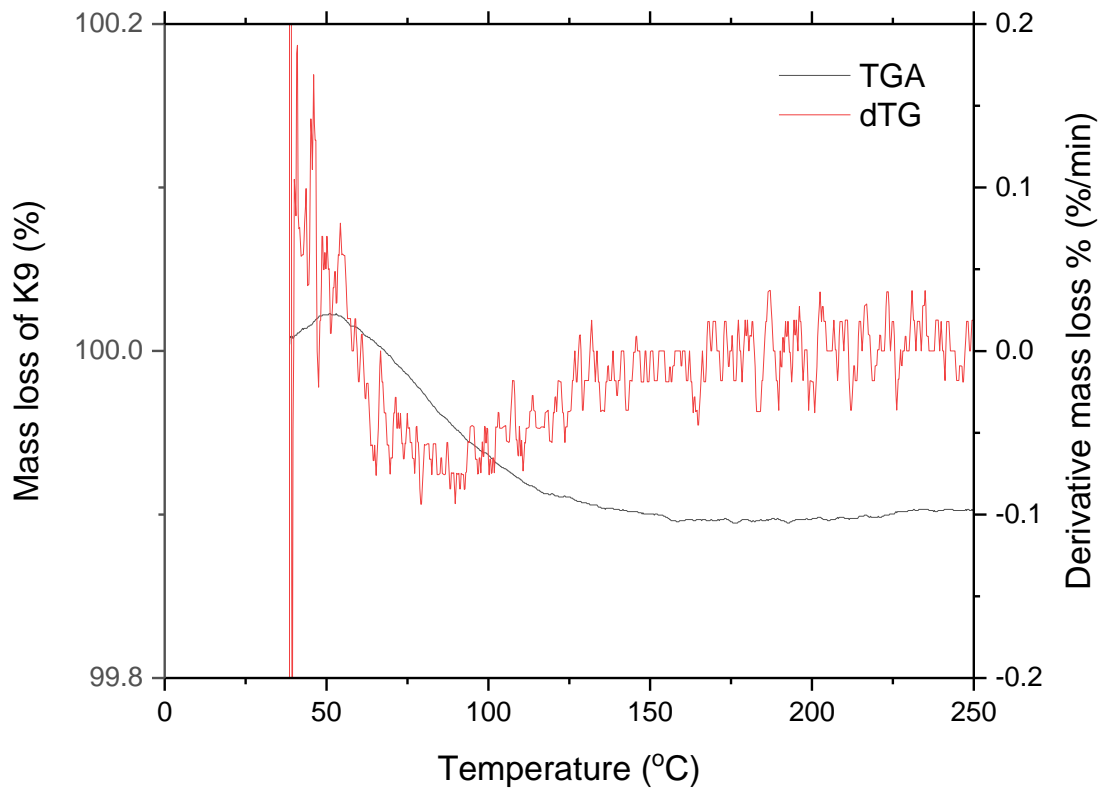The TGA and dTG profiles for K9 show a 0.1 % mass loss centred around 60 °C, whereas a 2 % mass loss is observed for K10, centred around 80 °C. By use of the TGA data and the BET surface area measurements (Table 5.3), the amount of water present in the TGA samples per surface area was calculated, the results of which are displayed in Table 5.5.

Table 5.5 Comparison of hydrophobicity defining parameters for K9 and K10

	K9	K10
Temperature at which the fastest mass loss is reached (°C)	62	80
Mass lost as water (mg)	0.040	0.699
Total surface area (m^2)	1.07	3.37
Amount of water per surface area (mg m^{-2})	0.037	0.208

The TGA data suggest K10 to be the more hydrophilic of the two catalysts, with over 560 % more water absorbed per surface area than K9. The temperature at which the fastest mass loss is reached is also lower for K9. On a hydrophobic material, the molecules in water interact with each other more strongly than with the surface of the material, resulting in larger contact angles[35]. The energy required for evaporation is therefore lower than on a hydrophilic surface, due to the reduced interaction[35]. These results conclude K9 to be the more hydrophobic and justify the use of K10 as the conventional hydrophilic catalyst.

5.2.4 X-ray photoelectron spectroscopy (XPS)

XPS is an important characterisation tool in catalysis and helps provide information on the surface of a solid sample. It enables the elemental composition to be determined, as well as quantification and identification of oxidation states of elements present on the sample surface. For the SiC catalysts (K7 − 9), the carbon 1s, silicon 2p, oxygen 1s, platinum 4f, and for K9, the titanium 2p orbitals

were probed using XPS. The carbon 1s scan for K7, K8 and K9 is shown in Figure 5.8.
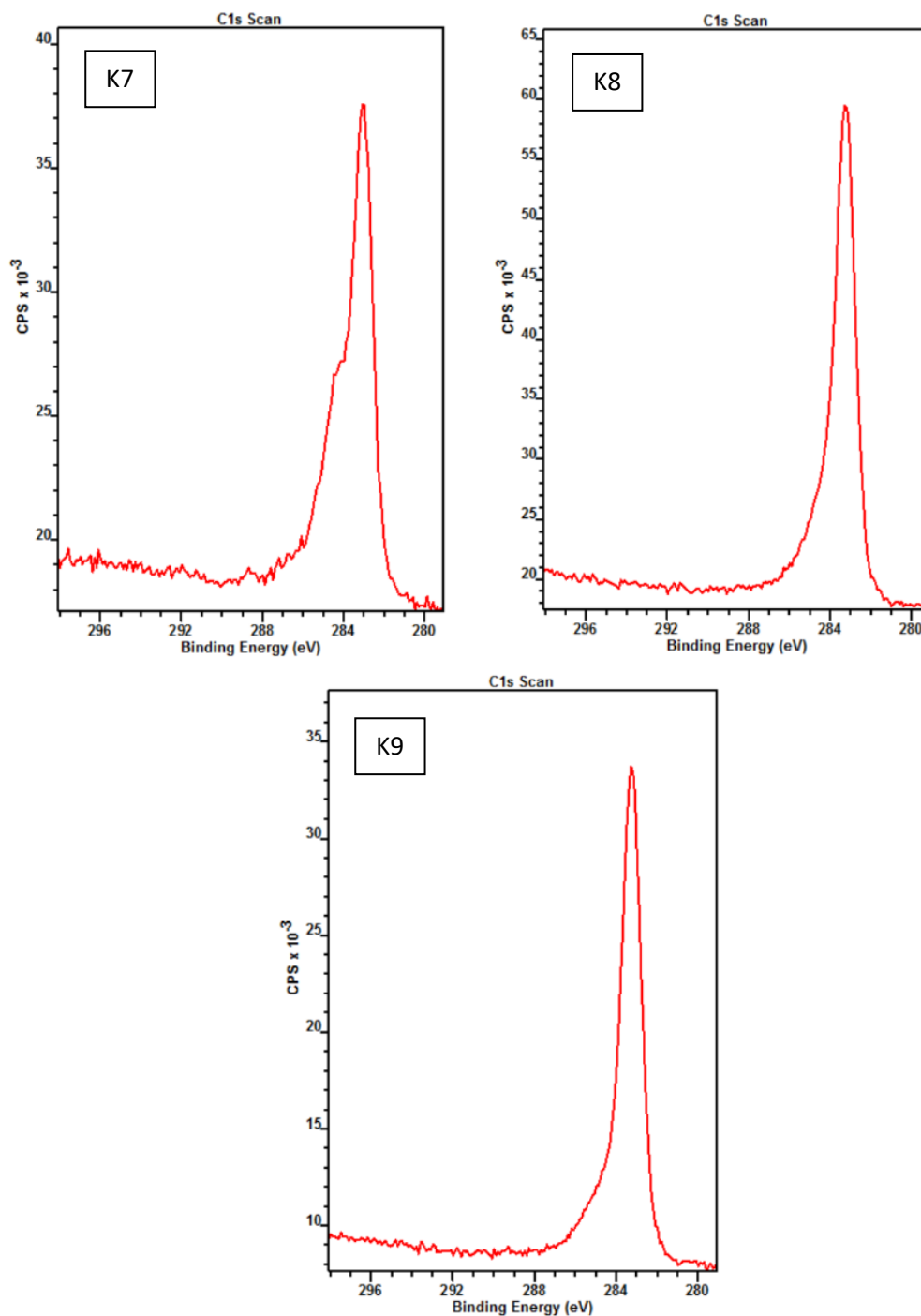
Figure 5.8 Carbon 1s XPS profile for K7 (top left), K8 (top right) and K9 (bottom middle)

The XPS profiles of K8 and K9 shows one well defined peak centred around a binding energy of 283.5 eV, indicating that the surface carbon in both catalysts is found in the same, singular environment. Although this peak is also shown in spectra for K7, the presence of the shoulder at a higher energy is indicative of a

second carbon environment, absent in K8 and K9. A probable explanation for a second carbon environment could be adventitious carbon left over from the decomposition of the metal precursor, $Pt(acac)_2$, although it is uncertain as to why this would be observed for K7 and not K8 and K9 given the identical preparation steps. Carbon deposition on platinum has been shown to be promoted by high temperatures[36,37] and it is possible the temperature reached during calcination may have promoted carbon deposition on the catalyst surface from the acetylacetonate, resulting in a second carbon environment.
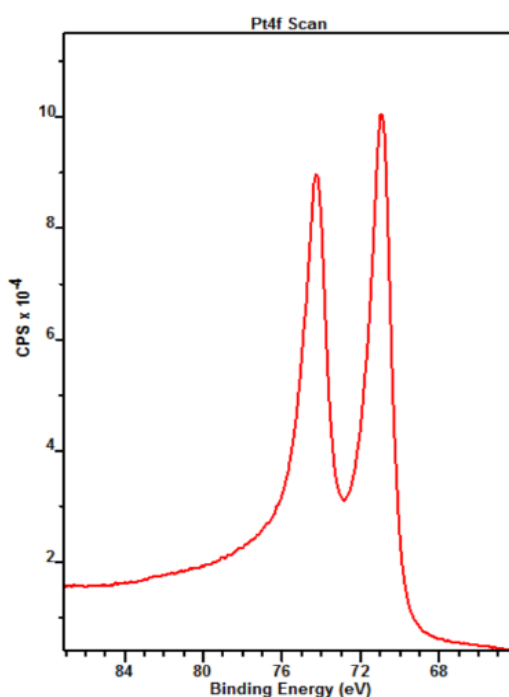
Figure 5.9 Platinum 4f XPS profile for K7

Figure 5.9 presents the XPS spectra of Pt 4f for K7, which shows two distinct peaks around 71 and 74.5 eV. According to the literature, the binding energies for Pt^0 $4f_{7/2}$ and $4f_{5/2}$ are 71.1 and 74.4 eV, respectively[38-40]. Thus, the XPS spectra of Pt 4f for K7 can be assigned to Pt^0, if PtO_2 were present, corresponding peaks for Pt^{2+} at binding energies of 73 and 76.3 eV would be expected[41]. The XRD pattern for K7 (Figure 5.1) established the presence of PtO_2, suggesting the oxide exists in the bulk of the catalyst, whilst the surface is almost exclusively metallic platinum. The Pt 4f profiles for K8 and K9 are also characteristic of metallic platinum and can be found in the appendix.
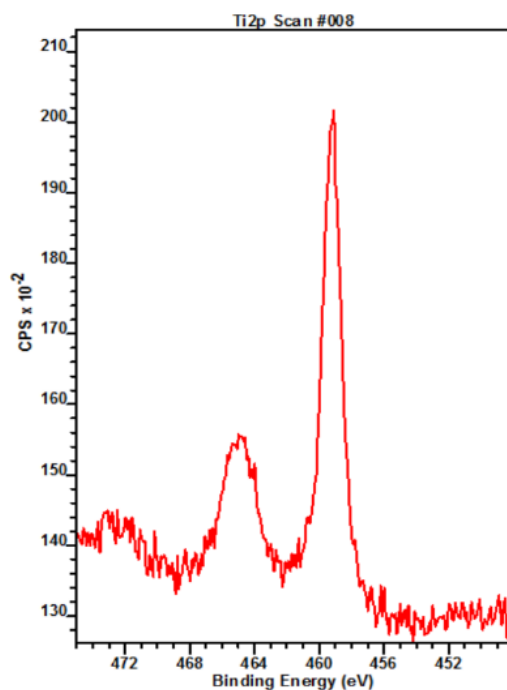
Figure 5.10 Titanium 2p XPS profile for K9

The peaks in the titanium 2p XPS profile for K9 (Figure 5.10) are typical of those seen for titanium in TiO_2, in a +4 oxidation state, at binding energies of 458.6 and 464.2 eV for Ti $2p_{3/2}$ and Ti $2p_{1/2}$ respectively[18,42,43]. It was previously discussed that during calcination K9 undergoes a mass related change, resulting in a loss of surface area. The oxidation of TiC to TiO_2 within the support was thought to be responsible and the Ti 2p spectra characteristic of TiO_2 further strengthens this hypothesis. The Ti 2p XPS spectra for TiC typically displays a peak at 455 eV[44], however, Ivanovskaya *et al.*[45] observed the Ti 2p spectra of commercial TiC samples to be more complex due the presence of various oxidised states of Ti on the TiC surface. A peak corresponding to the Ti – C bond was observed at 454.6 eV, the absence of a peak at this binding energy for K9 and presence of only one titanium environment, suggest all the TiC on the surface of the sample has been fully oxidised to TiO_2.

A second carbon environment would have also been expected in the C 1s spectra for K9 if TiC were present on the surface of the catalyst, typically occurring at 281 eV[46]. No TiO_2 peaks were observed in the XRD pattern for K9 (Figure 5.1), suggesting TiO_2 may be located in small layers primarily on the surface.
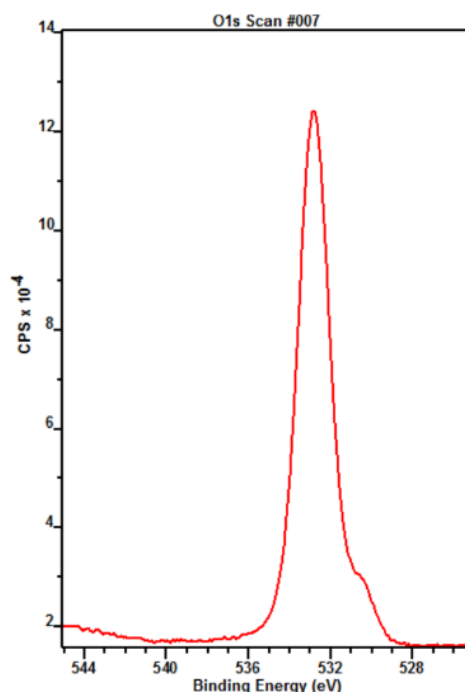
Figure 5.11 Oxygen 1s XPS profile for K9

Figure 5.11 shows the oxygen 1s spectra for K9; O 1s spectra can typically be split into three components, peaks around 529 eV correspond to lattice oxygen, whilst peaks occurring at 531 – 532 eV are characteristic of adsorbed oxygen species and peaks around 533 eV are typical of adsorbed H_2O[47]. The SiC catalysts all exhibited a distinct peak around 532 eV, characteristic of surface adsorbed oxygen species[41,48]. A small shoulder towards a lower binding energy accompanied the peak for K9, which could correspond to O^{2-} within TiO_2, typically occurring at 230 eV[45]. Oxygen in a TiO_2 environment would further confirm the oxidation of TiC during calcination, however, oxygen in adsorbed carbonate CO_3^{2-} groups has also been observed at a similar binding energy[47].

Higher percentages of surface oxygen species may promote oxidation reactions by influencing the surface characteristics and adsorption behaviour. Chemisorbed oxygen has been shown to be more active than lattice oxygen for oxidation processes, as it can more easily exchange with gas phase oxygen or molecules adsorbed on catalyst surface[25,49-51].

For K10, the aluminium 2p orbital, ruthenium 3d orbital and the cerium 3d orbital were probed. The Al 2p orbital revealed a single peak at a binding energy

of 74 eV[52], which is characteristic of alumina, the XPS profile for which can be found in the appendix. Figure 5.12 shows the Ru 3d and Ce 3d spectra of K10.
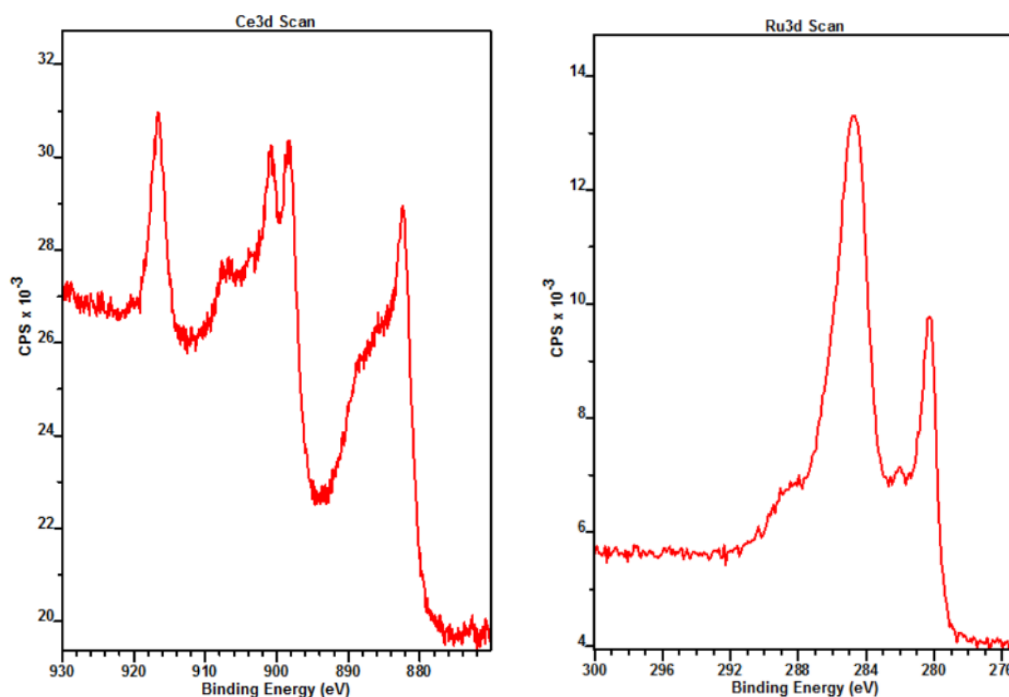
Figure 5.12 Cerium 3d (left) and ruthenium 3d (right) XPS profiles for K10

The complicated Ce 3d spectra is formed by two series of peaks consisting of $3d_{5/2}$ and $3d_{3/2}$ at $881 - 898$ eV and $900 - 918$ eV respectively[47]. The cerium 3d spectrum shows evidence of Ce^{3+} and Ce^{4+}, the peaks at 900 and 916 eV are characteristic of Ce^{4+}, whilst the lack of definition around the peak at 882 eV indicates the presences of both forms[53,54]. Rocha *et al.*[18] observed an increase in the ratio of Ce^{3+} : Ce^{4+} with increasing Ce loading for TiO_2-CeO_2 catalysts.

The Ru 3d spectra for K10 is characterised by the $3d_{5/2}$ peak located at 280.5 eV and $3d_{3/2}$ peak at 285 eV. The peak at the lowest binding energy and accompanying shoulder at 281 eV is typical of RuO_2[55,56]. If metallic ruthenium were present on the surface a peak closer to a binding energy of 280 eV would be expected[57]. The existence of RuO_2 and absence of Ru^0 are in agreement with the XRD pattern for K10.

XPS also provided elemental weight percentages (Table 5.6), which gave an interesting insight into the platinum concentration at the surface of K7, K8 and K9.

Table 5.6 Average atomic weight percentage of surface elements for catalysts K7, K8 and K9 measured using XPS

	Pt	Si	Ti	C	O
K7	11.1	33.9	-	20.8	34.2
K8	6.8	38.0	-	22.2	33.0
K9	2.9	39.1	1.0	18.6	38.3

Each catalyst was prepared with a 2 wt% loading of platinum, however the XPS analysis revealed a much higher percentage of the active metal. The catalysts were prepared by impregnation, and so it is expected that platinum be present primarily on the surface of the catalyst, but may be dispersed differently. Further characterisation techniques are required to get a full picture of metal distribution on the catalyst.

The weight percentage of oxygen on the surface of K9 is higher than seen for K7 and K8; possibly due to the oxidation of surface TiC to TiO_2. For activated carbon catalysts, a high percentage of surface oxygen species gave rise to increased activity for CWAO[58].

5.2.5 Scanning electron microscopy (SEM) and energy dispersive x-ray spectroscopy (EDX)

SEM is an analytical technique widely used to visually analyse the topography of a solid surface, often used in conjunction with EDX, which provides elemental analysis, to give an insight into particle shape, size and distribution.

5.2.5.1 Microscopy studies of K7 catalyst
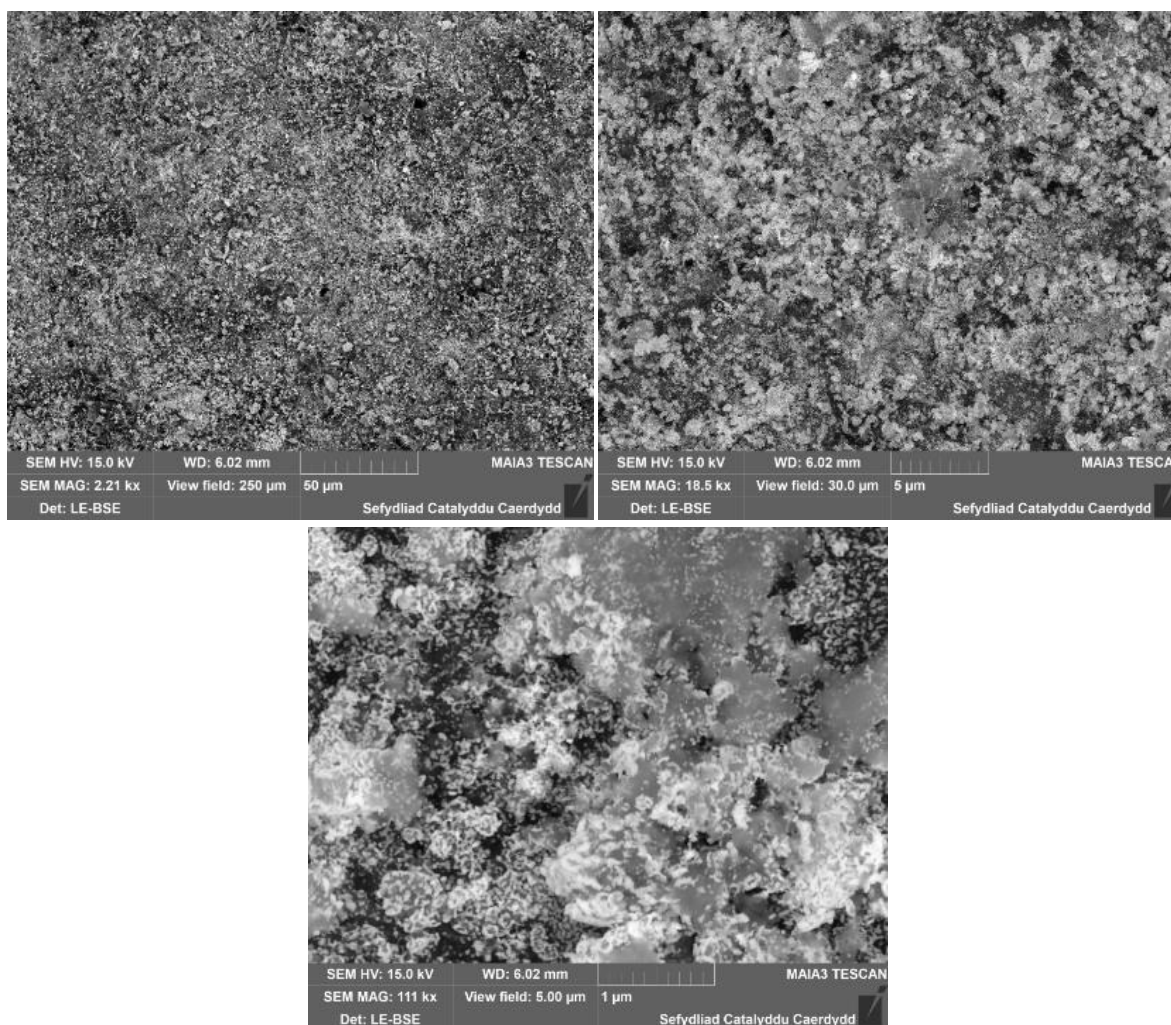
Figure 5.13 SEM images of K7 at 2.2, 18.5 and 111 kx magnification

Figure 5.13 displays the SEM images of catalyst K7, the bright spots on the images indicate the presence of platinum. At the higher magnification, and with the help of EDX mapping, the platinum appears to be densely spread over the external surface of the catalyst pellet, which could be responsible for the high metal weight percentages seen in the XPS.

The SiC catalyst support consisted of 1.6 mm trilobe shaped extrudates with a maximum length of 0.5 cm. A cross-section of the extruded pellet was obtained by dissecting the pellet width wise, by use of a scalpel. The cross-section was then re-examined under SEM to establish whether any platinum exists within the internal pore structure of the pellets. The cross-section SEM images of K7 can be seen in Figure 5.14.
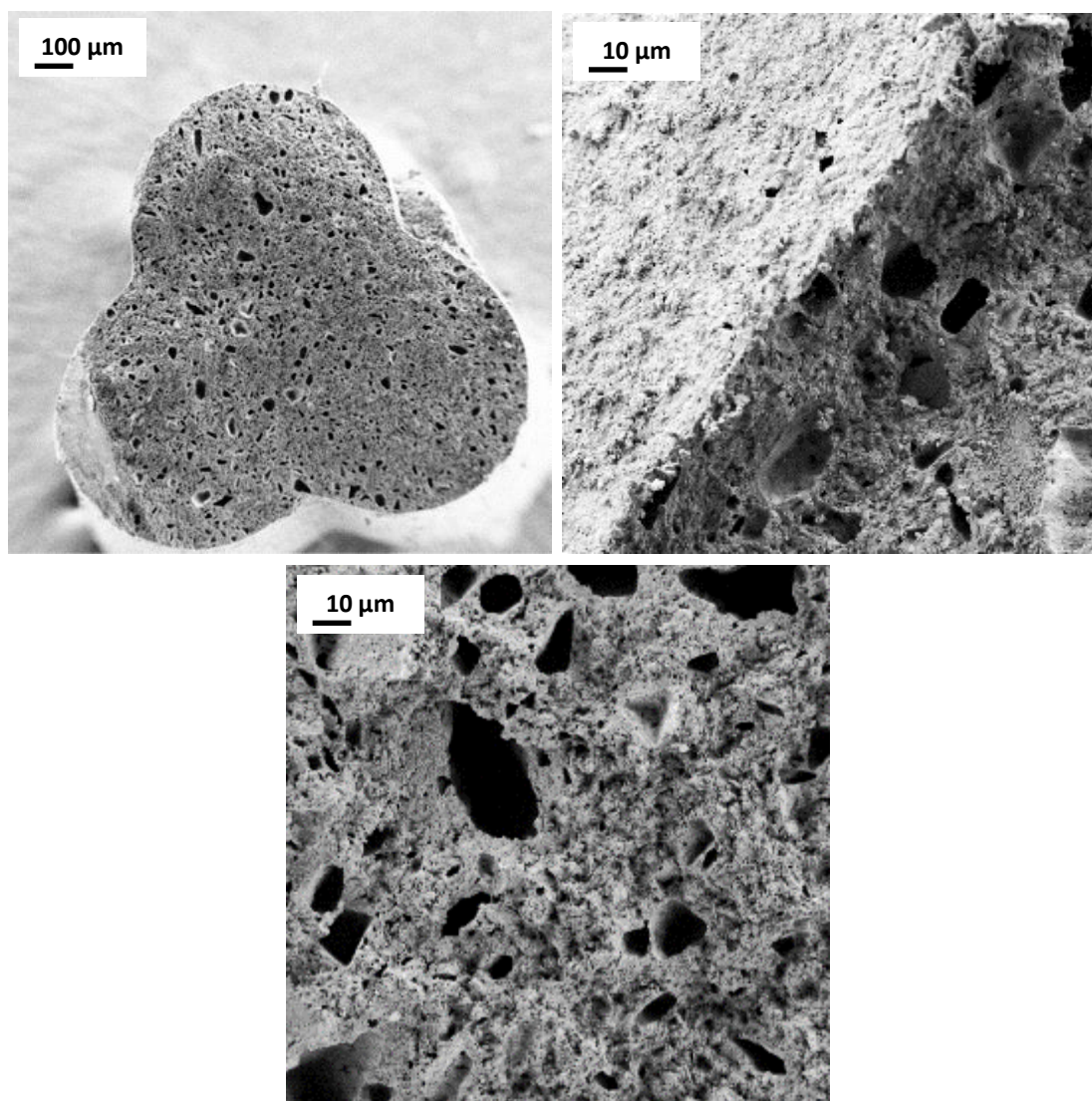
Figure 5.14 SEM images of K7 catalyst pellet cross section (top left), boundary between external surface and cross section (top right) and inner cross section (bottom middle)

The images of the dissected catalyst show a porous inner region in contrast to the less permeable outer external surface. The presence of platinum is only seen on the outer surface of the pellet, with no metal observed in the inner cross-section of any of the samples. This not only results in a high external pellet surface metal concentration, but also implies a low dispersion of the metal throughout the inner pore structure of the catalyst.

Inhomogeneous covering of catalyst supports by the active material has been previously seen for catalysts prepared by impregnation[59], and was the result of sufficiently weak interactions between the metal precursor and support material during preparation. The catalyst preparation *via* impregnation and low

porosity of SiC may both contribute to the low dispersion of platinum observed for K7.

5.2.5.2 Microscopy studies of K8 catalyst
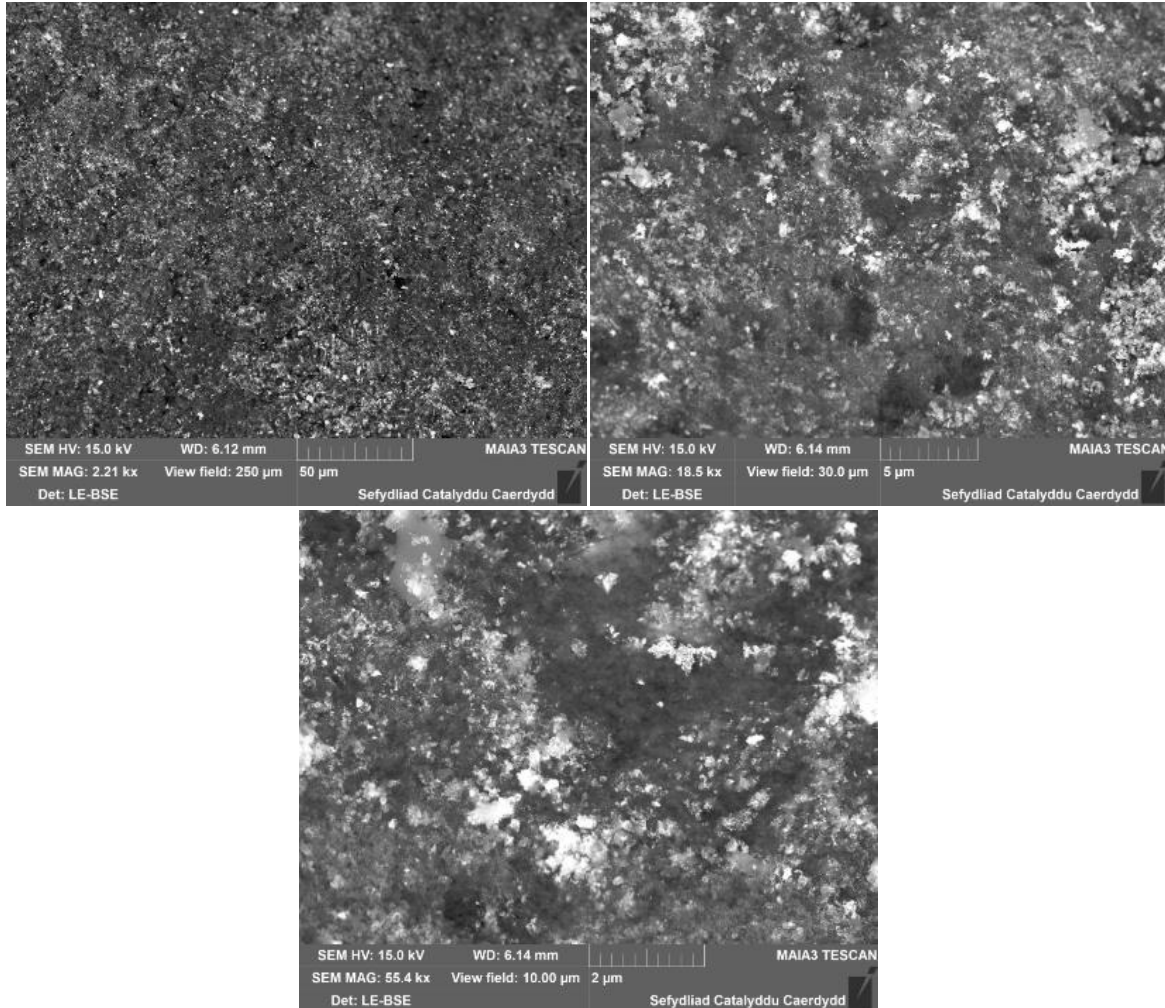
Figure 5.15 SEM images of K8 at 2.2, 18.5 and 55.4 kx magnification

The SEM images of K8 seen in Figure 5.15, appear similar to the images of K7, with the platinum localised on the external surface of the pellets. The platinum appears to exist in more distinguishable particles, unlike an almost continuous surface layer as seen for K7, which could be a result of the higher surface area of K8.

As with K7, a cross-section of the catalyst pellet was examined, the SEM images of which can be seen in Figure 5.16.
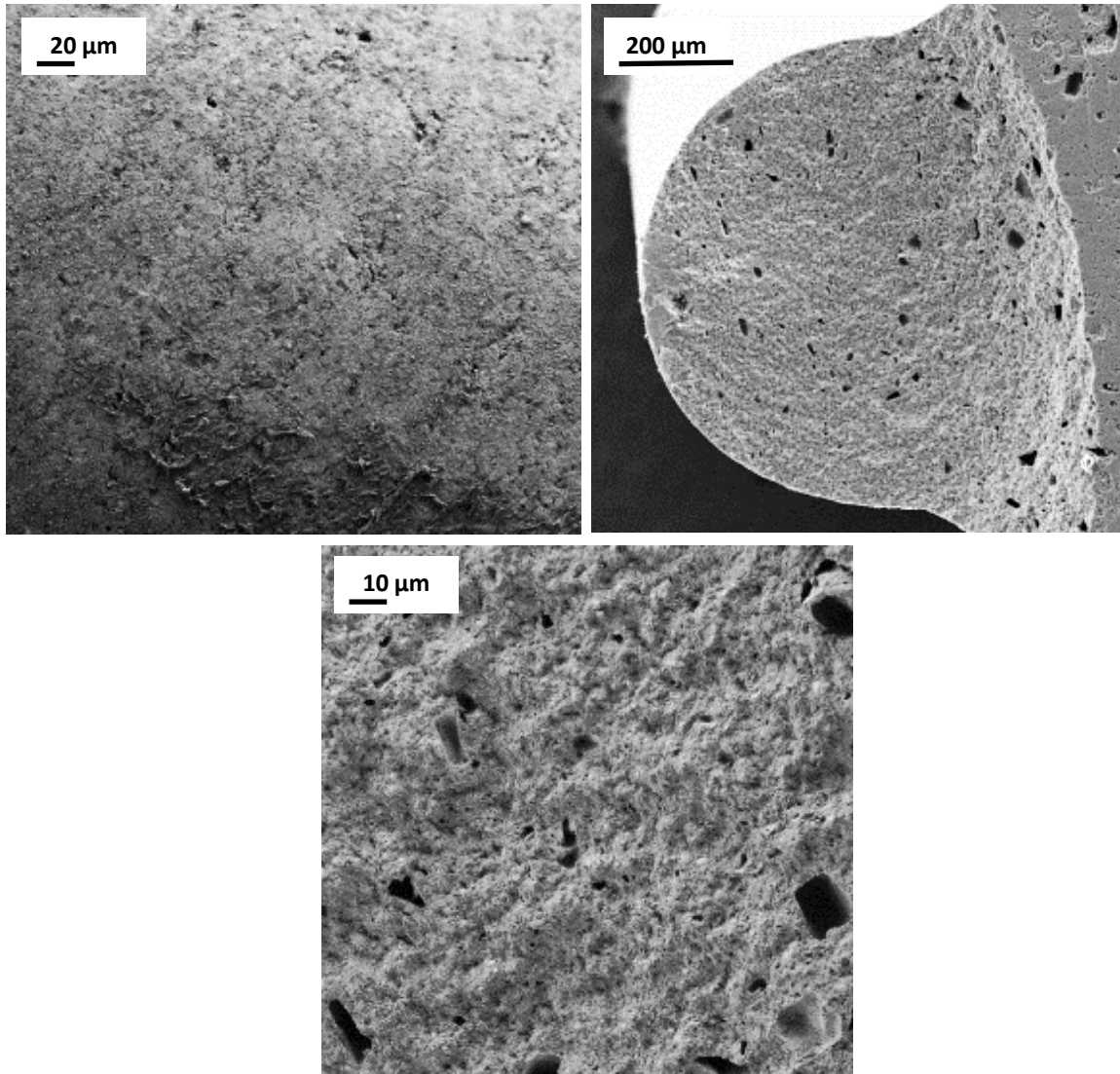
Figure 5.16 SEM images of K8 catalyst pellet external surface (top left), cross section (top right) and inner cross section (bottom middle)

From the cross-section SEM images of K8, it was clear the platinum did not permeate past the external surface of the SiC support pellets during impregnation, with no Pt observed within the cross-sectional area. The inner pores for K8 also appear smaller than those for K7.

5.2.5.3 Microscopy studies of K9 catalyst
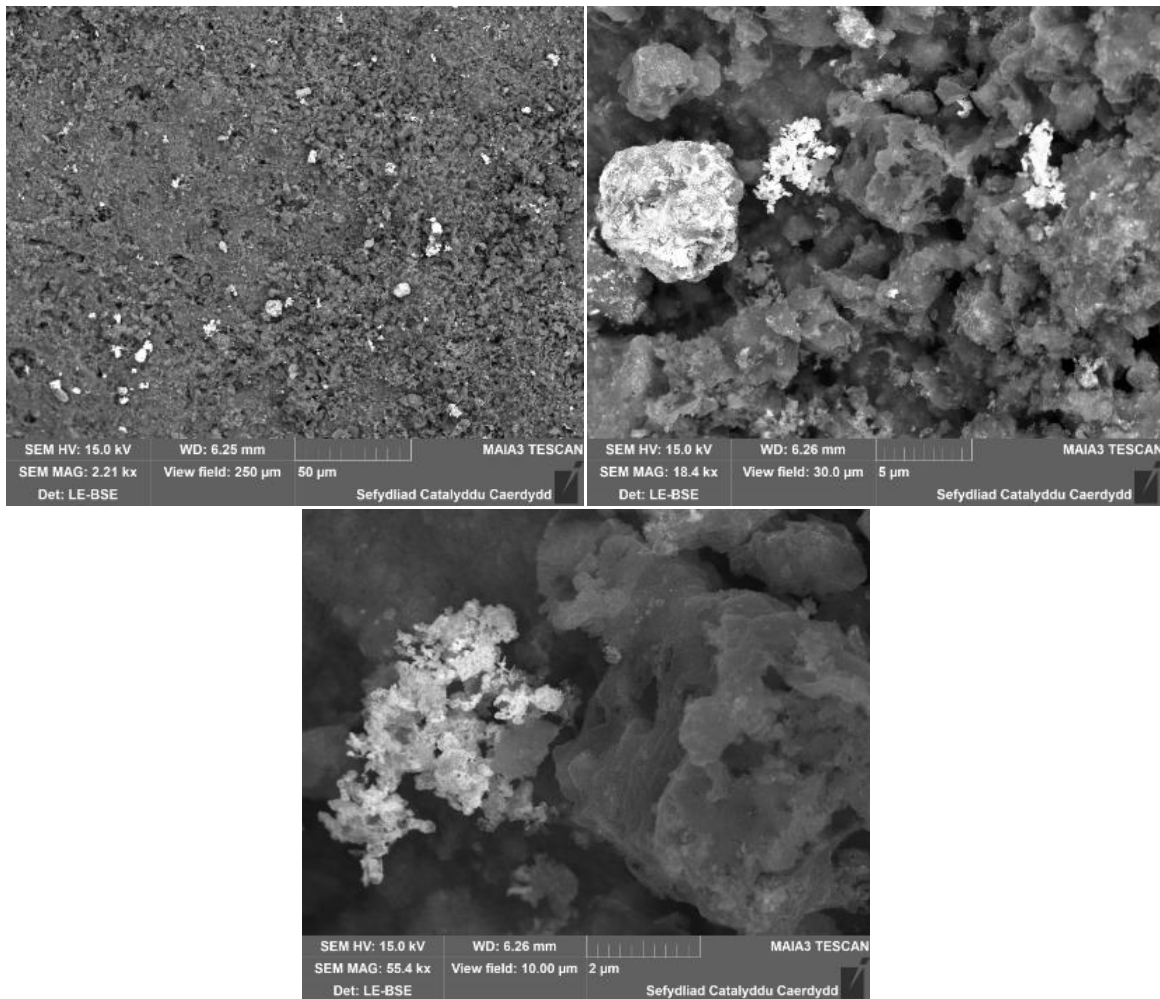
Figure 5.17 SEM images of K9 at 2.2, 18.5 and 55.4 kx magnification

The SEM images of K9 (Figure 5.17) show distinguishable platinum particles ranging from sizes 2 – 15 μm. The Pt particle size range achieved by K9 is larger than those typically seen in the literature for Pt supported metal catalysts[60,61].

The cross-section of the catalyst pellets for K9 was also analysed by SEM, the images of which can be seen in Figure 5.18.
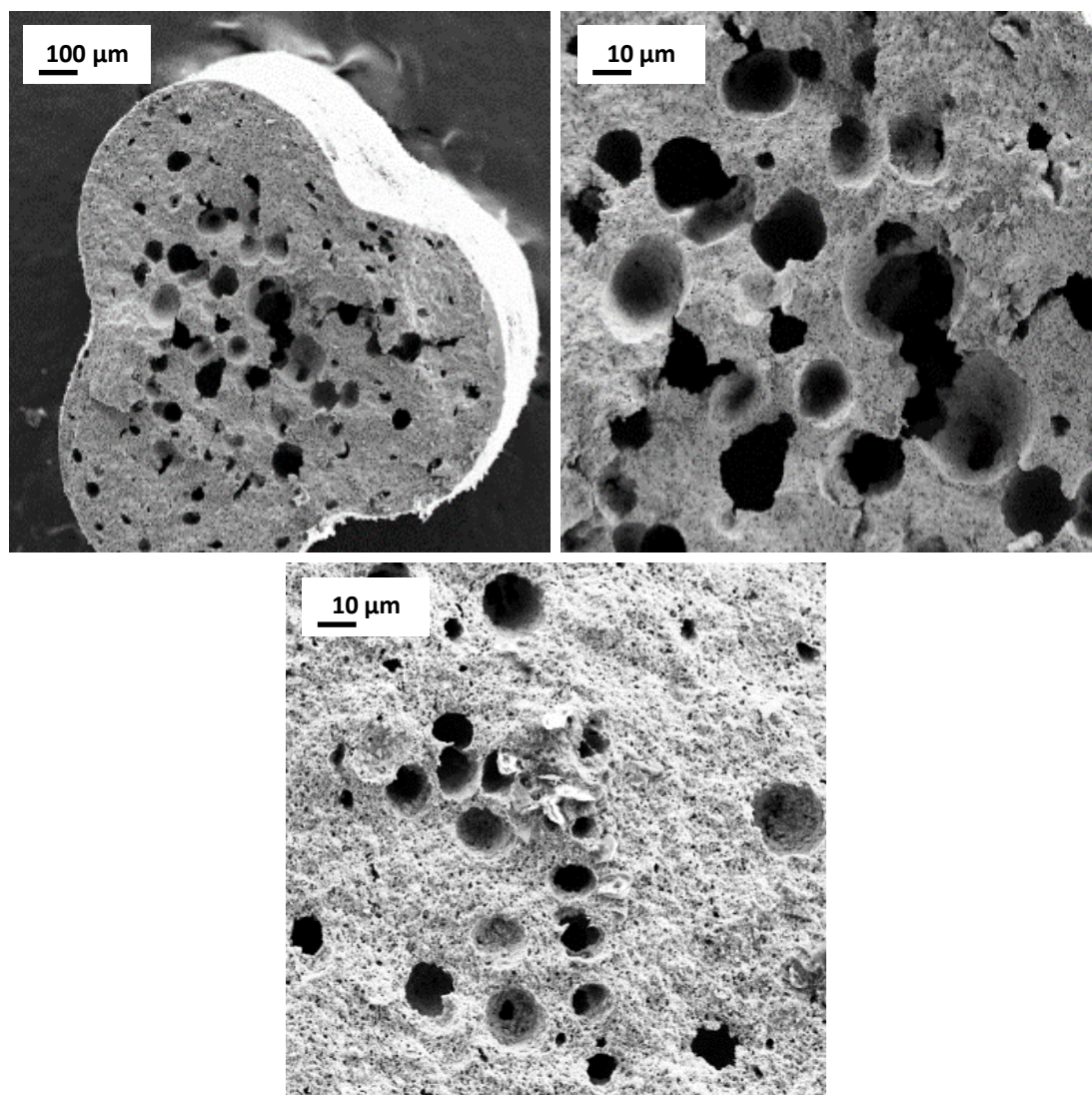
Figure 5.18 SEM images of K9 catalyst pellet cross section (top left) and inner cross section (top right and bottom middle)

Upon dissection of the K9 pellets, the catalyst pores appear larger than K7 and K8, possibly the result of TiC/TiO_2 within the SiC support.

5.2.5.4 EDX of silicon carbide catalysts

EDX was utilized to get a measure of the platinum loading throughout the catalyst. To help obtain a more accurate value for the metal loading, the catalysts were also ground into a powder using a pestle and mortar and subject to EDX analysis. Table 5.7 shows the average Pt weight percentages obtained from the external surface of the catalyst pellet, where the majority of the metal was

observed in SEM, from the inner cross-section of the dissected pellets and from samples of the powdered catalyst.

Table 5.7 Average EDX atomic weight percentage of platinum throughout the catalyst pellets

	External surface of pellet	Inner cross-section of pellet	Ground catalyst
K7	33.71	-	1.86
K8	57.2	-	1.60
K9	2.37	0.90	1.74

The EDX analysis identified the presence of Pt throughout the K9 catalyst pellet and inner cross-section, suggesting the metal is more highly dispersed than for K7 and K8. The less inflated Pt weight percentage observed by XPS is also agreement with this. The wt % of Pt on the surface exceeds the 2 % nominal loading, suggesting that whilst some Pt was impregnated into the inner pore structure of the support, the Pt is still primarily located on the external surface of the catalyst pellet.

Both K7 and K8 display highly inflated values compared with the 2 wt % nominal loading of Pt, with no metal observed in the cross-sectional areas of the catalyst pellets. The higher percentage of metal on the external surface of the support is typical of catalyst preparation methods such as impregnation, whereby the metal is added onto the support as opposed to methods such as co-precipitation, where the metal may be within the support.

By grinding the catalysts into a powder, a more accurate value of platinum loading was achieved. K7 exhibits the highest average platinum weight percentage, followed by K9 and finally K8. K9 indicates a more even distribution of platinum, but still with a higher percentage observed on the external catalyst surface than throughout the pellet.

The atomic weight percentages of the other catalyst elements were also measured *via* EDX and displayed in Table 5.8.

Table 5.8 Average EDX atomic weight percentages of K7, K8 and K9 elemental components

	Si	Ti	C	O
K7	38.35	-	46.81	9.14
K8	31.72	-	52.67	8.17
K9	34.80	4.15	40.87	19.20

The majority of the atomic weight percentages are as expected, with silicon and carbon being the primary elements. Of note is the higher oxygen content of K9, also shown in the XPS, compared with K7 and K8. Given the oxidation of TiC to TiO_2 during calcination, a higher oxygen content would therefore be expected for K9.

5.2.5.5 Microscopy studies of K10 catalyst

K10 was also analysed by SEM and EDX, the results of which can be seen in Figure 5.19 and Table 5.9 respectively.
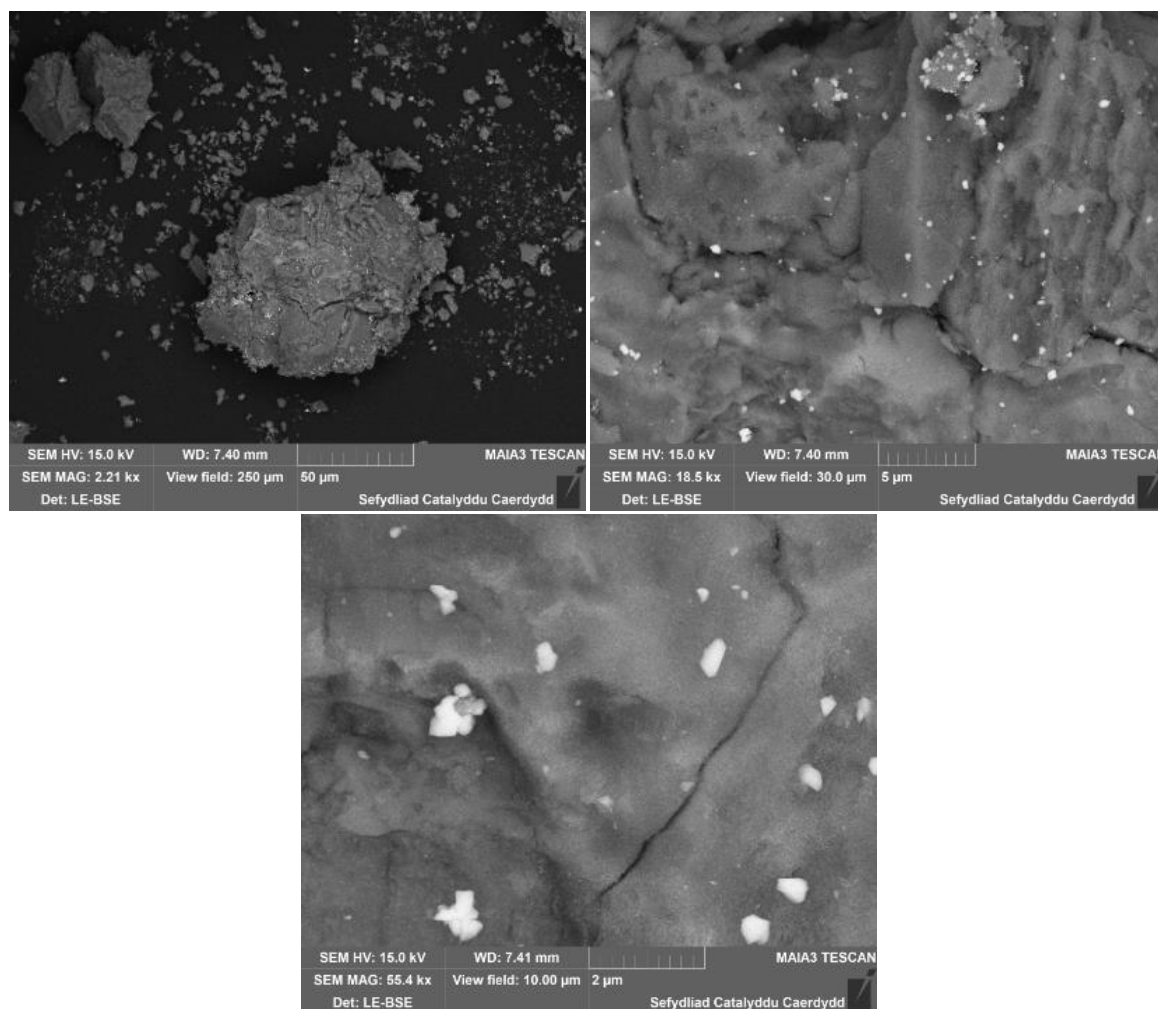
Figure 5.19 SEM images of K10 at 2.2, 18.5 and 55.4 kx magnification

Table 5.9 Average EDX atomic weight percentages of K10 elemental components

	Ru	Ce	Al	O
K10	2.11	4.03	50.73	43.48

The SEM images of K10 are far more typical of a heterogeneous catalyst. The bright spots, which are indicative of ruthenium, are well dispersed on the catalyst surface. The metal particles were observed in a size range between 10 µm – 100 nm, much smaller than the Pt particles observed for K7 – 9. Smaller particles offer a larger surface area of the active component, thus more potential active sites.

The EDX wt percentages for K10 are as expected, with the catalyst primarily consisting of Al and O, with an approximate weight percent of 2 and 5 % for Ru

and Ce respectively. The slight variations in Ru and ceria loadings may be due to unrepresentative sampling, which could be rectified by further analysis.

5.2.6 Temperature programmed reduction (TPR)

TPR can provide information regarding the oxidation state of platinum on the catalyst surface by measuring the consumption of hydrogen as a function of temperature. H_2-TPR profiles for the catalysts determined in the temperature range from 40 – 800 ^oC are shown in Figure 5.20.
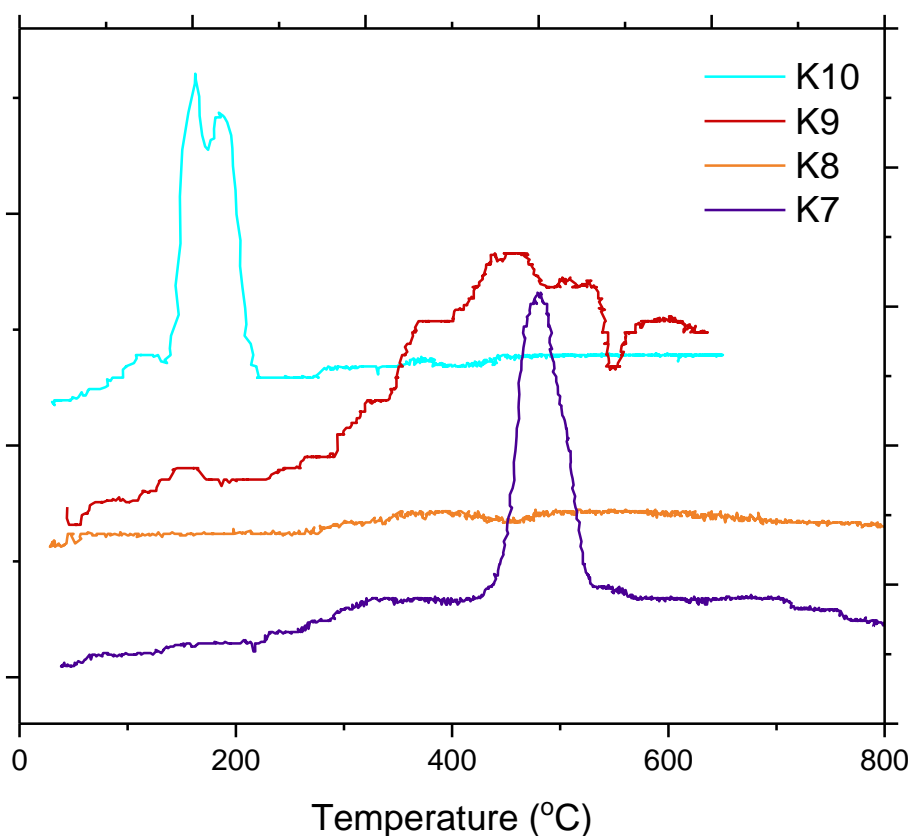
Figure 5.20 H_2-TPR profiles for K7, K8, K9 and K10

A singular peak between 440 – 525 ^oC is observed in the TPR profile for K7, attributed to the presence of platinum oxide. High temperature reduction peaks for monometallic Pt catalysts have been frequently reported in the literature[62-65]. Typically, hydrogen consumption below 300 ^oC is characteristic of the reduction of bulk PtO_x species weakly bound to the support, whereas H_2 consumption between 350 – 500 ^oC relates to more strongly interacting PtO_x being reduced[66]. The high

temperature reduction peak for K7 indicates that the SiC catalyst has more Pt bound in the metallic form and that any PtO_x species present are only strongly interacting[3]. This is in agreement with the XRD pattern of K7 which showed the presence of PtO_2, and with the XPS, which revealed no PtO_2 on the surface, suggesting PtO_2 is buried beneath the surface of the catalyst. Given the SEM-EDX analysis, which showed no impregnation of the metal into the centre of the SiC support pellets, it is most likely that PtO_2 is formed in an intermediate layer between the surface and bulk of the catalyst. It has also been proposed that higher reduction temperatures are indicative of strong metal support interactions[67,68].

The H_2-TPR profile of K9 appears more complex, with less distinct peaks than that for K7 or K10. Similar profiles have been observed for TiO_2 supported metal catalysts, with the partial reduction of the TiO_2 surface by H_2 beginning at 300 °C[69]. This low temperature reduction of surface TiO_2 to TiO_{2-x} is facilitated by Pt particles adjacent the TiO_2 surface[70,71]. The reduction of bulk oxygen in TiO_2 has been reported to occur at temperatures between 520 – 600 °C[72,73], and is thought to be responsible for the high temperature reduction peaks observed in the H_2-TPR profile for K9.

The TPR profile for K10 shows a pronounced peak just below 200 °C, characteristic of the reduction of RuO_2 particles[74-76].

5.3 Catalyst activity studies

For an initial comparison of the four catalysts, a common temperature and pressure was selected based on previous studies under which all catalysts would be expected to show phenol conversion[77]. The phenol oxidation reaction was carried out at 7 $bar_{(g)}$ and 120 °C for 4.5 hours, for which the phenol conversions as a function of time are displayed in Figure 5.21.
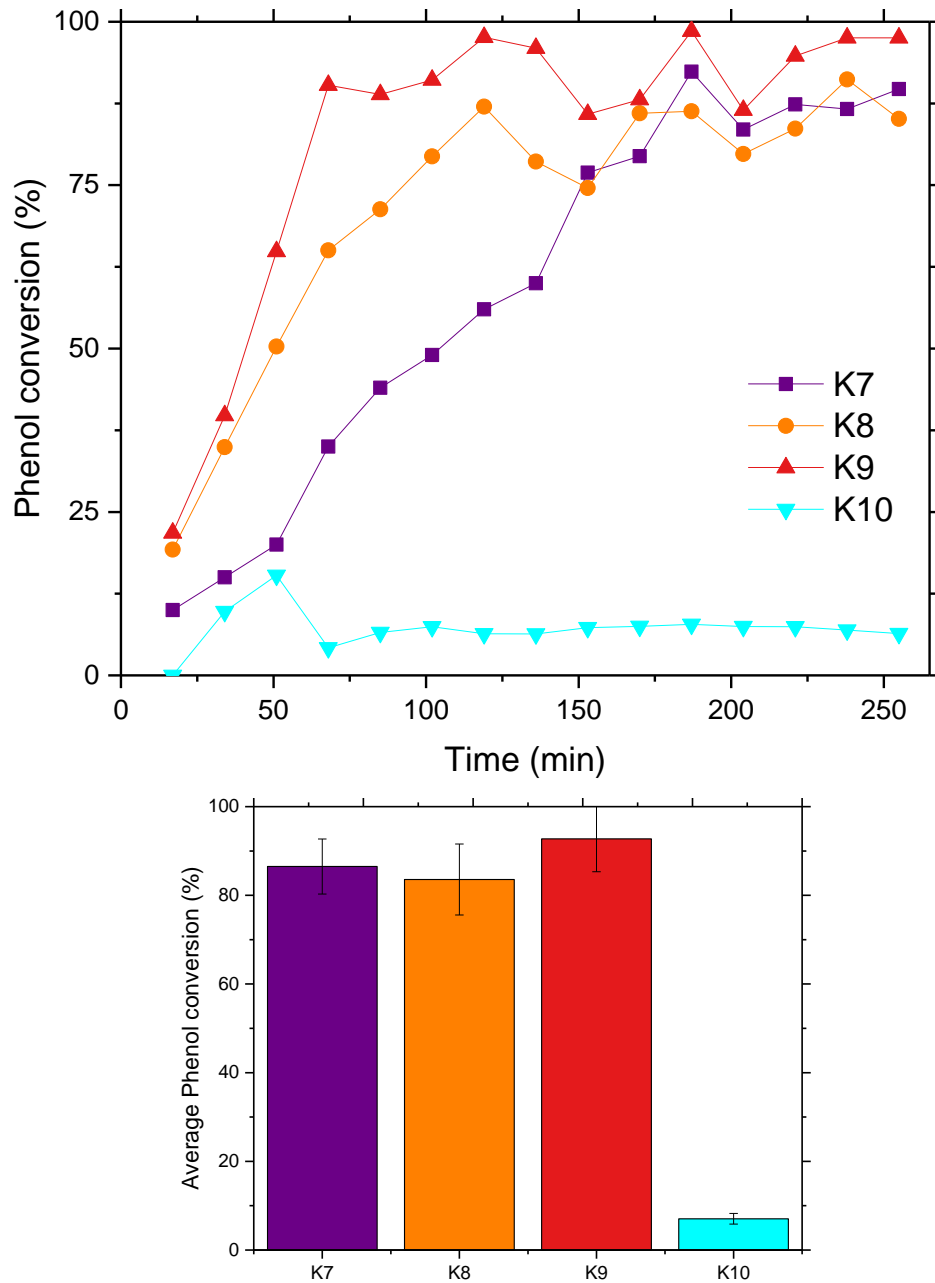
Figure 5.21 Phenol conversion vs time profiles for K7, K8, K9 and K10, at 7 bar$_{(g)}$ pressure and 120 °C (top) and average phenol conversion (bottom)

As with the catalysts reviewed in Chapter 4, an initial induction period was observed for the SiC catalysts, attributed to the necessary time required to achieve a critical concentration of organic radicals[78]. The longest induction period of >150 minutes was observed for K7, whilst K9 achieved steady conversions in approximately 70 minutes. Once the reaction reached a steady state, the average phenol conversions for K7 and K8 were within 3 % of each other. For K10, a much lower activity was achieved, the initial spike in conversion could be attributed to the adsorption of phenol onto the catalyst's active sites, creating a false positive

reaction rate, which quickly declines to the true conversion rate once the active sites have been saturated. From these results it can be deduced that surface area may not play a significant role in the abatement of phenol *via* CWAO. The catalyst with the highest surface area, K10 – 110 m^2g^{-1}, exhibited the lowest activity, whilst the catalysts with lower surface area, K7, K8, and K9 – 29 m^2g^{-1}, 35 m^2g^{-1} and 34 m^2g^{-1} respectively, displayed significantly higher activity.

Despite being a proven well performing catalyst in the literature[3], K10 does not compare to the SiC based catalysts at such low operating temperatures and pressures, furthering the hypothesis that a hydrophobic catalyst is better suited for CWAO of phenol.

To be able to effectively compare the SiC catalysts, the reaction was repeated at a lower temperature in order to operate at lower conversions; due to the low activity observed for K10 at 120 °C it was not included. Unfortunately, if the operating conditions were to remain within the active range for K10, K7 – 9 would all show near 100 % conversion. When conversions reach 100 %, it is not possible to gain a true representation of catalytic activity as only a portion of the active sites may be contributing to oxidation at any given time, making it difficult to differentiate between the catalysts. The phenol conversion profiles for K7 – 9 at 100 °C are displayed in Figure 5.22.
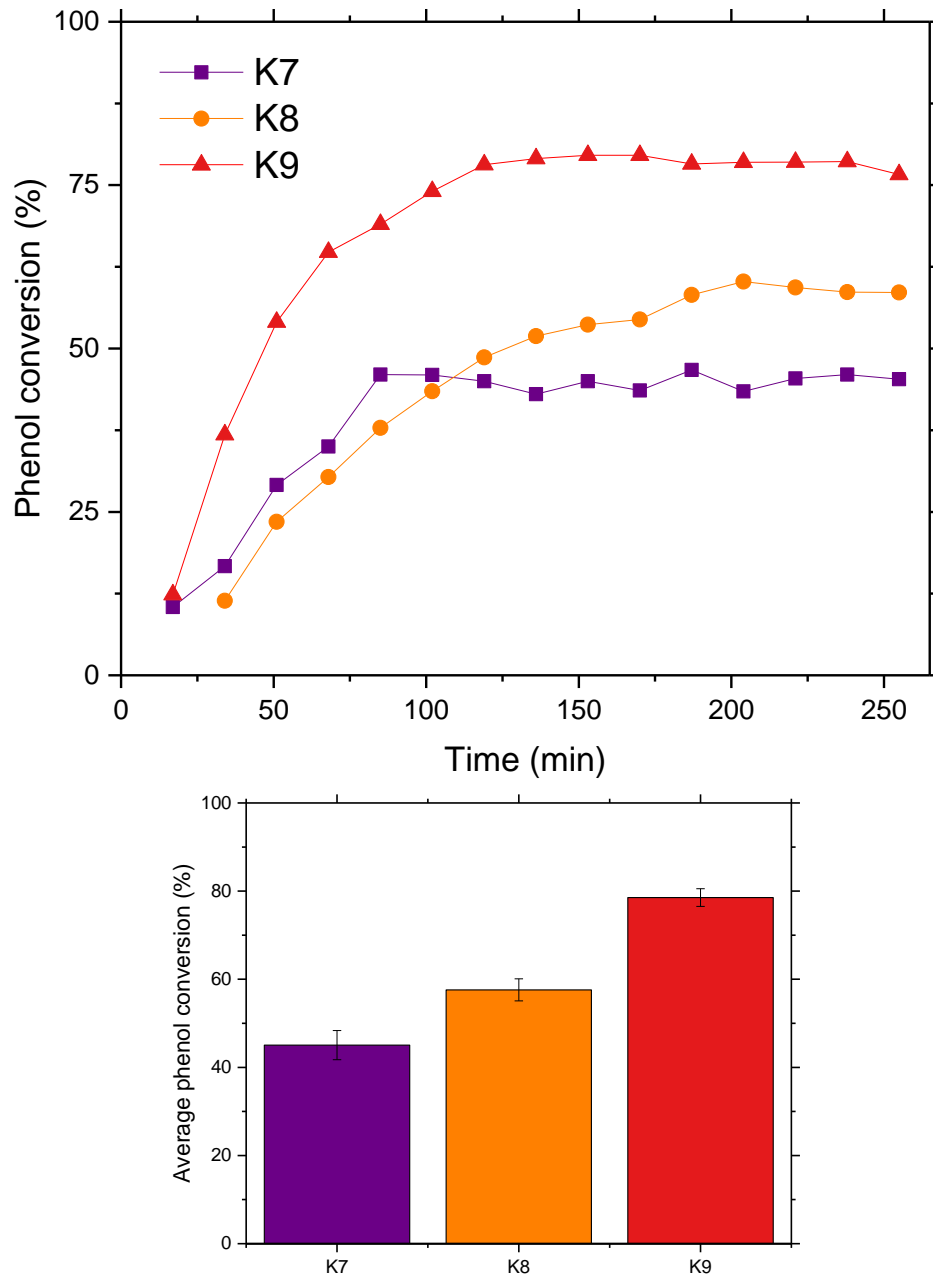
Figure 5.22 Phenol conversion vs time profiles (top) and average phenol conversion (bottom) for K7, K8 and K9, at 7 bar$_{(g)}$ pressure and 100 ^{o}C

As expected, larger differences in conversion become apparent when the temperature was reduced to 100 ^{o}C, with K9 remaining the most active followed by K8 and K7 respectively. The lower loading of metallic Pt, due to the presence of PtO$_2$, coupled with the lower surface area for K7 may be accountable for the lower activity observed.

The vast majority of catalysts investigated in the literature for CWAO of phenol operate under more extreme conditions than those used in this study. At 110 ^{o}C, the mixed metal oxide catalyst Mn$_x$-Ce$_x$-O$_x$, required an oxygen partial

pressure greater than 5 bar (equivalent to approximately 24 bar air pressure) to achieve a similar phenol conversion as K9[51]. When supported on Al_2O_3, Pt necessitated operating conditions of 175 °C and 25 bar oxygen pressure to achieve a phenol conversion of 95 %[79]. The SiC catalysts are active at a significantly lower temperature and pressure compared to catalysts seen in the literature for CWAO of phenol.

A steady state is reached for each catalyst in under approximately 100 minutes, whereas in some cases in the literature it has taken up to 20 hours for a catalyst to reach steady state under CWAO conditions[31]. K9 showed a higher initial reaction rate at both temperatures (100 °C and 120 °C) which can be beneficial to start-up of a CWAO reactor.

Given the almost equivalent surface areas of K8 and K9, the trend in activity cannot be attributed to increased surface area. Another contributing factor must be responsible for the higher activity observed for K9. The increased Pt dispersion and addition of TiO_2 in the SiC support may promote the oxidation reaction for K9.

Increased dispersion has been correlated with increased activity for Pt supported metal catalysts in oxidation reactions[80,81]. Keav *et al.*[82] observed platinum dispersion to have a significant effect on the reaction rate during the CWAO of phenol. Increased Pt dispersion for Pt/CeO_2 led to increased phenol conversion, however the nature of the active metal also played an important role, as Pt catalysts were more active compared with Ru/CeO_2 despite similar metal dispersions.

The addition of TiO_2 has also been shown to enhance catalytic reactions. A synergistic effect was observed when activated carbon was coupled with TiO_2, which was beneficial in the photocatalytic degradation of phenol[83]. The increased efficiency of the photocatalyst was explained by the adsorption of phenol on AC, followed by mass transfer to the photoactive titania. This synergistic effect has also been observed for TiO_2-graphene and TiO_2-CNT composites, with the carbon based material responsible for increasing the amount of surface adsorbed reactant species[84-86].

The addition of TiO_2 to Ru/ZrO_2 resulted in an increase in specific surface area of the catalyst and enhanced the activity for CWAO treatment of isothiazolone[87]. The increased catalytic performance was attributed to a higher percentage of Ru species on the catalyst surface, caused by an increase in bonding strength between RuO_x and the support, as well as an increase in surface area and Ru dispersion upon addition of TiO_2.

5.3.1 Catalyst activity studies as a function of temperature

From the Arrhenius equation (Equation 2.1) it is known that the reaction rate is dependent upon the temperature. Increasing the temperature increases the proportion of species with high enough energy to overcome the activation barrier for oxidation, leading to faster reaction rates and thus, higher conversions. By lowering the reaction temperature, it would be expected to have a negative impact on the catalyst activity. K9 was investigated over a range of temperatures, for which the subsequent phenol conversion vs temperature profile and Arrhenius plot are displayed in Figure 5.23.
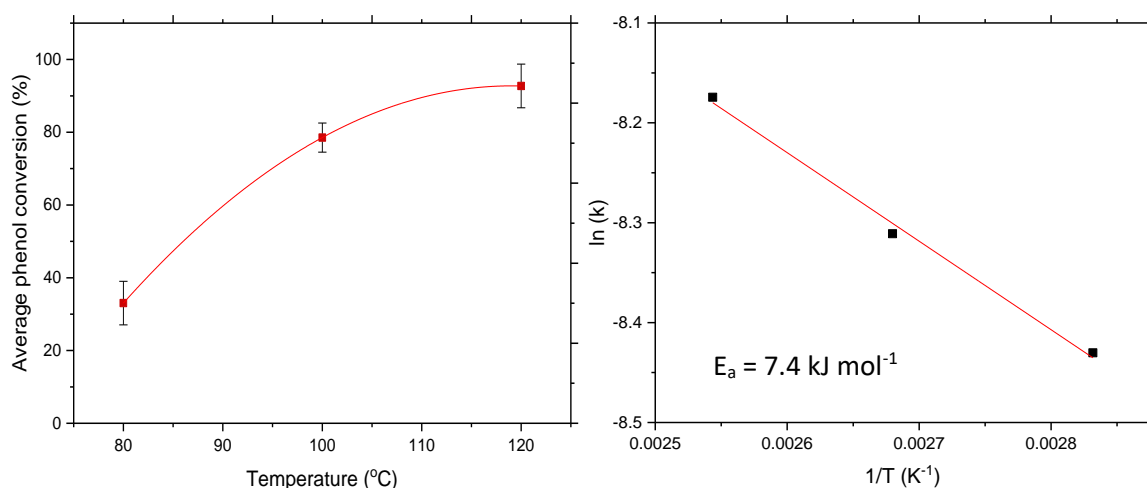
Figure 5.23 Phenol conversion as a function of temperature for K9 (left), and Arrhenius plot (right) at 7 bar pressure

As predicted, increasing the temperature had a positive effect on phenol conversion. The largest increase in conversion is seen when the temperature was increased from 80 °C to 100 °C, showing a strong temperature dependence below

100 $^{\circ}$C. The activation energy for K9 was calculated at 7.4 kJ mol^{-1} by use of the Arrhenius equation[88], significantly lower than the reported value of 21.1 kJ mol^{-1} for K10 under similar CWAO conditions[3]. Comparatively, activation energies of 24.5 − 238.7 kJ mol^{-1} have been previously reported for CWAO of phenol in the literature[89-93].

In general, there are two limiting factors to the speed of a surface reaction, the diffusion of reactants to the surface and the chemical or physical kinetics of the interaction between the analyte and substrate[94]. Reactions can be classified as either diffusion or reaction limited. Diffusion limited processes are those whereby the reaction rate is governed by the transportation of the reactants in solution and reaction limited processes are those in which there is a significant barrier for chemical transformation[95].

The activation energy for K9 is very low, and whilst high activation energies imply the process is strongly reaction limited, values between 5 − 10 kJ mol^{-1} suggest the reaction is diffusion limited[96]. In a heterogenous reaction sequence, external mass transfer of reactants must first take place from the bulk solution through the boundary layer (interphase diffusion), then diffuse through the catalyst pores (intraparticle diffusion) before adsorption onto the catalyst surface and subsequent reaction can take place[97]. The low activation energy for K9 (7.4 kJ mol^{-1}) suggests the reaction is limited by interphase and/or intra particle diffusion.

Diffusion limited processes are frequently encountered in heterogeneous catalysis whereby the reactants are in a different phase to the catalyst. External mass transfer is dependent on a multitude of factors including, but not limited to, the operating temperature and pressure, the choice of reactor, flow rate and catalyst particle size[98]. Varying these parameters can help reduce external mass transfer resistance[99]. Intraparticle diffusion in the pores of the catalyst particles can also influence the overall reaction rate and is strongly dependent on the pore diameter of the catalyst support[97].

The reduced wettability of a hydrophobic support, thought to be responsible for the increased activity seen for SiC catalysts *via* the transfer of

oxygen directly from the gas phase to the catalyst surface, may negatively impact the diffusion of phenol molecules. Diffusion limitations for phenol, as a result of lower liquid to catalyst contact area, may be responsible for the low activation energy observed for K9. Despite diffusion limitations, Pt/SiC remains a proficient catalyst for the CWAO of phenol and few catalysts in the literature are active over operating conditions as moderate as those used in this study. Keeping in mind the ultimate goal of achieving CWAO under ambient conditions, it is imperative to find a catalyst that is active at low temperatures and Pt/SiC-TiC has so far been shown to be promising start.

5.3.2 Catalyst activity studies as a function of pressure

A positive correlation would also be expected between phenol conversion and operating pressure. Increasing the pressure leads to a higher oxygen partial pressure, resulting in a higher concentration of both gaseous and dissolved oxygen available for reaction. Depending upon the primary reaction mechanism the catalyst follows, whether it would be reliant on gas phase or dissolved oxygen, a differing dependence on pressure would be observed. Since both concentrations of oxygen increase with increased pressure, a rise in activity would be predicted regardless of mechanism. However, if solely dependent on dissolved oxygen for oxidation, a higher reliance on pressure would be observed.

A hydrophilic catalyst would have a completely wetted surface during CWAO, and so oxygen must first be dissolved in the liquid phase in order for oxygen to access the catalyst active sites. A partially wetted hydrophobic catalyst, however, could facilitate oxygen transfer directly from the gas phase *via* the solid – gas interface at the catalyst surface. If solely reliant on dissolved oxygen, a hydrophilic catalyst would therefore be expected to show a greater pressure dependence, than a hydrophobic catalyst, since the concentration of dissolved oxygen is directly proportional to the oxygen partial pressure, which in turn is proportional to the reaction pressure.

Due to the large difference in activity towards phenol oxidation, K7 - K9 and K10 were tested over a range pressures but at different temperatures, the results of which can be seen in Figure 5.24.
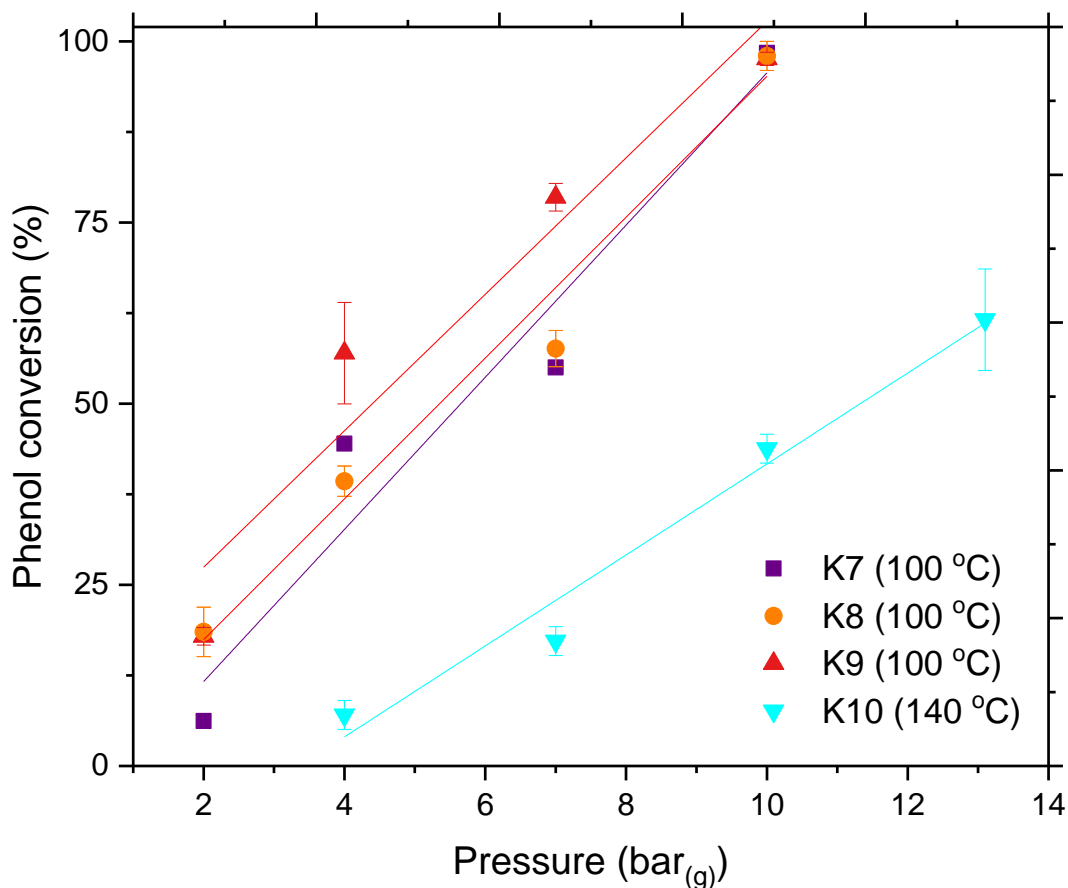
Figure 5.24 Phenol conversions as a function of pressure for K7, K8 and K9 at 100 °C, and for K10 at 140 °C

Each catalyst shows a positive correlation with pressure, at 10 bar$_{(g)}$ all the SiC catalysts reach near 100 % conversion, suggesting any further increase in pressure would not yield a higher conversion, thus oxygen saturation had been reached. A lower gradient is observed for the trendline of K10, with the catalyst promoting conversion from 17.2 % at 7 bar$_{(g)}$ to 61.6 % at 10 bar$_{(g)}$. Even at a higher temperature K10 requires much greater pressures to achieve activities close to those of the SiC catalysts.

K7 – K9 show near complete conversion at 10 bar$_{(g)}$, however at lower pressures K9 achieves higher conversions, a 23.5 % increase in activity is seen for K9 at 7 bar$_{(g)}$ and 12.5 % increase at 4 bar$_{(g)}$ compared with K7. It is possible the presence of PtO$_2$ and lower surface area are responsible for the lower activity

observed for K7, however K9 also out performs K8, a catalyst with similar surface area and exclusively metallic platinum. K9 exhibits a higher active metal dispersion, which, coupled with the presence of TiO_2 within the support, may promote phenol oxidation, allowing the catalyst to achieve higher conversions under milder conditions.

Since the catalysts were tested at different temperatures it makes it challenging to directly compare their pressure dependence. The concentration of dissolved oxygen is dependent upon both temperature and pressure; at higher temperatures any change in pressure will have a greater effect on the dissolved oxygen concentration[100]. However, if using consistent conditions, the SiC catalysts would show quasi-100 % conversions or quasi-0 % conversion in the case of K10, regardless of pressure. Using the equation laid out by Tromans *et al.*[100] (Equation 2.5), it is possible to calculate the concentration of dissolved oxygen at a given temperature and pressure. Since the requirement for dissolved oxygen is in question, the dissolved O_2 concentrations for each temperature and pressure were plotted against catalyst activity to help better evaluate the pressure dependence. The resulting phenol conversion as a function of concentration of dissolved oxygen (C_{aq}) plot for catalysts K9 and K10 is displayed in Figure 5.25.
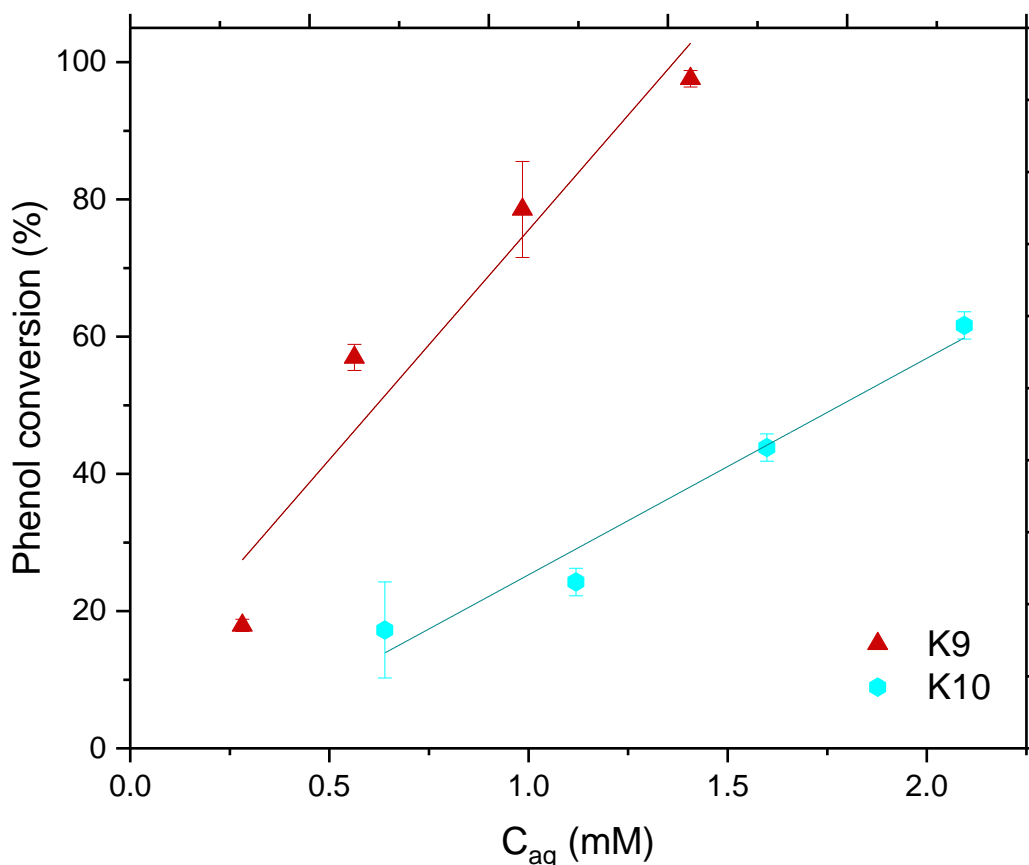
Figure 5.25 Phenol conversion as a function of dissolved oxygen concentration (C_{aq}) for K9 and K10

A linear relationship between the concentration of dissolved oxygen (C_{aq}) and the phenol conversion can be observed for both K9 and K10. At approximately 0.6 mM [$O_{2(aq)}$] there is a 40 % difference in phenol conversion between the catalysts. The steeper trendline observed for the hydrophobic K9 catalyst suggests there is a lower pressure dependence than for the hydrophilic alumina catalyst, as a smaller change in dissolved [O_2] correlates to a larger difference in phenol conversion. K10 requires a more pronounced increase in dissolved [O_2] to achieve the same increase in activity.

If the concentration of dissolved oxygen is the rate limiting factor for K10, increasing from a lower concentration would be expected to have more pronounced affect than increasing from a higher concentration of dissolved oxygen. At higher pO_2, there is a larger probability that the reaction is less limited by [O_2], therefore at higher pO_2 it is more likely that increasing the concentration of dissolved oxygen will give a smaller change in conversion. If this is true, the relationship between activity and [$O2_{(aq)}$] for K10 may not be strictly linear and

further testing at higher pressures may indicate a non-linear function. Unfortunately, due to time restraints, such experiments for K10, conducted above 14 bar$_{(g)}$ pressure, were not possible.

As mentioned previously, it is believed that the hydrophobic nature of the K9 support is responsible for the higher catalytic activity observed. The presence of gas bubbles within the pores would allow for oxygen adsorption directly from the gas phase, negating the requirement for the kinetically limiting step of oxygen dissolution. Since a portion of the catalyst surface would still be wetted by the reaction media, it is likely that K9 is able to oxidise phenol *via* both reaction pathways and so a dependence on [O2$_{(aq)}$] still exists for K9, but not exclusively as for K10.

Although the data suggests K9 is less dependent upon the operating pressure compared with K10, it must be considered whether this is strictly a fair comparison. The relative hydrophobicity of the catalysts may not be only contributing factor for the pressure dependence of each catalyst. The concentration of dissolved oxygen may also not be solely responsible for the differences in activity observed between them. The activation energy observed for CWAO of phenol over K9 alluded to the process being diffusion limited, whereas this may not be the case for K10. The ability of the reactants to diffuse within the pores of the catalyst particles can significantly influence the overall reaction rate, and thus the resulting phenol conversions. The literature values for E$_a$ for K10 (21.1 kJ mol^{-1})[3] under similar CWAO conditions implies the process is not diffusion limited. If the activity observed for K9 is influenced by diffusion limitations, whilst the activity observed for K10 is not, Figure 5.25 may not be an accurate comparison for the pressure dependence of either catalyst.

The change in the active metal, as opposed to hydrophilicity, may also be responsible for the variations in activity observed between K9 and K10. Renard *et al.*[101] reported higher activity and selectivity towards CWAO of stearic acid for Pt compared with Ru when supported on CeO$_2$. The differences in catalyst performance were a result of two potential oxidation mechanisms. Ru promoted intra-molecular cleavage of the C – C bond, which lead to high concentrations of

acetic acid, whereas Pt favoured decarboxylation. This may also be the case for K9 and K10, where Ru and Pt favour different oxidation pathways, although at temperatures >100 $^{\circ}$C, no reaction intermediates (of those measured by HPLC) were seen for either catalyst, and so further investigation would be required to confirm this. Different reaction pathways may have a different dependence on oxygen concentration, resulting in a variation in the dependence of [$O_{2(aq)}$].

5.3.3 Catalyst activity studies in relation to catalyst particle size

One of the many challenges in designing catalysts for continuous processes such as CWAO, is achieving a balance between the back pressure across the catalyst bed length and effective mass transfer of pollutants and O_2 within the reactor[77]. To investigate the optimum pellet size, the SiC-TiC support for K9 was obtained in the form of 2 mm pellets, then crushed and sieved to achieve particle size ranges between 1 – 0.6 mm and 450 – 600 µm, before impregnation with platinum. The resulting catalysts were subject to CWAO of phenol at 100 $^{\circ}$C and 7 bar$_{(g)}$ pressure, for which the phenol conversion vs time profiles can be seen in Figure 5.26.
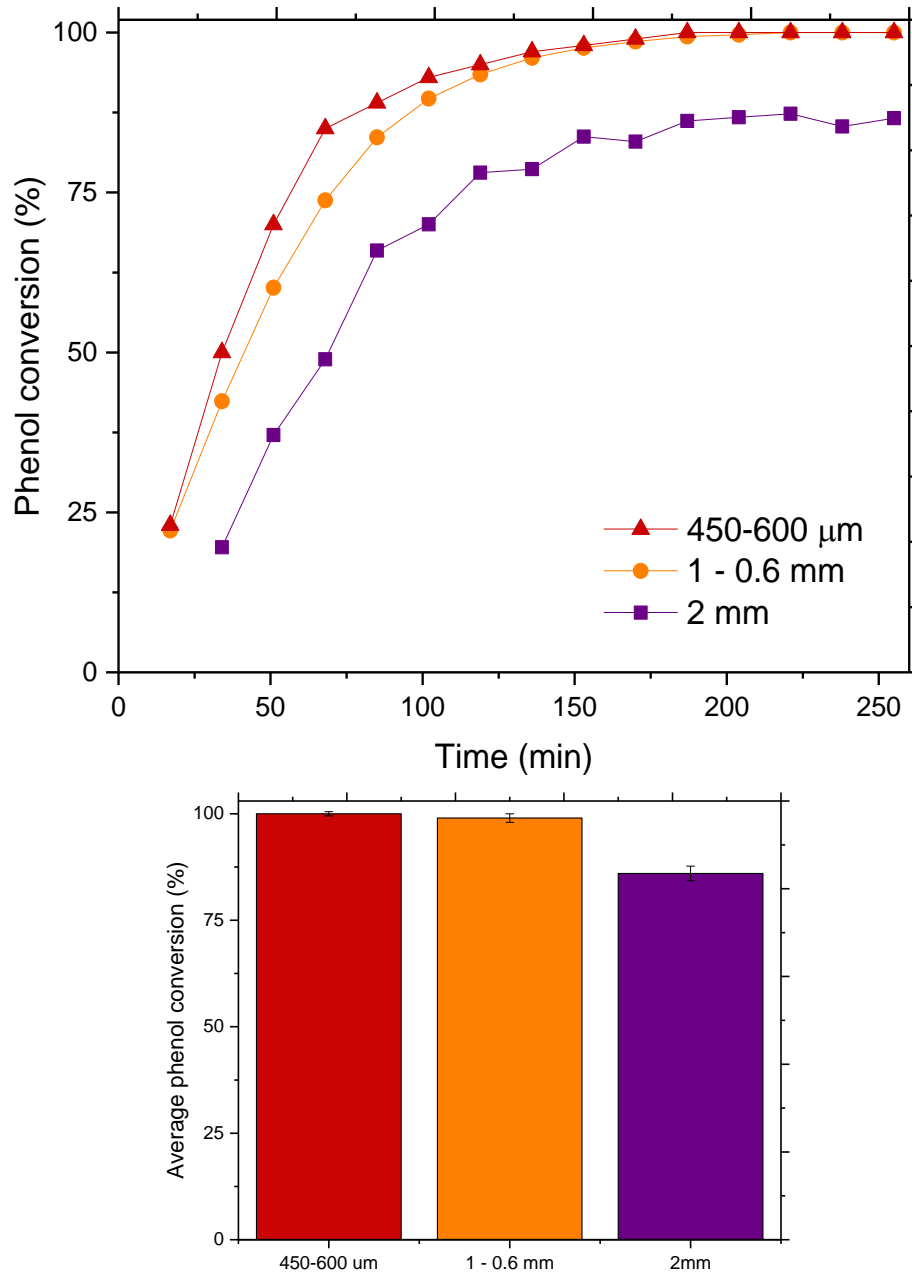
Figure 5.26 Phenol conversion vs time profile (top) and average phenol conversion (bottom) for a range particles sizes (2 mm, 1 − 0.6 mm, 450 − 600 µm) of K9, at 7 bar pressure and 100 °C

The larger 2 mm pellets achieved an average phenol conversion of 86 % once at steady state, whilst the 450 − 600 µm and 1 − 0.6 mm catalysts both reached 100 % conversion after 200 minutes. The higher activities seen for the smaller catalyst pellet sizes indicate mass transfer limitations within the 2 mm pellets. As discussed previously, a catalysts true activity cannot be determined if conversions reach 100 %, as only a portion of the active sites may be contributing. Both the smaller pellet sizes achieved 100 % conversion and so it is possible there

are still mass transfer limitations below 2 mm that cannot be expressed under these conditions.

Decreasing the pellet size can help optimise mass transfer and increases catalyst – phenol contact time as a result of more efficient packing. For this reason, powdered catalysts are commonly seen in the literature, however they bring about their own disadvantages. Powders can be difficult to handle and require more robust apparatus to hold the catalyst in place within the bed, and prevent the catalyst being washed through the reactor. Larger pellets can help avoid pressure drop issues as the inefficient packing offers less resistance to the liquid flow, however, this also causes reduced reactant – catalyst contact time[102]. Reduced contact time can result in some phenol passing through the reactor without adequate interaction with the catalyst. Often a compromise must be reached between the easier to handle pellets and the effective mass transfer of powders[103].

Stuber *et al.[102]* found that the optimal catalyst pellet size for CWAO needs to be small enough to provide sufficient catalyst – phenol contact time, but large enough to avoid pressure drop related problems. The shape and size of the catalyst pellets can also influence the heat transfer within the reactor[104].

5.3.4 Catalyst activity studies as a function of initial phenol concentration

Realistically industrial wastewaters are not always going to have consistent pollutant concentrations, and so it is important a catalyst is able to manage varying phenol concentrations. Figure 5.27 displays the initial phenol conversion as a function of the average phenol conversion and initial reaction rate.
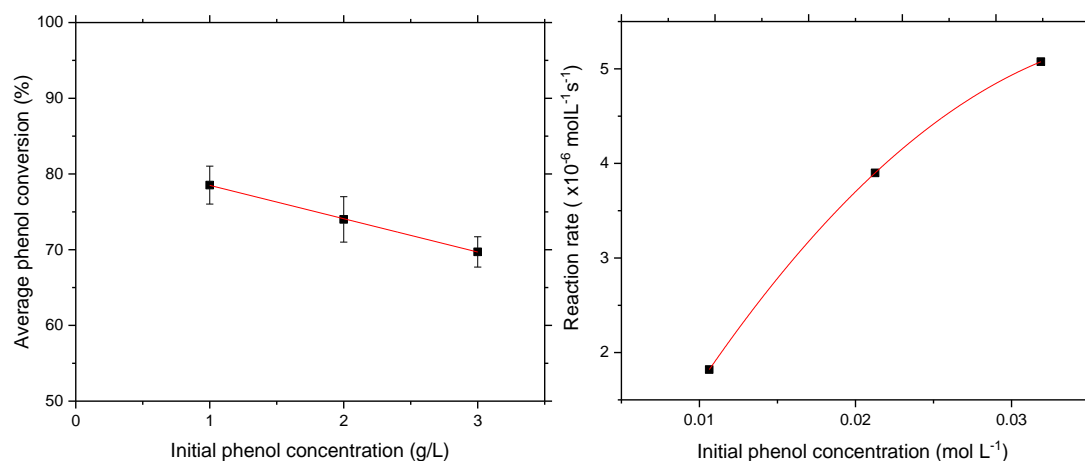
Figure 5.27 Initial phenol conversion as a function phenol concentration and reaction rate for K9 at 7 bar$_{(g)}$ and 100 ^{o}C

When the phenol concentration is triple that previously used, K9 is still able to achieve an average conversion of 69.7 % after 5 hours. Less than a 10 % reduction in average phenol activity is observed when the phenol concentration is increased to 3 g L^{-1}. A linear relationship is observed between the phenol conversion and initial phenol concentration under these conditions. When the concentration of phenol is increased, the ratio of phenol molecules to catalyst active sites increases and once the available active sites reach capacity, the catalyst becomes saturated causing excess phenol molecules to pass through the catalyst bed without being oxidised. The phenol conversion drops a result of this.

When expressing the reaction rate as a function of initial phenol concentration for K9, the relationship appears to be linear, although further data at different initial concentrations would help corroborate this. Hamoudi *et al.*[79] observed a linear dependence between reaction rate and initial phenol concentration, over Pt/Al$_2$O$_3$ and MnO$_x$-CeO$_x$ catalysts in a slurry reactor, for initial phenol concentrations up to 0.4 g L^{-1}. Similar profiles have been frequently reported in the literature[105,106]. Whilst Stuber *et al.*[102] observed that the reaction rate increased faster at lower initial phenol concentration than at higher concentrations. At first, the reaction rate increased linearly as a function of phenol concentration, implying the reaction was pseudo first order. When the initial phenol concentration exceeded 5 g L^{-1}, the reaction rate was independent of the initial phenol concentration, implying pseudo-zero order. The sensitivity of the

reaction rate at the higher concentrations was attributed to the increased deactivation by carbon deposition observed.

5.3.5 Catalyst activity studies under mild operating conditions

Thus far K9 has proven to be active for CWAO at temperatures and pressures lower than those observed in the literature. It is proposed that the hydrophobicity of SiC has allowed for a secondary oxidation pathway *via* the presence of gas bubbles located within the pores. To further the goal of achieving CWAO under ambient temperatures, where the contaminated water would not require elevated pressure to remain in the liquid phase, K9 was subjected to testing under 1 bar$_{(g)}$ pressure and 80 ^{o}C, the results of which are displayed in Figure 5.28. Reducing the severity of operating conditions consequently, reduces the environmental and economic impact of the process, as well as improving operational safety.
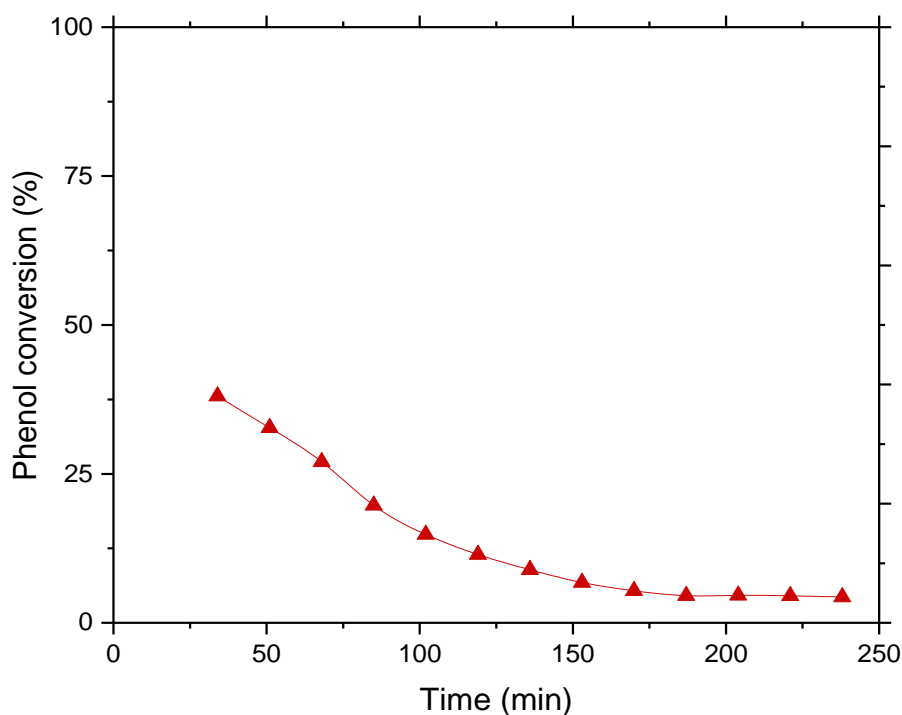
Figure 5.28 Phenol conversion as a function of time for K9 at 1 bar$_{(g)}$ and 80 ^{o}C

Under the reduced operating conditions an initial conversion of 38.1 % is observed, after which a gradual decrease in phenol conversion occurs until a

steady rate of 4 – 5 % is reached after 175 minutes. A conversion – time profile such as this is characteristic of catalyst deactivation. Catalyst deactivation of supported metal catalysts in CWAO operations typically results from build-up of carbonaceous deposits on the catalyst surface[107]. These carbon species then limit the oxygen transfer and access of reagents to the active sites, causing a decrease in catalytic activity.

During the CWAO of phenol under milder operating conditions, a low concentration (approximately 25 mg L^{-1}) of acetic acid was observed in the end stream. The formation of reaction intermediates in the CWAO of phenol has been shown to be sensitive to the reaction temperature, with substantial increase in intermediates observed when temperature is reduced below 100 ^{o}C[108,109]. The increased formation of partial oxidation products is often accompanied with a decline in activity, brought about by carbonaceous deposits accumulating on the catalyst surface[8].

Reduced selectivity towards CO_2 and H_2O, resulting in an increased concentration of reaction intermediates, with decreasing pO_2, has also been observed for CWAO of phenol over Pt/graphite[110]. As such, the deactivation of K9 observed under these conditions is most likely the result of the low temperature and pressure promoting partial oxidation, resulting in deactivation *via* carbonaceous deposits. Catalytic deactivation is discussed in further detail in Chapter 6.

5.4 Post-reaction catalyst characterisation

Characterisation of the catalysts post-reaction can provide details of any structural or compositional changes they may have undergone during the process, when compared to the characterisation of their fresh counterpart.

5.4.1 Powder x-ray diffraction (XRD)

Analysis of the used catalysts *via* XRD can provide evidence of any additional phases that accumulated during reaction, or whether the active metal underwent any oxidation. The XRD profiles for K7, K8, K9 and K10 after 5 hours testing at 7 bar$_{(g)}$ and 120 °C are shown in Figures 5.29 and 5.30.
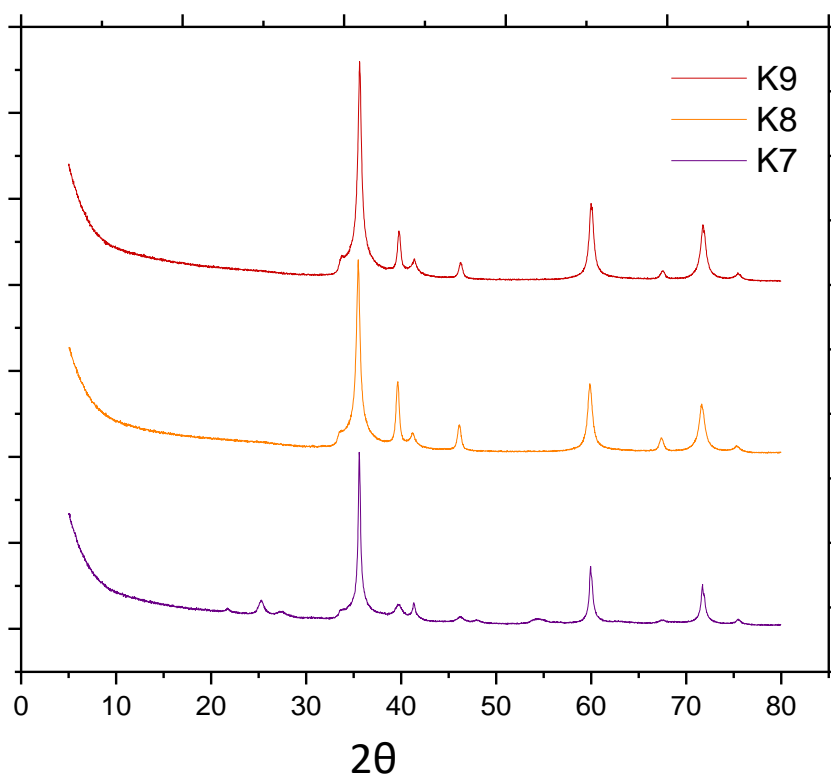
Figure 5.29 Powder XRD patterns of catalysts K7, K8 and K9 post-reaction

The XRD diffraction patterns for K7, K8 and K9 post-CWAO do not differ greatly from their pre-reaction patterns, suggesting the catalysts mostly remained unchanged. The PtO$_2$ peaks present only in the K7 XRD profile at 33.5° and 54.5°, have increased slightly indicating oxidation of the metallic platinum may have occurred within the rector. Oxidation of platinum particles on a catalyst surface has been previously reported for CWAO, accredited to the acidic and oxidising conditions associated with the process[111]. The XRD analysis of K8 and K9 showed no corresponding PtO$_2$ peaks suggesting no significant oxidation of the metal occurred for these catalysts.
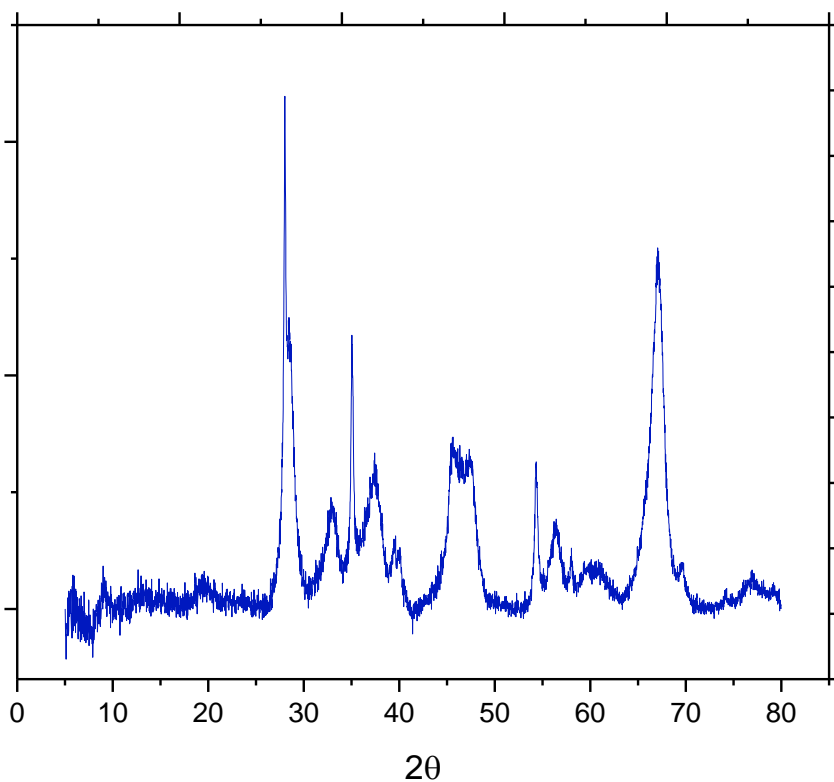
Figure 5.30 Powder XRD pattern of K10 post-reaction

The XRD pattern for K10 (Figure 5.30) also shows intact crystal structure with no reduction in RuO_2 or the presence of any additional species.

5.4.2 Thermogravimetric analysis (TGA)

Thermogravimetric analysis (TGA) is a technique often used as a measure of whether any catalyst deactivation due to adsorbed species on the catalyst surface may have occurred. Any carbon impurities present would be oxidised under the high temperatures and identified by the resulting mass loss. The TGA profiles taken after 5 hours testing at 7 bar$_{(g)}$ and 120 °C, are shown in Figure 5.31.
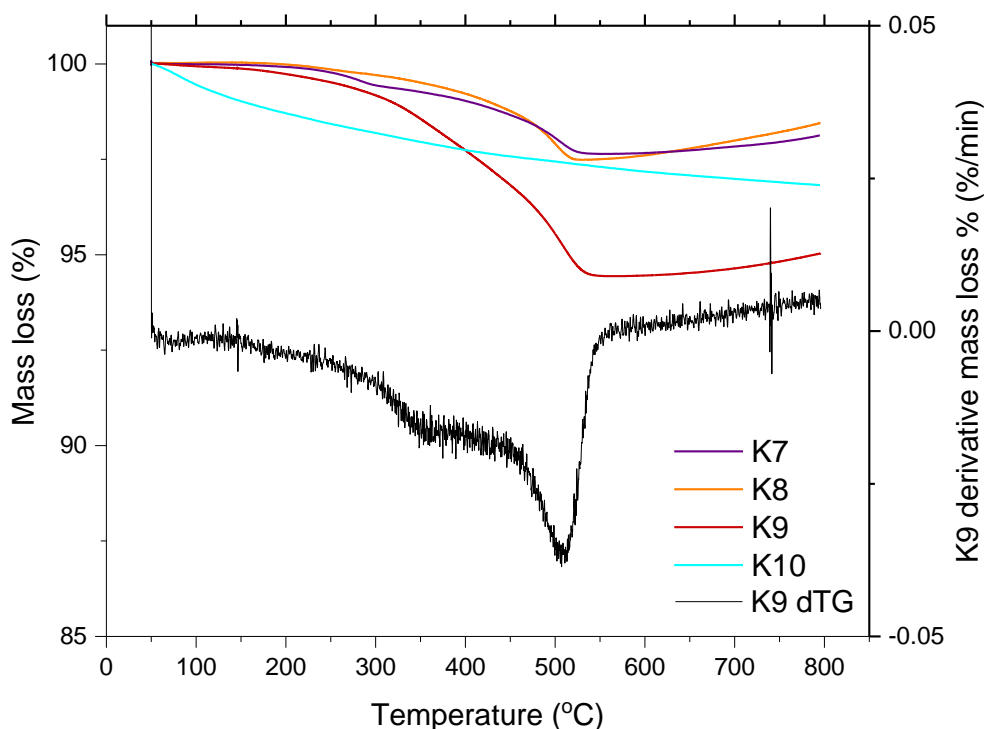
Figure 5.31 TGA profiles of K7, K8, K9 and K10 catalysts after testing, including the first derivative mass loss for K9

Although no catalysts showed deactivation during the 5 hours testing at 120 °C, the TGA revealed similar mass loss profiles for the SiC catalysts between 200 °C – 500 °C, typical of carbonaceous deposits. K9 showed the greatest mass loss, which the first derivative revealed to be in two steps centred around 350 and 510 °C. The initial mass loss is characteristic of the release of CO_2 from the decomposition of carboxylic acid groups present on the catalyst surface[107,112]. The secondary mass loss can be attributed to the decomposition of carbonyl and phenolic groups[113]. The accumulation of carbonaceous species is more pronounced for K9, compared with K7 and K8, suggesting deactivation may occur over a shorter timespan if testing were extended.

The TGA profile for K10 differs from the others with initial mass loss occurring at a lower temperature. Mass loss between 50 °C – 150 °C is likely water evaporating from the catalyst surface[114]. The profile of the fresh K10 catalyst resembles that of the used, indicating no significant concentration of species were adsorbed during the reaction.

5.5 Conclusion

In conclusion, K9 showed the highest activity towards CWAO of phenol under the conditions investigated. Increasing the surface area of the SiC support from 29 $m^2 g^{-1}$ to 35 $m^2 g^{-1}$ (K7 to K8), showed not only an increase in activity but also supressed the formation of metallic oxides on the surface. The higher activity observed for K9 is thought to be due to an increase in the Pt dispersion or the presence of TiO_2 within the SiC support. Calculation of the activation energy revealed the process is likely diffusion limited for K9.

The hydrophilic catalyst, K10, exhibited a stronger pressure dependence when evaluated as a function of dissolved oxygen concentration. Although not conclusive, this furthers the hypothesis of the secondary oxidation pathway being promoted by a hydrophobic catalyst support. Greater understanding of the relationship between dissolved oxygen concentration and reaction rate, as well as further understanding of the dependence on pressure for catalytic activity would help increase the reliability of these results. Testing the catalysts over a larger pressure range would also provide greater insight into whether the pressure dependence for both hydrophobic and hydrophilic catalysts is truly linear.

No catalyst deactivation was observed during the 5 hour testing periods at 120 °C, but accumulation of carbonaceous species were detected in the post-reaction TGA. Prolonged exposure to the acidic and oxidising CWAO conditions would be required to be definitive of any deactivation. Deactivation can also not be ruled out for the experiments where 100 % phenol conversion was reached, as this may give a false representation of true activity.

The conditions used in this study are considerably milder than any seen in the literature, even under near ambient conditions, Pt/SiC-TiC (K9) still achieved phenol conversion. K9 did however show signs of deactivation under such conditions, attributed to the accumulation of carbon species on the catalyst surface. If the thermal stabilisation of the support could be increased to maintain the larger surface area during heat treatment, it may be possible to achieve even higher conversions

5.6 References

(1)   Jones, C.; Cole, K. J.; Taylor, S. H.; Crudace, M. J.; Hutchings, G. J. Copper manganese oxide catalysts for ambient temperature carbon monoxide oxidation: effect of calcination on activity. *J. Mol. Catal. A: Chem.* **2009,** *305* (1-2), 121.

(2)   Mele, A.; Mele, I.; Mele, A. Preparation-properties relation of Mn-Cu hopcalite catalyst. *Am. J. Appl. Sci.* **2012,** *9* (2), 265.

(3)   Davies, D.; Catalytic Wet Air Oxidation: Developing a Continuous Process: Cardiff University PhD Thesis, **2016**.

(4)   Wang, F.-L. a. Z. L.-Y. a. Z. Y.-F. SiC Nanowires Synthesized by Rapidly Heating a Mixture of SiO and Arc-Discharge Plasma Pretreated Carbon Black. *Nanoscale research letters* **2008,** *4*, 153.

(5)   Voevodin, A. A.; Prasad, S. V.; Zabinski, J. S. Nanocrystalline carbide amorphous carbon composites. *Journal of Applied Physics* **1997,** *82* (2), 855.

(6)   Hyde, T.; Crystallite size of supported platinum catalysts by XRD. *Johnson Matthey Technology Review*: Platinum Metal Reviews, **2008**; Vol. 52.

(7)   Banerjee, R.; Liu, Q. L.; Tengco, J. M. M.; Regalbuto, J. R. Detection of Ambient Oxidation of Ultrasmall Supported Platinum Nanoparticles with Benchtop Powder X-Ray Diffraction. *Catalysis Letters* **2017,** *147* (7), 1754.

(8)   Masende, Z. P. G.; Kuster, B. F. M.; Ptasinski, K. J.; Janssen, F.; Katima, J. H. Y.; Schouten, J. C. Platinum catalysed wet oxidation of phenol in a stirred slurry reactor - The role of oxygen and phenol loads on reaction pathways. *Catalysis Today* **2003,** *79* (1-4), 357.

(9)   Levec, J.; Pintar, A. Catalytic wet-air oxidation processes: A review. *Catal. Today* **2007,** *124* (3-4), 172.

(10)   Monteros, A. E. d. l.; Lafaye, G.; Cervantes, A.; Del Angel, G.; Barbier Jr, J.; Torres, G. Catalytic wet air oxidation of phenol over metal catalyst (Ru,Pt) supported on TiO2–CeO$_2$ oxides. *Catalysis Today* **2015,** *258, Part 2*, 564.

(11)   Lafaye, G.; Barbier, J.; Duprez, D. Impact of cerium-based support oxides in catalytic wet air oxidation: Conflicting role of redox and acid-base properties. *Catalysis Today* **2015,** *253*, 89.

(12)   Joo, S. H.; Park, J. Y.; Renzas, J. R.; Butcher, D. R.; Huang, W. Y.; Somorjai, G. A. Size Effect of Ruthenium Nanoparticles in Catalytic Carbon Monoxide Oxidation. *Nano Letters* **2010,** *10* (7), 2709.

(13)   Ramani, M.; Synthesis and Characterization of Hydrous Ruthenium Oxide-Carbon Supercapacitors. *Journal of The Electrochemical Society,* **2001,** *148*.

(14)   McBride, J. R.; Graham, G. W.; Peters, C. R.; Weber, W. H. Growth and characterization of reactively sputtered thin-film platinum oxides. *Journal of Applied Physics* **1991,** *69* (3), 1596.

(15)   Hori, C. E.; Permana, H.; Ng, K. Y. S.; Brenner, A.; More, K.; Rahmoeller, K. M.; Belton, D. Thermal stability of oxygen storage properties in a mixed CeO$_2$-ZrO$_2$ system. *Applied Catalysis B-Environmental* **1998,** *16* (2), 105.

(16)   Damyanova, S.; Perez, C. A.; Schmal, M.; Bueno, J. M. C. Characterization of ceria-coated alumina carrier. *Applied Catalysis a-General* **2002,** *234* (1-2), 271.

(17)   Holzwarth, U. a. G. N. The Scherrer equation versus the 'Debye-Scherrer equation'. *Nature nanotechnology* **2011,** *6*, 534.

(18)   Lunagomez Rocha, M. A.; Del Angel, G.; Torres-Torres, G.; Cervantes, A.; Vazquez, A.; Arrieta, A.; Beltramini, J. N. Effect of the Pt oxidation state and Ce^{3+}/Ce^{4+} ratio on the Pt/TiO_2-CeO_2 catalysts in the phenol degradation by catalytic wet air oxidation (CWAO). *Catalysis Today* **2015,** *250*, 10.

(19)   Hargreaves, J. S. J. Some considerations related to the use of the Scherrer equation in powder X-ray diffraction as applied to heterogeneous catalysts. *Catalysis Structure & Reactivity* **2016,** *2* (1-4), 33.

(20)   Jiang, H. G.; Ruhle, M.; Lavernia, E. J. On the applicability of the x-ray diffraction line profile analysis in extracting grain size and microstrain in nanocrystalline materials. *Journal of Materials Research* **1999,** *14* (2), 549.

(21)   Zhang, Z.; Zhou, F.; Lavernia, E. J. On the analysis of grain size in bulk nanocrystalline materials *via* X-ray diffraction. *Metallurgical and Materials Transactions a-Physical Metallurgy and Materials Science* **2003,** *34A* (6), 1349.

(22)   Kim, S. W.; Iwamoto, S.; Inoue, M. Novel Synthesis Method of Alumina Having a Large Pore-Volume. *Topics in Catalysis* **2010,** *53* (7-10), 535.

(23)   Xu, J.; Ibrahim, A. R.; Hu, X. H.; Hong, Y. Z.; Su, Y. Z.; Wang, H. T.; Li, J. Preparation of large pore volume gamma-alumina and its performance as catalyst support in phenol hydroxylation. *Microporous and Mesoporous Materials* **2016,** *231*, 1.

(24)   Song, A. Y.; Lu, G. X. Catalytic wet oxidation of aqueous methylamine: comparative study on the catalytic performance of platinum-ruthenium, platinum, and ruthenium catalysts supported on titania. *Environmental Technology* **2015,** *36* (9), 1160.

(25)   Yang, S. X.; Zhu, W. P.; Jiang, Z. P.; Chen, Z. X.; Wang, J. B. The surface properties and the activities in catalytic wet air oxidation over CeO_2-TiO_2 catalysts. *Applied Surface Science* **2006,** *252* (24), 8499.

(26)   Moene, R.; Makkee, M.; Moulijn, J. A. High surface area silicon carbide as catalyst support characterization and stability. *Applied Catalysis a-General* **1998,** *167* (2), 321.

(27)   Roy, J.; Chandra, S.; Das, S.; Maitra, S. Oxidation behaviour of silicon carbide - a review. *Reviews on Advanced Materials Science* **2014,** *38* (1), 29.

(28)   Ji, Y. Q.; Zan, Q. F.; Wang, X. G.; Zhu, Y. Y.; Zhou, A. G.; Lin, X. P. High temperature oxidation resistance of Ti_3SiC_2 in air and low oxygen atmosphere. *International Journal of Applied Ceramic Technology* **2017,** *14* (5), 851.

(29)   Barsoum, M. W.; ElRaghy, T.; Ogbuji, L. Oxidation of Ti_3SiC_2 in air. *Journal of the Electrochemical Society* **1997,** *144* (7), 2508.

(30)   Gozzi, D.; Guzzardi, G.; Montozzi, M.; Cignini, P. L. Kinetics of high temperature oxidation of refractory carbides. *Solid State Ionics* **1997,** *101*, 1243.

(31)   Erjavec, B.; Kaplan, R.; Djinovic, P.; Pintar, A. Catalytic wet air oxidation of bisphenol A model solution in a trickle-bed reactor over titanate nanotube-based catalysts. *Applied Catalysis B-Environmental* **2013,** *132*, 342.

(32)   Bellucci, A.; Gozzi, D.; Latini, A. Overview of the TiC/TiO$_2$ (rutile) interface. *Solid State Ionics* **2004,** *172* (1-4), 369.

(33)   Digne, M.; Sautet, P.; Raybaud, P.; Euzen, P.; Toulhoat, H. Hydroxyl groups on gamma-alumina surfaces: A DFT study. *Journal of Catalysis* **2002,** *211* (1), 1.

(34)   Karim, A. M.; Rothstein, J. P.; Kavehpour, H. P. Experimental study of dynamic contact angles on rough hydrophobic surfaces. *Journal of Colloid and Interface Science* **2018,** *513*, 658.

(35)   Chieng, B.; Ibrahim N.; Abidin, N. A.; Chapter 8 - Functionalization of Graphene Oxide *via* Gamma-Ray Irradiation for Hydrophobic Materials. *Micro and Nano Technologies* **2019**, 177.

(36)   Ostrovskii, N. M. New models of catalyst deactivation by coke: I. Multilayer coke formation *via* the consecutive mechanism. *Kinetics and Catalysis* **2001,** *42* (3), 317.

(37)   Ostrovskii, N. M. New models of catalyst deactivation by coke: II. Coking of supported platinum catalysts. *Kinetics and Catalysis* **2001,** *42* (3), 326.

(38)   Xi, K.; Wang, Y.; Jiang, K.; Xie, J.; Zhou, Y.; Lu, H. F. Support interaction of Pt/CeO$_2$ and Pt/SiC catalysts prepared by nano platinum colloid deposition for CO oxidation. *Journal of Rare Earths* **2020,** *38* (4), 376.

(39)   Hatanaka, M.; Takahashi, N.; Tanabe, T.; Nagai, Y.; Suda, A.; Shinjoh, H. Reversible changes in the Pt oxidation state and nanostructure on a ceria-based supported Pt. *Journal of Catalysis* **2009,** *266* (2), 182.

(40)   Liu, Z. L.; Lin, X. H.; Lee, J. Y.; Zhang, W.; Han, M.; Gan, L. M. Preparation and characterization of platinum-based electrocatalysts on multiwalled carbon nanotubes for proton exchange membrane fuel cells. *Langmuir* **2002,** *18* (10), 4054.

(41)   Chen, L.; Xu, Z. W.; He, C.; Wang, Y. G.; Liang, Z. Y.; Zhao, Q. X.; Lu, Q. Gas-phase total oxidation of nitric oxide using hydrogen peroxide vapor over Pt/TiO$_2$. *Applied Surface Science* **2018,** *457*, 821.

(42)   Heponiemi, A.; Azalim, S.; Hu, T.; Vielma, T.; Lassi, U. Efficient removal of bisphenol A from wastewaters: Catalytic wet air oxidation with Pt catalysts supported on Ce and Ce-Ti mixed oxides. *Aims Materials Science* **2019,** *6* (1), 25.

(43)   Ihara, H.; Kumashiro, Y.; Itoh, A.; Maeda, K. Aspects of esca spectra of single-crystals and thin-films of titanium carbide. *Japanese Journal of Applied Physics* **1973,** *12* (9), 1462.

(44)   Rist, O.; Murray, P. T. Growth of tic films by pulsed laser evaporation (ple) and characterization by xps and aes. *Fresenius Journal of Analytical Chemistry* **1991,** *341* (5-6), 360.

(45) Ivanovskaya, M.; Ovodok, E.; Kotsikau, D.; Azarko, I.; Micusik, M.; Omastova, M.; Golovanov, V. Structural transformation and nature of defects in titanium carbide treated in different redox atmospheres. *Rsc Advances* **2020,** *10* (43), 25602.

(46) Halim, J.; Cook, K. M.; Naguib, M.; Eklund, P.; Gogotsi, Y.; Rosen, J.; Barsoum, M. W. X-ray photoelectron spectroscopy of select multi-layered transition metal carbides (MXenes). *Applied surface science* **2016,** *362,* 406.

(47) Heponiemi, A.; Azalim, S.; Hu, T.; Lassi, U. Cerium Oxide Based Catalysts for Wet Air Oxidation of Bisphenol A. *Topics in Catalysis* **2015,** *58* (14-17), 1043.

(48) Alderucci, V.; Pino, L.; Antonucci, P. L.; Roh, W.; Cho, J.; Kim, H.; Cocke, D. L.; Antonucci, V. XPS study of surface oxidation of carbon-supported Pt catalysts. *Materials Chemistry and Physics* **1995,** *41* (1), 9.

(49) Yang, S. X.; Feng, Y. J.; Wan, J. F.; Zhu, W. P.; Jiang, Z. P. Effect of CeO_2 addition on the structure and activity of RuO_2/gamma-Al_2O_3 catalyst. *Applied Surface Science* **2005,** *246* (1-3), 222.

(50) Rodriguez-Reinoso, F. The role of carbon materials in heterogeneous catalysis. *Carbon* **1998,** *36* (3), 159.

(51) Chen, H.; Sayari, A.; Adnot, A.; Larachi, F. Composition-activity effects of Mn-Ce-O composites on phenol catalytic wet oxidation. *Applied Catalysis B-Environmental* **2001,** *32* (3), 195.

(52) Nartova, A. V.; Gharachorlou, A.; Bukhtiyarov, A. V.; Kvon, R. I.; Bukhtiyarov, V. I. New Pt/Alumina model catalysts for STM and in situ XPS studies. *Applied Surface Science* **2017,** *401*, 341.

(53) Cuauhtemoc, I.; Del Angel, G.; Torres, G.; Navarrete, J.; Angeles-Chavez, C.; Padilla, J. M. Synthesis and characterization of Rh/Al_2O-CeO_2 catalysts: effect of the Ce^{4+}/Ce^{3+} ratio on the MTBE removal. *Journal of Ceramic Processing Research* **2009,** *10* (4), 512.

(54) Galtayries, A.; Sporken, R.; Riga, J.; Blanchard, G.; Caudano, R. XPS comparative study of ceria/zirconia mixed oxides: powders and thin film characterisation. *Journal of Electron Spectroscopy and Related Phenomena* **1998,** *88*, 951.

(55) Morgan, D. J. Resolving ruthenium: XPS studies of common ruthenium materials. *Surface and Interface Analysis* **2015,** *47* (11), 1072.

(56) Rochefort, D.; Dabo, P.; Guay, D.; Sherwood, P. M. A. XPS investigations of thermally prepared RuO_2 electrodes in reductive conditions. *Electrochimica Acta* **2003,** *48* (28), 4245.

(57) Sunol, J. J.; Bonneau, M. E.; Roue, L.; Guay, D.; Schulz, R. XPS surface study of nanocrystalline Ti-Ru-Fe materials. *Applied Surface Science* **2000,** *158* (3-4), 252.

(58) Santos, A.; Yustos, P.; Gomis, S.; Ruiz, G.; Garcia-Ochoa, F. Reaction network and kinetic modeling of wet oxidation of phenol catalyzed by activated carbon. *Chemical Engineering Science* **2006,** *61* (8), 2457.

(59) Schwarz, J. A.; Contescu, C.; Contescu, A. Methods for preparation of catalytic materials. *Chemical Reviews* **1995,** *95* (3), 477.

(60)   Maugans, C. B.; Akgerman, A. Catalytic wet oxidation of phenol in a trickle bed reactor over a Pt/TiO$_2$ catalyst. *Water Research* **2003,** *37* (2), 319.

(61)   Maugans, C. B.; Akgerman, A. Catalytic wet oxidation of phenol over a Pt/TiO$_2$ catalyst. *Water Research* **1997,** *31* (12), 3116.

(62)   Mazzieri, V. A.; Grau, J. M.; Yori, J. C.; Vera, C. R.; Pieck, C. L. Influence of additives on the Pt metal activity of naphtha reforming catalysts. *Applied Catalysis a-General* **2009,** *354* (1-2), 161.

(63)   Carvalho, L. S.; Pieck, C. L.; Rangel, M. C.; Figoli, N. S.; Grau, J. M.; Reyes, P.; Parera, J. M. Trimetallic naphtha reforming catalysts. I. Properties of the metal function and influence of the order of addition of the metal precursors on Pt-Re-Sn/gamma-Al$_2$O$_3$-Cl. *Applied Catalysis a-General* **2004,** *269* (1-2), 91.

(64)   Lieske, H.; Lietz, G.; Spindler, H.; Volter, J. Reactions of platinum in oxygen-treated and hydrogen-treated Pt-gamma-Al$_2$O$_3$ catalysts .1. temperature-programmed reduction, adsorption, and redispersion of platinum. *Journal of Catalysis* **1983,** *81* (1), 8.

(65)   LeNormand, F.; Borgna, A.; Garetto, T. F.; Apesteguia, C. R.; Moraweck, B. Redispersion of sintered Pt/Al$_2$O$_3$ naphtha reforming catalysts: An in situ study monitored by X-ray absorption spectroscopy. *Journal of Physical Chemistry* **1996,** *100* (21), 9068.

(66)   Contreras-Andrade, I.; Vazquez-Zavala, A.; Viveros, T. Influence of the Synthesis Method on the Catalytic Behavior of Pt and PtSn/Al$_2$O$_3$ Reforming Catalyst. *Energy & Fuels* **2009,** *23* (8), 3835.

(67)   Subramanian, S.; Temperature programmed reduction of platinum group metals catalysts. *Johnson Matthey Technology Review*, **1992**; Vol. 36 (2).

(68)   Hwang, C. P.; Yeh, C. T. Platinum-oxide species formed by oxidation of platinum crystallites supported on alumina. *Journal of Molecular Catalysis a-Chemical* **1996,** *112* (2), 295.

(69)   Pintar, A.; Batista, J.; Tisler, T. Catalytic wet-air oxidation of aqueous solutions of formic acid, acetic acid and phenol in a continuous-flow trickle-bed reactor over Ru/TiO$_2$ catalysts. *Applied Catalysis B-Environmental* **2008,** *84* (1-2), 30.

(70)   Sexton, B. A.; Hughes, A. E.; Foger, K. XPS investigation of strong metal support interactions on group iiia-va oxides. *Journal of Catalysis* **1982,** *77* (1), 85.

(71)   Perez-Hernandez, R.; Gomez-Cortes, A.; Arenas-Alatorre, J.; Rojas, S.; Mariscal, R.; Fierro, J. L. G.; Diaz, G. SCR of NO by CH$_4$ on Pt/ZrO$_2$-TiO$_2$ sol-gel catalysts. *Catalysis Today* **2005,** *107-08*, 149.

(72)   Zhang, C. B.; He, H.; Tanaka, K. Catalytic performance and mechanism of a Pt/TiO$_2$ catalyst for the oxidation of formaldehyde at room temperature. *Applied Catalysis B-Environmental* **2006,** *65* (1-2), 37.

(73)   Epling, W. S.; Cheekatamarla, P. K.; Lane, A. M. Reaction and surface characterization studies of titania-supported Co, Pt and Co/Pt catalysts for the selective oxidation of CO in H$_2$-containing streams. *Chemical Engineering Journal* **2003,** *93* (1), 61.

(74) Lu, L. L.; Wang, C.; Wang, M.; Song, Q. J. Catalytic Oxidation of Trichloroethylene over RuO_2 Supported on Ceria-zirconia Mixed Oxide. *Chemical Research in Chinese Universities* **2019,** *35* (1), 71.

(75) Yu, J.; Zhao, D.; Xu, X. L.; Wang, X.; Zhang, N. Study on RuO_2/SnO_2: Novel and Active Catalysts for CO and CH_4 Oxidation. *Chemcatchem* **2012,** *4* (8), 1122.

(76) Wang, L.; Abudukelimu, N.; Ma, Y. B.; Qing, S. J.; Gao, Z. X.; Eli, W. J. Enhanced Ru/Alumina catalyst *via* the adsorption-precipitation (AP) method for the hydrogenation of dimethyl maleate. *Reaction Kinetics Mechanisms and Catalysis* **2014,** *112* (1), 117.

(77) Saunders, K.; Davies, D.; Golunski, S.; Johnston, P.; Plucinski, P. Making the Most of Precious Metal Nanoparticles in the Purification of Industrial Wastewater by Catalytic Wet Air Oxidation Revealing synergy between platinum and catalyst support. *Johnson Matthey Technology Review* **2018,** *62* (4), 429.

(78) Luna, A. J.; Rojas, L. O. A.; Melo, D. M. A.; Benachour, M.; de Sousa, J. F. Total catalytic wet oxidation of phenol and its chlorinated derivates with MnO_2/CeO_2 catalyst in a slurry reactor. *Brazilian Journal of Chemical Engineering* **2009,** *26* (3), 493.

(79) Hamoudi, S.; Larachi, F.; Sayari, A. Wet oxidation of phenolic solutions over heterogeneous catalysts: Degradation profile and catalyst behavior. *Journal of Catalysis* **1998,** *177* (2), 247.

(80) Chen, X. N.; Chen, J. Y.; Zhao, Y.; Chen, M. S.; Wan, H. L. Effect of Dispersion on Catalytic Performance of Supported Pt Catalysts for CO Oxidation. *Chinese Journal of Catalysis* **2012,** *33* (12), 1901.

(81) Haneda, M.; Sasaki, M.; Hamada, H.; Ozawa, M. Effect of Pt Dispersion on the Catalytic Activity of Supported Pt Catalysts for Diesel Hydrocarbon Oxidation. *Topics in Catalysis* **2013,** *56* (1-8), 249.

(82) Keav, S.; de los Monteros, A. E.; Barbier, J.; Duprez, D. Wet Air Oxidation of phenol over Pt and Ru catalysts supported on cerium-based oxides: Resistance to fouling and kinetic modelling. *Applied Catalysis B-Environmental* **2014,** *150,* 402.

(83) Matos, J.; Laine, J.; Herrmann, J. M. Synergy effect in the photocatalytic degradation of phenol on a suspended mixture of titania and activated carbon. *Applied Catalysis B-Environmental* **1998,** *18* (3-4), 281.

(84) Woan, K.; Pyrgiotakis, G.; Sigmund, W. Photocatalytic Carbon-Nanotube-TiO_2 Composites. *Advanced Materials* **2009,** *21* (21), 2233.

(85) Upadhyay, R. K.; Soin, N.; Roy, S. S. Role of graphene/metal oxide composites as photocatalysts, adsorbents and disinfectants in water treatment: a review. *Rsc Advances* **2014,** *4* (8), 3823.

(86) Wang, W. D.; Serp, P.; Kalck, P.; Faria, J. L. Visible light photodegradation of phenol on MWNT-TiO_2 composite catalysts prepared by a modified sol-gel method. *Journal of Molecular Catalysis a-Chemical* **2005,** *235* (1-2), 194.

(87) Wei, H. Z.; Wang, Y. M.; Yu, Y.; Gu, B.; Zhao, Y.; Yang, X.; Sun, C. L. Effect of TiO_2 on Ru/ZrO_2 catalysts in the catalytic wet air oxidation of isothiazolone. *Catalysis Science & Technology* **2015,** *5* (3), 1693.

(88)   Atkins, P. W.; De Paula, J.; Atkins' Physical cehmistry. Tenth Edition ed.; *Oxford University Press*, **2014**.

(89)   Yu, J. G.; Zhao, X. H.; Yang, H.; Chen, X. H.; Yang, Q.; Yu, L. Y.; Jiang, J. H.; Chen, X. Q. Aqueous adsorption and removal of organic contaminants by carbon nanotubes. *Science of the Total Environment* **2014,** *482*, 241.

(90)   Eftaxias, A.; Font, J.; Fortuny, A.; Fabregat, A.; Stuber, F. Kinetics of phenol oxidation in a trickle bed reactor over active carbon catalyst. *Journal of Chemical Technology and Biotechnology* **2005,** *80* (6), 677.

(91)   Kulkarni, U. S.; Dixit, S. G. Destruction of Phenol from Wastewater by Oxidation with SO_3^{2-}-O_2. *Industrial and Engineering Chemistry Research* **1991,** *30* (8), 1916.

(92)   Sadana, A.; Katzer, J. R. Catalytic-oxidation of phenol in aqueous-solution over copper oxide. *Industrial & Engineering Chemistry Fundamentals* **1974,** *13* (2), 127.

(93)   Cybulski, A.; Trawczyński, J. Catalytic wet air oxidation of phenol over platinum and ruthenium catalysts. *Appl. Catal. B: Environmental* **2004** *47*, 1

(94)   Carroll, K. M.; Knoll, A. W.; Wolf, H.; Duerig, U. Explaining the Transition from Diffusion Limited to Reaction Limited Surface Assembly of Molecular Species through Spatial Variations. *Langmuir* **2018,** *34* (1), 73.

(95)   Lynggaard, H.; Andreasen, A.; Stegelmann, C.; Stoltze, P. Analysis of simple kinetic models in heterogeneous catalysis. *Progress in Surface Science* **2004,** *77* (3-4), 71.

(96)   Dittmeyer, R. a. E. G. Simultaneous Heat and Mass Transfer and Chemical Reaction. **2008**, 1727.

(97)   Klaewkla, R.; Arend, M.; Hölderich, W., A review of mass transfer controlling the reaction rate in heterogeneous catalytic systems. **2011**; Vol. 29.

(98)   Fogler, H. S.; Elements of chemcial reaction engineering. *Prentice Hall*, **1998**.

(99)   White, D. E.; Litt, M.; Heymach, G. J. Diffusion-limited heterogeneous catalytic reactions on a rotating-disk .1. hydrogenation of alpha-methylstyrene. *Industrial & Engineering Chemistry Fundamentals* **1974,** *13* (2), 143.

(100) Tromans, D. Temperature and pressure dependent solubility of oxygen in water: a thermodynamic analysis. *Hydrometallurgy* **1998,** *48* (3), 327.

(101) Renard, B.; Barbier-Jr, J.; Duprez, D.; Durecu, S. Catalytic wet air oxidation of stearic acid on cerium oxide supported noble metal catalysts. *Applied Catalysis B-Environmental* **2005,** *55* (1), 1.

(102) Stuber, F.; Polaert, I.; Delmas, H.; Font, J.; Fortuny, A.; Fabregat, A. Catalytic wet air oxidation of phenol using active carbon: performance of discontinuous and continuous reactors. *Journal of Chemical Technology and Biotechnology* **2001,** *76* (7), 743.

(103) Staples, C. A.; Dorn, P. B.; Klecka, G. M.; O'Block, S. T.; Harris, L. R. A review of the environmental fate, effects, and exposures of bisphenol A. *Chemosphere* **1998,** *36* (10), 2149.

(104) Taulamet, M. J.; Mariani, N. J.; Barreto, G. F.; Martinez, O. M. Prediction of thermal behavior of trickle bed reactors: The effect of the pellet shape and size. *Fuel* **2017,** *202*, 631.

(105) Lin, S. S. Y.; Chang, D. J.; Wang, C. H.; Chen, C. C. Catalytic wet air oxidation of phenol by CeO_2 catalyst - effect of reaction conditions. *Water Research* **2003,** *37* (4), 793.

(106) Yang, S. X.; Zhu, W. P.; Wang, J. B.; Chen, Z. X. Catalytic wet air oxidation of phenol over CeO_2-TiO_2 catalyst in the batch reactor and the packed-bed reactor. *Journal of Hazardous Materials* **2008,** *153* (3), 1248.

(107) Nousir, S.; Keav, S.; Barbier-Jr, J.; Bensitel, M.; Brahmi, R.; Duprez, D. Deactivation phenomena during catalytic wet air oxidation (CWAO) of phenol over platinum catalysts supported on ceria and ceria-zirconia mixed oxides. *Applied Catalysis B-Environmental* **2008,** *84* (3-4), 723.

(108) Lal, K.; Garg, A. Catalytic wet oxidation of phenol under mild operating conditions: development of reaction pathway and sludge characterization. *Clean Technologies and Environmental Policy* **2015,** *17* (1), 199.

(109) Suarez-Ojeda, M. E.; Fabregat, A.; Stuber, F.; Fortuny, A.; Carrera, J.; Font, J. Catalytic wet air oxidation of substituted phenols: Temperature and pressure effect on the pollutant removal, the catalyst preservation and the biodegradability enhancement. *Chemical Engineering Journal* **2007,** *132* (1-3), 105.

(110) Masende, Z. P. G.; Kuster, B. F. M.; Ptasinski, K. J.; Janssen, F.; Katima, J. H. Y.; Schouten, J. C. Platinum catalysed wet oxidation of phenol in a stirred slurry reactor - A practical operation window. *Applied Catalysis B-Environmental* **2003,** *41* (3), 247.

(111) Besson, M.; Gallezot, P. Deactivation of metal catalysts in liquid phase organic reactions. *Catalysis Today* **2003,** *81* (4), 547.

(112) Santiago, M.; Stuber, F.; Fortuny, A.; Fabregat, A.; Font, J. Modified activated carbons for catalytic wet air oxidation of phenol. *Carbon* **2005,** *43* (10), 2134.

(113) Alvarez, P. M.; Beltran, F. J.; Gomez-Serrano, V.; Jaramillo, J.; Rodriguez, E. M. Comparison between thermal and ozone regenerations of spent activated carbon exhausted with phenol. *Water Research* **2004,** *38* (8), 2155.

(114) Cardenas-Aguiar, E.; Gasco, G.; Paz-Ferreiro, J.; Mendez, A. Thermogravimetric analysis and carbon stability of chars produced from slow pyrolysis and hydrothermal carbonization of manure waste. *Journal of Analytical and Applied Pyrolysis* **2019,** *140*, 434.

Chapter 6

The CWAO of bisphenol-A

6.1 Introduction

In real world scenarios, wastewater streams will likely contain multiple pollutants, thus an effective catalyst for CWAO must be able to degrade other toxic organic compounds commonly found in wastewater. Among such pollutants is Bisphenol A (BPA).

Widely used as a monomer for the synthesis of epoxy and polycarbonate resins[1-3], BPA is classified as a synthetic endocrine disrupting chemical (EDC)[4], a compound capable of disrupting the endocrine system in humans and animals. EDCs can disrupt a multitude of hormones through mimicking, increasing or decreasing levels or blocking endogenous hormones[5]. BPA specifically, is able to bind with oestrogen and androgen receptors, disrupting the hormones leptin, insulin and thyroxine, causing mutagenic and carcinogenic effects[6,7]. Due to the complex and wide-ranging effects of this endocrine disruptor, BPA has been linked to numerous adverse health effects[8,9].

BPA has an annual production exceeding 3.8 million tons[10] and can be found in a variety of products including thermal papers[11], epoxy resins in plastic lining of food storage cans[12], polycarbonate plastics[13], medical equipment[14] and electronic parts[15]. BPA has been shown to migrate from polycarbonate resins into food stuffs and liquids, thus allowing BPA to enter our ecosystems *via* plastic bottles, packaging and through wastewaters from industry associated with BPA processing and degradation of certain polymers[16,17]. The abundance of BPA and its harmful nature make its removal from the environment essential.

6.1.1 BPA as a pollutant
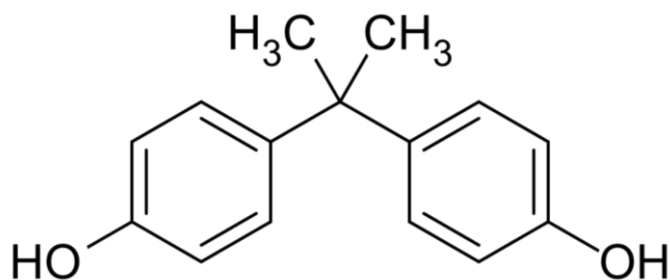
Figure 6.1 Molecular structure of Bisphenol A (BPA)

The chemical structure of BPA, shown in Figure 6.1, is composed of two hydrophenol groups. BPA exists as a white crystalline solid with a low water solubiltiy of 120 mg L^{-1} at 25 °C[3]. The presence of the two hydroxyl groups governs the reactivity of BPA[10].

BPA is historically synthesized from a condensation reaction between one mole of acetone and two equivalents of phenol in the presence of a catalyst. Typically, a large excess of phenol is used to ensure complete condensation[18], thus, wastewater streams associated with BPA production often also contain phenol and phenolic compounds.

Much like phenol, the oxidation pathway of BPA can proceed *via* the formation of numerous intermediates. Figure 6.2 shows the degradation pathway of BPA proposed by Hans *et al.*[19].
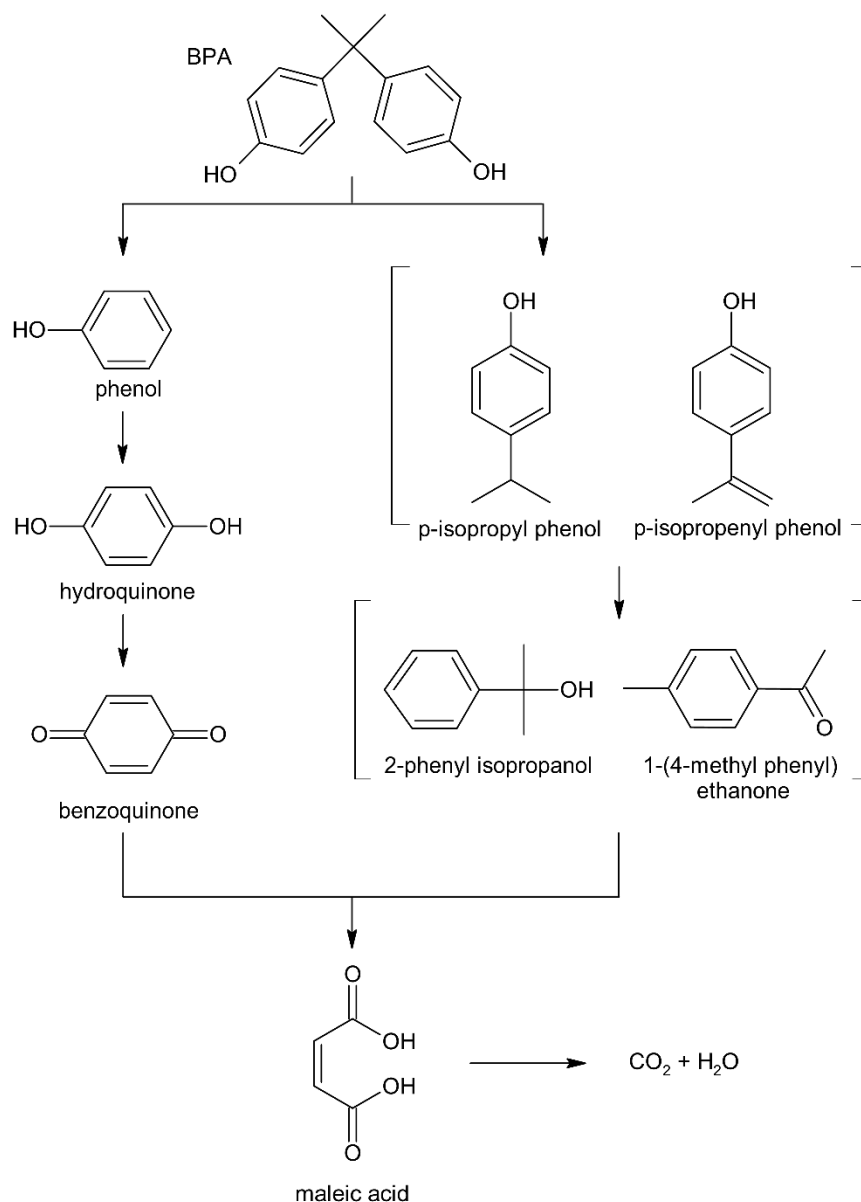
Figure 6.2 BPA degradation pathway proposed by Han et al.[19]

The degradation of BPA can proceed *via* a number of routes, including oxidation to phenol. The reaction mechanism goes through many of the same intermediates encountered during phenol oxidation, including benzoquinone, maleic acid and hydroquinone before mineralising to water and CO_2. Since Pt/SiC has proven to be an effective catalyst for the CWAO of phenol thus far, a similar trend would be expected for the oxidation of BPA. Jiao *et al.*[20] and Chen *et al.*[21] also proposed similar mechanisms, with two main degradation paths for BPA proceeding *via* phenol and isopropenyl phenol. Propionic, acetic, oxalic and formic acids, which were observed as intermediates during phenol oxidation, were likewise observed in the end stream during BPA oxidation.

Serra-Perez *et al.*[22] proposed that the oxidation of BPA by hydroxyl radicals can also proceed through an attack on one of the aromatic rings of BPA, illustrated in Figure 6.3. The electrophilic OH group attack occurs at the ortho-position due to orientation effects of substituted bi-phenols. The oxidation reaction then proceeds through numerous intermediates, all of which can be degraded to carboxylic acids, before mineralization to CO_2 and H_2O.
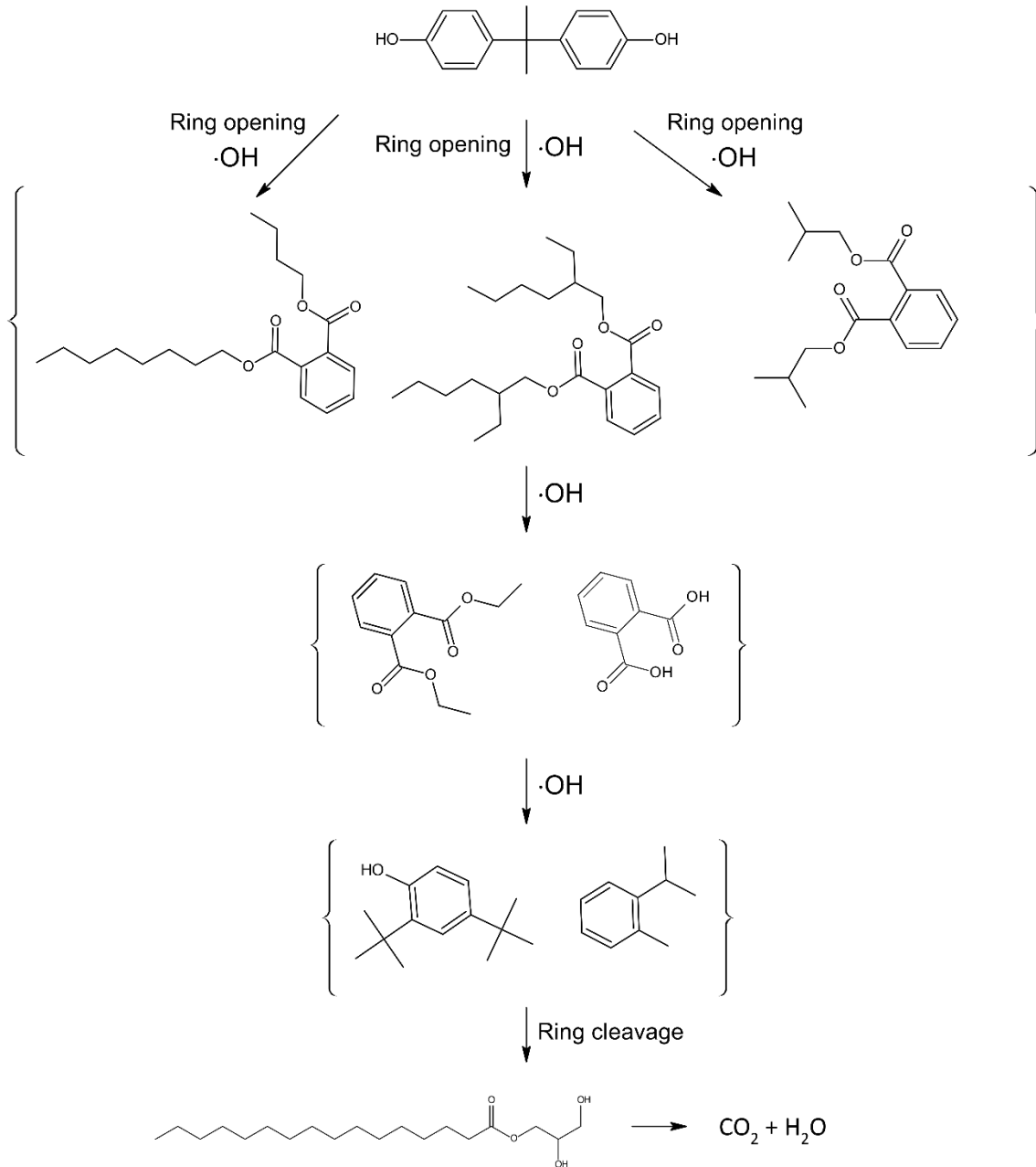
Figure 6.3 BPA degradation pathway via hydroxyl radicals for the CWAO of BPA[22]

Irrespective of which reaction scheme may be prevalent, both include the formation of many stable partial oxidation products. The presence of phenol and certain quinones (compounds with a higher toxicity than BPA) as derivatives for BPA degradation, may result in an increase in the toxicity of the previously 'treated' water[3,23]. Although degradation of BPA is important, the overall water quality must also be considered.

A variety of technologies exist for the treatment of BPA and EDC contaminated wastewaters and an appropriate selection must be made before the water can be safely integrated back into the environment.

6.1.2 Current treatment methods

Many current wastewater treatment plants are not specifically designed for the elimination of micropollutants such as BPA, thus these pollutants are able to pass through untreated[24]. In recent years, as the full environmental and health implications of EDCs are being realised, technologies capable of removing EDCs have received increased attention. The methods for removal of EDCs from wastewaters are diverse and frequently used in tandem, they also fall into similar categories as those used for phenolic wastewater treatment.

6.1.2.1 Removal of BPA by biodegradation

Biodegradation processes are typically the most cost-effective, and thus often opted as the method of choice[25]. EDC removal *via* activated sludge has shown great efficiency for treating compounds such as estradiols[25], however many micropollutants are not completely removed and can be absorbed by the biological sludge[26]. Conventional biological wastewater treatment plants are applied to wastewaters with low effluent concentrations and suffer from long residence times[27]. Biodegradation of BPA can be very slow and conventional

biological treatment cannot always effectively eliminate BPA from contaminated wastewaters[19].

6.1.2.2 Removal of BPA by physical adsorption

EDC removal *via* adsorption has the advantage of producing minimal harmful secondary products; the application of effective adsorbents is critical to guarantee the efficiency of the process[28]. The high specific surface area and low surface polarity of activated carbon have made it a desirable absorbent for BPA removal[29,30], as well as porous carbon[31], carbon nanotubes[32] and graphene oxide[33]. Despite evidence of high BPA abatement for adsorption processes, there are still inherent limitations and adsorption is not well suited for large scale treatment of pollutants[34].

6.1.2.3 Removal of BPA by membrane separation

Nanofiltration and reverse osmosis have emerged as promising membrane technologies for the removal of EDCs and other low molecular weight organic micropollutants. However, the membrane can be considered a reservoir of contaminants and studies have shown some retained EDCs permeating through the membrane, and being released back into the liquid phase[35]. Membrane fouling can also lead to high operational and maintenance costs[19].

6.1.2.4 Advanced oxidation processes

The limitations of conventional treatment methods for low concentrations of BPA have brought more focus to advanced oxidation processes (AOP). Strong oxidising agents such as highly reactive hydroxyl (HO·) or sulfate (SO4$^-$·) radicals, produced from thermal, UV and activation of oxidants can degrade EDCs to

intermediates, CO_2 and H_2O[36]. AOPs investigated for wastewater treatment include Fenton's reaction[37], ozonation[38], photocatalysis[39] and catalytic wet air oxidation (CWAO). CWAO has achieved significant abatement of organic contaminants under milder conditions than uncatalyzed wet air oxidation, typically ranging between temperatures and pressures of $110 - 230\ ^{o}C$ and $20 - 50$ bar for BPA removal[40].

CWAO is able to degrade EDCs at higher concentrations than conventional methods, however, further investigation is still required to increase the long-term stability of the catalysts and further lower operating conditions, improving the environmental and economic impact of the process.

6.1.3 Current catalyst benchmark

Table 6.1 shows the current standard of solid heterogeneous catalysts being investigated in the literature, the corresponding BPA conversions (X_{BPA}) achieved and the operating conditions at which they are active.

Table 6.1 Active catalysts for CWAO of BPA at temperature (T), O_2 partial pressure (pO_2), initial BPA concentration ([BPA]) and conversion rates (X_{BPA})

Catalyst	[BPA] (mg L^{-1})	T (^{o}C)	pO^2 (bar)	X_{BPA} (%)	Ref
Titanate nanotubes	10	210	10	99	40
Ru/TiO$_2$	20	230	10	100	23
Ru/CNS	20	130	5	>99	22
Pt/CeO$_2$	60	160	5	97	41
Ag/Ce$_{0.85}$Zr$_{0.15}$O$_2$	60	160	5	76	42
Titanate nanotubes	10	200	10	90	43
TiO$_2$	10	210	10	80	44

High BPA conversions were all achieved over a variety of catalysts during CWAO, however, the lowest pO_2 observed in the literature was 5 bar, equivalent to >20 bar air pressure. Pressures as high as this are used to increase the

concentration of dissolved oxygen, and thus reduce its potential as the rate limiting step. Uncatalyzed wet air oxidation (WAO) was also active under the operating conditions used for Ru/CNS[22] which may have contributed to the total BPA conversion (X_{BPA}).

The catalytic wet peroxide oxidation (CWPO) of BPA was also studied with iron supported on activated carbon catalysts, achieving complete BPA degradation at 80 °C with stoichiometric amount of hydrogen peroxide[45].

Heponiemi *et al.*[42] and Erjavec *et al.*[43] both observed BPA oxidation to be independent on catalyst surface area, similar to what was observed for CWAO of phenol for K7 – K10.

The aim of this study is to evaluate the efficiency of Pt/SiC for CWAO of BPA and to see whether the hydrophobicity of SiC can allow for high conversion rates at much lower pressures than those previously seen in the literature.

6.2 Pre-reaction catalyst characterisation

The catalysts used in this study were equivalent to those used in Chapter 5 and thus the pre-catalyst characterisation previously seen holds true for this chapter as well. Rather than repeat the data, a short summary of the catalyst characterisation is given instead. As a reminder, the shorthand key used to identify the catalysts is shown in Table 6.2.

Table 6.2 A shorthand key used to distinguish between catalysts

Code	Active component(s)	Support
K7	2 % Platinum	Silicon carbide - 1.6 mm Trilobe extrudate, 25 m ^{2}g^{-1} nominal surface area
K8	2 % Platinum	Silicon carbide - 1.6 mm Trilobe extrudate, 30 m^{2}g^{-1} nominal surface area
K9	2 % Platinum	Silicon carbide and titanium carbide composite - 1.6 mm Trilobe extrudate, 90 m^{2}g^{-1} nominal surface area
K10	2 % Ruthenium, 5 % ceria	Alumina – 450 – 600 μm granules

6.2.1 K7 – 2% Pt/SiC

The XRD diffraction pattern (Figure 5.1) revealed the presence both of PtO$_2$ and metallic platinum for K7; PtO$_2$ has been shown to be less active for CWAO of phenol compared with metallic platinum on identical supports[46]. K7 exhibited the lowest surface area, 29 m^2 g^{-1}, of the investigated catalysts, calculated using BET N$_2$ adsorption. The TGA revealed no significant mass changes up to 600 ºC (Figure 5.3), with similar stabilities seen for all catalysts.

When probed with XPS, a second carbon environment was observed on the surface of K7 (Figure 5.8), which was attributed to remaining carbon persisting from the breakdown of the platinum precursor (Pt(acac)$_2$). K7 displayed lower phenol conversions when compared with K8 and K9, which is believed to be resultant of this amorphous carbon layer blocking a portion of the active sites. No Pt oxide was observed in the XPS Pt 4f spectra (Figure 5.9), further analysis with H$_2$-TPR (Figure 5.20) suggested that any PtO$_2$ present is strongly interacting with the SiC support.

The SEM images (Figures 5.13 and 5.14) showed the Pt species existed exclusively on the external surface of the catalyst pellets. EDX analysis of catalyst

samples, which were ground into a powder to give a more accurate representation of the metal loading, revealed a Pt loading of 1.86 wt %.

6.2.2 K8 – 2% Pt/SiC

The XRD pattern for K8 (Figure 5.1) showed the presence of metallic platinum with no diffraction peaks characteristic of PtO_x species, this was confirmed in the H_2-TPR profile (Figure 5.20). The specific surface area was found to be 35 $m^2\,g^{-1}$, the highest observed for the SiC catalysts. The TGA profile (Figure 5.3) revealed no significant mass changes up to 600 ^{o}C.

Unlike K7, no second carbon environment was seen in the XPS (Figure 5.8) for K8. The SEM images (Figures 5.15 and 5.16) showed the platinum existed exclusively on the surface of the external surface of the SiC pellet. EDX analysis revealed an active metal loading of 1.6 wt %.

K8 exhibited a lower phenol conversion compared with K9, but higher than K7, achieving 57 % conversion at 7 $bar_{(g)}$ and 100 ^{o}C.

6.2.3 K9 – 2% Pt/SiC-TiC

A specific surface area of 34 $m^2\,g^{-1}$ was observed for K9, comparable with K8; whilst the XRD (Figure 5.1) showed the presence of metallic platinum, with no metal oxide species observed. The TGA profile of the uncalcined K9 support (Figure 5.4) showed a 3.5 % mass increase, which resulted in a large loss of specific surface area. The XPS Ti 2p spectra (Figure 5.10) was typical of titanium in a TiO_2 environment. Coupled with the H_2-TPR profile (Figure 5.20) which was characteristic of TiO_2 supported metal catalysts[47], and given the oxidation of TiC to TiO_2 seen in the literature for Ti_xSiC_x compounds[48,49], it is thought the surface area loss is resultant of TiC oxidation to TiO_2 during heat treatment. A surface area loss during calcination was not observed for K7 and K8 as no TiC is present in the

catalyst support for these samples. Once calcined, K9 showed no further significant mass changes in the TGA profile (Figure 5.5) up to temperatures of 600 ^{o}C.

The SEM images (Figures 15.17 and 15.18) of K9, show distinguishable Pt particles between 2 – 15 μm, with EDX identifying presence of the metal throughout the catalyst pellet. K9 achieved the highest phenol conversions out of the catalysts investigated, although some deactivation was observed under mild operating conditions (Figure 5.28).

6.2.4 K10 – 2% Ru/5% ceria/alumina

K10, a typical heterogenous catalyst for CWAO, was used as a comparison for the hydrophobic SiC catalysts. The relative hydrophilicity was confirmed using TGA (Figure 5.7) showing a higher water retention compared to K9. K10 had the highest surface area of all the catalysts, measured at 110 $m^2 g^{-1}$. The XRD pattern (Figure 5.2) revealed the presence of RuO_2, with no peaks corresponding to metallic ruthenium. The XPS data was in agreement with this, with the Ru 3d spectra (Figure 5.12) characteristic of ruthenium oxide. The XPS Ce 3d spectra also showed the presence of Ce^{3+} and Ce^{4+} for K10. The SEM images of K10 (Figure 5.19) show the highest metal dispersion of the catalysts investigated, with ruthenium particles observed in a size range between 10 μm – 100 nm.

The characterisation of K10 was indicative of a well performing catalyst, however the testing revealed K10 to exhibit the lowest phenol conversions observed of all the catalysts tested.

6.3 Catalyst activity studies

For the investigation into CWAO of BPA, the activity testing was carried out at the National Institute of Chemistry in Ljubljana, Slovenia. CWAO was conducted

using a PID Microactivity continuous-flow trickle bed reactor, the reactor set-up and operational parameters for which are described in Chapter 3.

Due to the decrease in the size of the catalyst bed within the reactor, to ensure sufficient packing and catalyst contact times, the catalysts were lightly crushed using a pestle and mortar to avoid any pressure drop related problems. Unfortunately, it was not possible to assess the catalyst pellet size at this point and so a definitive particle size range, below the 1.6 x 5 mm extrudates, cannot be given.

In the absence of any catalyst, the concentration of BPA remained stable in water and no degradation was observed over 24 hours under 7 bar$_{(g)}$ and 120 ^{o}C, showing no contribution from WAO under these conditions.

6.3.1 A comparison of CWAO of BPA and phenol

To be able to fully compare the results obtained for CWAO of phenol with those obtained for BPA, the reaction conditions were chosen to best emulate those previously used. To account for the smaller reactor volume and reduced catalyst mass, the liquid flow rate was lowered to 0.275 mL min^{-1} to maintain the same liquid hourly space velocity (LHSV) of 26.6 h^{-1}. The gas composition was chosen to mimic compressed air, as this was previously used for phenol oxidation. BPA has a lower water solubility than phenol, thus it was not possible to maintain the same initial pollutant concentration of 1 g L^{-1}. Instead, 10 mg L^{-1} concentration of BPA was selected as this was in accordance with concentrations frequently seen in the literature and representative of concentrations encountered in surface water[40,43]. Catalyst K9 was chosen for initial testing as it previously displayed the highest activity towards CWAO of phenol, and the standard operating conditions of 7 bar$_{(g)}$ and 120 ^{o}C were utilized. The resulting BPA conversion as a function of time is displayed in Figure 6.4.
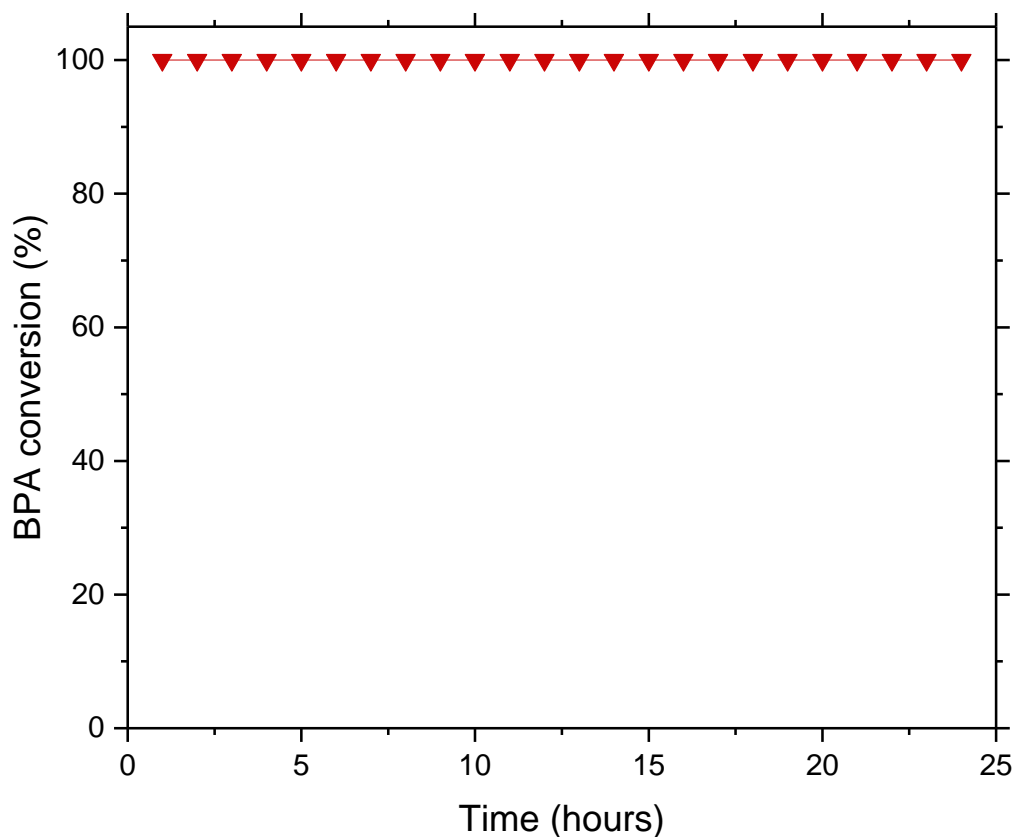
Figure 6.4 BPA conversion as a function of time for K9, at 7 bar$_{(g)}$, 120 °C, liquid flow rate = 0.275 mL min^{-1}, [BPA]$_0$ = 10 mg L^{-1}

The BPA conversion was analysed periodically every hour over a 24 hour period, much longer than any previous testing. K9 achieved complete BPA conversion throughout with no apparent deactivation. Comparatively, K9 achieved a phenol conversion of 94 % under similar reactor conditions, over the course of 5 hours.

Steady state was reached comparatively fast, within the first 60 minutes, whereas, during the CWAO of phenol under consistent operating conditions, induction periods between 100 – 150 minutes were observed, before stable conversion rates were reached.

Sadana *et al.*[50] observed shorter induction periods for the oxidation of phenol when using smaller quantities of catalyst. Similar findings have been reported for other free radical oxidation reactions, in which the induction period is increased with higher catalyst concentrations[51,52]. Varma *et al.*[53] observed an increase in reaction rate up to a critical catalyst concentration, after which no

reaction occurred. If small amounts of H_2O_2 were added however, the reaction would proceed immediately, suggesting there also exits a critical H_2O_2 to catalyst ratio, below which the reaction does not proceed. As discussed in Chapter 4, the decomposition of H_2O_2 leads to the formation of hydroxyl and perhydroxyl radicals, which then propagate the oxidation reaction. This critical catalyst concentration phenomenon was explained by the presence of two distinct adsorption sites on the catalyst surface, inactive adsorption sites which preferentially adsorb H_2O_2 and active adsorption sites which are responsible for the production of radicals[54]. When the concentration of H_2O_2 is low, the majority of it is used to saturate the inactive sites and since these sites do not contribute to radical formation, the reaction proceeds slowly. This explains the long induction periods observed with larger catalyst concentrations, as more H_2O_2 is required to saturate the larger number of inactive sites.

The lowered concentration of pollutant may also be responsible for the lack of induction period observed. As established in Chapter 5, lower initial phenol concentrations lead to increased conversion. When operating at 100 % conversion, only a fraction of active sites may be contributing and so a true conversion profile may not be apparent under these conditions.

To effectively evaluate the catalyst activity and stability, conversions below 100 % are required, thus the operating conditions were further adjusted, starting with the liquid flow rate. K9 was tested for BPA oxidation under the same operating conditions as before, but with steadily increasing flow rates to evaluate whether the catalyst activity was maintained under higher LHSVs. The BPA and TOC conversions are shown in Figure 6.5.
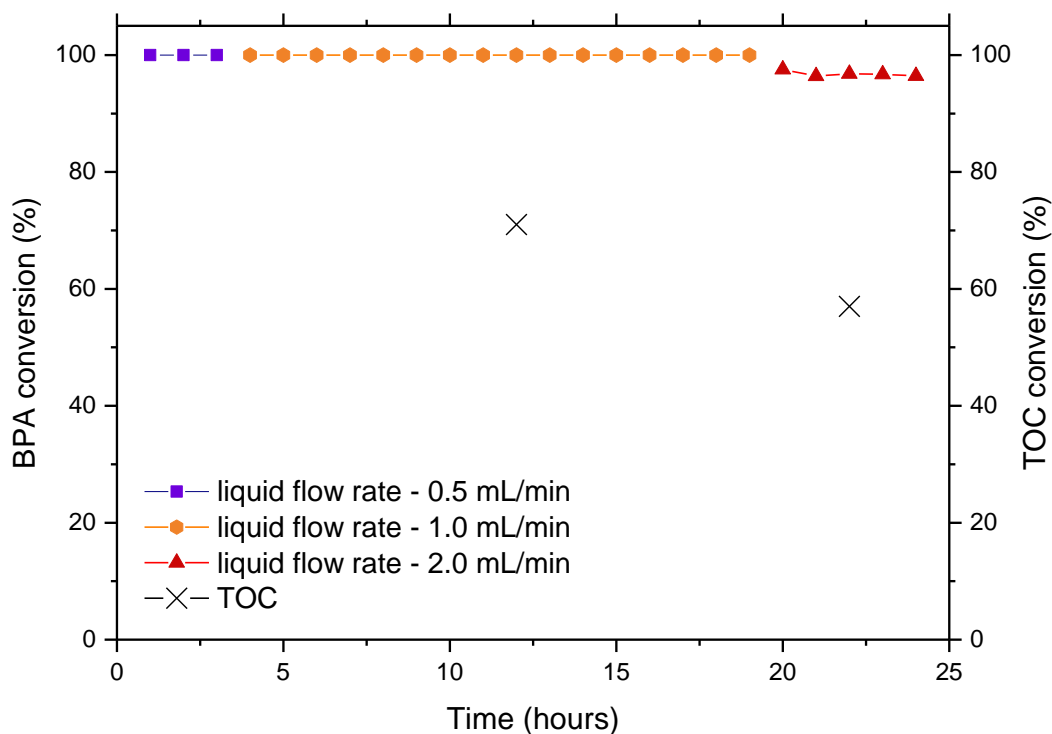
Figure 6.5 BPA conversion as a function of time and TOC conversions as a function of time for K9, at 7 bar$_{(g)}$, 120 ^{o}C, [BPA]$_0$ = 10 mg L^{-1} between liquid flow rates of 0.275 – 2.0 mL min^{-1}

Only when the flow rate is increased to 2 mL min^{-1} (after 20 hours) does the BPA conversion drop below 100 %. At the higher flow rate, a LHSV of 8 times greater than used for CWAO of phenol, K9 achieved 96.7 % BPA conversion. The TOC measurements showed a TOC conversion of 71 % and 57 % at flow rates of 1 mL min^{-1} and 2 mL min^{-1} respectively. The lower removal of TOC compared with BPA conversions indicates some non-BPA organic carbon content remaining in the off-stream, likely arising from the presence of reaction intermediates formed by partial oxidation. Short chain carboxylic acids, primarily formic and acetic acid, have been reported on multiple occasions in the end stream of CWAO experiments for BPA degredation[42,43].

The operating conditions of the reaction were further altered, focusing on temperature, pressure, flow rate and initial BPA concentration until suitable reaction conditions were established for catalyst comparison. The BPA activity plot used to determine appropriate reaction conditions can be found in the appendix.

6.3.2 CWAO of BPA

Once suitable operating conditions had been established, K7 – K10 were tested over 48 hours at 7 bar$_{(g)}$ and 60 ^{o}C, with a liquid flow rate of 1.0 mL min^{-1} and an initial BPA concentration of 60 mg L^{-1}. The BPA conversion as a function of time is displayed in Figure 6.6.
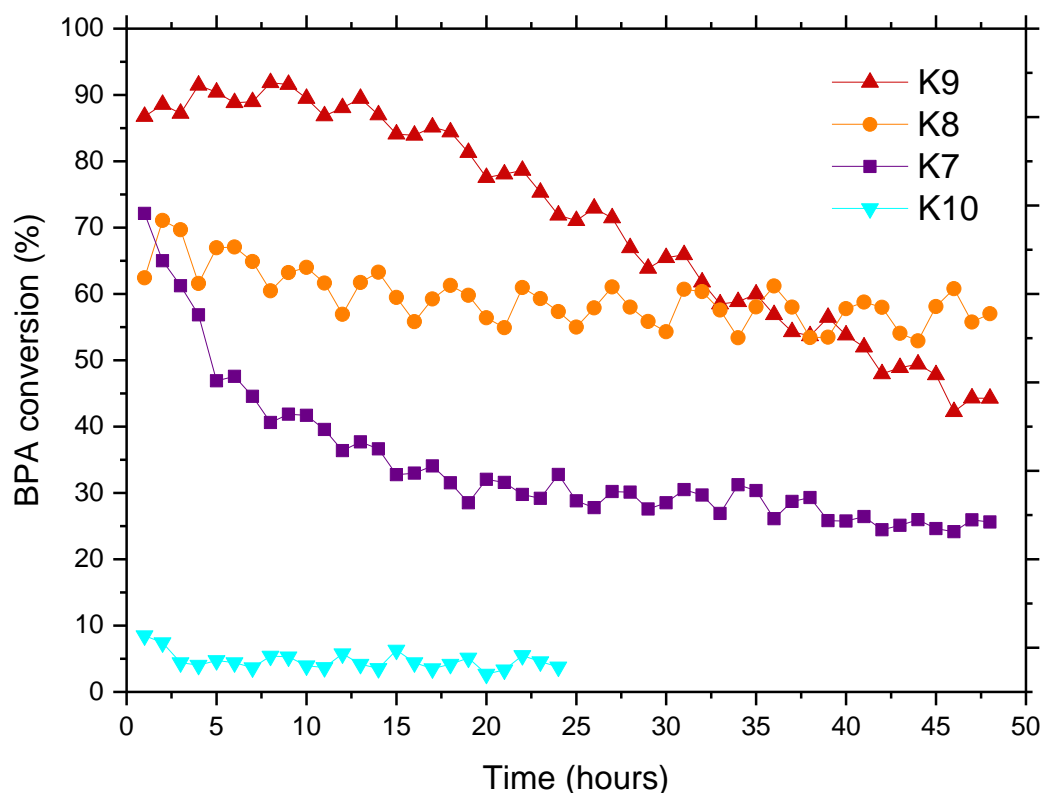
Figure 6.6 BPA conversions as a function of time profiles for K7, K8, K9 and K10, at 7 bar$_{(g)}$ and 60 ^{o}C, liquid flow rate = 1.0 mL min^{-1}, [BPA]$_0$ = 60 mg L^{-1}

During the half of the experiment, the catalysts demonstrated the same trend in activity observed for phenol oxidation, with K9 displaying the highest conversion, followed by K8, K7 and finally K10. After 15 hours however, the activity of K9 begins to decrease steadily with conversion reaching a minimum of 44.3 % after 48 hours. A decrease in activity is also observed for K7, with the majority occurring within the first 10 hours. After 30 hours on stream, the BPA conversion for K7 reaches a steady state with an average conversion of 27.5 %. The lowest activity was observed for K10, which achieved an average BPA conversion of only 4.4 %, as such the catalyst testing was ceased after 24 hours.

The decrease in activity of K9 is characteristic of catalyst deactivation; deactivation can arise from a variety of causes, including but not limited to, poisoning, fouling, thermal degradation and vapour or solid compound formation[55]. Specifically, for CWAO, deactivation caused by coke deposition, metal leaching and poisoning have all been reported[56]. The most common cause of catalyst deactivation reported in the literature for supported metal catalysts during CWAO, is the build-up of carbonaceous deposits on the catalyst surface, limiting accessibility of the pollutants and oxygen to the active sites. Despite the economic and environmental drive for lower operating conditions, low reaction temperatures (120 – 135 ^{o}C) can promote adsorptive interactions on the catalyst surface, leading to higher concentrations of carbon deposits[57]. Leaching of the active metal under the acidic conditions of CWAO can also be a cause of deactivation[58]. As the oxidation reaction proceeds and acidic intermediates, such as carboxylic acids, are formed, the pH of the liquid phase decreases, increasing the possibility of metal ions being leached from the supports; thus, leaching can increase with pollutant degradation[59].

Deactivation was not observed during initial testing, although, it is possible deactivation was not previously seen due to the 100 % conversion achieved or the shorter duration of the tests. When operating at complete conversion, the turn over frequency (TOF) at individual sites is going to be very high and as such, a proportion of the sites may not be active at any given time. Since only a fraction of the sites may be contributing to oxidation, even if deactivation begins immediately, there may be a delay before it impacts the conversion. No deactivation is observed for K9 until after 17 hours on stream, while the catalysts were only previously tested for phenol oxidation for 5 hours, during which deactivation may not have yet begun. The post-reaction catalyst characterisation, will help to determine the specific cause of deactivation.

The deactivation profile for K7, involving a rapid decrease in activity followed by stabilisation at a lower conversion, has been previously observed for noble metal catalysts during CWAO, and is often attributed to leaching of the active metal. Grosjean *et al.*[60] reported rapid leaching of the active metal during

the first 100 minutes, resulting in a decrease in activity, after which conversions stabilised. Leaching was more significant on Pt catalysts, compared with Pd and Ru, when supported on TiO_2 and ZrO_2. The oxidation state of the metal may also be of importance, Pd^{2+} was shown to be more susceptible to leaching during phenol oxidation compared with metallic Pd[61]. Given the presence of PtO_2, and corresponding lack of deactivation observed for the purely metallic Pt catalyst, K8, it is possible the initial deactivation seen for K7 may be the result of metal leaching from PtO_2 species.

The results show K10 remains the least active of the catalysts, with little BPA conversion displayed under these conditions. The CWAO of BPA has been shown to be independent of catalyst specific surface area[42,43], which is in agreement with the results of the study, as the higher specific surface area of K10 ($110\ m^2\,g^{-1}$) did not have significant impact on conversion.

The TOC conversions, along with the pH value of the off stream were measured after 21 and 47 hours for K7 – 9, the results can be seen in Table 6.3. The average pH value of the initial aqueous BPA solution was 6.54.

Table 6.3 TOC conversion (%) and pH values of off stream for CWAO of BPA at 7 bar$_{(g)}$ and 60 ^{o}C, liquid flow rate = 1.0 mL min^{-1}, [BPA]$_0$ = 60 mg L^{-1}, measured after 21 and 47 hours

	t = 21 hours		t = 47 hours	
Catalyst	pH	TOC (%)	pH	TOC (%)
K7	5.39	26	4.92	16
K8	4.98	40	5.54	41
K9	6.04	60	6.58	37

With regards to K7 and K8, the trend for average TOC conversion is in agreement with the trend observed for average BPA conversion. The decrease in TOC conversion for K9 coincides with the catalytic deactivation observed, whilst the TOC conversion for K8 remains consistent. The TOC conversions are lower than the equivalent BPA conversions, suggesting partial oxidation products remained in the off-stream.

The shift to a more acidic pH of the contaminated wastewater is attributed to the oxidation of BPA through acidic intermediates which remain in the water after CWAO as partial oxidation products. The reduction of pH values to the region of 5, as observed for K7 and K8, has been attributed to the formation of formic and acetic acids in the literature[40,41]. Heponiemi *et al.*[42] observed a pH range between 5.4 – 6.6 for wastewater after CWAO treatment of BPA over CeO_2 catalysts, similar to the pH range observed here. As the reaction proceeds, the pH value for K9 reverts towards the initial value observed for the BPA solution. A shift towards a more acidic pH might be expected if partial oxidation is occurring, as seen for K7 and K8, however, if the intermediates are remaining on the surface of the catalyst a lower pH might not be observed. This may also explain the cause of deactivation for K9, due to carbonaceous deposits accumulating on the surface, blocking the active sites.

Of the four catalysts tested K8 exhibits the most potential given its more stable activity whilst maintaining an average conversion of 56.9 %. The fluctuations observed in the data for all the catalysts can be attributed to fluctuating reactor conditions, such as periodic heating and pressurising of the reactor to maintain the desired operating conditions.

6.3.3 Catalyst activity studies as a function of pressure

The effect of pressure was investigated for the CWAO degradation of BPA by K9, shown in Figure 6.7, between $0 - 9$ bar$_{(g)}$ with an initial [BPA] = 60 mg L^{-1} at 80 °C. Given the positive correlation between reaction pressure and phenol oxidation a similar trend is expected for BPA oxidation. The TOC conversion was measured after 20 hours on stream.
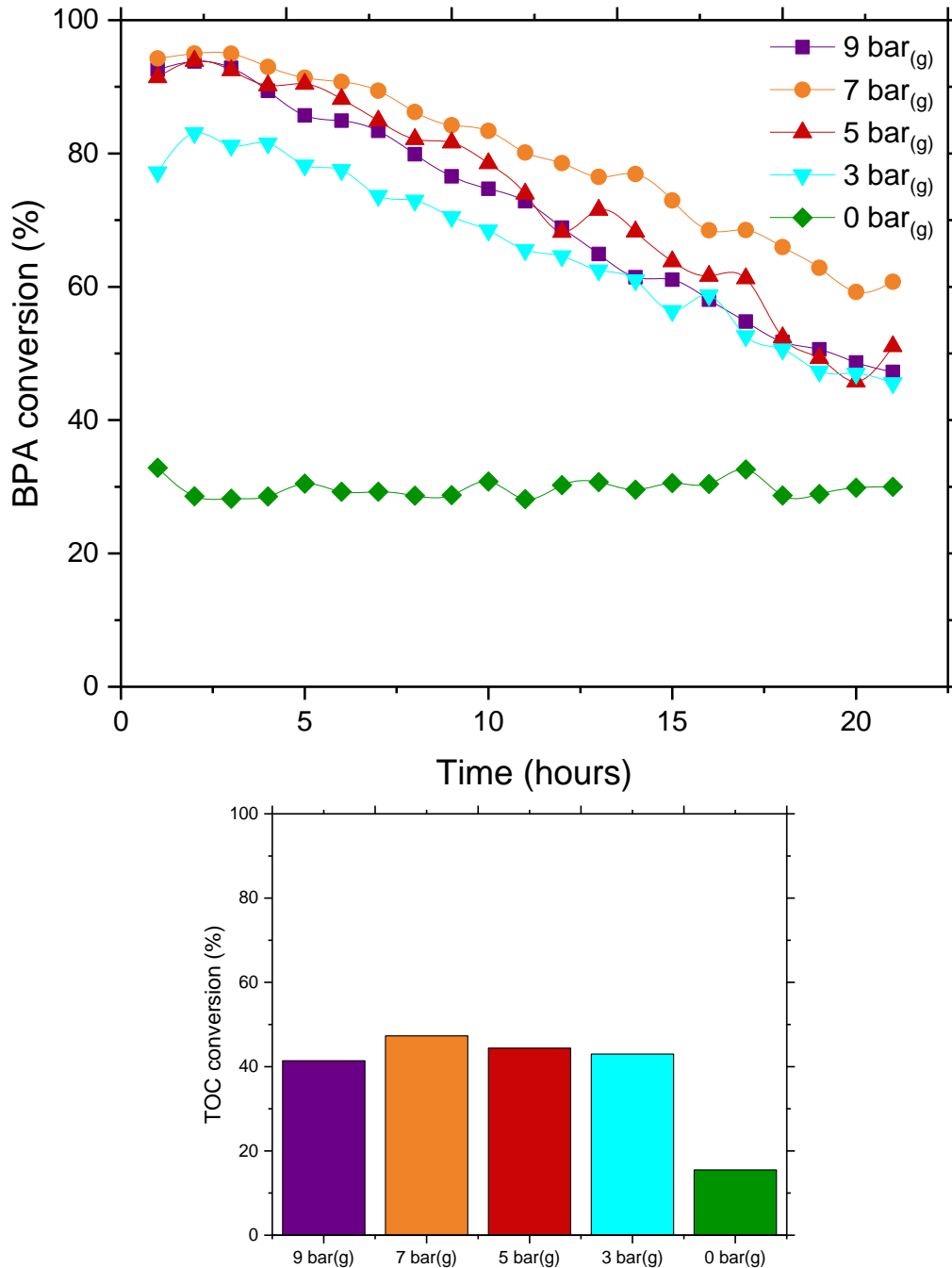
Figure 6.7 BPA conversion as a function of time for K9 between 0 - 9 bar$_{(g)}$, 80 °C, liquid flow rate = 1.0 mL min^{-1}, [BPA]$_0$ = 60 mg L$^-$1 and TOC conversion measured at t = 20 hours

It can be observed that the change in reaction pressures between 3 – 9 bar$_{(g)}$ did not have a pronounced effect on BPA removal. The catalyst underwent deactivation for all experiments within this pressure range, making it difficult to discern any trend in activity.

The TOC conversions at 3 – 9 bar$_{(g)}$ are within 41.4 – 47.3 %; the small TOC range indicates similar intermediates may remain after each reaction. The pH

range of the TOC samples was 5.7 – 6.32, with the increase in acidity attributed to the presence of short chain carboxylic acids.

When K9 was tested at atmospheric pressure (0 bar$_{(g)}$) no significant decrease in BPA conversion was observed. Despite the lower conversion of ≈25 % (±3 %), the lack of deactivation is an improvement and suggests that the cause of deactivation seen here may not be prevalent at atmospheric pressure. Dijkgraaf *et al.*[62] studied the deactivation of a Pt/C catalyst during the oxidation of aqueous D-gluconate and observed decreased deactivation at lower oxygen partial pressures (pO_2). The deactivation was attributed to coverage of the platinum surface with oxygen, followed by penetration of oxygen atoms into the metallic platinum lattice. Lowering the pressure, and therefore the pO_2, decreased the fraction of surface platinum covered by O_2, which resulted in decreased deactivation. The over oxidation of active platinum surfaces was also reported by Masende *et al.*[63] during the CWAO of phenol. At higher oxygen pressure, lower phenol conversion and selectivity towards CO_2 was observed, attributed to the over oxidation of Pt species. This method of deactivation was temporary and could be reversed under reducing conditions, however, the over oxidation of the Pt surface favoured the formation of ρ-benzoquinone, resulting in the formation of polymeric products and permeant deactivation of the catalyst *via* surface poisoning. The presence of chemisorbed unreactive oxygen species and subsequent over oxidation of metal surface has been attributed to deactivation of platinum catalysts during oxidation reactions on numerous occasions[64-69].

The concentration of oxygen in the aqueous phase was found to be a significant factor concerning deactivation of Pt catalysts by strong chemisorption of oxygen, and subsequent penetration of the Pt lattice, forming PtO_x species[70]. The availability of dissolved oxygen at the catalyst surface is necessary for the oxidation reaction to occur. Henry's law states that the concentration of dissolved oxygen in the liquid phase is proportional to the partial pressure of oxygen in the gas phase. As such, higher pressures typically lead to higher conversion and mineralisation of organic compounds. Moreover, the concentration of free radicals increases with increased oxygen pressure, which also enhances the

degradation of organic pollutants[71]. Increasing the pressure, however, leads to a more oxidative environment which may result in over oxidation of the active metal species[72]. For K9 at atmospheric pressure and 80 °C, the fraction of platinum sites covered by oxygen species may be low enough that deactivation is no longer prevalent by this mechanism.

Disregarding the potential for deactivation, typically, when increasing the pressure, the concentration of dissolved oxygen in the liquid phase increases, which increases the oxygen available to the catalyst surface and thus, increases the reaction rate. This hypothesis however, does not consider the availability of a secondary pathway where oxygen transfers directly from the gaseous phase onto the catalyst surface[73]. A hydrophobic catalyst could facilitate this oxygen transfer through reduced wettability of the catalyst surface, creating a solid – gas interface. If this secondary pathway is available, the increase in oxygen partial pressure is less crucial to the reaction, provided the total concentration of oxygen is sufficient for the reaction to proceed. The concentration of oxygen required is not the same as the concentration of dissolved oxygen required.

Using Equation 2.5 (Tromans *et al.*[74]), the average BPA conversion was plotted as a function of dissolved oxygen concentration, shown in Figure 6.8.
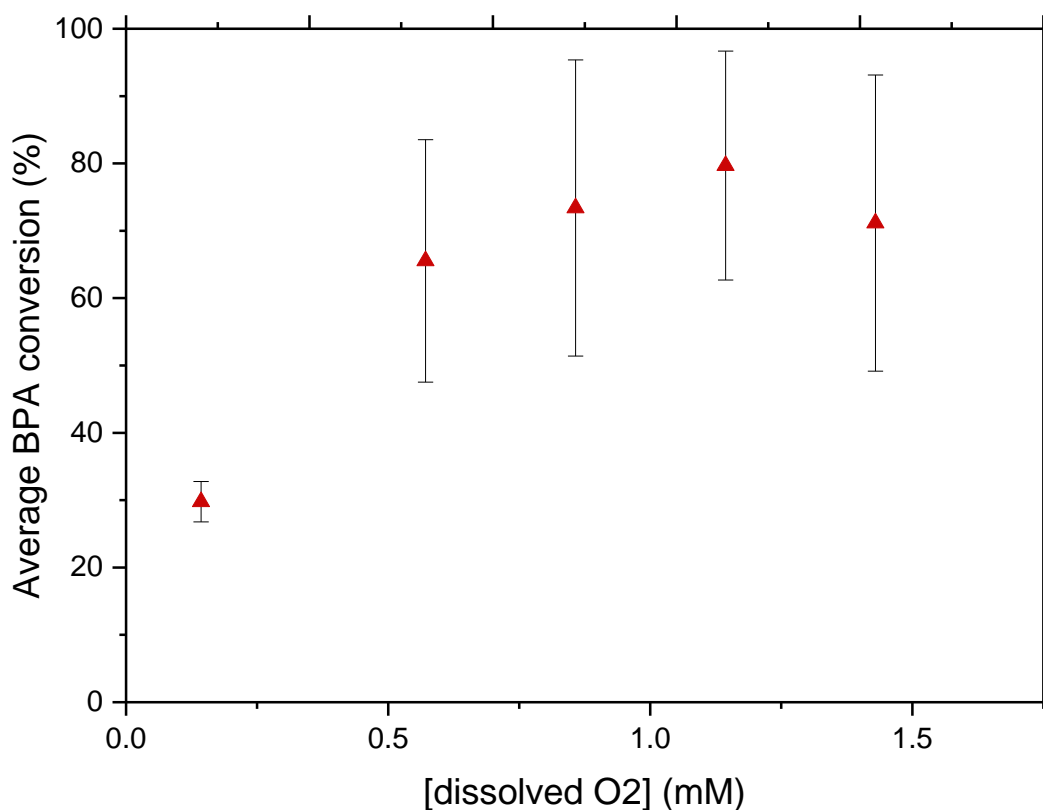
Figure 6.8 BPA conversion as a function of dissolved oxygen concentration for K9 at 60°C, liquid flow rate = 1.0 mL min^{-1}, [BPA]0 = 60 mg L^{-1}

For the CWAO of phenol, K9 exhibited an almost linear trend between pollutant conversion and concentration of dissolved oxygen concentration, however, due the prevalence of catalyst deactivation during reaction, the same cannot be conclusively said for BPA oxidation.

At atmospheric pressure the concentration of dissolved oxygen is 0.143 mM, yet K9 still achieves an average BPA conversion of 29.7 %. At dissolved oxygen concentrations as low as these, negligible conversion would be expected if the reaction was entirely reliant on oxygen dissolution. Under these conditions, a hydrophilic catalyst, with a completely wetted surface, would be expected to show very minimal activity due to the total reliance on dissolved oxygen. The observed activity of K9 at 0 bar$_{(g)}$ is suggestive of the presence of a gas bubbles within the catalyst pores allowing for a secondary gaseous oxygen transfer route.

6.3.4 Prolonged catalyst testing

To provide a better insight into the deactivation observed for K9, CWAO of BPA was carried out over an extended time period of 7 days (172 hours), at 7 bar$_{(g)}$ and 60 °C, the results of which can be seen in Figure 6.9.
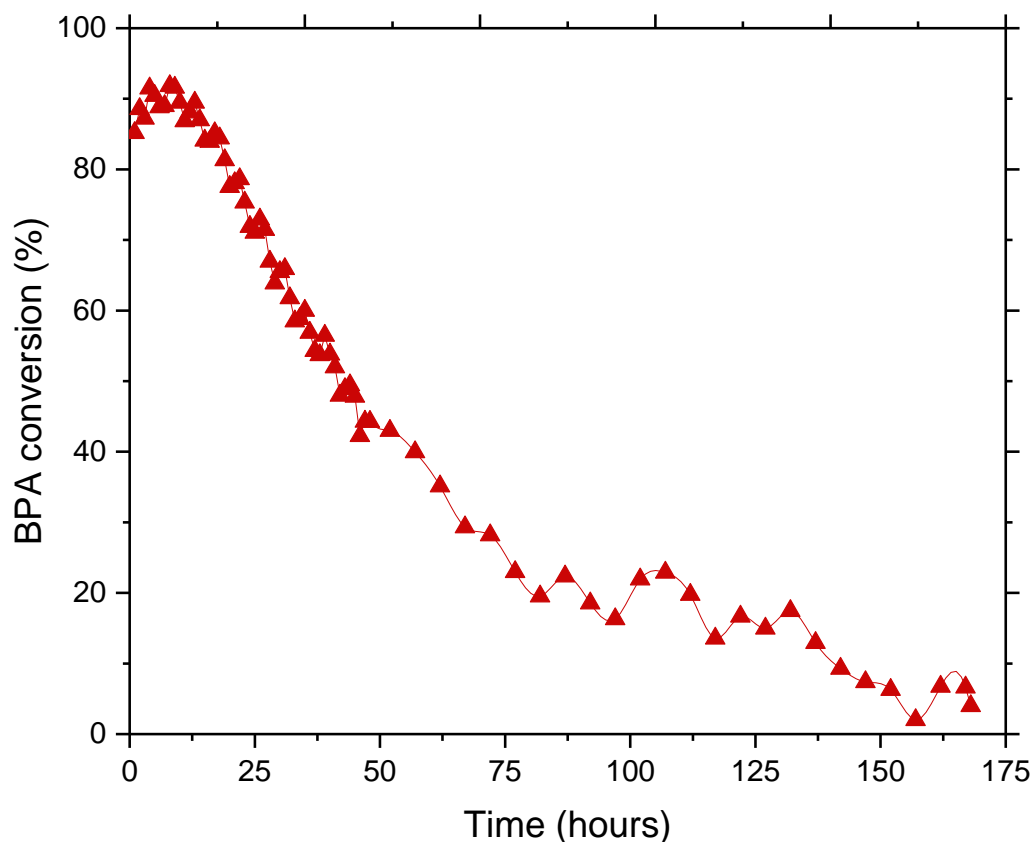
Figure 6.9 BPA conversion profile for K9 at 7 bar$_{(g)}$ and 60 °C over 172 hours

Complete deactivation of K9 can be observed after 172 hours, with a maximum conversion of 92.1 % falling to <3 %. This data is conclusive that K9 cannot be regarded as an efficient long-term catalyst for CWAO of BPA.

For the CWAO of phenol, the catalyst activity studies were only conducted for a maximum of 5 hours, in which time no deactivation occurred. The greater catalyst mass may have also decreased the rate of deactivation. To determine whether deactivation would also occur for phenol oxidation under similar conditions, the prolonged activity test was repeated using phenol as the model pollutant. It was not possible to monitor the concentration of phenol throughout, and thus, the TOC content was measured to provide an indication of the extent of

phenol oxidation. The comparative TOC conversions for BPA and phenol over K9 can be seen in Figure 6.10.
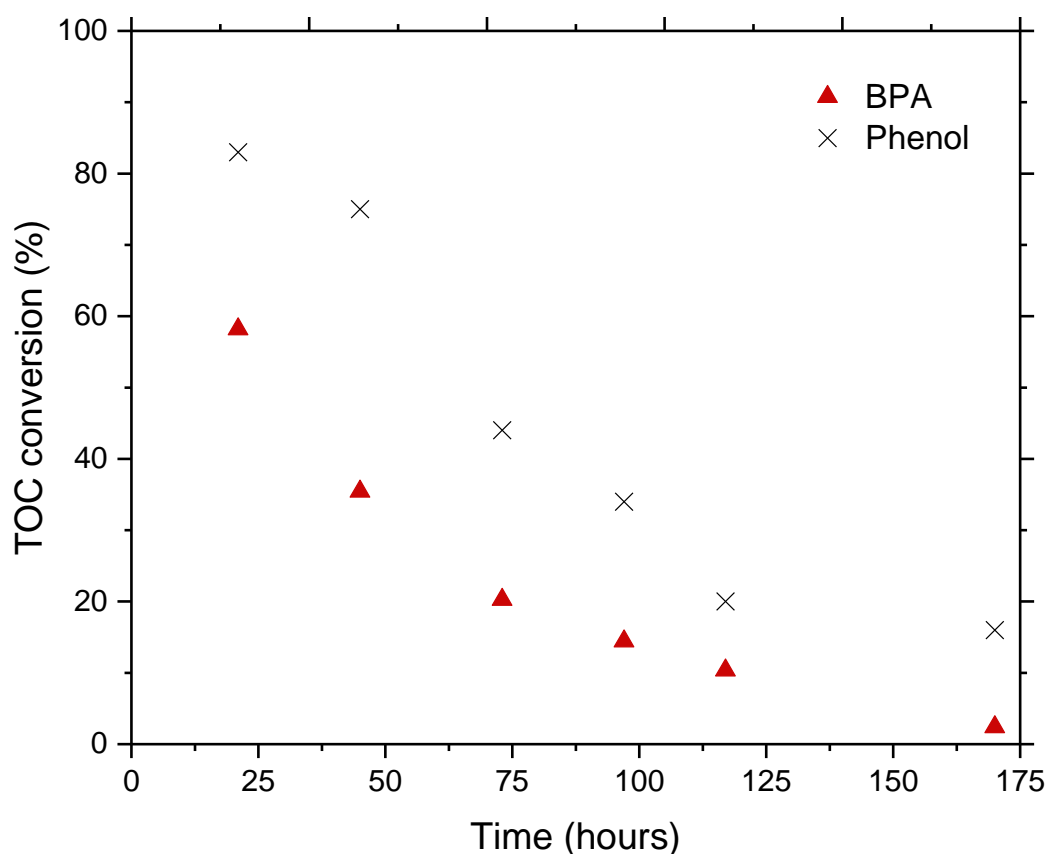
Figure 6.10 TOC conversions as a function of time for CWAO of BPA and phenol by K9 at 7 bar$_{(g)}$, 60 °C, liquid flow rate = 1.0 mL min^{-1} and [BPA]$_0$ = 60 mg L^{-1} over 172 hours.

The TOC conversions for CWAO of phenol are higher compared with BPA, but both follow a similar deactivation profile. This suggests K9 shows a higher selectivity towards CO_2 for phenol oxidation, however the catalyst still undergoes deactivation. Given the similar profile, the same mechanism(s) of deactivation is likely responsible. Post-reaction characterisation of K9 should help determine the specific cause or causes of the deactivation observed.

The deactivation was not previously observed for phenol oxidation when reaction times were below 5 hours; however, when the reaction length was increased, the TOC conversion decreased in the same trend as for TOC conversions during BPA oxidation. Thus, concluding that deactivation also occurs for CWAO of phenol under these conditions.

6.4 Post-reaction catalyst characterisation

A variety of catalyst characterisation techniques were employed to investigate any structural or compositional changes the catalyst may have undergone during the oxidation reaction. Post-reaction catalyst characterisation was also used to provide insight into the mechanism of catalyst deactivation.

6.4.1 Catalyst deactivation

XRD, TGA, and EDX analysis were all used to help identify the cause of catalytic deactivation observed for K9 during the CWAO of BPA.

6.4.1.1 Energy dispersive x-ray (EDX) analysis of K9

Energy dispersive x-ray (EDX) spectroscopy was utilized to accurately measure the platinum loading of the catalysts. Due to the high concentration of platinum on the external surface of the catalyst pellets, the catalysts were ground into powder to a more accurate value of metal loading. The average platinum weight percentage of K9, evaluated after 48 hours and 172 hours on stream at 7 $bar_{(g)}$ and 60 °C, is displayed in Table 6.4.

Table 6.4 Average EDX weight percentage of platinum of K9 - fresh, 48 hours and 172 hours on stream at 7 $bar_{0)}$, 60 °C, liquid flow rate = 1.0 mL min^{-1} and $[BPA]_0$ = 60 mg L^{-1}

Catalyst	Average weight % of platinum
K9 – fresh	1.74
K9 – 48 hours on stream	1.71
K9 – 172 hours on stream	1.43

A decrease in the platinum loading of K9 can been seen after CWAO experiments, with a 0.31 wt% decrease between the fresh catalyst and after 172 hours testing. Given the similar values between the catalyst after 48 hours on

stream and the fresh catalyst, coupled with the 2 – 5 % error associated with the EDX analysis, it is possible leaching did not occur during this period. Leaching of the active metal has been reported for CWAO, with the formation of certain reaction intermediates leading to increasingly acidic conditions being cited as the primary cause. Besson *et al.*[75] observed rapid leaching of Ru and Pt from supported catalysts when oxidation reaction proceeded *via* methylamines. Kouraichi *et al.*[59] reported deactivation of MnO_x-CeO_x mixed metal oxide catalysts during the CWAO of phenol; the formation of carbonaceous deposits and leaching of manganese were confirmed as the deactivation mechanisms responsible. The poor stability of MnO under acidic reaction conditions made manganese susceptible to leaching.

The CWAO of BPA proceeded through acidic intermediates, mostly likely carboxylic acids, which is confirmed by the decrease in pH of the liquid phase. The generation of catechol and oxalic acid as intermediates have been linked to active metal leaching during CWAO[76]. A decrease in surface concentration of Pd was observed for Pd-Fe/TiO_2 catalysts when treated with catechol and oxalic acid, with oxalic acid responsible for a larger extent of Pd leaching than catechol[77]. An increase in oxalic acid production was observed for Pt/SiC during the CWAO of phenol (Chapter 4). If BPA oxidation over K9 proceeds *via* phenol, through the same intermediates, an increase in oxalic acid concentration as the reaction progresses may be responsible for Pt leaching observed after 172 hours.

6.4.1.2 Powder x-ray diffraction (XRD) of K9

Analysis of the used catalyst *via* XRD can help provide evidence of any additional phases that may have accumulated during reaction, or whether the active metal underwent any oxidation. The XRD pattern for K9 after 172 hours testing and fresh catalyst (0 hours testing) are displayed in Figure 6.11.

Metallic platinum (Pt) ----------
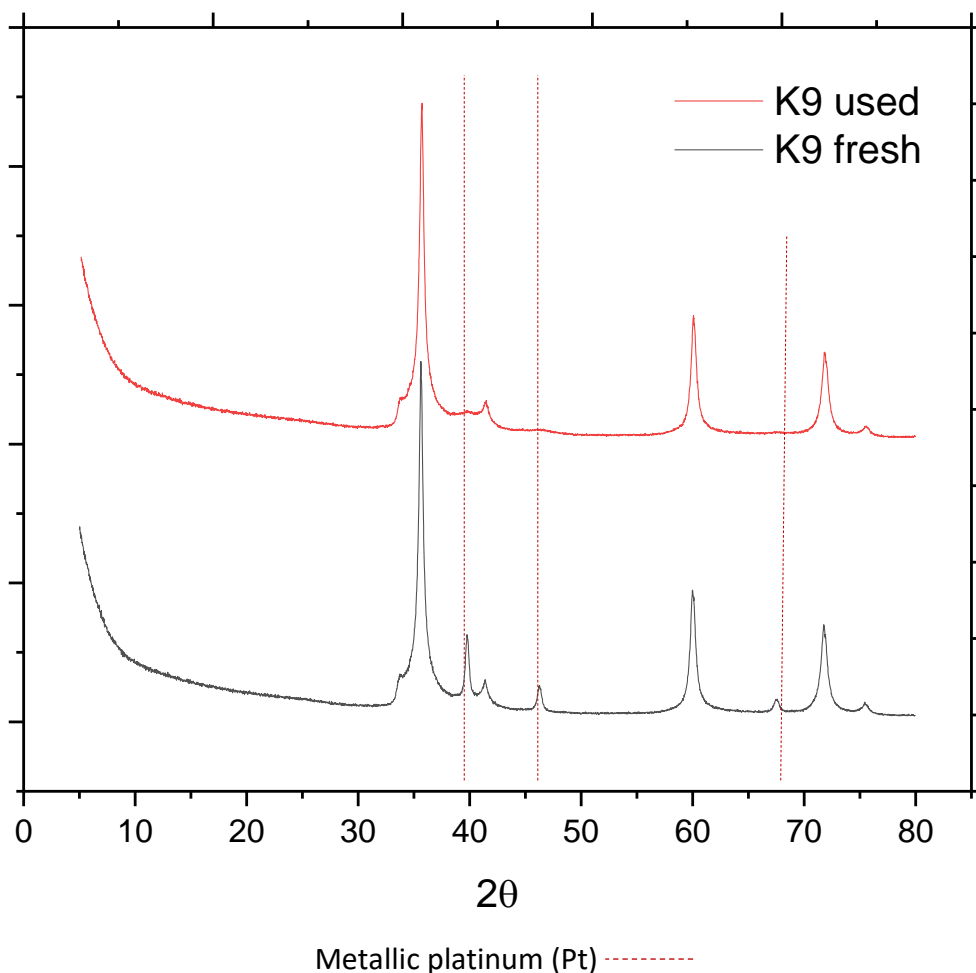
Figure 6.11 Powder XRD pattern for K9 (fresh catalyst) and K9 post-CWAO reaction with BPA (172 hours on stream)

A significant decrease in the intensity of the peaks occurring at 40°, 46° and 67.5°, which are characteristic of metallic platinum, can be seen for the used catalyst in comparison with fresh K9. The EDX analysis revealed some leaching of the active meal occurred, however, over 80 % of the Pt was retained for K9 after 172 hours.

Tauster *et al.*[78] reported similar findings for Pt/TiO_2 catalysts, where the XRD pattern for Pt/TiO_2 was pattern indistinguishable from TiO_2 pattern, with no intensity observed in the regions where principal diffraction peaks for Pt were expected. The lack of diffraction peaks characteristic of Pt was attributed to strong metal support interactions (SMSI) between the noble metal and titanium species, such interactions have been previously reported for Pt/TiO_2 systems[47]. SMSI effects were associated with bond formation between Pt and Ti cations, it was

proposed that the metal – metal bonding resulted from overlapping of the occupied d orbitals of the noble metal with the vacant d orbitals of Ti^{4+} [79]. The formation of a support 'over layer', such as TiO_x, which spreads over the surface of the noble metal has also been reported for similar Pt/TiO_2 systems[80,81]. If the interaction between the Pt and support changes, due to SMSI, the shape of Pt particles may also change. Stronger interactions may cause the Pt particles to flatten, which will then affect the peak size and width of the corresponding peaks in the diffraction pattern.

A reduction in the intensity of diffraction peaks in XRD, often accompanied by an increase in peak width, could also be an indication that the Pt particles are reducing in size or becoming less crystalline[82]. As the metal is being leached, the corresponding metal particles will shrink in size, resulting in less material available for diffraction.

6.4.1.3 Thermogravimetric analysis (TGA) of K9

Thermogravimetric analysis (TGA) was used to quantify the amount of any adsorbed species on the catalyst surface which may be responsible for the deactivation observed during CWAO. The TGA profiles of K9 taken after 48 hours and 172 hours testing at 7 $bar_{(g)}$ and 60 °C can be seen in Figure 6.12.

Figure 6.12 TGA profiles of K9 post-reaction at 7 bar$_{(g)}$, 60 °C, liquid flow rate = 1.0 mL min^{-1} and [BPA]$_0$ = 60 mg L^{-1} for 48 and 172 hours on stream

The TGA profiles after BPA oxidation are comparable with those after phenol oxidation with the mass loss for K9 occurring over a temperature range between 200 – 550 °C. The mass loss increased from 5.5 % to 10 % during complete catalyst deactivation after 172 hours, indicating an increase in concentration of carbonaceous deposits present on the catalyst. The first derivative of the TGA profiles for K9 after 48 and 172 hours are shown in Figure 6.13 and 6.14 respectively.

Figure 6.13 TGA profile and 1st derivative mass loss (dTG) of K9 post-reaction at 7 bar(g), 60 °C, liquid flow rate = 1.0 mL min-1 and [BPA]0 = 60 mg L-1 after 48 hours on stream

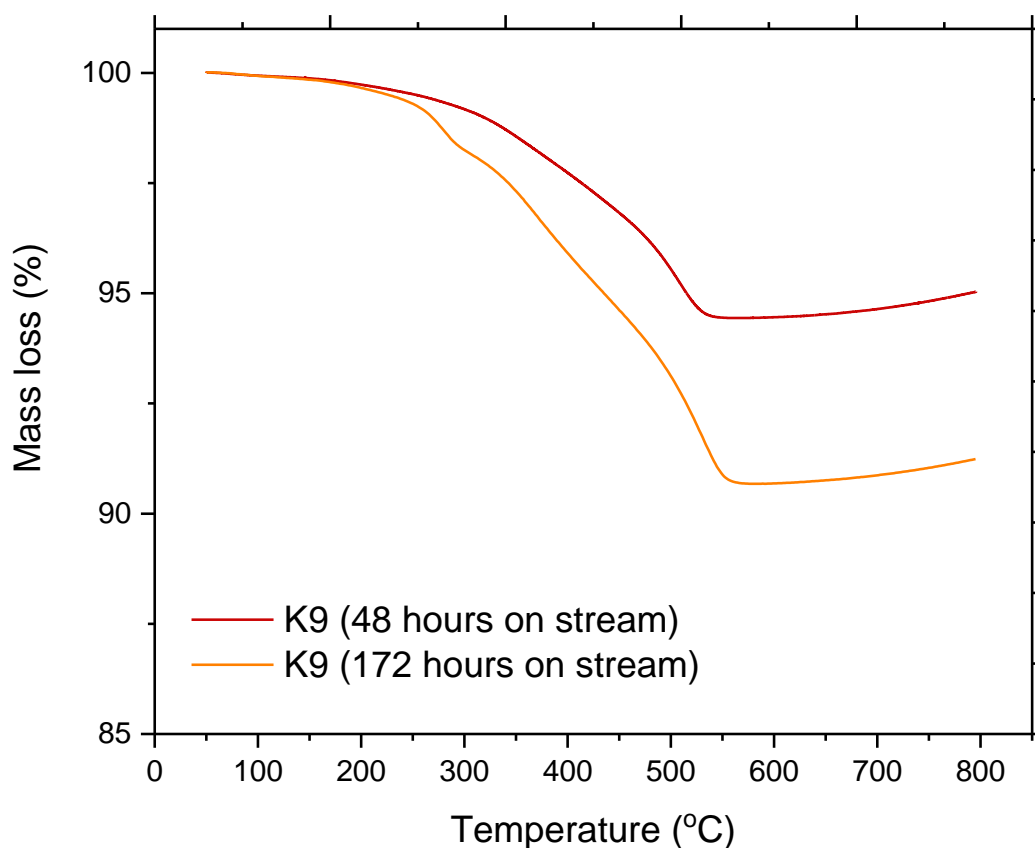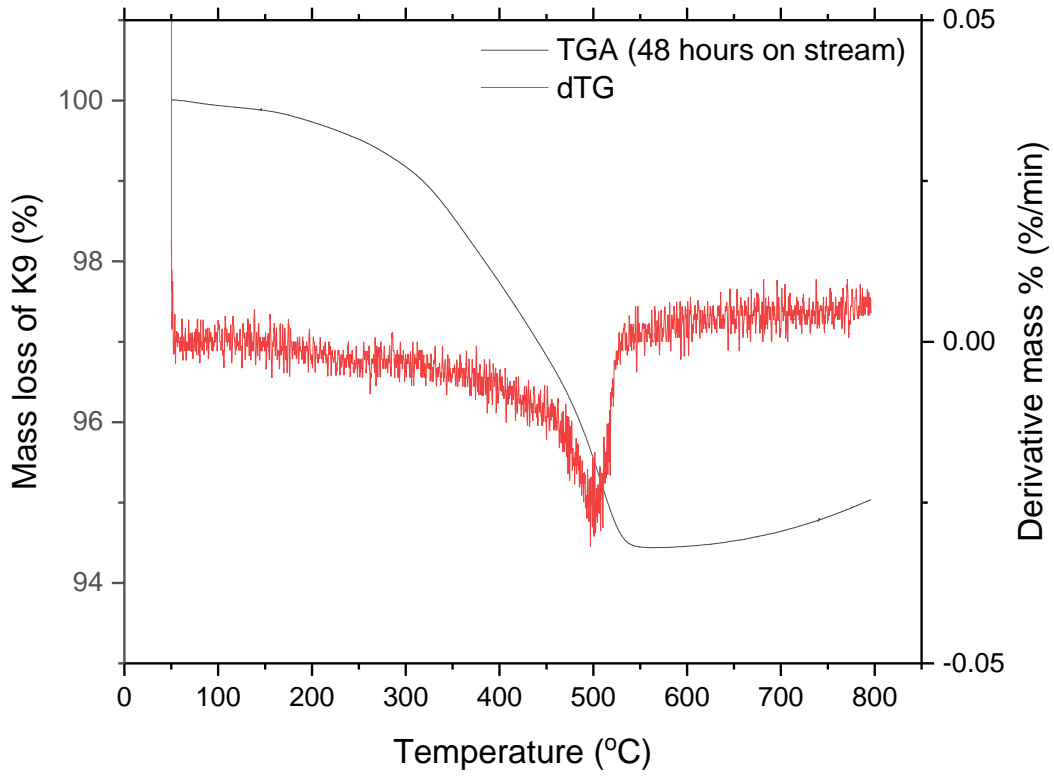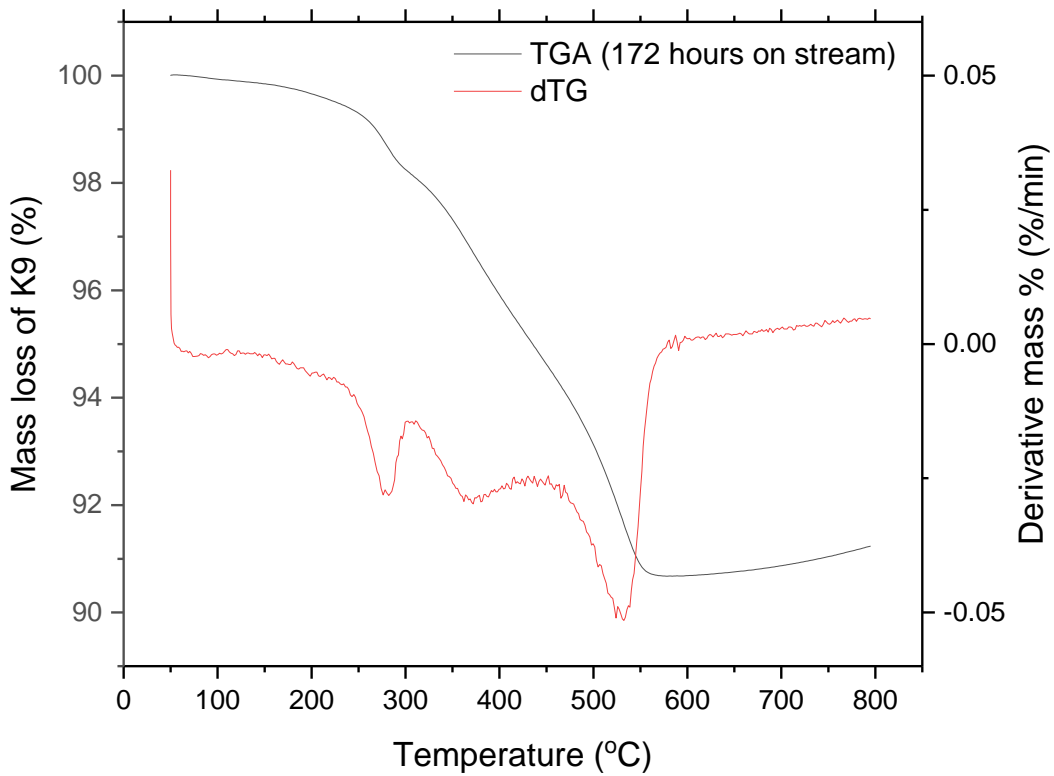*Figure 6.14 TGA profile and 1st derivative mass loss (dTG) of K9 post-reaction at 7 bar(g), 60 °C, liquid flow rate = 1.0 mL min-1 and [BPA]0 = 60 mg L-1 after 172 hours on stream*

The dTG profile after 48 hours testing shows a distinct mass loss peak centred around 500 °C, whereas the dTG profile after 172 hours shows further mass loss peaks around 280 and 360 °C. The mass loss occurring above 500 °C, observed for both catalyst samples is likely due to the decomposition of carbonyl and phenolic groups[83]. The mass loss observed between 250 – 400 °C can be attributed to the release of CO_2 from the decomposition of various carboxylic acid groups on the catalyst surface[84,85]. Leaching of Pt was observed between 48 – 172 hours and so it is possible the carboxylic acid groups adsorbed onto the surface may also be responsible for the metal leaching.

As carbonaceous deposits adsorb onto the catalyst surface, the active sites become concealed, limiting the access of pollutants onto the catalyst, thus decreasing catalyst activity. This increase in concentration of carbon deposits over time is likely a contributing factor for the deactivation observed.

Deactivation by this mechanism has been frequently reported in the literature. Pintar *et al.*[86] observed deactivation of Ru/TiO_2 catalysts during the CWAO of phenol, which was attributed to the strong adsorption of partially oxidised intermediates on the catalyst surface. The adsorption of C-6 intermediates, responsible for the deactivation, was not observed when reaction temperatures exceeded 190 °C, suggesting that the desorption of these particular phenol oxidation intermediates was a temperature activated process.

Keav *et al.*[87] reported the deactivation of Ru and Pt/CeO_2 catalysts for phenol oxidation *via* the accumulation of adsorbed carbon species on the catalyst surface. Interestingly, a trend between the oxygen storage capacity of the catalyst and the formation of adsorbed heavy species was observed; catalysts with higher oxygen storage capacity promoted the formation of the carbonaceous deposits responsible for deactivation. A higher concentration of oxygen was seen for K9 compared with K7 and K8, due to the oxidation of TiC within the support to TiO_2 during calcination. The presence of TiO_2, thought to promote oxidation, may also be responsible for an increased accumulation of carbonaceous deposits.

Although less severe reaction conditions offer economic and environmental advantages, low temperatures have been shown to promote stronger adsorptive interactions on catalyst surfaces, which accordingly facilitates the accumulation of carbonaceous deposits[88]. The deactivation of K9 *via* deposition of carbonaceous deposits could be promoted by the lower operating temperatures (60 – 80 °C) used in this study, however, deactivation was not observed for all the catalysts tested. Masende *et al.*[89] observed deactivation *via* fouling to be more severe for Pt catalysts with higher metal dispersion. It was thought that the catalysts with higher metal dispersions had active sites located deeper within the pores of the support. The formation of carbon species, blocking the access of the reactants to the pores, was more likely to cause significant deactivation in catalysts with a higher portion of active sites located deeper within the pores. A higher Pt dispersion was observed for K9, compared with K7 and K8, and could be responsible for the increased deactivation observed.

6.4.1.4 Catalyst deactivation conclusion

The post-reaction characterisation of K9 shows evidence of metal leaching and accumulation of carbonaceous deposits on the catalyst surface during CWAO of BPA. Both deactivation mechanisms have been previously observed for CWAO reactions and are likely contributing to the overall catalytic deactivation of K9.

The absence of deactivation observed at atmospheric pressure (Figure 6.7) also suggested deactivation at higher pressures may have occurred due to over oxidation and PtO_x formation. For PGMs, the oxidation state of metal surface can affect the potential of the metal being leached during reaction[90]. If over oxidation resulted in Pt^{2+} species on the surface of the metal particles, which are more susceptible to leaching compared with Pt^0, this may have resulted in leaching of the metal and decrease in Pt wt % observed for K9 post-reaction. Further analysis of the spent catalysts, by techniques such as XPS and MP-AES, would be necessary to confirm this.

Catalytic deactivation can have far reaching effects, other than simply decreased activity. Moreover, leaching of the active metal can result in toxic metal ions within the wastewater, which then require additional treatment to recover. Extensive research has gone into the modification of catalysts to avoid or reduce deactivation brought about by metal leaching or accumulation of carbonaceous deposits.

The influence of promoters such as lead and bismuth can decrease the vulnerability of noble metals to poisoning, whilst improving reaction rates and selectivity[91]. Furthermore, Besson *et al.*[92] suggested promoters can also protect noble metals against over oxidation

Hussain *et al.*[93] reduced the formation of heavy polymers on Mn-Ce-O catalysts during the CWAO of phenol *via* doping with potassium. Potassium formed K_2O, which subsequently formed O_2^- and contributed to the production of more peroxide, allowing for oxidation to occur more rapidly with high efficiency, reducing the formation of carbonaceous deposits[94].

6.4.2 Thermogravimetric analysis (TGA)

Thermogravimetric analysis (TGA) was used to evaluate the remaining catalysts (K7, K8 and K10) for the presence of any adsorbed species on the catalyst surface. The TGA profiles shown in Figure 6.13, were taken after 48 hours testing, with the exception of K10 which was taken after 24 hours testing, at 7 bar$_{(g)}$ and 60 °C.
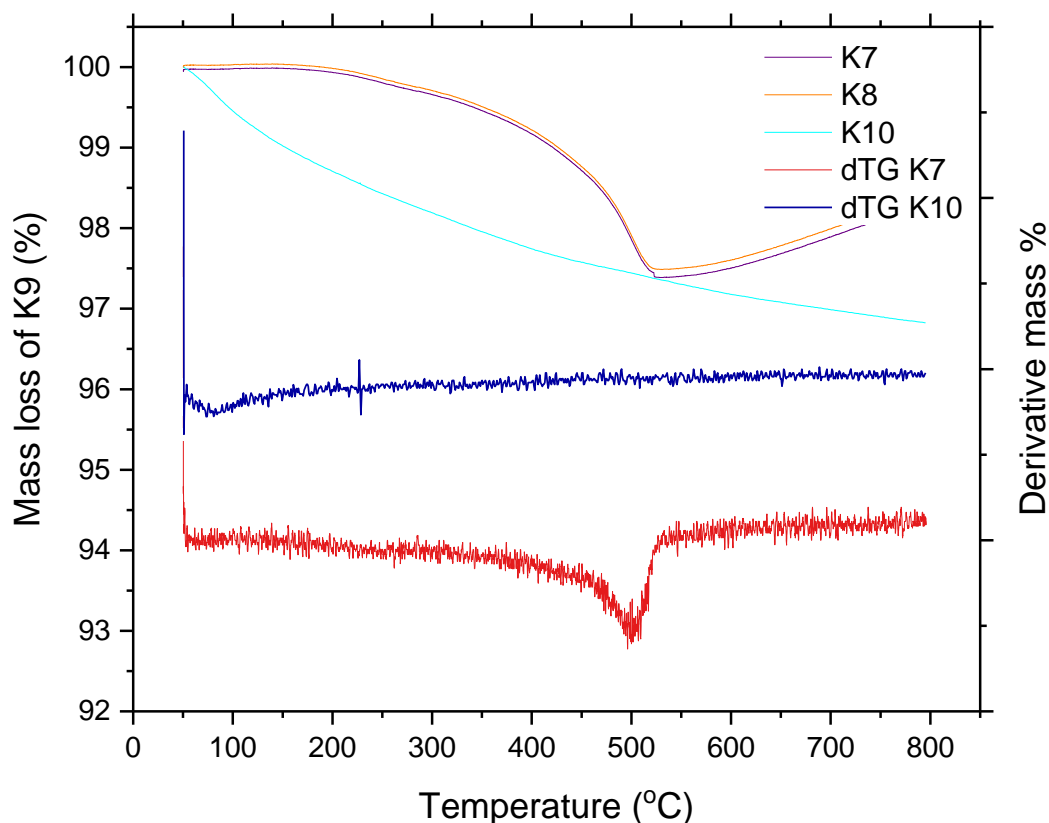
Figure 6.13 TGA profiles of K7, K8 and K10 post-reaction at 7 bar(g), 60 °C, t = 48 hours (K7 and K8) and 24 hours (K10), including and dTG of K7 and K10

K7 and K8 showed similar mass loss profiles with ≈2.5 % mass loss centred around 500 °C, which can be attributed to carbonyl and phenolic species adsorbed onto the catalyst surface during CWAO. In post-reaction analysis of K9 after 48 and 172 hours on stream, a similar mass loss is observed over the same temperature range, indicating the adsorbed species are likely similar in nature.

The dTG profile for K10 shows mass loss occurring below 100 °C, which is characteristic of water evaporating from the catalyst surface. The TGA profile for the fresh K10 catalyst (Figure 5.5) shows a similar mass loss curve, indicating no significant carbon deposition occurred on K10 during CWAO.

6.4.3 Energy dispersive x-ray (EDX) spectroscopy

Energy dispersive x-ray (EDX) spectroscopy was utilized to measure the active metal loading of K7, K8 and K10. As with K9, the catalysts were ground into

powder to provide a more accurate value of metal loading. Table 6.5 displays the average active metal weight percentage of K7 and K8, evaluated after 48 hours, and K10 after 24 hours on stream, at 7 bar$_{(g)}$ and 60 ^{o}C.

Table 6.5 Average EDX weight percentages of platinum for K7 and K8, and ruthenium for K10 after 24 and 48 hours on stream at 7 bar$_{0)}$, 60 ^{o}C, liquid flow rate = 1.0 mL min^{-1} and [BPA]$_0$ = 60 mg L^{-1}

	Average weight % of active metal	
	Fresh catalyst	**Catalyst after 48 hours testing**
K7	1.86	1.47
K8	1.60	1.63
K10	2.11	1.81 (24 hours testing)

Decreases in the platinum and ruthenium loading can be seen for K7 and K10 respectively. K7 showed a 0.39 wt % decrease, similar to the percentage of Pt lost for K9 after 172 hours on stream, suggesting that Pt leaching occurred at a faster rate for K7 than K9. A 0.3 wt % reduction in Ru was observed for K10 after only 24 hours on stream.

The BPA conversion for K7 (Figure 6.6) showed a rapid decrease in activity within the first 10 hours, before establishing a stable conversion. The conversion profile was similar to those observed in the literature and suggested the deactivation was the result of active metal leaching. The EDX analysis further supports this hypothesis, with a 0.39 wt % loss of Pt loading observed post-reaction. The pre-reaction characterisation established the presence of PtO$_2$ for K7, whereas exclusively metallic Pt was observed for K8. Other than a marginal increase in specific surface area of 6 m^2 g^{-1}, the presence of platinum oxide is the primary difference between the two catalysts. K8 however, showed no significant deactivation during CWAO, despite similar accumulation of carbon species observed in the post-reaction TGA. Therefore, the leaching of Pt for K7 is likely responsible for deactivation observed, and in agreement with the literature, suggests ionic platinum may be more susceptible to leaching under these conditions than metallic platinum.

A minor increase in the average Pt wt % was observed for K8 post-reaction, however, the associated error with EDX spectroscopy should be considered. The EDX values were also taken as an average over multiple sample points and thus, the difference in Pt wt % is likely the result of averaging, since it is not possible for an increase in platinum loading to occur during CWAO.

6.5 Conclusion

The CWAO of BPA was investigated for platinum based SiC catalysts and a hydrophilic Ru/ceria/alumina catalyst. Under similar operational parameters as previously used for the CWAO of phenol, K9 achieved complete BPA degradation over a 24 hour period. When the severity of the reaction conditions was increased to temperatures <80 °C, K9 began to exhibit deactivation, with a complete loss of activity observed after 172 hours. From the post-reaction catalyst characterisation, the mechanism of deactivation was shown to be a combination of platinum leaching and accumulation of carbonaceous deposits blocking the active sites on the catalyst surface.

K10, the comparatively more hydrophilic catalyst, displayed the lowest activity towards BPA oxidation, with less than 5 % BPA conversion achieved over 24 hours. Post-reaction characterisation of both K10 and K7 also showed leaching of active metal ions. The deactivation observed for K7 occurred during the initial 10 hours, before reaching a stable conversion and was attributed to the leaching of Pt from PtO_x species on the catalyst.

K8 showed consistent activity for BPA oxidation over 48 hours and was the only catalyst not to undergo deactivation caused by leaching of the active metal. An average BPA conversion of 57 % was observed for K8 at temperatures of 60 °C, considerably lower than any temperature observed in the literature, making K8 a very promising catalyst for CWAO reactions.

6.6 References

(1)   Furhacker, M.; Scharf, S.; Weber, H. Bisphenol A: emissions from point sources. *Chemosphere* **2000,** *41* (5), 751.

(2)   Yamamoto, T.; Yasuhara, A.; Shiraishi, H.; Nakasugi, O. Bisphenol A in hazardous waste landfill leachates. *Chemosphere* **2001,** *42* (4), 415.

(3)   Staples, C. A.; Dorn, P. B.; Klecka, G. M.; O'Block, S. T.; Harris, L. R. A review of the environmental fate, effects, and exposures of bisphenol A. *Chemosphere* **1998,** *36* (10), 2149.

(4)   Lindholst, C.; Pedersen, K. L.; Pedersen, S. N. Estrogenic response of bisphenol A in rainbow trout (Oncorhynchus mykiss). *Aquatic Toxicology* **2000,** *48* (2-3), 87.

(5)   Schug, T. T.; Janesick, A.; Blumberg, B.; Heindel, J. J. Endocrine disrupting chemicals and disease susceptibility. *Journal of Steroid Biochemistry and Molecular Biology* **2011,** *127* (3-5), 204.

(6)   Wetherill, Y. B.; Akingbemi, B. T.; Kanno, J.; McLachlan, J. A.; Nadal, A.; Sonnenscheing, C.; Watson, C. S.; Zoeller, R. T.; Belcher, S. M. In vitro molecular mechanisms of bisphenol A action. *Reproductive Toxicology* **2007,** *24* (2), 178.

(7)   Yoshida, T.; Horie, M.; Hoshino, Y.; Nakazawa, H. Determination of bisphenol A in canned vegetables and fruit by high performance liquid chromatography. *Food Additives and Contaminants Part a-Chemistry Analysis Control Exposure & Risk Assessment* **2001,** *18* (1), 69.

(8)   Sharpe, R. M.; Drake, A. J. Bisphenol A and Metabolic Syndrome. *Endocrinology* **2010,** *151* (6), 2404.

(9)   Rubin, B. S. Bisphenol A: An endocrine disruptor with widespread exposure and multiple effects. *Journal of Steroid Biochemistry and Molecular Biology* **2011,** *127* (1-2), 27.

(10)   Michalowicz, J. Bisphenol A - Sources, toxicity and biotransformation. *Environmental Toxicology and Pharmacology* **2014,** *37* (2), 738.

(11)   Liao, C. Y.; Kannan, K. Widespread Occurrence of Bisphenol A in Paper and Paper Products: Implications for Human Exposure. *Environmental Science & Technology* **2011,** *45* (21), 9372.

(12)   Rosenfeldt, E. J.; Linden, K. G. Degradation of endocrine disrupting chemicals bisphenol A, ethinyl estradiol, and estradiol during UV photolysis and advanced oxidation processes. *Environmental Science & Technology* **2004,** *38* (20), 5476.

(13)   Frye, C. A.; Bo, E.; Calamandrei, G.; Calza, L.; Dessi-Fulgheri, F.; Fernandez, M.; Fusani, L.; Kah, O.; Kajta, M.; Le Page, Y.; Endocrine Disrupters: A Review of Some Sources, Effects, and Mechanisms of Actions on Behaviour and Neuroendocrine Systems. *Journal of Neuroendocrinology* **2012,** *24* (1), 144.

(14)   Chen, D.; Kannan, K.; Tan, H. L.; Zheng, Z. G.; Feng, Y. L.; Wu, Y.; Widelka, M. Bisphenol Analogues Other Than BPA: Environmental Occurrence, Human Exposure, and Toxicity-A Review. *Environmental Science & Technology* **2016,** *50* (11), 5438.

(15)   Huang, Y. Q.; Wong, C. K. C.; Zheng, J. S.; Bouwman, H.; Barra, R.; Wahlstrom, B.; Neretin, L.; Wong, M. H. Bisphenol A (BPA) in China: A review of sources, environmental levels, and potential human health impacts. *Environment International* **2012,** *42*, 91.

(16)   Mercea, P. Physicochemical Processes Involved in Migration of Bisphenol A from Polycarbonate. *Journal of Applied Polymer Science* **2009,** *112* (2), 579.

(17)   Lin, K.; Liu, W.; Gan, J. Oxidative Removal of Bisphenol A by Manganese Dioxide: Efficacy, Products, and Pathways. *Environmental Science & Technology* **2009,** *43* (10), 3860.

(18)   Mishra, M.; Feidler, A. Ullmann's encyclopedia of industrial chemistry, fifth edition. *Journal of the American Chemical Society* **1998,** *120* (24), 6197.

(19)   Han, Q.; Wang, H. J.; Dong, W. Y.; Liu, T. Z.; Yin, Y. L.; Fan, H. K. Degradation of bisphenol A by ferrate(VI) oxidation: Kinetics, products and toxicity assessment. *Chemical Engineering Journal* **2015,** *262*, 34.

(20)   Jiao, Z. J.; Chen, L. G.; Zhou, G. L.; Gong, H. F.; Zhang, X. M.; Liu, Y. Q.; Gao, X. Degradation of Bisphenol A by CeCu Oxide Catalyst in Catalytic Wet Peroxide Oxidation: Efficiency, Stability, and Mechanism. *International Journal of Environmental Research and Public Health* **2019,** *16* (23).

(21)   Chen, W. J.; Zou, C. J.; Liu, Y.; Li, X. K. The experimental investigation of bisphenol A degradation by Fenton process with different types of cyclodextrins. *Journal of Industrial and Engineering Chemistry* **2017,** *56*, 428.

(22)   Serra-Perez, E.; Alvarez-Torrellas, S.; Agueda, V. I.; Delgado, J. A.; Ovejero, G.; Garcia, J. Insights into the removal of Bisphenol A by catalytic wet air oxidation upon carbon nanospheres-based catalysts: Key operating parameters, degradation intermediates and reaction pathway. *Applied Surface Science* **2019,** *473*, 726.

(23)   Bistan, M.; Tisler, T.; Pintar, A. Catalytic and Photocatalytic Oxidation of Aqueous Bisphenol A Solutions: Removal, Toxicity, and Estrogenicity. *Industrial & Engineering Chemistry Research* **2012,** *51* (26), 8826.

(24)   Luo, Y. L.; Guo, W. S.; Ngo, H. H.; Nghiem, L. D.; Hai, F. I.; Zhang, J.; Liang, S.; Wang, X. C. C. A review on the occurrence of micropollutants in the aquatic environment and their fate and removal during wastewater treatment. *Science of the Total Environment* **2014,** *473*, 619.

(25)   Liu, Z. H.; Kanjo, Y.; Mizutani, S. Removal mechanisms for endocrine disrupting compounds (EDCs) in wastewater treatment - physical means, biodegradation, and chemical advanced oxidation: A review. *Science of the Total Environment* **2009,** *407* (2), 731.

(26)   Esplugas, S.; Bila, D. M.; Krause, L. G. T.; Dezotti, M. Ozonation and advanced oxidation technologies to remove endocrine disrupting chemicals (EDCs) and pharmaceuticals and personal care products (PPCPs) in water effluents. *Journal of Hazardous Materials* **2007,** *149* (3), 631.

(27)   Clara, M.; Kreuzinger, N.; Strenn, B.; Gans, O.; Kroiss, H. The solids retention time - a suitable design parameter to evaluate the capacity of wastewater treatment plants to remove micropollutants. *Water Research* **2005,** *39* (1), 97.

(28)   Xu, J.; Wang, L.; Zhu, Y. F. Decontamination of Bisphenol A from Aqueous Solution by Graphene Adsorption. *Langmuir* **2012,** *28* (22), 8418.

(29)   Liu, G. F.; Ma, J.; Li, X. C.; Qin, Q. D. Adsorption of bisphenol A from aqueous solution onto activated carbons with different modification treatments. *Journal of Hazardous Materials* **2009,** *164* (2-3), 1275.

(30)   Toledo, I. B.; Ferro-Garcia, M. A.; Rivera-Utrilla, J.; Moreno-Castilla, C.; Fernandez, F. J. V. Bisphenol A removal from water by activated carbon. Effects of carbon characteristics and solution chemistry. *Environmental Science & Technology* **2005,** *39* (16), 6246.

(31)   Asada, T.; Oikawa, K.; Kawata, K.; Ishihara, S.; Iyobe, T.; Yamada, A. Study of removal effect of bisphenol A and beta-estradiol by porous carbon. *Journal of Health Science* **2004,** *50* (6), 588.

(32)   Yu, J. G.; Zhao, X. H.; Yang, H.; Chen, X. H.; Yang, Q.; Yu, L. Y.; Jiang, J. H.; Chen, X. Q. Aqueous adsorption and removal of organic contaminants by carbon nanotubes. *Science of the Total Environment* **2014,** *482*, 241.

(33)   Jin, Z. X.; Wang, X. X.; Sun, Y. B.; Ai, Y. J.; Wang, X. K. Adsorption of 4-n-Nonylphenol and Bisphenol-A on Magnetic Reduced Graphene Oxides: A.Combined Experimental and Theoretical Studies. *Environmental Science & Technology* **2015,** *49* (15), 9168.

(34)   Husain, Q.; Qayyum, S. Biological and enzymatic treatment of bisphenol A and other endocrine disrupting compounds: a review. *Critical Reviews in Biotechnology* **2013,** *33* (3), 260.

(35)   Zhang, Y.; Causserand, C.; Aimar, P.; Cravedi, J. P. Removal of bisphenol A by a nanofiltration membrane in view of drinking water production. *Water Research* **2006,** *40* (20), 3793.

(36)   Sharma, J.; Mishra, I. M.; Dionysiou, D. D.; Kumar, V. Oxidative removal of Bisphenol A by UV-C/peroxymonosulfate (PMS): Kinetics, influence of co-existing chemicals and degradation pathway. *Chemical Engineering Journal* **2015,** *276*, 193.

(37)   Torres, R. A.; Sarantakos, G.; Combet, E.; Petrier, C.; Pulgarin, C. Sequential helio-photo-Fenton and sonication processes for the treatment of bisphenol A. *Journal of Photochemistry and Photobiology a-Chemistry* **2008,** *199* (2-3), 197.

(38)   Irmak, S.; Erbatur, O.; Akgerman, A. Degradation of 17 beta-estradiol and bisphenol A in aqueous medium by using ozone and ozone/UV techniques. *Journal of Hazardous Materials* **2005,** *126* (1-3), 54.

(39)   Ahmed, S.; Rasul, M. G.; Brown, R.; Hashib, M. A. Influence of parameters on the heterogeneous photocatalytic degradation of pesticides and phenolic contaminants in wastewater: A short review. *Journal of Environmental Management* **2011,** *92* (3), 311.

(40)   Mezohegyi, G.; Erjavec, B.; Kaplan, R.; Pintar, A. Removal of Bisphenol A and its Oxidation Products from Aqueous Solutions by Sequential

Catalytic Wet Air Oxidation and Biodegradation. *Industrial & Engineering Chemistry Research* **2013,** *52* (26), 9301.

(41)   Heponiemi, A.; Azalim, S.; Hu, T.; Vielma, T.; Lassi, U. Efficient removal of bisphenol A from wastewaters: Catalytic wet air oxidation with Pt catalysts supported on Ce and Ce-Ti mixed oxides. *Aims Materials Science* **2019,** *6* (1), 25.

(42)   Heponiemi, A.; Azalim, S.; Hu, T.; Lassi, U. Cerium Oxide Based Catalysts for Wet Air Oxidation of Bisphenol A. *Topics in Catalysis* **2015,** *58* (14-17), 1043.

(43)   Erjavec, B.; Kaplan, R.; Djinovic, P.; Pintar, A. Catalytic wet air oxidation of bisphenol A model solution in a trickle-bed reactor over titanate nanotube-based catalysts. *Applied Catalysis B-Environmental* **2013,** *132*, 342.

(44)   Erjavec, B.; Tisler, T.; Kaplan, R.; Pintar, A. Titanate Nanotubes As a Novel Catalyst for Removal of Toxicity and Estrogenicity of Bisphenol A in the CWAO Process. *Industrial & Engineering Chemistry Research* **2013,** *52* (35), 12559.

(45)   Mena, I. F.; Diaz, E.; Rodriguez, J. J.; Mohedano, A. F. CWPO of bisphenol A with iron catalysts supported on microporous carbons from grape seeds activation. *Chemical Engineering Journal* **2017,** *318*, 153.

(46)   Davies, D.; Catalytic Wet Air Oxidation: Developing a Continuous Process: Cardiff University PhD Thesis, **2016**

(47)   Sexton, B. A.; Hughes, A. E.; Foger, K. XPS investigation of strong metal support interactions on group III-V oxides. *Journal of Catalysis* **1982,** *77* (1), 85.

(48)   Ji, Y. Q.; Zan, Q. F.; Wang, X. G.; Zhu, Y. Y.; Zhou, A. G.; Lin, X. P. High temperature oxidation resistance of Ti_3SiC_2 in air and low oxygen atmosphere. *International Journal of Applied Ceramic Technology* **2017,** *14* (5), 851.

(49)   Barsoum, M. W.; ElRaghy, T.; Ogbuji, L. Oxidation of Ti_3SiC_2 in air. *Journal of the Electrochemical Society* **1997,** *144* (7), 2508.

(50)   Sadana, A.; Katzer, J. R. Catalytic-oxidation of phenol in aqueous-solution over copper oxide. *Industrial & Engineering Chemistry Fundamentals* **1974,** *13* (2), 127.

(51)   Neuburg, H. J.; Basset, J. M.; Graydon, W. F. Heterogeneous liquid-base oxidation of cyclohexene with manganese-dioxide as catalyst. *Journal of Catalysis* **1972,** *25* (3), 425.

(52)   Vreugdenhil, A. D. Mechanism of the silver-on-silica catalyzed oxidation of cumene in the liquid phase. *Journal of Catalysis* **1973,** *28* (3), 493

(53)   Varma, G. R.; Graydon, W. F. Heterogeneous catalytic-oxidation of cumene (isopropyl benzene) in liquid-phase. *Journal of Catalysis* **1973,** *28* (2), 236.

(54)   Mukherjee, A.; Graydon, W. F. Heterogeneous catalytic oxidation of Tetralin. *The Journal of Physical Chemistry* **1967,** *71* (13), 4232.

(55)   Bartholomew, C. H. Mechanisms of catalyst deactivation. *Applied Catalysis a-General* **2001,** *212* (1-2), 17.

(56) Kim, K.-H.; Ihm, S.-K. Heterogeneous catalytic wet air oxidation of refractory organic pollutants in industrial wastewaters: A review. *Journal of Hazardous Materials* **2011,** *186* (1), 16.

(57) Masende, Z. P. G.; Kuster, B. F. M.; Ptasinski, K. J.; Janssen, F.; Katima, J. H. Y.; Schouten, J. C. Platinum catalysed wet oxidation of phenol in a stirred slurry reactor - The role of oxygen and phenol loads on reaction pathways. *Catalysis Today* **2003,** *79* (1-4), 357.

(58) Arena, F.; Giovenco, R.; Torre, T.; Venuto, A.; Parmaliana, A. Activity and resistance to leaching of Cu-based catalysts in the wet oxidation of phenol. *Applied Catalysis B-Environmental* **2003,** *45* (1), 51.

(59) Kouraichi, R.; Delgado, J. J.; Lopez-Castro, J. D.; Stitou, M.; Rodriguez-Izquierdo, J. M.; Cauqui, M. A. Deactivation of Pt/MnO_x-CeO_2 catalysts for the catalytic wet oxidation of phenol: Formation of carbonaceous deposits and leaching of manganese. *Catalysis Today* **2010,** *154* (3-4), 195.

(60) Grosjean, N.; Descorme, C.; Besson, M. Catalytic wet air oxidation of N,N-dimethylformamide aqueous solutions: Deactivation of TiO_2 and ZrO_2-supported noble metal catalysts. *Applied Catalysis B-Environmental* **2010,** *97* (1-2), 276.

(61) Underhill, R.; The *in-situ* generation of H_2O_2 from H_2 and O_2 for use in oxidation reactions. Cardiff University PhD Thesis, **2017**

(62) Dijkgraaf, P. J. M.; Rijk, M. J. M.; Meuldijk, J.; Vanderwiele, K. Deactivation of platinum catalysts by oxygen .1. Kinetics of the catalyst deactivation. *Journal of Catalysis* **1988,** *112* (2), 329.

(63) Masende, Z. P. G.; Kuster, B. F. M.; Ptasinski, K. J.; Janssen, F.; Katima, J. H. Y.; Schouten, J. C. Platinum catalysed wet oxidation of phenol in a stirred slurry reactor - A practical operation window. *Applied Catalysis B-Environmental* **2003,** *41* (3), 247.

(64) Sarkany, J.; Gonzalez, R. D. Support and dispersion effects on silica-supported and alumina-supported platinum catalysts .2. Effect on the CO-O_2 reaction. *Applied Catalysis* **1983,** *5* (1), 85.

(65) Cant, N. W. Metal crystallite size effects and low-temperature deactivation in carbon-monoxide oxidation over platinum. *Journal of Catalysis* **1980,** *62* (1), 173.

(66) Ostermaier, J. J.; Katzer, J. R.; Manogue, W. H. Platinum catalyst deactivation in low-temperature ammonia oxidation reactions .1. Oxidation of ammonia by molecular-oxygen. *Journal of Catalysis* **1976,** *41* (2), 277.

(67) Dirkx, J. M. H.; Vanderbaan, H. S. The oxidation of glucose with platinum on carbon as catalyst. *Journal of Catalysis* **1981,** *67* (1), 1.

(68) Dirkx, J. M. H.; Vanderbaan, H. S. The oxidation of gluconic acid with platinum on carbon as catalyst. *Journal of Catalysis* **1981,** *67* (1), 14.

(69) Minh, D. P.; Gallezot, P.; Besson, M. Treatment of olive oil mill wastewater by catalytic wet air oxidation 3. Stability of supported ruthenium catalysts during oxidation of model pollutant p-hydroxybenzoic acid in batch and continuous reactors. *Applied Catalysis B-Environmental* **2007,** *75* (1-2), 71.

(70)   Dijkgraaf, P. J. M.; Duisters, H. A. M.; Kuster, B. F. M.; Vanderwiele, K. Deactivation of platinum catalysts by oxygen .2. Nature of the catalyst deactivation. *Journal of Catalysis* **1988,** *112* (2), 337.

(71)   Lin, S. S. Y.; Chang, D. J.; Wang, C. H.; Chen, C. C. Catalytic wet air oxidation of phenol by CeO_2 catalyst - effect of reaction conditions. *Water Research* **2003,** *37* (4), 793.

(72)   Sushma; Kumari, M.; Saroha, A. K. Performance of various catalysts on treatment of refractory pollutants in industrial wastewater by catalytic wet air oxidation: A review. *Journal of Environmental Management* **2018,** *228*, 169.

(73)   Lavelle, K.; McMonagle, J. B. Mass transfer effects in the oxidation of aqueous organic compounds over a hydrophobic solid catalyst. *Chemical Engineering Science* **2001,** *56* (17), 5091.

(74)   Tromans, D. Temperature and pressure dependent solubility of oxygen in water: a thermodynamic analysis. *Hydrometallurgy* **1998,** *48* (3), 327.

(75)   Besson, M.; Descorme, C.; Bernardi, M.; Gallezot, P.; di Gregorio, F.; Grosjean, N.; Minh, D. P.; Pintar, A. Supported noble metal catalysts in the catalytic wet air oxidation of industrial wastewaters and sewage sludges. *Environmental Technology* **2010,** *31* (13), 1441.

(76)   Perathoner, S.; Centi, G. Wet hydrogen peroxide catalytic oxidation (WHPCO) of organic waste in agro-food and industrial streams. *Topics in Catalysis* **2005,** *33* (1-4), 207.

(77)   Underhill, R.; Lewis, R. J.; Freakley, S. J.; Douthwaite, M.; Miedziak, P. J.; Akdim, O.; Edwards, J. K.; Hutchings, G. J. Oxidative Degradation of Phenol using in situ Generated Hydrogen Peroxide Combined with Fenton's Process Supported palladium-iron catalysts for the removal of model contaminants from wastewater. *Johnson Matthey Technology Review* **2018,** *62* (4), 417.

(78)   Tauster, S. J.; Fung, S. C.; Garten, R. L. Strong metal-support interactions - group-8 noble-metals supported on TiO_2. *Journal of the American Chemical Society* **1978,** *100* (1), 170.

(79)   Dickson, J. G.; Katz, L.; Ward, R. Compounds with hexagonal barium titanate structure. *Journal of the American Chemical Society* **1961,** *83* (14), 3026.

(80)   Tauster, S. J.; Fung, S. C. strong metal-support interactions - occurrence among binary oxides of groups IIA-VB. *Journal of Catalysis* **1978,** *55* (1), 29.

(81)   Subramanian, S.; Temperature programmed reduction of platinum group metals catalysts. *Johnson Matthey Technology Review*, **1992**; Vol. 36 (2).

(82)   Holder, C. F.; Schaak, R. E. Tutorial on Powder X-ray Diffraction for Characterizing Nanoscale Materials. *Acs Nano* **2019,** *13* (7), 7359.

(83)   Alvarez, P. M.; Beltran, F. J.; Gomez-Serrano, V.; Jaramillo, J.; Rodriguez, E. M. Comparison between thermal and ozone regenerations of spent activated carbon exhausted with phenol. *Water Research* **2004,** *38* (8), 2155.

(84)   Santiago, M.; Stuber, F.; Fortuny, A.; Fabregat, A.; Font, J. Modified activated carbons for catalytic wet air oxidation of phenol. *Carbon* **2005,** *43* (10), 2134.

(85)   Cardenas-Aguiar, E.; Gasco, G.; Paz-Ferreiro, J.; Mendez, A. Thermogravimetric analysis and carbon stability of chars produced from slow pyrolysis and hydrothermal carbonization of manure waste. *Journal of Analytical and Applied Pyrolysis* **2019,** *140*, 434.

(86)   Pintar, A.; Batista, J.; Tisler, T. Catalytic wet-air oxidation of aqueous solutions of formic acid, acetic acid and phenol in a continuous-flow trickle-bed reactor over Ru/TiO$_2$ catalysts. *Applied Catalysis B-Environmental* **2008,** *84* (1-2), 30.

(87)   Keav, S.; de los Monteros, A. E.; Barbier, J.; Duprez, D. Wet Air Oxidation of phenol over Pt and Ru catalysts supported on cerium-based oxides: Resistance to fouling and kinetic modelling. *Applied Catalysis B-Environmental* **2014,** *150*, 402.

(88)   Kim, K. H.; Ihm, S. K. Heterogeneous catalytic wet air oxidation of refractory organic pollutants in industrial wastewaters: A review. *Journal of Hazardous Materials* **2011,** *186* (1), 16.

(89)   Masende, Z. P. G.; Kuster, B. F. M.; Ptasinski, K. J.; Janssen, F.; Katima, J. H. Y.; Schouten, J. C. Support and dispersion effects on activity of platinum catalysts during wet oxidation of organic wastes. *Topics in Catalysis* **2005,** *33* (1-4), 87.

(90)   Atia, T. A.; Wouters, W.; Monforte, G.; Spooren, J. Microwave chloride leaching of valuable elements from spent automotive catalysts: Understanding the role of hydrogen peroxide. *Resources Conservation and Recycling* **2021,** *166*.

(91)   Besson, M.; Gallezot, P. Selective oxidation of alcohols and aldehydes on metal catalysts. *Catalysis Today* **2000,** *57* (1-2), 127.

(92)   Besson, M.; Lahmer, F.; Gallezot, P.; Fuertes, P.; Fleche, G. Catalytic-oxidation of glucose on bismuth-promoted palladium catalysts. *Journal of Catalysis* **1995,** *152* (1), 116.

(93)   Hussain, S. T.; Sayari, A.; Larachi, F. Novel K-doped Mn-Ce-O wet oxidation catalysts with enhanced stability. *Journal of Catalysis* **2001,** *201* (1), 153.

(94)   Hussain, S. T.; Jamil, S.; Mazhar, M. Catalytic wet oxidation of phenol: The role of promoter and ceramic support. *Environmental Technology* **2009,** *30* (5), 511.

Chapter 7

Conclusions

In this study a range of catalysts were tested for CWAO of phenol and BPA with the primary aim of developing a catalyst which would be active under ambient conditions.

A comprehensive introduction into wastewater treatment methods was provided, along with the various advantages and disadvantages of each process. The primary focus was on advanced oxidation processes (AOPs), namely, catalytic wet air oxidation (CWAO).

Several batch and continuous chemical reactors were explored, with a trickle bed reactor established as the most appropriate for CWAO operations. An overview of catalysis, long with the current benchmark of catalysts reported in the literature was discussed, focusing on supported noble metal catalysts.

Initially the effect of the metal loading of platinum and ruthenium supported on silicon were investigated for phenol oxidation. Thrifting of the platinum loading by partial substitution with ruthenium showed no reduction in the phenol conversion. The platinum containing catalysts all achieved complete conversion at 160 ^{o}C and 7 bar$_{(g)}$. When co-impregnated, an increase in the initial reaction rate, with only a minor drop in selectivity was observed. When fully substituted with ruthenium, phenol conversion dropped below 7 %, concluding that when supported on SiC, platinum is intrinsically more active for CWAO than ruthenium.

Platinum impregnated on a range of SiC supports with differing surface areas (K7 – K10), were extensively studied for CWAO of phenol. A comparatively hydrophilic catalyst (K10) was tested alongside the SiC catalysts. The relative hydrophilicity and hydrophobicity of K9 and K10 was explored using TGA, with the

hydrophobic SiC catalysts achieving higher conversion rates under all investigated temperatures and pressures. The comparatively hydrophilic catalyst K10, showed the lowest activity towards both phenol and BPA oxidation, despite its higher surface area and smaller metal particle size. The effect of temperature, pressure, initial phenol concentration and catalyst particle size on CWAO of phenol were explored.

When the pollutant was changed to bisphenol A (BPA), catalytic activity was observed for the SiC catalysts at temperatures as low as 60 ^{o}C and atmospheric pressures. The catalysts were tested for upwards of 24 – 172 hours, with complete BPA conversion achieved by K9 at 7 bar$_{(g)}$ and 120 ^{o}C. When reaction temperatures and pressures were decreased K9 showed evidence of catalytic deactivation. Post-reaction characterisation revealed both metal leaching and carbonaceous deposits to be primarily responsible for the deactivation seen.

The conditions used in this study are considerable milder than any previously seen in the literature, and under near ambient conditions Pt/SiC was able to achieve 5 % and 25 % phenol and BPA conversions respectively.

To conclude, SiC was shown to be a very effective catalyst support for CWAO of organic pollutants, allowing the reaction to carried out under reduced temperatures and pressures. Reducing the severity of the operating conditions, furthers the technology as an environmentally friendly and cost-effective process for industrial wastewater treatment.

Appendix

HPLC calibration

==== Shimadzu LabSolutions Calibration Curve ====

ID#   : 1
Name   : Formic acid
Quantitative Method   : External Standard
Function   : f(x)=3118.74*x+0
   Rr1=0.9995512 Rr2=0.9991026 RSS=1.824325e+009
   MeanRF: 3.263407e+003 RFSD: 4.031657e+002 RFRSD: 12.354136
FitType   : Linear
ZeroThrough   : Through
Weighted Regression   : None
Detector Name   : Detector A
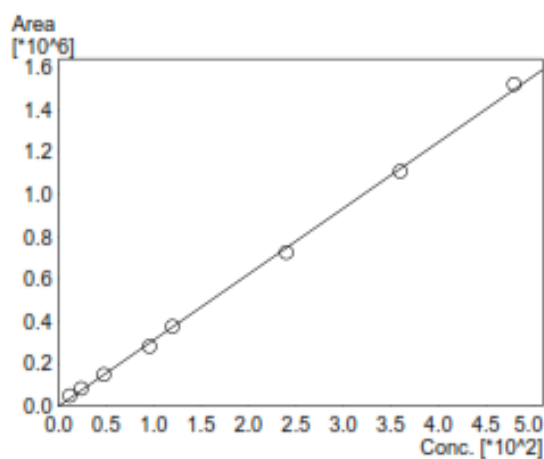
#	Conc.(Ratio)	MeanArea	Area
1	12	50163	50163
2	24	83569	83569
3	48	149007	149007
4	96	281895	281895
5	120	375665	375665
6	240	725716	725716
7	360	1109228	1109228
8	480	1520983	1520983

ID#   : 2
Name   : Oxalic acid
Quantitative Method   : External Standard
Function   : f(x)=57687.2*x+0
   Rr1=0.9977464 Rr2=0.9954978 RSS=2.633398e+011
   MeanRF: 6.437887e+004 RFSD: 1.055446e+004 RFRSD: 16.394292
FitType   : Linear
ZeroThrough   : Through
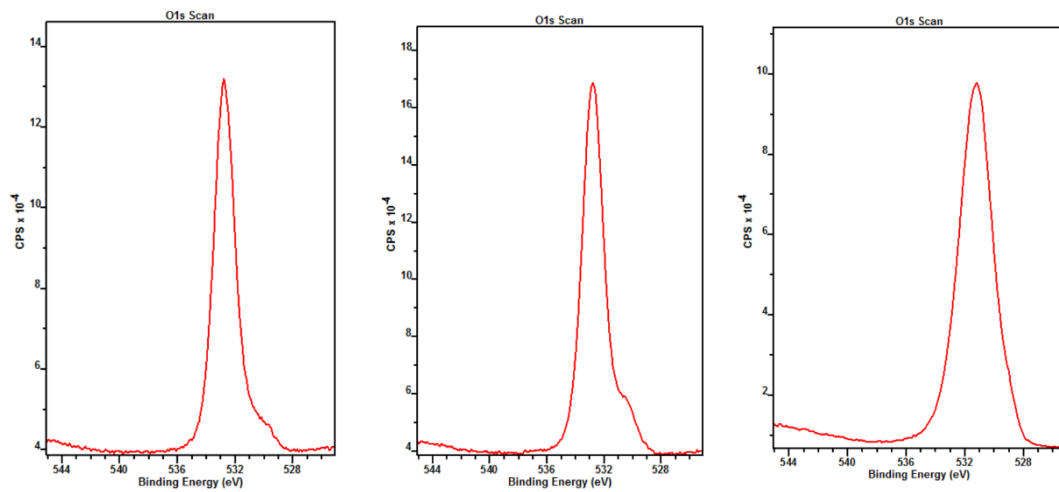Weighted Regression   : None
Detector Name   : Detector A
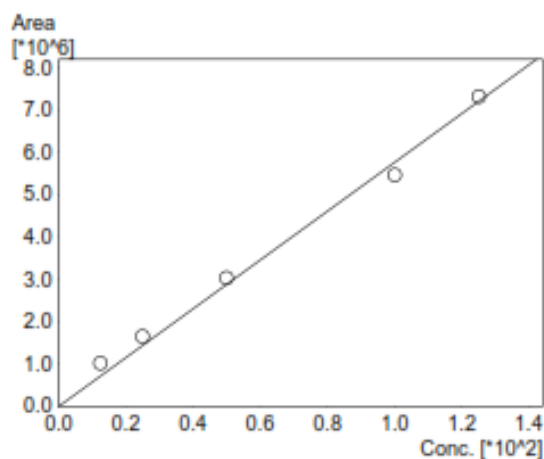
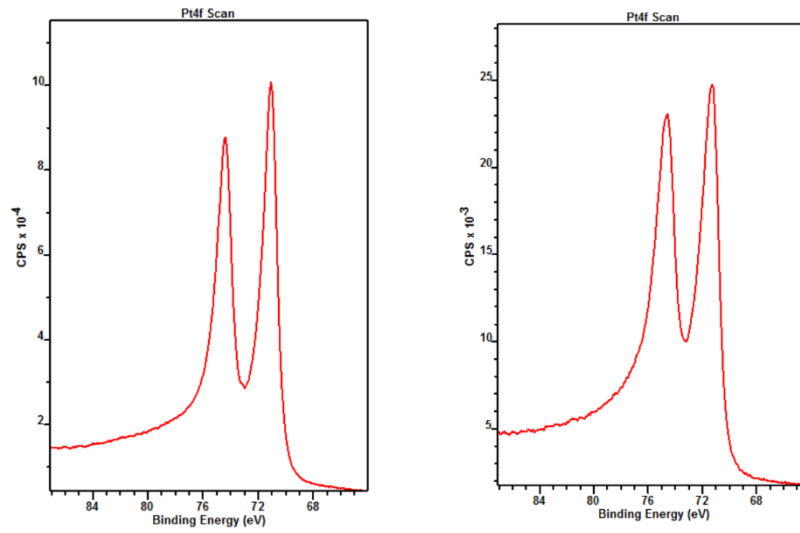| #	Conc.(Ratio)	MeanArea	Area
1	12.5	1021256	1021256
2	25	1656826	1656826
3	50	3035355	3035355
4	100	5464866	5464866
5	125	7320628	7320628

XPS data

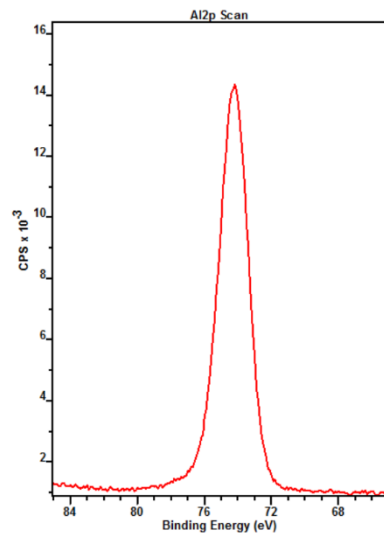Silicon 2p profile of K7 (left), K8 (middle) and K9 (right)
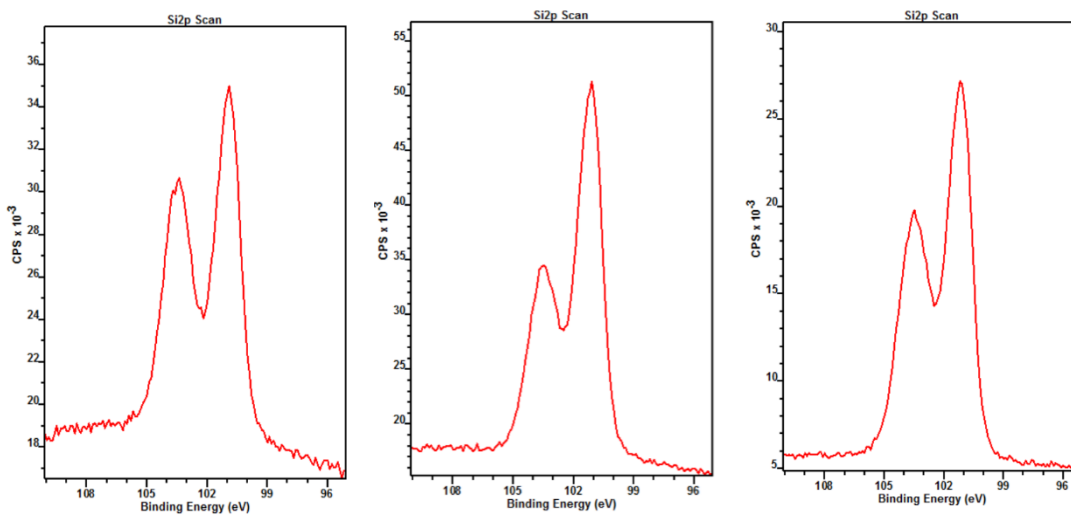
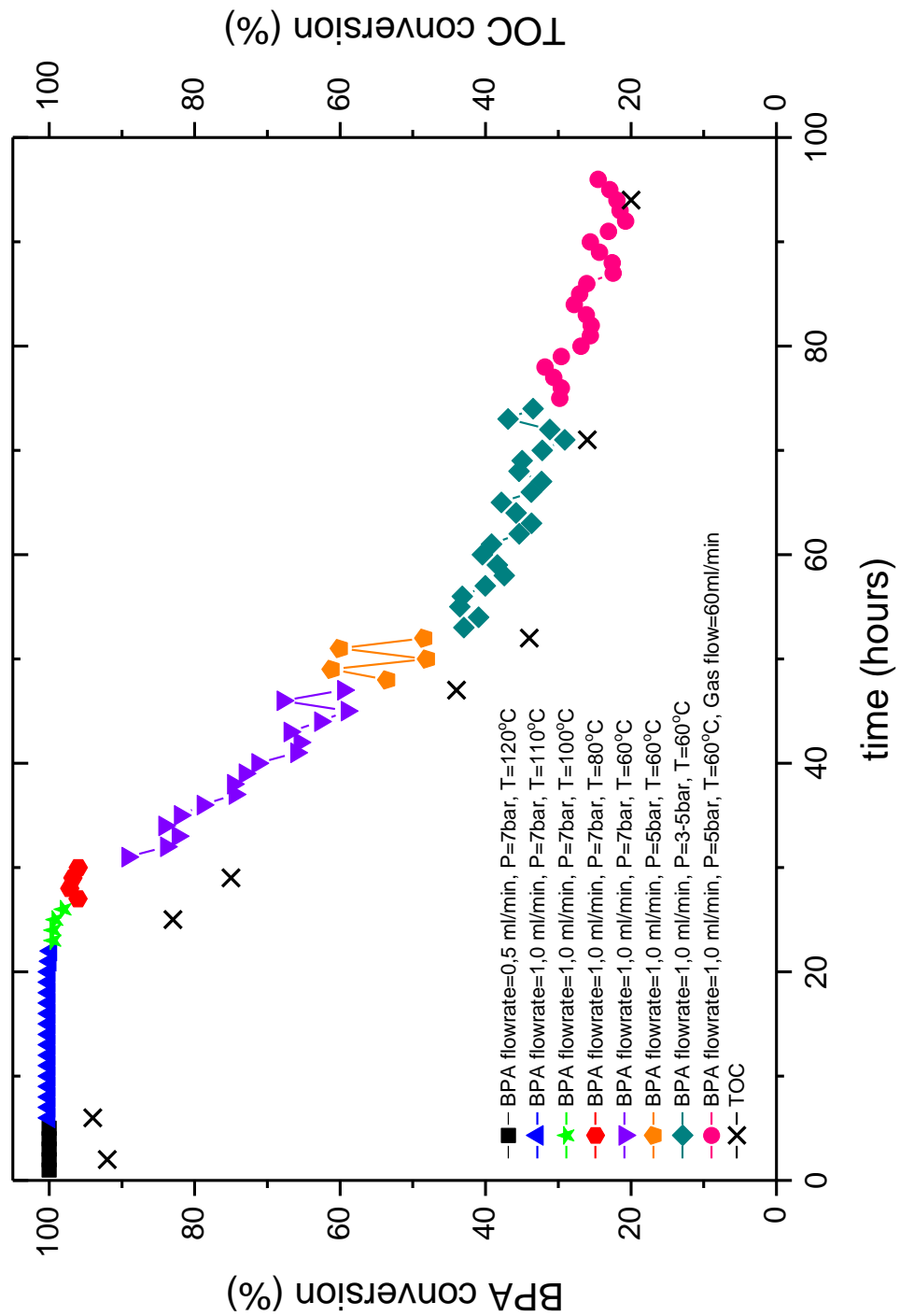Oxygen 1s profile of K7 (left), K8 (middle) and K10 (right)

Platinum 4f profile of K8 (left) and K9 (right)

Aluminium 2p profile of K10

BPA plot to determine appropriate conditions for further testing

The decrease in activity was initially thought to be due to lower rates at the lower temperatures/pressures, but after further experiments it became obvious it was caused by deactivation.